Aptamer-based optical biosensors

Von der Naturwissenschaftlichen Fakultät

der Gottfried Wilhelm Leibniz Universität Hannover

und

dem Senat des Technion – Israel Institute of Technology

Zur Erlangung des Grades

Doktorin der Naturwissenschaften (Dr. rer. nat.)

und

Doctor of Philosophy (PhD)

genehmigte Dissertation

von

Katharina Urmann, M.Sc.

geboren am 19.01.1987 in Würzburg

Referenten:
Prof. Thomas Scheper
Assoc. Prof. Ester Segal

Tag der Promotion:

21.Oktober 2016

Aptamer-based optical biosensors

Research Thesis

In Partial Fullfillment of the Requirements

for the Degree of Doctor of Philosophy

and

Doktor der Naturwissenschaften (Dr. rer. nat.)

Katharina Urmann

Submitted to the Senate of the Technion – Israel Institute of Technology

and

Der Naturwissenschaftlichen Fakultät

der Gottfried Wilhelm Leibniz Universität Hannover

Haifa, September 2016

ביוסנסורים אופטיים מבוססי אפטמרים

חיבור על מחקר

לשם מילוי חלקי של הדרישות לקבלת תואר דוקטור לפילוסופיה

-ו

תואר דוקטור במדעי הטבע (Dr. rer. nat.)

קטרינה אורמן

הוגש לסנט הטכניון – המכון הטכנולוגי לישראל

ואל

Naturwissenschaftliche Fakultät

der Gottfried Wilhelm Leibniz Universität Hannover

חיפה, ספטמבר 2016

Acknowledgement

The Research Thesis Was Done Under the Joint Supervision of Prof. Ester Segal in the Department of Biotechnology and Food Engineering (Technion) and Prof. Thomas Scheper at the Institute of Technical Chemistry (Leibniz University). The Generous Financial Help of the German Research Foundation, the Technion, and the Leventhal Family Fellowship, Administered by the Irwin and Joan Jacobs Graduate School, Is Gratefully Acknowledged.

List of Publications

1. **Urmann, K.**, Reich, P., Walter, J.-G., Beckmann, D., Segal, E., Scheper, T. (2016): *Rapid and Label-Free Detection of Protein A by Aptamer-Tethered Porous Silicon Nanostructures*. [Invited contribution to a Special Issue of the Journal of Biotechnology, submitted]

2. Modh, H., Witt, M., **Urmann, K.**, Lavrentieva, A., Segal, E., Scheper, T., Walter, J.-G. (2016): *Magnetic bead-based aptamer-assisted detection of ATP using qPCR (Apta-qPCR).* [submitted to ACS Sensors]

3. **Urmann, K.**, Mordrejewski, J., Walter, J.-G. (2016): *Aptamer-modified Nanomaterials: Principles and Applications*. Invited review to the Special Issue “Biofunctionalization” in BioNanoMaterials DOI: 10.1515/bnm-2016-0012

4. **Urmann, K.**, Arshavsky-Graham, S., Walter, J.-G., Scheper, T., Segal, E. (2016): *Whole cell detection of live Lactobacillus Acidophilus on aptamer-decorated porous silicon biosensors*. Analyst 141, 5432-5440

5. **Urmann, K.**, Tenenbaum, E., Walter, J.-G., Segal, E. (2015): *Porous silicon biosensors employing emerging capture probes* in Springer Series in Materials Science: *Electrochemically engineered nanoporous materials: methods, properties and applications* edited by D. Losic and A. Santos, Springer.

6. **Urmann, K.**, Walter, J.-G., Scheper, T., Segal, E. (2015): *Label-free optical biosensors based on aptamer-functionalized porous silicon scaffolds,* Analytical Chemistry 87(3), 1999-2006.

7. Woeller, K.-H., **Urmann, K.** (2012): *Optimised hydrogel matrix system containing emulsifiers*. Patent WO2012010465, PCT/EP2011061868

Conferences

Oral presentations

1. **Urmann, K.**, Sailor, M. J., Scheper, T., Segal, E. (2016): *Porous Si nanoparticles for the investigation of tethered receptor-target interactions by microscale thermophoresis*. [Porous Semiconductors – Science and Technology Conference, Tarragona - Spain, 06.-11. March 2016]

2. **Urmann, K.**, Walter, J.-G., Segal, E., Scheper, T. (2014): *Label-free optical biosensors based on aptamer-modified porous silicon scaffolds*. [**Keynote Lecture**] [Biosensors 2014 – World Conference on Biosensors, Melbourne - Australia, 27.-30. May 2014]

3. **Urmann, K.**, Segal, E., Walter, J.-G., Scheper, T. (2014): *Porous silicon-based aptasensors*. [Aptamers 2014 – 1st Oxford Symposium on Aptamers, Oxford - England, 24.-25. March 2014]

4. **Urmann, K.**, Walter, J.-G., Scheper, T., Segal, E. (2014): *Highly generic aptamer-based porous Si optical biosensors*. [Porous Semiconductors – Science and Technology Conference, Alicante - Spain, 09.-14. March 2014]

5. **Urmann, K.**, Walter, J.-G., Segal, E., Scheper, T. (2013): *Aptamer-based optical biosensors*. [2nd Conference of the Israel Society for Biotechnology Engineering, Tel Aviv - Israel, 01. December 2013]

Posters

1. **Urmann, K.**, Arshavsky-Graham, S., Walter, J.-G., Scheper, T., Segal, E. (2016): *Aptamer-functionalized porous Si optical biosensors for bacteria detection*. [Porous Semiconductors – Science and Technology Conference, Tarragona - Spain, 06.-11. March 2016]

2. **Urmann, K.**, Sailor, M. J., Scheper, T., Segal, E. (2016): *Porous Si nanoparticles for the investigation of tethered receptor-target interactions by microscale thermophoresis*. [3rd Conference of the Israel Society for Biotechnology Engineering, Tel Aviv - Israel, 13. December 2015]

3. **Urmann, K.**, Walter, J.-G., Segal, E., Scheper, T. (2015): *Aptamers and porous silicon – two talents for universal biosensing applications.* [9. German Biosensor Symposium , Munich, 11.-13. March 2015]

4. **Urmann, K.**, Walter, J.-G., Segal, E., Scheper, T. (2015): *Aptamers and porous silicon – two talents for universal biosensing applications.* [Conference for Scientific Cooperation between Lower Saxony and Israel, Hannover, 10.-11. March 2015]

5. Urmann, K., Walter, J.-G., Scheper, T., **Segal, E.** (2014): *Label-free Optical Biosensors Based on Aptamer-Modified Porous Silicon Scaffolds* [Gordon Research Conferences Bioanalytical Sensors, Newport - USA, 22.-27. June 2014]

6. **Urmann, K.**, Walter, J.-G., Segal, E., Scheper, T. (2013): *Aptamer-based optical biosensors*. [Poster and short-talk] [2nd Conference of the Israel Society for Biotechnology Engineering, Tel Aviv - Israel, 01. December 2013]

7. **Urmann, K.**, Segal, E., Walter, J.-G., Scheper, T. (2013): *Aptamer-based optical biosensors.* [First Conference for Scientific Cooperation between Lower Saxony and Israel, Hannover, 06.-07. October 2013]

8. **Urmann, K.**, Segal, E., Walter, J.-G., Scheper, T. (2013): *Aptamer-based optical sensor system.* [8. German Biosensor Symposium , Wildau, 10.-13. March 2013]

Table of Contents

List of Figures

List of Tables

Abstract

English

Early, sensitive, and selective detection of various analytes is a critical step in quality assurance, environmental monitoring, clinical diagnostics and industrial process control (e.g. biotechnological production of recombinant therapeutic proteins). Conventional procedures are often time-consuming, laborious and require highly specific equipment, complex sample processing, and well trained staff. A promising approach for highly specific and rapid detection of various compounds is the development of biosensors. To date, available sensor systems are mostly based on fluorescence detection or include complicated assay schemes.

In order to overcome these limitations, we designed biosensors based on oxidized porous silicon (PSi), which is used as the optical transducer, conjugated with target-specific aptamers. Exposure of these scaffolds to analyte molecules or cells, results in capture of analytes within the nanostructure or on the PSi surface respectively. These binding events induce predictable changes in the thin-film optical interference spectrum of the biosensor - or a decrease of the signal intensity - and can easily be monitored in real time by a simple spectrometer. Through the novel combination of aptamers and PSi, these biosensors have prolonged shelf-lives and outstanding stability in aqueous environment for repeated cycles of biosensing when the aptamer allows for elution of the bound target.

The biosensors presented in this work are a novelty with regard to their tunable design, which can be tailored for many other relevant targets. Exchanging the conjugated aptamer while retaining immobilization chemistry and other system parameters, allows to easily build a new biosensor capable of specific detection of the respective aptamer ligand. These aptamer-based, label-free sensor schemes provide tremendous advantages in terms of speed and cost of measurement, as well as simplicity and portability of the system.

Keywords: optical biosensor, aptamer, label-free, porous silicon

Deutsch

Die schnelle, sensitive und spezifische Detektion unterschiedlichster Substanzen ist essentiell in Diagnostik, Qualitätskontrolle, Umweltüberwachung und vielen Produktionsprozessen (z.B. in der biotechnologischen Produktion pharmazeutisch relevanter Proteine). Konventionelle Detektionsmethoden sind oftmals zeitintensiv, arbeitsaufwändig und erfordern spezielles Equipment sowie komplexe Probenaufarbeitung und deshalb gut ausgebildetes Personal. Ein vielversprechender Ansatz für eine hochspezifische und schnelle Detektion verschiedener Moleküle ist die Entwicklung von Biosensoren. Moderne optische Biosensoren basieren meist auf Fluoreszenz-Messungen oder beinhalten komplizierte Assays.

Um diese Einschränkungen zu überwinden, wurden Biosensoren entwickelt, die oxidierte porösen Silizium-Schichten (PSi) als optische Transducer verwenden. Analyt-spezifische Aptamere sind hier als Biorezeptoren kovalent an dieser Matrix immobilisiert und das Aufgeben von Analyt-Proben resultiert in deren Bindung innerhalb der Porenstruktur, bzw. an der PSi-Oberfläche. Diese spezifischen Bindungen führen zu vorhersagbaren Veränderungen im Reflektionsspektrum des Biosensors bzw. zu einem Signalabfall und können in Echtzeit mit einem Spektrometer verfolgt werden. Durch die neuartige Kombination von Aptameren und PSi besitzen diese Biosensoren eine deutlich verlängerte Lagerstabilität und verbesserte Korrosionsresistenz in wässrigen Medien. Zudem können dieselben Biosensoren für mehrere Detektionszyklen verwendet werden, wenn das entsprechende Aptamer eine Elution des Analyten zulässt.

Die in dieser Arbeit präsentierten Biosensoren stellen eine Neuheit im Hinblick auf ihre universelle Anwendung dar. Durch Austausch der Aptamer-Sequenz, lässt sich mit geringem Aufwand ein neuer Biosensor zur spezifischen Detektion des jeweiligen Aptamer-Targets herstellen. Diese Aptamer-basierten markierungsfreien Biosensoren haben enorme Vorteile im Hinblick auf Schnelligkeit, Kosten der Messungen, sowie Einfachheit und Tragbarkeit des Systems.

Keywords: optischer Biosensor, Aptamer, markierungsfrei, poröses Silizium

Hebrew

בתהליכי בקרת איכות וייצור ובניטור סביבתי, נדרש לא פעם זיהוי מוקדם, רגיש וסלקטיבי של מגוון חומרים. בפרט, בתהליכים ביוטכנולוגיים, מעקב אחר ריכוז או נוכחות אנליטים שונים (analyte) הינו הכרחי. התפתחות החיישנים הביולוגיים (ביוסנסורים) מהווה גישה מבטיחה לזיהוי ספציפי ומהיר של מגוון תרכובות.

שיטות קונבנציונליות לזיהוי תרכובות שונות וחיידקים אורכות לעיתים זמן רב. השיטות הללו דורשות מכשור מעבדתי מורכב ויקר, הכנה מורכבת של דוגמאות ולפיכך, גם כוח אדם מיומן. החיישנים הקיימים כיום מבוססים על שיטות זיהוי פלורוסנטיות או על בדיקות מורכבות.

כדי להתגבר על חסרונות אלו תכננו ופיתחנו חיישנים מבוססים על סיליקון פורוזיבי מחומצן אשר משמש כמתמר אופטי אליו מצומדים אפטמרים הספציפיים לאנליט המטרה. כאשר החיישן נחשף לדוגמאות המכילות את חלבוני המטרה או החיידק, הם נקשרים אל האפטמרים ונלכדים בתוך המבנה הננומטרי של הסיליקון הפורוזיבי או בפני השטח שלו, בהתאמה. תהליכי הקישור הספציפיים הללו יוצרים שינויים צפויים בספקטרום ההחזרה האופטי של הסיליקון או לירידה בעוצמת הסיגנל, ואת שניהם ניתן לנטר בקלות ובזמן אמת עם ספקטרומטר פשוט. נוסף על כך, הודות לשילוב החדשני של האפטמרים עם סיליקון פורוזיבי, לחיישנים אלה יש חיי מדף ארוכים ויציבות מצוינת בסביבה מימית במספר מחזורי חישה, המתאפשרים על ידי אלוציה של האנליט.

החיישנים הביולוגיים המוצגים בעבודה זו הינם חדשניים בגמישותם ויכולת התאמתם למגוון אפליקציות. שינוי של האפטמר המצומד, תוך שמירה על הכימיה ופרמטרים אחרים במערכת, מאפשרת יצירה של חיישן חדש המאפשר זיהוי ספציפי של ליגנד שונה. החיישנים הללו לא דורשים סימון מקדים ומקנים יתרונות עצומים מבחינת מהירות המדידה, עלות, פשטות וניידות המערכ.

List of Abbreviations

3D	Three dimensional
6H7	His-tag binding aptamer
APTES	3-Aminopropyl(triethoxyl)silane
ATR	Attenuated Total Reflectance
CCD	Charge Couple Device
CLSM	Confocal Laser Scanning Microscopy
DMSO	Dimethylsulfoxide
DNA	Deoxyribonucleic acid
EB	Elution buffer
EDC	1-Ethyl-3-(3-dimethylaminopropyl)carbodiimide
EDIPA	Ethyldiisopropylamine
EDTA	Ethylenediaminetetraacetic acid
e.g.	For example
EOT	Effective Optical Thickness
FFT	Fast Fourier Transform
FTIR	Fourier Transform Infrared Spectroscopy
GA	Glutaraldehyde
Hemag1P	*Lactobacillus acidophilus*-binding aptamer
HEPES	4-(2-hydroxyethyl)-1-piperazineethanesulfonic acid
HF	Hydrofluoric acid
HR/SEM	High Resolution / Scanning Electron Microscope
i.e.	id est
IgG	Immunoglobulin G
ITC	Isothermal titration calorimetry
LB	Luria broth
MES	2-Morpholinoethanesulfonic acid
MPTMS	(3-Mercaptopropyl)trimethoxysilane

MRS	de Man, Rogosa and Sharpe medium
MST	Microscale thermophoresis
PA	Protein A
PAA	Protein A-binding aptamer
PBS	Phosphate Buffer Saline
PNA	Peptide nucleic acid
PSi	Porous Si
$PSiO_2$	Oxidized PSi
RI	Refractive index
RIFTS	Reflective Interferometric Fourier Transform Spectroscopy
RNA	Ribonucleic acid
RT	Room Temperature
SB	Selection buffer
SELEX	Systematic Evolution of Ligands by Exponential Enrichment
Si	Silicon
SLIM	Spectroscopic Liquid Infiltration Method
SPR	Surface Plasmon Resonance
ssDNA	Single Stranded DNA
TE	Tris and EDTA containing buffer
TRIS	2-Amino-2-(hydroxymethyl)-1,3-propanediol

1. Preamble

Early and rapid detection, as well as identification of different analytes, is a critical step in food safety and quality assurance, environmental monitoring, industrial processes and of utmost importance in disease diagnostics. As intensive research discovers more and more disease-specific biomarkers (e.g. overexpressed proteins, DNAs, short and micro RNAs etc.) and scandals about environmental toxins in food (e.g. herbicides, antibiotics or bacterial contaminations) repeatedly flood news reports, the need for new assays to reliably detect and quantify such analytes is emphasized.

A promising approach for highly specific and rapid detection of target analytes (ranging from small molecules to whole cells) is the development of biosensors. Most conventional biosensor schemes rely on natural bioreceptors like antibodies, enzymes or matching DNA/RNA sequences, which are not readily available for all analytes and implicate significant limitations. For instance, antibody-function is dependent on near-physiological conditions and the regeneration of antibody-based biosensors is hampered by their tendency to irreversibly denature. Also the selectivity of the capture probe can significantly restrict the biosensor's performance, especially for detection in complex samples, e.g., of clinical origin, food or wastewater samples. Direct biosensing approaches without tedious pre-treatment of samples are desired to lower the overall assay time and to pave the way towards point-of-care application of biosensors in a simple and portable manner outside the laboratory environment.

A novel category of bioreceptors is represented by aptamers. These are short single stranded oligonucleotides that can exhibit specific target affinity as a product of an iterative selection process called SELEX (Systematic Evolution of Ligands by Exponential Enrichment), which was first established in 1990 [1, 2]. In brief, during this process, a large library of random RNA or DNA sequences is screened for their ability to capture the desired target under the given experimental conditions (i.e. sample matrix compositions). Following a separation step, only target-affine sequences are amplified and form the starting library for the next

cycle. After a number of iterations, the final library is sequenced and usually yields only a small number of different but often similar sequences that can then be synthesized and characterized for their precise binding properties individually.

As the prices for synthetic oligonucleotides as well as sequencing services have decreased significantly over the last few years; while methods for selection and characterization have been facilitated and firmly established, it is believed that aptamers may have the potential to replace antibodies in most fields in the near future [3]. The main disadvantage of antibodies is their often poor characterization and unreliable production. A study from 2008 has shown that only half of 6000 commercially available antibodies were indeed recognizing their specific target [4] . Andrew Bradbury, Andreas Plückthun, and 110 more co-signatories are pillorying the waste of research time and budget caused by non-standardized antibodies in their Comment in Nature [5] and are calling for action to create an accessible database for all types of binding reagents.

Further advantages of aptamers are their high binding affinities, while their production is performed fully *in vitro* and thus fast, low-cost, and with constant high quality [6, 7]. Employed as capture probes, biosensors especially profit from the aptamers' versatile chemical modification options, small molecule size and high stability. During synthesis, aptamers can be modified with a wide range of functional groups either on their 5' or 3' terminus to allow for facile conjugation in the desired immobilization orientation and density [8-10]. Aptamer-modified biosensors – depending on the nature of the transducer – may have long shelf lives due to the aptamers' excellent stability and ability to reversibly fold and unfold their active secondary structure. Aptamers can be designed to bind virtually any desired target [6] and their selection under conditions of the native target conformation and surrounding matrix, foster a highly selective and affine aptamer sequence as a result.

An ideal transducer for the beneficial combination with aptamers as receptor probes seems porous silicon. Its history, material properties and fabrication for the use as optical transducers are described in the following section (taken and

adapted from the book chapter “Porous Silicon Biosensors Employing Emerging Capture Probes” which appeared 2015, see appendix).

Although porous silicon (PSi) was already discovered in the 1950s, it only gained scientific attention in the 1990s when Leigh Canham reported bright photoluminescence of the material [11]. While the interest in PSi for optoelectronic switches, displays and lasers quickly faded due to its poor chemical and mechanical stability, it became a material of choice for sensors design. PSi unique combination of properties i.e., high surface area and volume, tunable nanostructure, versatile surface chemistry and compatibility with other silicon microfabrication technologies, allow for the design of sophisticated biosensing platforms [11, 12]. Indeed, a growing number of biosensing schemes employing PSi as a transducer are reported in recent years. By 2013, the yearly number of new publications already reached 40. Included here are not only electrochemical biosensors taking advantage of the semiconductor electrical properties, but also many optical biosensing schemes, which utilize the unique optical properties of this nanostructured material.

The most common fabrication method of PSi is electrochemical etching in the presence of hydrofluoric acid (HF) and in a two-electrode setup: a platinum wire serves as electrode and aluminum on the Si-backside is the counter-electrode (see Fig. 1.1). The reaction equation for PSi formation is shown in Fig. 1.2.

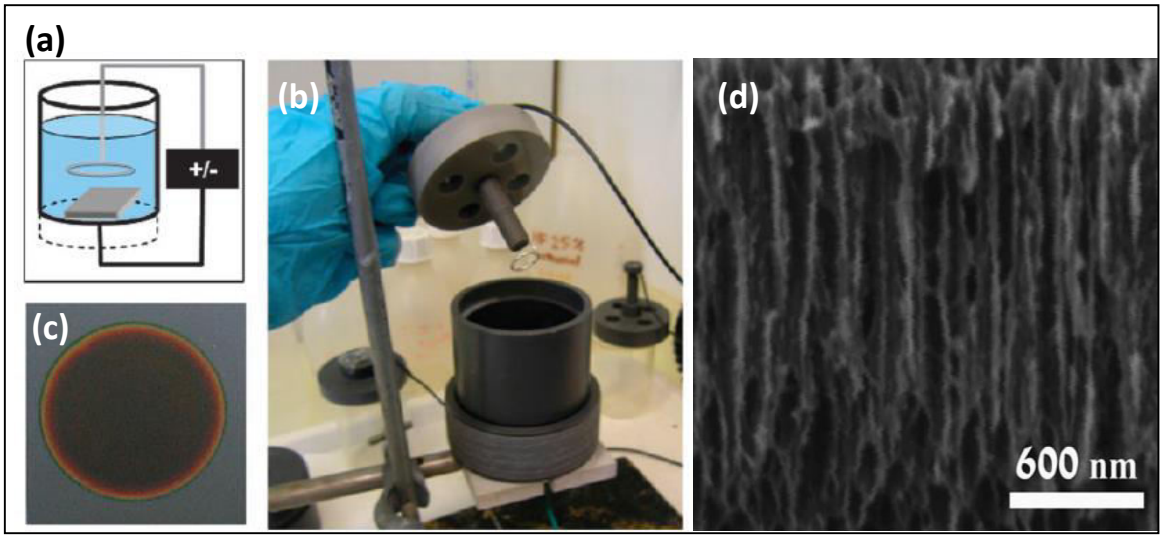

Figure 1.1. (a) A scheme and (b) a photograph of an electrochemical-etching cell used for anodization of Si. (c) A photograph of a PSi sample etched in this apparatus. (d) Cross-sectional view SEM micrograph of a thin layer of PSi etched under conditions to yield cylindrical pores. Adapted from ref. [13].

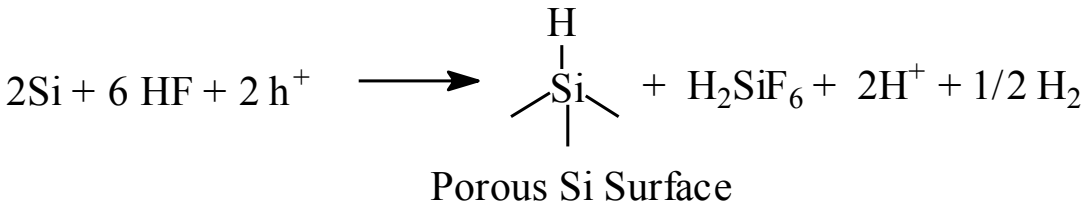

Figure 1.2. Reaction scheme for galvanostatic etching. “h+” indicates the positively charg ed hole in the crystal structure due to doping with boron.

This method allows to easily define the properties of the formed porous layer in terms of pore dimensions, morphology and porosity, by adjustment of the etching parameters (e.g., current density, anodization time, HF concentration) [14],[15]. By controlling the current density during the etching process, different porous

structures can be fabricated such as single porous layers, double layers,microcavities and rugate filters (see Fig. 1.3) [12].

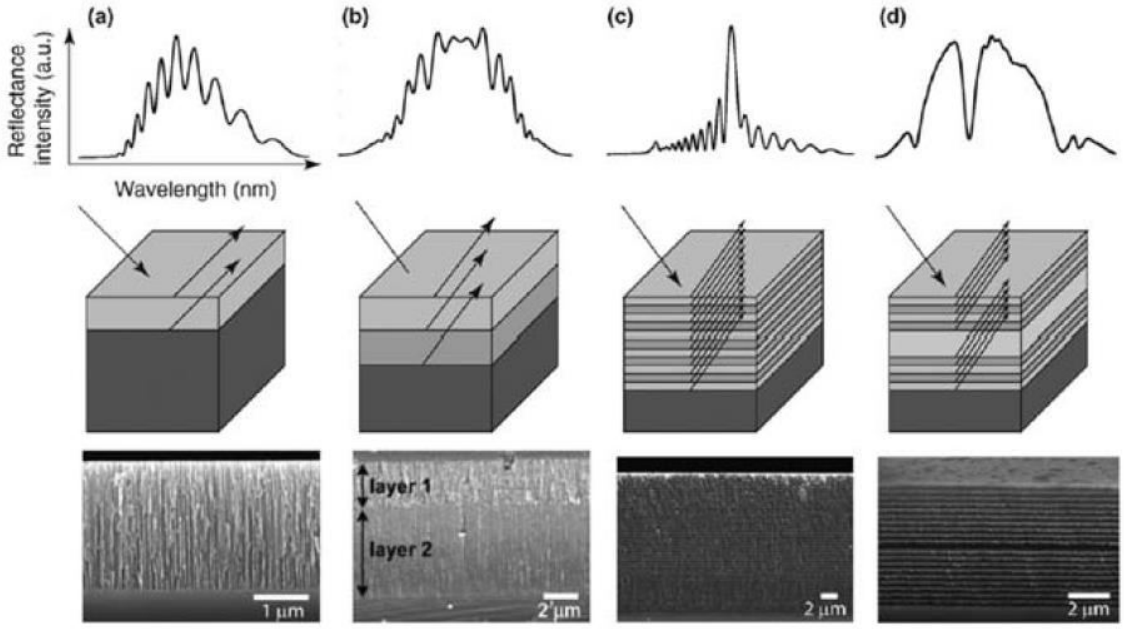

Figure 1.3. Bottom to top: HR-SEM micrographs, schematics and corresponding reflectance spectra of different PSi structures. (a) Single layer; (b) Double layer; (c) Multilayer (Rugate filter); (d) Microcavity. Adapted from ref. [12].

The freshly-etched PSi is unstable in ambient environment and in aqueous medium as the Si hydride-terminated surface is prone to nucleophilic attack by water molecules. A simple method to stabilize PSi is to grow an oxide layer on the surface to slow spontaneous oxidation ($PSiO_2$ formation). The resulting $PSiO_2$ layer provides a convenient means for subsequent surface modification, as it enables the simple reaction with different alkyl silanes [12, 13, 16]. Reactive groups at the distal end of the silane molecules, such as amines and thiols, provide attachment points for biorecognition elements. Silanization of oxidized PSi has been used to create biorecognition interfaces composed of DNA [16], antibodies [17-19] and small molecules [20].

Porous silicon has proven to be a suitable transducer, showing excellent sensitivity, and allowing for label-free detection of many analytes of interest [21, 22]. PSi optical biosensors are based on changes in the photoluminescence or the

reflectivity spectra upon exposure to the target analyte, which replace the media in the pores. A change in the refractive index (RI) of the liquid in the pores affects the average RI of the porous film, and is commonly observed as quenching of the PSi photoluminescence or as a wavelength shift in the reflectivity spectrum. For analytes that are size excluded from penetrating into the porous nanostructure, changes in the reflected light intensity are observed as a result from a change in the RI contrast at the PSi-medium (air or other) interface [(23)].

Optical transducers received significant attention in the field of PSi-based biosensors since the pioneering work of Sailor and co-workers [(24-26)], and there are already few commercially-available optical sensing systems (Silicon Kinetics, Inc.). Nevertheless, PSi is also studied as an electrochemical transducer for biosensing applications [(27)]. The two main electrochemical transduction types are potentiometry and amperometry. Potentiometric biosensors measure the potential difference occurring as a result of an acidic/basic substance formation. These substances are usually a product of an enzymatic reaction, where the catalyzing enzyme is immobilized to the PSi surface. Amperometric biosensors measure current density resulting from redox reactions, catalyzed by immobilized enzymes. Amperometric PSi-based biosensors are less applicable due to the relatively poor conductivity of PSi and therefore, coupling of metal electrodes to the PSi may increase their sensitivity [(27, 28)].

Apart from the transducer quality, the properties of the biorecognition elements to be used for analyte binding have a critical effect on the performance of any biosensor system. The use of novel capture probes is emerging for new assay designs and for targeting a wide variety of analytes. These capture probes: aptamers, peptide nucleic acid (PNA), synthetic antibodies, antimicrobial peptides (AMPs) or enzymes, hold in store many advantages over the common bioreceptors. These include improved conformational stability, higher affinity towards the target analyte, and reduced production costs. We believe that the integration of these novel biorecognition elements with the advantageous properties of PSi will improve the performance of PSi-based biosensors

dramatically, especially in terms of sensitivity. Low limits of detection will allow these biosensors to meet the requirements in the fields of food safety, medical diagnostics or homeland security.

In this work, we show the first examples for the implementation of aptamer receptors in optical prorous silicon biosensors. While stressing the simplicity of optical systems based on PSi nanostructures, we highlight the advantages of aptamers and demonstrate regenerability of the recognition element, selective and sensitive detection, not only for protein targets, but also for whole cell capture. Furthermore, we show the possibility to obtain system-specific affinity constants for the utilized aptamer/target pairs by non-linear regression of the optical signal vs. the target concentration and to determine the limit of detection of the optical biosensor.

2. Literature survey

2.1 Book chapter: Porous Silicon Biosensors Employing Emerging Capture Probes

The following literature survey is based on and adapted from the book chapter "Porous Silicon Biosensors Employing Emerging Capture Probes" which appeared 2015 in the Springer Series in Material Science book entitled "Electrochemically Engineered Nanoporous Materials – Methods, Properties and Applications" edited by Dusan Losic and Abel Santos (see Apendix).

2.1.1 Emerging Bioreceptors

All biosensors rely on an element facilitating molecular recognition – the so-called bioreceptor, which specifically binds the target analyte. Binding between the bioreceptor and the analyte occurs due to biomolecular recognition which is based on the complementarities of the surfaces of the two binding partners [(29)]. Different molecular interactions can contribute to binding: Hydrogen bonding, van der Waals forces, electrostatic interactions, π-π interactions, and combination of thereof are working in concert to enable high specific and high affinity binding. Moreover, during the binding event, successive replacement of water from the binding sites of the bioreceptor and the analyte takes place, resulting in an increase of enthalpy making binding favorable. In aqueous solutions – which are most often the media to be analyzed by biosensors – this so-called hydrophobic effect has a profound role and may even dominate the bioreceptor-analyte complex formation [(30)].

In this section a brief overview on bioreceptors will be given with an emphasis on emerging new types of recognition elements. This section makes no claim to be complete, more comprehensive reviews can be found elsewhere (e.g. [(31, 32)]).

2.1.1.1 Natural Bioreceptors

The first biosensor systems utilized bioreceptors provided by living organisms. Examples for such biological recognition elements are antibodies and enzymes. These naturally occurring receptors have been developed by nature via evolutional processes. Today, biotechnology allows not only the construction of completely

new bioreceptors, which will be discussed in the section 2.1.2.2, but also facilitates rational modification of naturally occurring bioreceptors e.g. manipulation of their binding site to permit new specificities. Therefore, a precise discrimination between natural and synthetic bioreceptors is difficult and the line between them is blurred. In this subsection we are summarizing some naturally occurring bioreceptors as well as engineered variants derived from these molecules.

2.1.1.1.1 Antibodies

The most prominent example for bioreceptors may be antibodies. In nature, antibodies are produced by the immune system by an evolutional process resulting in high affinity and specificity. The human immune system is estimated to possess a repertoire of 10^{15} distinct antibody structures from which appropriate antibodies are chosen by recombinant selection [(33)]. This allows the production of antibodies directed against numberless potential antigens. This diversity in combination with the well-established techniques of antibody development and production are responsible for the broad use of antibodies in biosensing systems. The dominance of antibodies was especially boosted by the development of monoclonal antibody technology, facilitating the production of large amounts of antibodies directed against one single epitope of the antigen in cell culture. Instead of using the complete, intact antibody, Fab fragments or even smaller fragments can be used as bioreceptors [(34-36)].

Based on their generation in living organisms – cells or animals - antibodies possess some limitations. For instance, antibodies directed against small molecules in general, and especially against toxic or non-immunogenic molecules, are difficult to generate. Here the analyte has to be coupled to a protein before immunization [(37)] and the obtained antibodies have to be purified in order to isolate the fraction binding to the target of interest. The development of antibodies against small molecules is thus laborious, time-consuming and expensive.

Detailed understanding of the genetic background of antibodies has resulted in the possibility to manipulate antibodies structure [(35)]. Recombinant expression of antibodies allows the design of chimeric antibodies; the binding sites of antibodies

can be selected by phage display techniques using genetic engineered phage libraries. In antibody phage display, the minimized antibodies are fused to a coat protein of the virus, resulting in phages presenting the antibody on the phage surface. The phages are then used for the selection of antibody fragments with the desired binding properties, they not only display the antibody fragment on their surface, but they also carry the corresponding genetic information and can thus be used for the amplification of these features [(38)].

Although these modern selection techniques have overcome the limitations associated with the development of antibodies in living organisms, other problems remain unsolved. These include poor antibody stability and their limitation to near-physiological conditions.

2.1.1.1.2 Enzymes

Enzymes do not only bind a substance – the so-called substrate – they also convert it in a product. The binding of the substrate into the active binding pocket of the enzyme is driven by the forces described above and results in high specificity. Moreover, the catalytic process results in detectable reaction products like protons and electrons, which can be exploited for signal amplification. Enzymes were the first recognition elements used in biosensors. The pioneering work of Clark and Lyons [(39)], immobilizing glucose oxidase on an electrode to allow for the determination of glucose concentration, has boosted the development of numerous enzymatic biosensor platforms, which exploit the outstanding specificity of enzymes [(40)].

Drawbacks of naturally occurring enzymes are their rather low stability with regard to environmental conditions (temperature and pH) [(41)], and the lack of specific enzymes for all analytes of interest. Here, genetic engineering can broaden up the diversity of possible substrates and fine-tune the characteristics of the bioreceptor [(42)]. An interesting approach to develop enzymes, which can be tailored to allow the detection of specific analytes of interest, was described by Ostermeier (2005) [(44)]. Target binding sites were engineered and inserted into the regulatory subunit

of an allosteric enzyme. Binding of the target to the regulatory subunit resulted in a structural switch affecting the activity of the catalytic site [43, 44].

2.1.1.2 Synthetic Receptors

As already mentioned, natural bioreceptors are limited by their low stability, poor performance in organic solvents, and/or their availability against a specific analyte. Therefore, technologies have been developed to advance naturally occurring bioreceptors or to even completely substitute them by novel types of bioreceptors. Using modern DNA technology naturally occurring bioreceptors can be further evolved to result in engineered receptors with improved properties. In addition, completely synthetic bioreceptors are developed by rational design, computational chemistry, combinatorial chemistry, molecular imprinting, self assembly or combinations of these techniques [45].

2.1.1.2.1 DNA and PNA

DNA oligonucleotides can be used as bioreceptors for the detection of complementary DNA sequences. Here, the hybridization between the DNA and the oligonucleotide is exploited for the detection of the DNA - or more specifically - the source of the DNA. Thus, oligonucleotides are most valuable for a variety of targets ranging from pathogens in infectious diseases [46] and food-borne contaminations [47], cancer biomarkers [48], to the diagnosis of genetic diseases by microarray-based multiplexed detection of genes and gene alterations [49-51].

One drawback associated with DNA oligonucleotides as bioreceptors is their susceptibility to degradation by nucleases. In this context, the use of phosphorothioates can improve DNA stability [52] and locked nucleic acids (LNAs) have been developed which contain at least one bicyclic furanose unit which, nucleases do not accept as a substrate [53]. Other disadvantages associated with DNA are the limited sensitivity and rapidity of the sensing. Conventionally, the DNA originating from the sample to be analyzed needs to be amplified via PCR prior to sensing, resulting in a lengthy procedure. Moreover, the negatively charged phosphate backbone of the oligonucleotides is also the source of some concerns. The negative charge results in electrostatic repulsion, which further increases upon

duplex-formation and causes Coulomb blockage of the hybridization [54, 55]. To circumvent these problems, a new type of nucleic acid oligomers has been developed. In peptide nucleic acids (PNAs) [56], the negatively charged phosphate backbone of natural oligonucleotides is replaced by a neutral peptide-like backbone composed of repeated N-(2-aminoethyl)glycine units linked by amide bonds. The number of bonds between the bases in the obtained PNA is similar to that in DNA, resulting in a proper inter-base spacing, which allows for hybridization of DNA and PNA. The use of PNA in DNA biosensors offers some major advantages. PNA is not recognized by nucleases and proteases and is thus stable in biological fluids. Due to the lack of electrostatic repulsion, which exists between two DNA oligonucleotides, the binding between PNA and DNA is even stronger and more specific than the formation of DNA duplexes. Thus, PNA is considered to offer extraordinary specific detection of DNA to facilitate the identification of single-nucleotide mismatches [57].

Despite their improved properties, PNAs are limited to the detection of DNA sequences. Another type of oligonucleotide – termed aptamer – broadens up the specificity of oligonucleotide-based detection to virtually all types of analytes.

2.1.1.2.2 Aptamers

Aptamers are single-stranded oligonucleotides composed of RNA or DNA generated by *in vitro* selection techniques like SELEX (systematic evolution of ligands by exponential enrichment) [58-60], modified SELEX procedures [61, 62] MonoLEX [63]. During the selection, aptamers are isolated from combinational oligonucleotide libraries containing up to 10^{15} individual sequences based on their affinity and specificity towards the desired target molecules. Once an aptamer sequence has been identified, the aptamer can be produced by chemical synthesis.

In contrast to conventional DNA, which binds complementary DNA based on Watson-Crick base-pairing and is usually thought of as a rather linear molecule, aptamers fold into unique three-dimensional (3D) structures that enable the molecular recognition of their corresponding targets [64, 65]. Thus, they are often

described as nucleic acid-based alternatives to antibodies. While the development of antibodies depends on the immunization of animals and their production via cell culture techniques, aptamers are selected by *in vitro* techniques and can be produced via chemical synthesis. Consequently, aptamers can be selected against virtually all types of targets, including those with low immunogenicity or high toxicity. Moreover, aptamers can be selected under non-physiological conditions in order to generate aptamers that are functional under desired conditions. Thus, in case of aptamers, a tailor-made bioreceptor can be designed and optimized to meet the requirements of specific applications [(66, 67)].

In the special context of biosensing, the major advantages of aptamers over their amino acid-based counterparts include their superior stability, ease of regeneration (to allow subsequent usage in multiple sensing cycles), and highly reproducible production by chemical synthesis. During this synthesis the aptamer can be modified at defined positions; for instance linker molecules can be incorporated to facilitate highly controlled immobilization of the aptamer on the transducer surface. Moreover, due to their oligonucleotide nature, aptamers offer completely new biosensing schemes, as we reviewed recently [(68, 69)]. For instance, oligonucleotides complementary to the target-binding site of the aptamer can be designed and hybridized to the aptamer. Thus, in the presence of the target, the target will replace the complementary oligonucleotide, while the release of the oligonucleotide can be detected and quantified via different labeling techniques. This strategy has been already successfully applied for the detection of ethanolamine, which is the smallest analyte against which an aptamer has been selected [(70)]. In more sophisticated sensing schemes, the aptamer can simultaneously act as both the bioreceptor and the transducer. In these so called aptamer beacons, the aptamer can be modified with a quencher and a fluorophore positioned in close proximity, resulting in low fluorescence in the absence of the target. Binding to the target results in conformational changes; fluorophore and quencher depart from each other to yield an increase in the of fluorescence intensity [(71)].

One concern associated with aptamers is their sensitivity to degradation by nucleases. Today this problem can be easily overcome by different modifications [72] and even non-modified aptamers are already successfully applied in complex biological samples [73, 74]. In addition, the high negative charge presented by the aptamer molecule may result in failure to select of aptamers, which are directed against negatively charged species, and may also induce non-specific binding to aptamer-modified surfaces. To overcome these issues, PNA aptamers have been developed in recent years. Lee et al. have synthesized a PNA aptamer using the same base sequence known from a DNA aptamer directed against thrombin [75]. However, it remains uncertain whether this simple transition from DNA to PNA may be applicable for other aptamers, in which the folding of the aptamer may be influenced strongly by the negatively charged phosphate backbone. In this context, the direct selection of aptamers from a PNA library, which has already been used to develop PNA aptamers directed against dihydrofolate reductase [76], may prove to be a more versatile tool.

2.1.2 Porous Silicon-Based Biosensors

Over the past decade, a great number of PSi-based biosensors were reported in the literature [12, 22, 77]. With its most attractive property, the large surface area of up to 500 m^2/cm^3, PSi allows dense immobilization of different capture probes: enzymes [78], DNA fragments [79], antibodies [17], or any of the aforementioned emerging bioreceptors. Optical biosensors make up for the largest share in PSi-based assays and can be further categorized to two subgroups, based on the optical transduction mechanism, to include biosensors based on changes in photoluminescence [20, 80] and those based on changes in reflectivity [16, 81]. Upon infiltration of the target analyte molecules into the porous layer and their subsequent binding to the respective bioreceptors, which are immobilized onto the pore walls, a change in the RI of the thin film can be observed, as a modulation in the photoluminescence or as a wavelength shift in the reflectivity spectra, respectively. Other biosensors based on PSi are mainly electrochemical, relying on PSi semiconductor characteristics [82]. Examples include voltammetric

approaches [83] as well as amperometric [84], potentiometric characterization [85] and impedance-based sensors [86].

Another appealing characteristic of PSi transducers is the ability to easily tailor their nanostructure [11]: pore sizes to accommodate the interacting species, pore architecture, as well as surface chemistry, can be varied and tuned to meet the needs of any specific application.

2.1.2.1 Optical Biosensors

While the discovery of photoluminescence in PSi kick-started scientists' attention on the material, this emission of secondary photons upon light induced excitation has not established itself as a prevalent transduction methodology for biosensors development. This is in spite of the promising early studies by Starodub *et al.* [87], in which specific protein binding to the corresponding antibody was demonstrated by a decrease in the PSi photoluminescence. The complex photoluminescence mechanisms, associated with electron transfer and interfacial charging [11, 88, 89], pose a major challenge in the development of reliable biosensors [90]. Yet, a recent study demonstrated the quenching of a reporter-label inside the porous structure in a very interesting manner [91].

Fluorescent labels have also been used in assays to combine both a fluorescent signal and reflectivity spectra [92] or electrical impedance [93], respectively. Nonetheless, label-free methods are often preferred. The necessity of additional steps for labeling the capture probes or target, add cost and complexity to the assay and may interfere with target recognition. Other disadvantages of labeled approaches include the rapid photobleaching of fluorescent organic dyes conjugated to the biomolecules of interest, as well as challenges associated with quantitative analysis due to the fluorescence signal bias, as the number of fluorophores on each molecule cannot be precisely controlled [94].

For label-free PSi biosensors based on reflectance, two different signals can be monitored: the shift in the wavelength due to RI variation [26] and a change in the intensity of the reflected light due to scattering effects [95]. Different PSi

architectures e.g., single and double layers [96, 97], microcavities [78, 98], and photonic crystals [99, 100], have been used for the construction of reflectivity-based optical biosensors. The tunable architecture of PSi allows incorporating additional functionalities within the optical transducer, such as internal reference channels, and size exclusion features. Pacholski *et al.* [101] demonstrated a double layer biosensor, where a layer with smaller pore size serves for separation of biomolecules by size exclusion and also as an internal signal reference channel. This nanostructure allowed for simultaneous detection of a macromolecule (*bovine* serum albumin) and a small molecule (sucrose). This concept was later exploited by Bonanno and DeLouise [98] using a microcavity structure for filtering, enabling a label-free detection of rabbit IgG in complex media (such as whole blood samples).

We believe that a combination of the advantageous properties of the novel capture probes, described in the previous section, with PSi can bring forth a new generation of high performance biosensing concepts.

2.1.2.2 Electrochemical Biosensors

In electrochemical biosensors, the investigated reaction usually produces or consumes an electro-active moiety due to the activity of the recognition element in the device. An important characteristic of these biosensors is a direct spacial contact between the electrochemical transducer and the bioreceptor, enabling a measurement of either current (amperometric), potential or charge accumulation (potentiometric) between the electrodes [102, 103]. These changes in electrical properties of the biosensor system are induced by the occurrence of analyte attachment to the recognition element. A similar technique that does not require labeling, relies on the measurement of impedance spectra. Here, the observed change in the characteristic impedance spectrum of the sensor is solely based on the binding of the target molecule.

The dielectric constant, space-charge distribution and therefore conductance and capacitance of the PSi transducer are the signal-producing properties in different electrochemical sensing techniques. These depend on the Si-dopant, the

interacting surface area (hence layer thickness and porosity), as well as the number of available binding sites [12, 16, 77, 104]. In order to sensitively follow changes of these properties during target capture, a thorough characterization of the biosensor surface in respect to all relevant parameters is essential.

2.2 Aptamer-conjugated nanomaterials

The following part of the literature survey is based on and adapted from the review article “Aptamer-modified Nanomaterials: Principles and Applications” which appeared 2016 in a special issue “Biofunctionalization” of the journal BioNanoMaterials (see Apendix).

2.2.1 Introduction

Aptamers are synthetic short single stranded oligonucleotides composed of DNA or RNA. Based on their unique three-dimensional structure, aptamers exhibit specific binding to their corresponding target molecule, which can be a small molecule, a macromolecule, or a complete cell. Due to this specificity and their high affinity, aptamers can be used to substitute antibodies in different applications. In comparison to antibodies, aptamers offer several advantages which are mainly based on their *in-vitro* generation and their oligonucleotide nature: aptamers are selected in an *in-vitro* process termed systematic evolution of ligands by exponential enrichment (SELEX)[105]. Due to this animal-free process, aptamers can be selected to exhibit binding of the target under non-physiological conditions and the selection of aptamers is also possible for highly toxic or non-immunogenic molecules [106]. Once aptamers are selected and their sequence is revealed, they can be produced by chemical synthesis, a process not only resulting in high and consistent product quality, but also facilitating the precise introduction of labels or other modifications at defined positions within the aptamer sequence.
Aptamers have already been applied successfully e.g. for the detection of proteins and small molecules [107, 108], the purification of proteins [109-111] and depletion of small molecules [112], as well as in cell targeting and drug delivery [113-115]. In most of the developed aptamer-based methods, the aptamer has to be immobilized on a solid support, which might be a nano-structured surface. Aptamer binding to the

corresponding target molecule depends on the correct three-dimensional folding of the aptamer [116]. Therefore, it is crucial to immobilize aptamers without affecting their ability to fold into this binding-competent structure. Herein, we highlight factors that may interfere with correct folding of aptamers on solid supports and give general suggestions for the immobilization of functional aptamers.

2.2.2 Immobilization of Aptamers

As mentioned before, functional groups can be incorporated into the aptamer sequence and can subsequently be used for the immobilization of the aptamer on a solid support. For different types of materials, different modifications can be utilized, for example the introduction of terminal thiol groups is allowing for the straight-forward immobilization of aptamers on gold surfaces. Since the chemical synthesis enables precise control of the position of functional groups, the aptamer can be immobilized in a highly controlled orientation, *i.e.* via one of the termini of the aptamer. This controlled orientation facilitates high binding activity by avoiding a loss of functionality resulting from immobilization in random orientation. Nonetheless, several factors influencing aptamer folding have to be carefully considered during the immobilization of aptamers and in many cases, optimization of aptamer conjugation has to be performed to obtain functional aptamer-modified surfaces [117].

2.2.2.1 Effects of immobilization to aptamer performance

In order to immobilize aptamers in a functional manner, the conjugation process must not interfere with aptamer folding [118, 119]. Here, the user has to consider that during most of the selection processes, aptamers are present free in solution. Thus, aptamers can adopt their binding-competent folding while they are in solution but might lose their binding competence after immobilization mainly due to three different factors [117]:

First, the surface may directly interfere with aptamer folding. This is especially problematic when truncated versions of the aptamer sequence are used. To overcome steric hindrance caused by too close proximity of aptamer and surface, the use of spacer molecules can be recommended. Here, rather simple spacers

like polyethylenglycol moieties can be used and either be provided on the surface or fused between the aptamer sequence and the aptamer modification used for immobilization chemistry [120]. Also the elongation of the aptamer sequence, *e.g.* by introduction of several thymine bases, can provide additional space to allow for proper aptamer folding. One other factor that might interfere with correct folding of the aptamer is its orientation. Therefore, a screening of different aptamer orientations (3' terminal versus 5' terminal immobilization) may be useful to optimize aptamer performance.

The second feature of aptamers that has to be considered is their highly negative charge. Immobilizing aptamers on positively charged surfaces may result in complete unfolding of aptamers - which interact with the surface electrostatically. This can be prevented by capping of the surface [117].

Finally, the third factor influencing the folding of conjugated aptamers is the immobilization density. While generally, high immobilization densities are desired to guarantee high binding capacity for the aptamer target, too high aptamer density may prevent formation of the correct three-dimensional structure. Here, one has to consider that the immobilized aptamer must be provided with sufficient space to fold encountering no steric interference caused by neighboring aptamers. Moreover, the negative charge of aptamers can provoke electrostatic repulsion of neighboring aptamers, thereby forcing the aptamers to erect into a rather linear conformation not able to bind the target molecule. Therefore, the aptamer density, which can be easily influenced by the aptamer concentration applied during the immobilization process, has to be optimized experimentally.

2.2.2.2 Methods to investigate immobilized aptamers

As elaborated briefly in the previous subsection, several parameters including the aptamer density, aptamer orientation, surface charge, and the presence of spacers influence the performance of immobilized aptamers. Thus, methods for the investigation and optimization of aptamer conjugation are needed. Surface plasmon resonance (SPR) measurements allow for the quantitative investigation of the binding affinities of immobilized aptamers. SPR measurements are especially useful to reveal immobilization-induced reduction of aptamer affinity

when they are compared with immobilization-free methods for the determination of dissociation constants such as isothermal titration calorimetry (ITC) or microscale thermophoresis (MST) [121]. The comparison of dissociation constants obtained by different methods may uncover negative effects evoked by immobilization. Nonetheless, SPR measurements suffer from a limited degree of parallelization, thus require a large set of experiments to screen different immobilization conditions and additionally require rather large amounts of aptamer and target. Aptamer microarrays have shown to be a suitable alternative for the systematic investigation and optimization of aptamer immobilization [117, 120, 122]. Here, many different immobilization conditions (e.g. different aptamer orientations and immobilization densities, as well as different spacer moieties) can be screened in parallel on one single microarray. When aptamers are utilized as a receptor probe in a biosensing scheme, depending on the type and complexity, optimization of aptamer-conjugation directly within the biosensing platform may be the most suitable approach. Aptamer performance can be set in relation with the output signal and optimized accordingly.

2.2.3 Aptamer-modified nanostructured surfaces

Many different materials are accessible to a wide variety of surface chemistries for the attachment of biomolecules, such as aptamers. One reason for immobilization of aptamers to nanostructured surfaces specifically can be to increase the aptamer-density on the material due to higher surface area of such materials and thus increased area of interaction between aptamer and target analyte [123, 124]. Another main reason are the desirable intrinsic properties of nanostructured materials in combination with the binding characteristics of the immobilized aptamers which are opening possibilities for a variety of applications. In the following chapter, some of the main considerations when conjugating aptamers to nanomaterials are discussed.

2.2.3.1 Special considerations for aptamer immobilization on nanostructured surfaces

Nanomaterials and nanostructured materials of different kinds have recently gained increased attention for their application in concert with aptamer-receptors tethered to their surface [125-127]. Applications thereof can mainly be found in the field of biosensors and for the capture and purification of cellular targets (*e.g.* cancer cells, bacteria cells). However, in contrast to immobilization of oligonucleotides on planar surfaces, aptamer-conjugation to nanomaterials requires a number of additional considerations which are discussed in the following.

Increased immobilization-density of aptamers conjugated to a surface (*i.e.* by means of larger surface area in nanomaterials), also brings the risk of higher steric hindrance effects, commonly occurring [108, 128-130]. This phenomenon was recently studied by Daniel *et al.* on a planar gold-coated prism for surface plasmon resonance measurements with the thrombin-binding aptamer as model [131]. The researchers conducting the study consequently compared binding affinities of the thrombin to surface-immobilized aptamers and in a competitive mode when additional aptamers are present in solution. They varied grafting-density as well as concentrations of free aptamer and found that increasing grafting-density has a negative effect on the binding affinity (K_D) of the surface-conjugated aptamer, while it has no effect on the K_D of aptamer in solution. In order to ensure sufficient spacing and thus maintain aptamer-functionality, even on this planar surface, additional spacing between aptamer and surface had to be applied.

Nanoscale surface features (e.g. roughness, groves, pores) and spatial confinement of aptamers when immobilized on nanomaterials adds another dimension to the challenge of controlling steric hindrance effects. Even though close proximity of capture probe and target supported by nanostructure architecture (*e.g.* in a porous matrix) can enhance their interaction [132], high grafting-density and crowding within the nanostructures can hamper aptamer-functionality and accessibility of the target-binding sites [129, 130]. Herein, also electrostatic interactions can have a particular effect: high amounts of negative

charges accumulated by conjugated aptamers on a surface can prevent access of target analytes to the binding sites, which is enhanced by spatial confinement and limited free surface. Hence, besides reduced crowding, reduced negative charges can be a reason for better capture efficiency at lower aptamer immobilization densities [130, 133]. Furthermore, while enhanced surface roughness due to nanoscale features on the surface can improve interaction of the target (*i.e.* cells) with the substrate, it may also render it prone to unspecific adsorption (*e.g.* matrix components) [134, 135]. Thus, when nanomaterials are functionalized with aptamers, special attention has to be paid to careful optimization of spacer-arms and immobilization density as well as to orientation of the aptamer.

3. Research Aims

The general objective of this research was the development of a universal biosensor platform utilizing aptamers as capture probes for the real-time and label-free detection of the aptamer target analytes. The biosensor is based on functional porous silicon nanostructures, enabling simple optical monitoring of target capture onto or within the porous scaffold. In particular, the broad range of aptamer-target pairs, ranging from small molecules to whole cells, was to be demonstrated with model-systems, highlighting the great potential of these easily tunable aptamer-based biosensors.

Specific aims were:

1. Fabrication and characterization of nanostructured oxidized porous Si ($PSiO_2$) films.
2. Evaluation of different immobilization strategies for aptamers onto $PSiO_2$ and verification of successful conjugation.
3. Development of biosensing schemes for the specific and reversible detection of different aptamer targets (*i.e.* proteins and bacteria cells).
4. Characterization of obtained biosensors in terms of their performance.
5. Direct comparison between $PSiO_2$-based biosensors utilizing aptamers or antibodies as capture probes.

4. Experimental

4.1 Materials

Highly doped p-type Si wafers (0.0008 Ω cm resistivity, ⟨100⟩-oriented, B-doped) were purchased from Siltronix Corp. Aqueous HF (48%) and ethanol absolute were supplied by Merck. (3-Aminopropyl)triethoxysilane (APTES), *N*-(3-(dimethylamino)propyl)-*N*-ethylcarbodiimide hydrochloride (EDC), succinic acid, (3-Mercaptopropyl)trimethoxysilane (MPTMS), maleimide, ethylenediaminetetraacetic acid (EDTA), 5,5′-dithiobis-(2-nitrobenzoic acid) (DTNB, Ellman reagent), glutaraldehyde 25% solution (GA), sodium cyanoborohydride, ethyldiisopropylamine (EDIPA), culturing media components and all buffer salts were purchased from Sigma-Aldrich Chemicals. Buffers and media were all prepared with deionized water (18.2 MΩ cm) and filtered prior to use. Media were autoclaved prior to their use. Solvents (toluene, acetone) were purchased from Gadot Israel. All used aptamer and oligonucleotide sequences, including their original publication source and modification are listed in table 1. Oligonucleotides were manufactured by Integrated DNA Technologies.

Table 1. Aptamer and oligonucleotide sequences and their modification

Sequence name	Sequence	Modification
6H7 *(136)*	GCTATGGGTGGTCTGGTTGGGATTGGCCC CGGGAGCTGGC	5′-Amino
6H7 *(136)*	GCTATGGGTGGTCTGGTTGGGATTGGCCC CGGGAGCTGGC	5′-Amino, 3’-Cy5
6H7 *(136)*	GCTATGGGTGGTCTGGTTGGGATTGGCCC CGGGAGCTGGC	5′-Acrydite
Hemag1P *(137)*	AGCAGCACAGAGGTCAGATGTAGCCCTTC AACATAGTAATATCTCTGCATTCTGTGTGC CTATGCGTGCTACCGTGAA	5′-Acrydite

T10-Hemag1P	TTTTTTTTTTAGCAGCACAGAGGTCAGATG TAGCCCTTCAACATAGTAATATCTCTGCAT TCTGTGTGCCTATGCGTGCTACCGTGAA	5′-Acrydite
PAA *(138)*	ATACCAGCTTATTCAATTAGCAACATGAGG GGGATAGAGGGGGTGGGTTCTCTCGGCT	3'-Amino
DNA-Pool	NNNNNNNNNNNNNNNNNNNNNNNNNNNNN NNNNNNNNNNNN	5'-Amino

N – Random nucleotide, IDT machine mix. During synthesis all bases are allowed to react simultaneously.

6H7 was selected in 50 mM K_2HPO_4, 150 mM NaCl, and 0.05% Tween 20 (this buffer composition is subsequently abbreviated as 6H7-SB-T). As Tween 20 is known to be responsible for partial blocking of amino-modified surfaces, immobilization and washing steps, as well as renaturation of the aptamer were carried out in 6H7-SB-T without Tween 20 (abbreviated as 6H7-SB). For elution, 6H7-SB was supplemented with 500 mM Imidazole (referred to as 6H7-EB). Hemag1P was selected in 50 mM Tris-HCl (pH 7.4), 100 mM NaCl, 5 mM KCl, 1 mM $MgCl_2$ (this buffer composition is subsequently abbreviated as SB). TE-buffer was composed of 10 mM Tris-HCl (pH 8.0) and 1 mM EDTA. PBS-buffer was composed of 137 mM NaCl, 2.7 mM KCl, 10 mM Na_2HPO_4 and 1.8 mM KH_2PO_4 (pH 7.0). MES buffer was composed of 100 mM MES, pH 6. Tris washing buffer was composed of 50 mM Tris-HCl (pH 7.4). HEPES buffer was composed of 0.1 M HEPES (pH 7.4). PAA was selected in 20 mM Tris-HCl (pH 7.6), 100 mM NaCl, 5 mM KCl, 10 mM $MgCl_2$ and 1 mM $CaCl_2$ (subsequently referred to as BBKC). BBKC supplemented with 0.005% Tween 20 was used for sample dilutions (BBKCT). Mouse anti-his antibody was obtained from Enco. Streptavidin and biotinylated protein A were purchased from Sigma-Aldrich Chemicals. Proteins for biosensing experiments included casein, IgG from human serum, trypsin from porcine, recombinant Protein A from *Staphylococcus aureus* (all Sigma-Aldrich Chemicals), 6xhis T6 lipase from *Geobacillus stearothermophilus*, referred to as lipase, generously supplied by Prof. Ayelet Fishman. *Escherichia coli* strain JL-102

and K12 (generously supplied by Prof. Sima Yaron – Technion IIT) were cultured in Luria broth (LB) medium (10 g/L casein peptone, 10 g/L NaCl, 5 g/L yeast extract, all purchased from Sigma-Aldrich Chemicals). Bacteria strain *Lactobacillus acidophilus* ATCC 4356 was obtained from Gamidor Diagnostics and was cultured in MRS medium (CM0359, OXOID).

4.2 Preparation of PSi nanostructures

Si wafers (single side polished, ⟨100⟩ oriented and heavily doped, p-type) were electrochemically etched in a 3:1 (v/v) solution of aqueous HF (48%) and ethanol under conditions as outlined in table 2. Caution: HF is a highly corrosive liquid, and it has to be handled with extreme care and under secured working conditions! Si wafers with an exposed area of 1.33 cm^2 were contacted on the back side with a strip of aluminum foil and mounted in a Teflon etching cell; a platinum mesh was used as the counter electrode. After etching, the surface of the wafer was rinsed with ethanol several times and dried under dry nitrogen gas flow.

Table 2. Electrochemical etching conditions

Etching conditions	Constant current density [mA/cm^2]	Duration [s]
(1)	300	30
(2)	24	375
(3)	375	30

For condition (3), the etched PSi layer was dissolved in 0.1 M NaOH and rinsed and dried again before exposure to a mixture of HF:EtOH:H_2O 1:1:3 for 2 min. Then etching was repeated under the respective conditions. The freshly etched PSi samples were thermally oxidized in a tube furnace (Thermolyne) at 800 °C for 1 h in ambient air resulting in oxidized PSi ($PSiO_2$) scaffolds.

4.3 Characterization of PSi nanostructures

Spectroscopic ellipsometry. Spectroscopic ellipsometry measurements of the neat $PSiO_2$ scaffold were carried out with a Woolam M-2000 UI Ellipsometer. Measurements were fitted with an effective medium approximation.

Scanning Electron Microscopy. High-resolution scanning electron microscopy (HRSEM) of the $PSiO_2$ scaffolds were performed using a Carl Zeiss Ultra Plus HRSEM with an accelerating voltage of 1 keV.

Gravimetry. For gravimetric characterization, the silicon samples were weighed prior (m_1) and after etching and oxidation (m_2). Subsequently, the oxide layer was dissolved in a 3 : 1 (v/v) solution of aqueous HF (48%) and ethanol and the remnant porous layer was removed by incubation in 1 M aqueous KOH solution. The remaining sample was weighed again (m_3) and the porosity (P) was determined by the following equation: [11]

$$P(\%) = \frac{m_1 - m_2}{m_1 - m_3} \cdot 100$$

Spectroscopic liquid infiltration method. The SLIM method provides a nondestructive determination of thickness and porosity based on data from reflectance spectra obtained while different liquids infiltrate into the pores [11]. The differences between the spectra are attributed to the change in optical thickness as the medium in the pores changes, under the assumption that all void spaces are filled equally [139]. The optical thickness ($2nL$, where n is the average refractive index of the porous film and L is its thickness) of the $PSiO_2$ is determined from the interferometric reflectance spectrum of the porous film in air and while immersed in ethanol and acetone, having refractive indices of 1.359 and 1.357, respectively. The refractive index of the SiO_2 portion of the film is assumed to be 1.455. Values of $2nL$ are then fitted to a two-component Bruggeman model of refractive index for the composite-layer, which yields a unique solution for both the porosity and the thickness of the samples [139, 140].

4.4 Biofunctionalization

Conjugation of amino-modified oligonucleotides. The $PSiO_2$ samples were incubated with a solution of 42 mM APTES in toluene for 1 h. After the solution was removed, the surface was rinsed with toluene, ethanol, and acetone and dried under a nitrogen stream. The APTES-modified surface was then immersed in a freshly prepared solution of 100 mg of succinic acid in 4.7 mL of DMSO and 300

µL of 0.1 M $NaHCO_3$, pH 9.4 for 30 min. After removal of the solution, the surface was washed extensively with DMSO two times and with purified water.

A 52 mM EDC solution (dissolved in MES or respective selection buffer) was allowed to react for 1 h. Subsequently, 50 µL of 75 µM aptamer solution (diluted from aqueous stock with either MES or respective selection buffer) was applied to the sensor for 1 h, followed by thorough washing with 10 mL of 50 mM Tris buffer and a final folding of the aptamer by incubation in selection buffer for 30 min. Alternatively, after aptamer-immobilization, the surface was blocked by reaction with 100 mM aqueous ethanolamine solution for 30 min. In cases where aptamers were immobilized in MES, an additional washing step with boiling deionized water was performed before the final rinsing and incubation in selection buffer.

Conjugation of acrydite-modified oligonucleotides. For $PSiO_2$ biofunctionalization, the porous film was incubated in a solution of 20 mM MPTMS in toluene for 1 h. After removal of the solution, the surface was rinsed with toluene, ethanol and acetone (for 2 min each) and dried under a stream of nitrogen. The silanized sample was rinsed with TE buffer prior to 1 h incubation with the aptamer solutions (50 µL dissolved in TE) and successive rinsing with TE and PBS buffers. 2 mg mL^{-1} maleimide were dissolved in PBS, then applied to the aptamer-modified sample, and allowed to react for 1 h. Subsequently, the resulting biosensor was rinsed with PBS and finally incubated (30 min) in SB to allow proper aptamer folding.

Antibody-conjugation. For unoriented conjugation with antibodies, $PSiO_2$ samples were first incubated with a solution of 1% APTES and 1% EDIPA in water for 30 min. After removing the solution, the sample was rinsed with toluene, ethanol and acetone, then dried under a nitrogen stream. Afterwards, the surface was incubated in a 2% aqueous glutaraldehyde solution for 30 min. Subsequently, the sample was washed with water and again dried under a stream of nitrogen. In the next step, the sample was mounted in the same type of custom made Plexiglas flow cell and 50 µl of 100 µg/ml anti-his antibody solution were injected. The sample was first incubated for 1 h at room temperature and then stored over night

at 8 ˚C. Prior to the biosensing experiments, unbound antibodies were removed by thorough washing with PBS and residual reactive groups were capped by incubation of the sensor with 0.1 M aqueous solution of ethanolamine for 30 min.

For oriented immobilization of antibodies, silanization and modification with GA were performed as described above, followed by an incubation with 50 mM sodium cyanoborohydride in HEPES for 30 min. After washing with HEPES, $PSiO_2$ samples were placed in a humidity chamber and 100 µL of a freshly prepared streptavidin solution (100 µg/mL in PBS) are pipetted on the sample and incubated for 1 h. Thorough rinsing with PBS was performed before a repetition of the incubation in sodium cyanoborohydride as described before. Before incubation with biotinylated protein A (100 µL; 100 µg/mL in PBS) for 1 h in a humidity chamber, the streptavidin-surface was blocked with ethanolamine (as described previously). Finally, the samples were rinsed with PBS and incubated with the antibody (50 µL; 100 µg/mL in PBS; humidity chamber) for 1 h at room temperature and then overnight in the fridge. On the next day, repeated blocking of residual groups with ethanolamine after rinsing with PBS was performed, concluding the oriented immobilization of the anti-his-tag-antibodies.

4.5 Confirmation of aptamer-conjugation

Fourier transform infrared spectroscopy. Surface modifications were verified using attenuated total reflectance Fourier transform infrared (ATR-FTIR) spectroscopy. Spectra were recorded using a Thermo 6700 FTIR instrument equipped with a Smart iTR diamond ATR device.

Confocal laser scanning microscopy. For confocal microscopy studies, samples were scanned immediately after sensor functionalization, using a Cy5-labeled aptamer for immobilization. A LSM 700 confocal laser-scanning microscope (Carl Zeiss, Inc.) linked to a Zeiss inverted microscope equipped with a Zeiss X63 oil immersion objective was utilized. Laser lines of 405 nm were irradiated for the excitation of the $PSiO_2$ structure. Signals for $PSiO_2$ and the Cy5-labeled aptamers were obtained at 420 and 635 nm, respectively. For three-dimensional image projection of the porous structure, z-scans in 0.35 µm

increments were taken over a depth of ~10 µm and projected by using standard Carl Zeiss software (ZEN 2009).

Ellmann assay. Silanization of the samples with MPTMS was characterized by the Ellmann assay for free thiol groups [(141)]. Herein, the silanized $PSiO_2$ samples were incubated for 15 min in 2.5 mL Ellman buffer (100 mM sodium phosphate, pH 8.0, 1 mM EDTA) supplemented with 50 µl Ellman solution (4 mg mL^{-1} of DNTB in Ellman buffer). The supernatant was collected after the reaction and its absorbance was measured at 412 nm using a Varioskan flash plate reader (Thermo Scientific).

4.6 Sample preparation and bacteria culturing

Culturing for whole bacteria samples. *L. acidophilus* was grown in MRS medium (CM0359, OXOID) under 5% CO_2 atmosphere at 37 °C. Bacterial growth was monitored by optical density (OD) measurements at 600 nm in order to determine the logarithmic phase of growth. To correlate OD_{600} values with bacteria cell concentration, a standard plate-counting technique [(142)] was performed. Briefly, bacteria were grown to the mid-logarithmic phase (OD_{600} of 0.44) and plated on MRS agar plates in replicates. Plates were then incubated for 48 h in 5% CO_2 atmosphere at 37 °C and the formed colonies were counted. Based on counting, an OD_{600} value of 0.44 was correlated to a cell concentration of 3.5×10^7 CFU mL^{-1}.

E. coli K12 was cultivated in Luria–Bertani (LB) medium (composed of 5 g of NaCl, 5 g of yeast extract and 10 g of tryptone in 1 L of deionized water) at 37 °C while shaking. Bacterial growth was monitored by OD measurements and bacteria concentration was calculated from OD_{600} value according to the correlation of 1 $OD_{600} = 10^8$ cells per mL [(95)].

For biosensing experiments, *L. acidophilus* was grown overnight in MRS medium and a subculture was grown the next morning until a cell density corresponding to an OD_{600} value of 0.44. *E. coli* K12 was grown overnight in LB medium and a subculture was grown the next morning until an OD_{600} value of 0.5. Samples of the cultures (1 mL) were spun down in a standard lab centrifuge (10 min at 5000*g*),

replacing the supernatant by 1 mL SB. Following the re-suspension of the cell pellet, the centrifugation and buffer replacement were repeated two more times before the final cell suspension was either further diluted or used directly for biosensing experiments.

For the biosensing experiments with mixed bacterial populations, upon the final centrifugation and supernatant replacement, a bacteria pellet was re-suspended in 1 mL SB, after which, another bacteria pellet was introduced to form a mixed culture suspension.

For biosensing experiments with non-viable bacteria, bacteria suspensions were heat-treated as suggested by Bunthof *et al.* [143]. Bacterial suspensions were placed on a dry heating block for 15 min at 70 °C and then stored on ice until further use.

Preparation of lysates. A shaking flask with 20 mL of sterile LB medium was inoculated with 100 µL of a freeze culture of *E. coli* JL-102 (free of plasmids) and cultured overnight, shaking at 37 °C. The resulting culture was used for biosensing experiments to mimic a biologically relevant complex fluid.

A volume of 2 mL of bacteria culture was spun down in a standard lab centrifuge, replacing the supernatant by 1 mL of PBS selection buffer. Following the resuspension, the culture was ultrasonicated at 4 °C (Labsonic M, Sartorius Stedim Biotech). Following removal of cell debris, the suspension was centrifuged again and the supernatant was taken to a fresh tube and further used as the bacterial lysate.

4.7 Biosensing experiments

4.7.1 Protein biosensing

Interferometric reflectance spectra of the samples were collected using an Ocean Optics charge-coupled device (CCD) USB 4000 spectrometer fitted with a microscope objective lens coupled to a bifurcated fiber-optic cable. A tungsten light source was focused onto the center of the sample surface with a spot size of

approximately 1–2 mm^2. Reflectivity data were continuously recorded every 30 s in the wavelength range of 400–1000 nm with a spectral acquisition time of 100 ms. Both illumination of the surface and detection of the reflected light were performed along an axis coincident with the surface normal. All the optical experiments were conducted in a fixed cell to ensure that the sample reflectivity is measured at the same spot during all measurements. Spectra were collected using a CCD spectrometer and analyzed by applying fast Fourier transformation (FFT), as previously described by Massad-Ivanir *et al.* [(95)]. Figure 3.1 depicts representative reflectivity spectra of the $PSiO_2$ nanostructure before and after binding of the target molecules, as well as the fast Fourier transformation (FFT) of the reflectivity spectra, leading to a single peak, whose position (corresponds to the value of 2 nL, EOT) was monitored. In the present work, the data is presented as relative EOT and defined as:

$$\frac{EOT}{EOT_0} = \left(\frac{EOT_{readout}}{EOT_{at\ baseline}}\right)$$

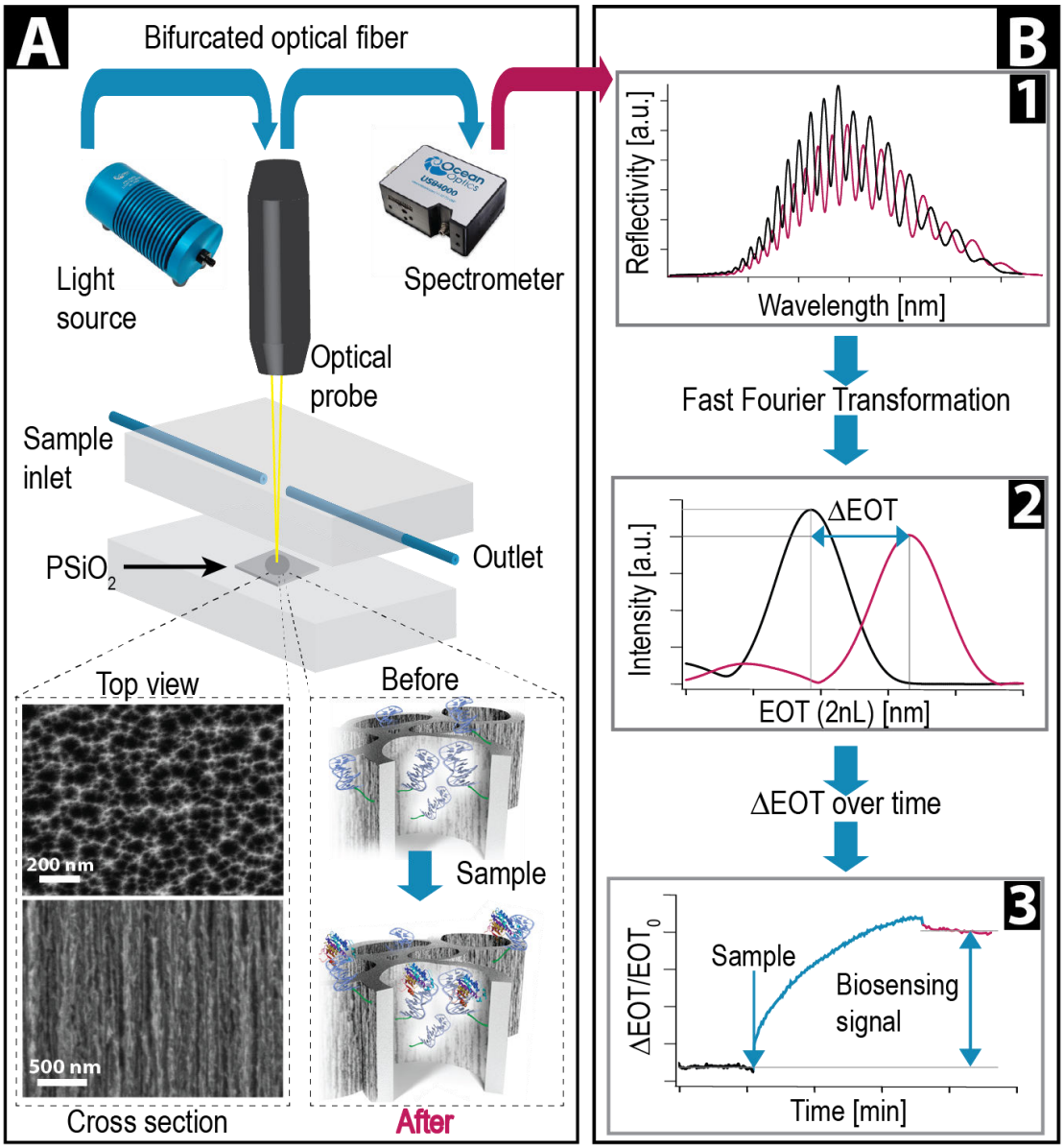

Figure 4.1. Schematic illustration of the experimental setup depicting instrumentation and flow-cell configuration. The lower panels show HRSEM micrographs of porous silicon nanostructures (left) and schematics of aptamer-functionalized $PSiO_2$ before and after target capture (right). B: RIFTS signal processing steps. Reflectivity spectra were recorded (1) and a fast Fourier transformation was applied (2). The signal was then expressed as the relative change in EOT over the course of the experiment (3). The final biosensing result was extracted as the relative change in EOT before and after exposure of the aptamer-functionalized $PSiO_2$ scaffold to the sample solution (3).

Please note that the term EOT_0 refers to the averaged EOT obtained during baseline establishment at the beginning of the optical experiments. In a typical optical biosensing experiment, a freshly prepared aptamer-functionalized $PSiO_2$ sample was incubated with selection buffer for 30 min to allow proper folding of the aptamer and to acquire a baseline signal. Thereafter, the protein sample was introduced and allowed to incubate with the biosensor for 1 h. After removal of the sample and thorough flushing of the cell with selection buffer, the biosensor was incubated for 30 min in selection buffer. Note that during buffer exchange and rinsing steps, optical measurements were shortly paused to allow a thorough washing of the biosensor and the flow cell. For elution of the protein from the biosensor surface, following the previously described protocol, the biosensor was incubated with 6H7-EB for 15 min and then rinsed and incubated with 6H7-SB anew (30 min).

4.7.2 Bacteria biosensing

The biosensors were placed in fixed flow cell apparatus and their interferometric reflectance spectra were collected using an Ocean Optics charge-coupled device (CCD) USB 4000 spectrometer fitted with a microscope objective lens coupled to a bifurcated fiber-optic cable. A tungsten light source was focused onto the center of the flow cell with a spot size of approximately 1–2 mm^2. Reflectivity data were continuously recorded every minute in the wavelength range of 400–1000 nm, with a spectral acquisition time of 100 ms. As previous work on probiotic bacteria indicated their sensitivity to light [144, 145], a shutter was used to block the light from reaching the sample surface between the measurements. This is to exclude the possible effect of light on bacteria growth, behavior, and interaction with the aptamer-conjugated surface. Both illumination of the surface and detection of the reflected light were performed along an axis coincident with the surface normal. The collected spectra were analyzed by applying fast Fourier transformation (FFT), as previously described by Massad-Ivanir *et al.* [95] with the FFT intensity changes expressed as percentages and calculated using the following equation:

$$Intensity\ decrease\ (\%) = \frac{I_1 - I_2}{I_1} \cdot 100\%$$

where I_1 is the average intensity during the baseline establishment and I_2 is the average intensity during the incubation of the sensor with SB after exposure to the bacteria and the respective subsequent washing step.

In a typical optical biosensing experiment, a freshly prepared aptamer-functionalized $PSiO_2$ sample was incubated with SB for 30 min to allow proper folding of the aptamer and to acquire a baseline signal. Thereafter, the respective bacteria suspensions (in SB) were introduced and allowed to incubate with the biosensor for 20 min. After removal of the bacteria suspension and thorough flushing of the cell with SB, the sample was incubated for 10 min in SB. Optical measurements were recorded every 1 min throughout the experiment. Note that during buffer exchange and rinsing steps, optical measurements were shortly paused to allow a thorough washing of the biosensor and the flow cell.

To confirm the bacteria capture on the biosensor surface, the biosensor was removed from the flow cell and immediately examined under a light microscope (ZEISS upright). Images were taken using the microscope camera (Axio Cam MRc, ZEISS).

5. Results

This result section consists of the three original articles that were published (or are currently under review) in peer-reviewed journals.

5.1 Label-free optical biosensors based on aptamer-functionalized porous silicon scaffolds

This work presents the first optical porous silicon biosensor employing an aptamer-capture probe. It provides the proof-of-concept for a simple label-free and reagentless biosensing platform that demonstrates reliability and robustness as well as its regenerability. Herein, we describe the fabrication and characterization of aptamer-conjugated $PSiO_2$ biosensors in detail, where a previously characterized his-tag binding aptamer (6H7) is used as model system. Exposure of the aptamer-functionalized $PSiO_2$ to the target proteins as well as to complex fluids results in robust and well-defined changes in the optical interference spectrum ascribed to specific aptamer-protein binding events occurring within the nanoscale pores monitored in real time. Specifically, we highlight the performance of the biosensor in highly relevant biological fluids, such as bacteria lysates, with an abundance of nonspecific proteins. The biosensors show exceptional stability and moreover can be easily regenerated by a short rinsing step for multiple biosensing analyses, emphasizing again the advantages of aptamers as recognition elements in this biosensing platform. In the biosensor working range (0-56 µM), we show a linear correlation of the biosensor response and target-protein concentration and the very low signals from unspecific adsorption of non-target molecules. This proof-of-concept study demonstrates the possibility to design highly stable and specific label-free optical $PSiO_2$ biosensors, employing aptamers as capture probes. Such biosensors hold immense potential for application in detection of a broad range of targets, in a simple yet reliable manner.

analytical chemistry

Article

pubs.acs.org/ac

Label-Free Optical Biosensors Based on Aptamer-Functionalized Porous Silicon Scaffolds

Katharina Urmann,[†,‡] Johanna-Gabriela Walter,[†] Thomas Scheper,[†] and Ester Segal*[,‡]

[†]Institute of Technical Chemistry, Leibniz University of Hannover, Callinstrasse 5, 30167 Hannover, Germany

[‡]Department of Biotechnology and Food Engineering, Technion Israel Institute of Technology, Technion City, 32000 Haifa, Israel

Supporting Information

ABSTRACT: A proof-of-concept for a label-free and reagentless optical biosensing platform based on nanostructured porous silicon (PSi) and aptamers is presented in this work. Aptamers are oligonucleotides (single-stranded DNA or RNA) that can bind their targets with high affinity and specificity, making them excellent recognition elements for biosensor design. Here we describe the fabrication and characterization of aptamer-conjugated PSi biosensors, where a previously characterized his-tag binding aptamer (6H7) is used as model system. Exposure of the aptamer-functionalized PSi to the target proteins as well as to complex fluids (i.e., bacteria lysates containing target proteins) results in robust and well-defined changes in the PSi optical interference spectrum, ascribed to specific aptamer-protein binding events occurring within the nanoscale pores, monitored in real time. The biosensors show exceptional stability and can be easily regenerated by a short rinsing step for multiple biosensing analyses. This proof-of-concept study demonstrates the possibility of designing highly stable and specific label-free optical PSi biosensors, employing aptamers as capture probes, holding immense potential for application in detection of a broad range of targets, in a simple yet reliable manner.

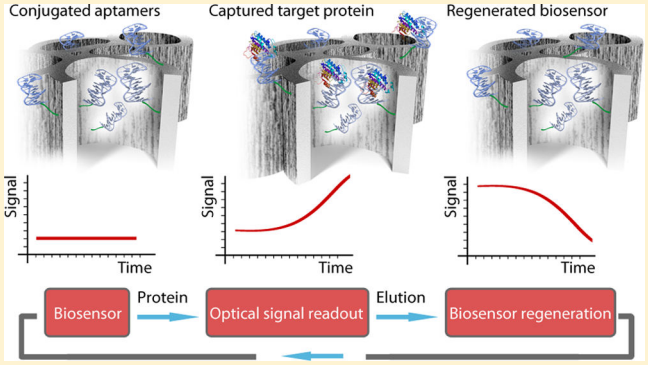

Since the establishment in 1990 of an *in vitro* selection process for short, single-stranded oligonucleotides with a desired target affinity, these molecules are referred to as aptamers[1,2] and have emerged as promising capture probes for biosensing applications. Aptamers can be designed to capture virtually any desired target, e.g., whole cells, proteins, and small molecules,[3] by using the Systematic Evolution of Ligands by Exponential Enrichment (SELEX) process for their development. When used as receptor molecules, these synthetic oligonucleotides present significant advantages compared to antibodies, while easily accessible in high and constant quality.[3] Aptamers exhibit exceptional stability, their small size facilitates high surface coverage, and their ability for reversible folding enables the design of sensitive yet regenerable biosensing schemes.[3,4] Aptamers were already selected for many different targets including ions, small organic molecules (dyes, amino acids, ATP, vitamins, antibiotics, several drugs), peptides, proteins, cells, or microorganisms and the catalogue is steadily growing.[3,5,6] In addition to this diversity in targets, aptamers can be modified during their synthesis either on the 5′ or 3′ terminus of the oligonucleotide to introduce functional groups, which allow their facile immobilization onto a variety of surfaces.[7]

Over the past decade, aptamer-based biosensors, also called aptasensors, have been extensively developed, presenting an immense potential to replace traditional antibody-based assays, due to their high sensitivity and stability.[4,5,8−11] Additionally, their unique selection process opens up the possibility to target substances that do not have alternative specific receptors available, emphasizing their suitability as a receptor element for biosensing.

Various aptasensor schemes are reported in the literature, ranging from label-dependent methods such as electrochemistry, fluorescence, and chemiluminescence[12−14] to label-free optical methods, which are mainly limited to surface plasmon resonance (SPR).[15−19] SPR is inarguably a well-established and highly sensitive method; nevertheless, a particular challenge in SPR application is the limited sensor area, leading to a diminished capacity.[20] In addition, SPR-based transducers are particularly sensitive to ambient temperature drift and, for maximal performance, this parameter must be controlled, making the instrumentation complex and expensive.[21] Thus, SPR analysis requires highly skilled-personnel and is mostly confined to a laboratory setting.

In recent years, porous silicon (PSi) has emerged as a promising nanomaterial for the design of different optical label-free biosensing platforms, owing to its large surface area, versatile chemistry, and straightforward fabrication.[22−35] PSi-

Received: December 2, 2014
Accepted: December 30, 2014
Published: December 30, 2014

DOI: 10.1021/ac504487g
Anal. Chem. 2015, 87, 1999−2006

based interferometers, in which a change in refractive index of the solution contained within the porous nanostructure can be measured, are most common and the technique is often referred to as reflective interferometric Fourier transform spectroscopy (RIFTS).[30,33,36,37] Briefly, the reflectivity spectrum of a PSi sensor is comprised of a series of Fabry−Pérot interference fringes resulting from reflections at the top and bottom interfaces of the porous thin film. The position of the peak along the *x*-axis in the RIFTS spectrum corresponds to the effective optical thickness (EOT), which equals $2nL$ (where n is the effective refractive index and L is the physical thickness of the porous layer). Changes in n or L lead to proportional shifts in the reflectivity spectra and therefore in the EOT value.[38] Thus, the biosensing concept relies on monitoring changes in the EOT of PSi with a conjugated capture probe as a response to target binding. So far, PSi-based biosensors have employed only conventional receptor molecules, such as antibodies or enzymes.[33,39−42]

Herein, we describe, for the first time, the design and characterization of a label-free optical PSi-based aptasensor. An oxidized porous silicon nanostructure (Fabry-Pérot thin film), used as the optical transducer, is conjugated with a well-characterized his-tag binding aptamer (6H7).[43−45] This aptamer system has been previously used for protein purification processes and was thoroughly investigated in microarray applications as described by Walter et al.[46] We confirm successful immobilization of the aptamer throughout the oxidized PSi ($PSiO_2$) scaffold by attenuated total reflectance Fourier transform-infrared (ATR-FT-IR) spectroscopy and confocal microscopy. Aptamer-protein binding events, occurring within the nanoscale pores, are monitored in real time, confirming affinity of the aptamer-immobilized $PSiO_2$ toward the target proteins in the micromolar range as anticipated by this specific aptamer binding characteristics.[43] The high selectivity and specificity of this biosensing scheme is demonstrated also in complex biological fluids such as bacteria lysates. Furthermore, as the aptamer is engineered to withstand repeated cycles of denaturation and renaturation, the biosensor exhibits outstanding stability and reusability for numerous subsequent experiments.

EXPERIMENTAL SECTION

Materials. Highly doped p-type Si wafers (0.0008 Ω cm resistivity, ⟨100⟩-oriented, B-doped) were purchased from Siltronix Corp. Aqueous HF (48%) and ethanol absolute were supplied by Merck. (3-Aminopropyl)triethoxysilane (APTES), *N*-(3-(dimethylamino)propyl)-*N*-ethylcarbodiimide hydrochloride (EDC), succinic acid, and all buffer salts were purchased from Sigma-Aldrich Chemicals. All solutions were prepared with Milli-Q water (18.2 MΩ cm) and filtered prior to use. Anti-His Tag aptamer 6H7 (5′-GCT ATG GGT GGT CTG GTT GGG ATT GGC CCC GGG AGC TGG C-3′) sequence was taken from the U.S. patent specification U.S. 7329742 (Doyle and Murphy, 2008). 6H7 was selected in 50 mM K_2HPO_4, 150 mM NaCl, and 0.05% Tween 20 (this buffer composition is subsequently abbreviated as PBS-T). As Tween 20 is known to be responsible for partial blocking of amino-modified surfaces, immobilization and washing steps, as well as renaturation of the aptamer were carried out in PBS-T without Tween 20 (abbreviated as PBS). Aptamers were purchased with a 5′-amino modification from BioSpring. Additional aptamers with 5′-amino modification as well as 3′-Cy5 fluorescent dye for laser confocal microscopy imaging were purchased from Integrated DNA Technologies. Proteins for biosensing experiments included casein, IgG (Sigma-Aldrich Chemicals) and 6xhis T6 lipase from *Geobacillus stearothermophilus*, referred to as lipase, generously supplied by Prof. Ayelet Fishman. As a negative control, *Escherichia coli* strain JL-102 was cultured in Luria broth (LB) medium (10 g/L casein peptone, 10 g/L NaCl, 5 g/L yeast extract, all purchased from Sigma-Aldrich Chemicals).

Preparation of Bacteria and Their Lysates. A shaking flask with 20 mL of sterile LB medium was inoculated with 100 μL of a freeze culture of *E. coli* JL-102 (free of plasmids) and cultured overnight, shaking at 37 °C. The resulting culture was used for biosensing experiments to mimic a biologically relevant complex fluid.

A volume of 2 mL of bacteria culture was spun down in a standard lab centrifuge, replacing the supernatant by 1 mL of PBS selection buffer. Following the resuspension, the culture was ultrasonicated at 4 °C (Labsonic M, Sartorius Stedim Biotech). Following removal of cell debris, the suspension was centrifuged again and the supernatant was taken to a fresh tube and further used as the bacteria lysate.

Preparation of Oxidized PSi. Si wafers (single side polished, ⟨100⟩ oriented and heavily doped, p-type) were electrochemically etched in a 3:1 (v/v) solution of aqueous HF (48%) and ethanol for 30 s at a constant current density of 300 mA/cm^2. Caution: HF is a highly corrosive liquid, and it has to be handled with extreme care and under secured working conditions! Si wafers with an exposed area of 1.33 cm^2 were contacted on the back side with a strip of aluminum foil and mounted in a Teflon etching cell; a Platinum mesh was used as the counter electrode. After etching, the surface of the wafer was rinsed with ethanol several times and dried under dry nitrogen gas flow. The freshly etched PSi samples were thermally oxidized in a tube furnace (Thermolyne) at 800 °C for 1 h in ambient air resulting in oxidized PSi ($PSiO_2$) scaffolds.

Scanning Electron Microscopy. High-resolution scanning electron microscopy (HRSEM) of the neat $PSiO_2$ scaffold was performed using a Carl Zeiss Ultra Plus HRSEM with an accelerating voltage of 1 keV.

Characterization of $PSiO_2$ Films. The structural properties, i.e., thickness and porosity, of the $PSiO_2$ layers were characterized by HRSEM, gravimetry (for porosity), and SLIM (spectroscopic liquid infiltration method) methods, as we previously described.[47] Detailed description regarding the application of gravimetry and SLIM for the characterization of PSi nanomaterials can be found elsewhere.[48] Spectroscopic ellipsometry measurements of the neat $PSiO_2$ scaffold were carried out with a Woolam M-2000 UI Ellipsometer. Measurements were fitted with an effective medium approximation.

Functionalization of $PSiO_2$ Films. The $PSiO_2$ samples were incubated with a solution of 42 mM APTES in toluene for 1 h. After the solution was removed, the surface was rinsed with toluene, ethanol, and acetone and dried under a nitrogen stream. The APTES-modified surface was then immersed in a freshly prepared solution of 100 mg of succinic acid in 4.7 mL of DMSO and 300 μL of 0.1 M $NaHCO_3$, pH 9.4 for 30 min. After removal of the solution, the surface was washed extensively with DMSO two times and with purified water.

In order to follow the reflectivity changes upon the surface modifications, the sample was mounted in a custom-made Plexiglas flow cell and fixed underneath the light source. An O-

DOI: 10.1021/ac504487g
Anal. Chem. 2015, 87, 1999−2006

ring inside the cell limits the modified area and an in- and outlet allow the injection of solutions for the different reaction steps (see Table 1). Table 1 summarizes the detailed procedure

Table 1. Synthetic Steps Followed for Aptamer Immobilization onto $PSiO_2$ and Details of Protein Biosensing Experiment

reaction step	details	volume	incubation time
washing/wetting	PBS	10 mL	*a*
EDC activation	52 mM EDC in PBS	1 mL	1 h
aptamer immobilization	75 μM aptamer in PBS	50 μL	1 h
washing	50 mM Tris buffer	10 mL	*a*
elution	PBS-T, 1 M imidazole	10 mL	30 min
aptamer folding	PBS	10 mL	30 min
sensing	protein diluted in PBS-T	50 μL	1 h
washing	PBS	10 mL	*a*
readout	PBS	10 mL	30 min
elution	PBS-T, 1 M imidazole	10 mL	30 min
regeneration	PBS	10 mL	30 min

[a]Sensor is gently rinsed in a time interval of 2 min.

followed for the biosensor preparation. Briefly, a 52 mM EDC solution was injected to the flow cell and allowed to react for 1 h. Subsequently, 50 μL of 75 μM aptamer solution was applied to the sensor for 1 h, followed by thorough washing with 10 mL of 50 mM Tris buffer and a final folding of the aptamer by incubation in PBS for 30 min.

Measurement of Interferometric Reflectance Spectra. Interferometric reflectance spectra of the samples were collected using an Ocean Optics charge-coupled device (CCD) USB 4000 spectrometer fitted with a microscope objective lens coupled to a bifurcated fiber-optic cable. A tungsten light source was focused onto the center of the sample surface with a spot size of approximately 1−2 mm^2. Reflectivity data were continuously recorded every 15 s in the wavelength range of 400−1000 nm, with a spectral acquisition time of 100 ms. Both, illumination of the surface and detection of the reflected light were performed along an axis coincident with the surface normal. All the optical experiments were conducted in a fixed cell to ensure that the sample reflectivity is measured at the same spot during all measurements. Spectra were collected using a CCD spectrometer and analyzed by applying fast Fourier transformation (FFT), as previously described by Massad-Ivanir et al.[49] Figure S-1 (see the Supporting Information) depicts representative reflectivity spectra of the $PSiO_2$ nanostructure before and after binding of the target molecules, as well as the fast Fourier transformation (FFT) of the reflectivity spectra, leading to a single peak, whose position (corresponds to the value of 2 nL, EOT) was monitored. In the present work, the data is presented as relative EOT and defined as

$$\mathrm{EOT/EOT_0} = \left(\frac{\mathrm{EOT_{readout}}}{\mathrm{EOT_{at\ baseline}}}\right)$$

Please note that the term EOT_0 refers to the averaged EOT obtained during baseline establishment at the beginning of the optical experiments.

Infrared Spectroscopy. Surface modification was verified using attenuated total reflectance Fourier transform-infrared (ATR-FT-IR) spectroscopy. Spectra were recorded using a Thermo 6700 FT-IR instrument equipped with a Smart iTR diamond ATR device.

Protein Biosensing. Biosensing experiments were carried out in a flow cell configuration, described for the functionaliza-

Scheme 1. Surface Modification and Immobilization Steps[a]

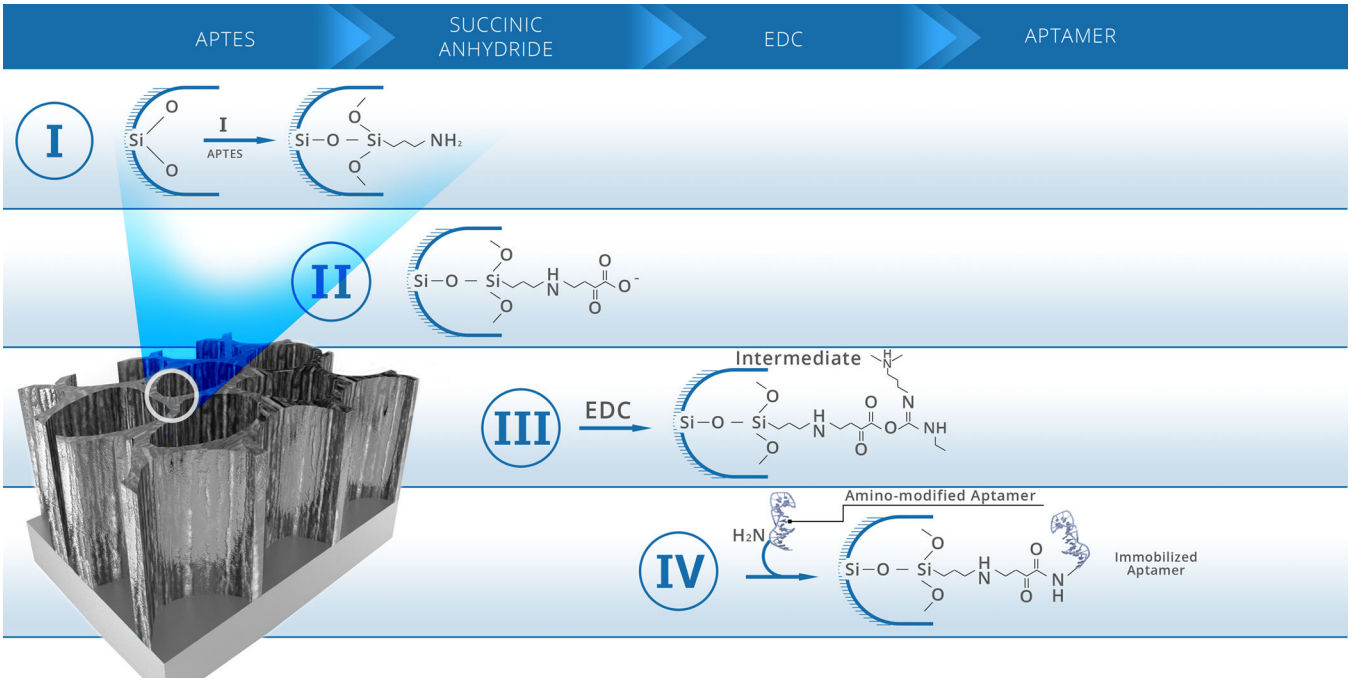

[a](I) Silanization of the $PSiO_2$ surface. (II) Carboxylation and (III) EDC-induced formation of the active intermediate. (IV) Covalent binding of the amino-modified aptamer.

DOI: 10.1021/ac504487g
Anal. Chem. 2015, 87, 1999−2006

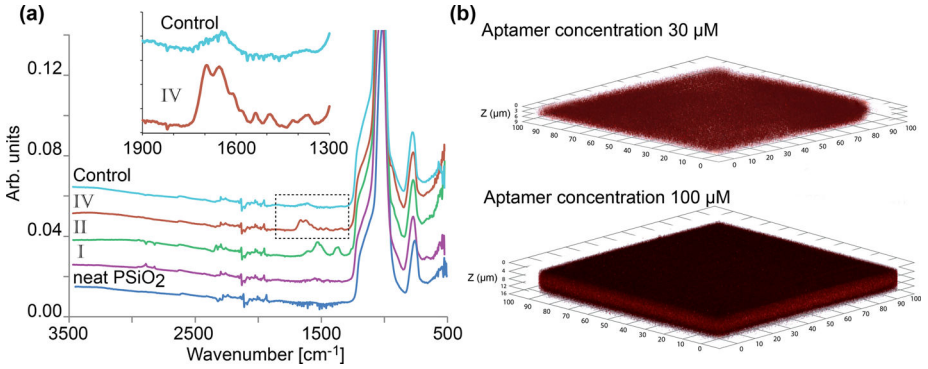

Figure 1. (a) ATR-FT-IR of the different functionalization steps (illustrated in Scheme 1) followed for the preparation of aptamer-immobilized $PSiO_2$: (I) APTES-modified surface, (II) succinic anhydride-modified surface, and (IV) 6H7-modified surface. As a control, neat $PSiO_2$ was incubated with the 6H7 aptamer solution under similar conditions and washed with PBS. (b) Confocal microscope z-stack images of $PSiO_2$ sensors conjugated with different aptamer-concentrations (30 and 100 μm of Cy5-labeled 6H7 aptamer).

tion of $PSiO_2$ scaffolds, immediately following the preparation of the biosensor. The aptamer-functionalized $PSiO_2$ samples were incubated with the protein solution (in PBS-T) for 1 h. After removal of the protein solution and flushing the cell with PBS, the sample was incubated for 30 min in PBS (see Table 1). For the regeneration of the biosensor, the protein was eluted with 1 M imidazole, followed by the renaturation of aptamers in PBS (see Table 1). Optical measurements were recorded every 15 s throughout the whole experiment. Please note that during buffer exchange and rinsing steps, EOT measurements were shortly paused to allow for a thorough washing of the biosensor and the flow cell.

Confocal Laser Microscopy. For confocal microscopy studies, samples were scanned immediately after sensor functionalization, using a Cy5-labeled aptamer for immobilization. A LSM 700 confocal laser-scanning microscope (Carl Zeiss, Inc.) linked to a Zeiss inverted microscope equipped with a Zeiss X63 oil immersion objective was utilized. Laser lines of 405 nm were irradiated for the excitation of the $PSiO_2$ structure. Signals for $PSiO_2$ and the Cy5-labeled aptamers were obtained at 420 and 635 nm, respectively. For three-dimensional image projection of the porous structure, z-scans in 0.35 μm increments were taken over a depth of ~10 μm and projected by using standard Carl Zeiss software (ZEN 2009).

RESULTS AND DISCUSSION

Functionalization of $PSiO_2$ Films with Amino-Modified Aptamers. The PSi films were prepared from a highly doped p-type crystalline Si wafer by an electrochemical etching process at 300 mA/cm^2 for 30 s. The resulting freshly etched PSi film was then thermally oxidized at 800 °C to create a hydrophilic $PSiO_2$ scaffold.[38] The average values for scaffold characterization are summarized in Table S-1 (see the Supporting Information). Briefly, the resulting porous layers are around 5400 nm thick and the calculated porosity is approximately 80%. The SLIM results are in excellent agreement with spectroscopic ellipsometry experiments, in which fitting with the effective medium approximation results in a calculated layer thickness of 5000 nm and porosity of 79%. HRSEM studies (top-view and cross-section) of the films reveal their highly porous nature and depict interconnecting cylindrical pores ranging in diameter from 50 to 80 nm (see Figure S-2, Supporting Information). It should be noted that the resulting nanostructure is characterized by a high specific surface area and porous volume over a small working area (980 cm^2 STP cm^{-2} and 3.24 × 10^{-4} cm^3 STP cm^{-2},[50] respectively, with STP being standard temperature and pressure), facilitating an effective large volume for monitoring reactions/events occurring within the pores.

The synthetic approach for grafting the amino-modified aptamers onto the $PSiO_2$ surfaces is based on well-established silanization and coupling chemistries, which we have previously employed for conjugation of single-stranded DNA onto PSi nanostructures.[39] The detailed synthesis scheme is outlined in Scheme 1. First, the $PSiO_2$ film was treated with APTES in toluene, resulting in an amino-silanized surface (Scheme 1,I). In the following step, the amino groups were capped by succinic anhydride, forming a carboxylated surface (Scheme 1,II). Finally, the amine-terminated oligonucleotide was conjugated via EDC coupling chemistry (Scheme 1,III,IV), resulting in an aptamer-functionalized $PSiO_2$.

To confirm the immobilization of the aptamer to the $PSiO_2$ scaffold, samples were characterized using ATR-FT-IR spectroscopy. Figure 1a shows the ATR-FT-IR spectra of the porous film following the different modification steps. The spectrum of the neat $PSiO_2$ surface shows a typical $-(O_ySiH_x)$ vibration mode at 801 cm^{-1} and a peak at 1039 cm^{-1} that is related to the Si−O−Si stretching mode. The APTES-modified surface spectrum (Figure 1a,I) depicts two additional peaks; the 1641 cm^{-1} is ascribed to the bending of primary amine and the 1555 cm^{-1} to the bending of protonated amines.[51] Following the modification with succinic anhydride, the spectrum shows two strong bands near 1400 and 1570 cm^{-1} for the symmetric and the antisymmetric stretching vibration, respectively, indicative of the deprotonated carboxylate group (Figure 1a,II).[52,53] Characteristic DNA bands, around 1688 cm^{-1} (carbonyl), as well as around 1230 cm^{-1} (phosphate groups), are observed after conjugation of the aptamer (Figure 1a,IV). As a control, the neat $PSiO_2$ was incubated with the 6H7 aptamer solution under similar conditions, followed for aptamer conjugation, and washed with PBS prior to FT-IR analysis. The resulting spectrum (Figure 1a, control trace) shows minor changes in comparison to the neat $PSiO_2$, which may be ascribed to electrostatic interaction of the negatively charged-aptamer and highly porous film.[3,54]

Immobilization onto the PSi nanostructure was also validated by confocal laser microscopy imaging using an aptamer sequence with a Cy5-dye conjugated to its 3′ end. Figure 1b depicts z-stack images of $PSiO_2$ films with two different aptamer concentrations (30 and 100 μM). These images reveal

DOI: 10.1021/ac504487g
Anal. Chem. 2015, 87, 1999−2006

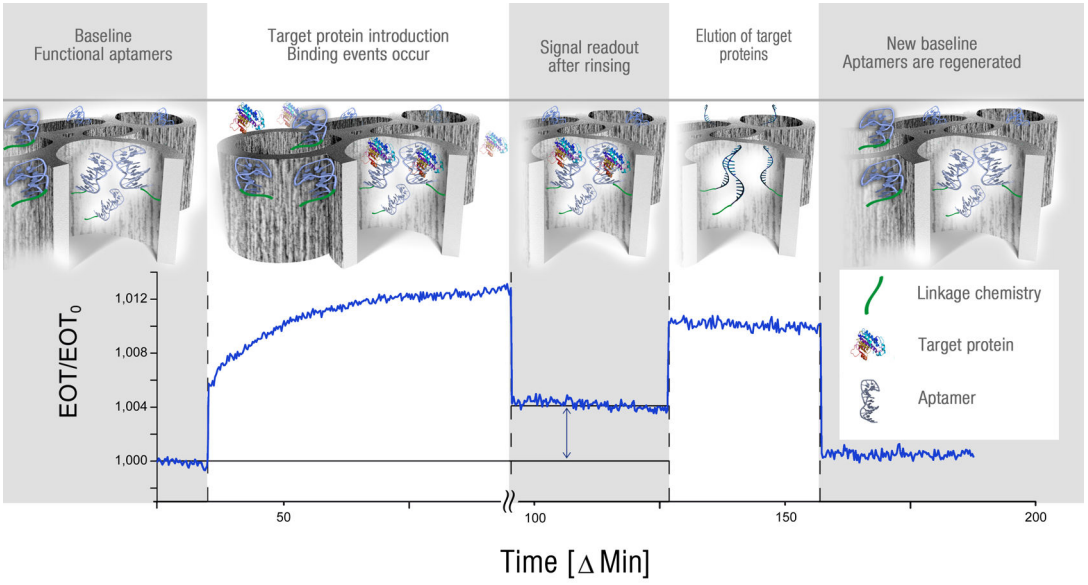

Figure 2. Relative EOT value vs time of 6H7-functionalized $PSiO_2$ during a typical biosensing experiment. A baseline is obtained in buffer solution followed by the introduction of lipase solution, binding events occur, and the signal increases rapidly. After a rinse step to remove unbound molecules, a stable readout signal is attained. Competitive elution with 1 M imidazole leads to the release of the captured target protein and the rapid removal of such in the following rinse step. Following a short incubation in the aptamer's selection buffer, the biosensor can be restored for subsequent use. Note that during buffer exchange and rinsing, EOT measurements are briefly paused.

that the aptamer was immobilized both on the top surface and throughout the entire porous scaffold. Using low and high aptamer concentrations, results in significant differences in the fluorescence signal intensity, ascribed to different surface coverage values. For the subsequent biosensing experiments, we used an intermediate aptamer concentration of 75 μM. It is crucial for target recognition, that the aptamers maintain their ability to fold in their specific 3D-structure; thus, based on our preliminary results (data not shown) an intermediate aptamer concentration was employed to provide sufficient surface coverage by the aptamers yet allowing spacing for folding and target recognition.[55,56] In line with these findings and to ensure a high yield of functional aptamers, we have introduced an additional step of aptamer refolding (in PBS) following the aptamer conjugation to the PSi scaffold (see Table 1).

Optical Biosensing Experiments. As a model system we chose the 6H7 aptamer,[43] which is designed to target the polyhistidine tag (his-tag) of proteins. In our previous work we have thoroughly characterized this aptamer and demonstrated its binding affinity to his-tagged proteins.[45,46] A typical dissociation constant (calculated from the Langmuir isotherm) of 4.6 μM was determined for the aptamer when immobilized onto magnetic particles.[43] To investigate the potential of the 6H7-functionalized $PSiO_2$ for biosensing, we have studied its optical response to a variety of his-tagged (6× His) protein targets, characterized by different properties and molecular weights. In a typical biosensing experiment, the 6H7-functionalized $PSiO_2$ is exposed to a solution containing the target protein and the reflectivity spectra of the porous film is monitored in real time and corresponding EOT values are computed. Figure 2 presents the change in the relative EOT values (EOT/EOT_0) upon exposure of the 6H7-functionalized $PSiO_2$ to lipase (T6 from *Geobacillus stearothermophilus*, molecular weight 44 kDa) at a concentration of 19 μM. First, PBS buffer was introduced into the flow cell to acquire a stable EOT baseline. Following this step, the lipase solution was introduced and the sample was incubated with the solution. Immediately after the introduction of the lipase, a rapid increase in the relative EOT value was observed, after which the signal steadily increased until a constant EOT value was attained (after ~1 h). The increase in the EOT is attributed to the infiltration of the protein solution into the pores and to binding events of the his-tagged protein to the 6H7 aptamer. Next, the protein solution was removed and the biosensor surface extensively rinsed with PBS (during this washing step, EOT acquisition was briefly paused). Subsequently, because of removal of the unbound protein molecules, the relative EOT sharply decreased and a stable EOT value was obtained, corresponding to a net EOT shift of 40 nm. This significant EOT shift is attributed to binding of the target protein to the aptamer-functionalized surface. The stability of the EOT signal during the rinsing step implies that the captured protein molecules are tightly bound to the aptamer under these conditions. It should be emphasized that exposure of the biosensor to non his-tagged proteins, e.g, casein and human IgG, did not induce significant changes in the relative EOT (see Figure S-3, Supporting Information). This clearly indicates that the developed surface chemistry protocol in combination with the high surface coverage by the aptamers, provide an effective passivation of the sensor surface and minimize effects of nonspecific binding.

One of the main advantages of aptamers over conventional recognition elements (e.g., antibodies) is their ability to undergo reversible changes of conformation with variations in temperature or salt concentration, rendering aptamer-based sensors as potentially recyclable.[57] Alternatively, gentle elution conditions can be predefined during SELEX to facilitate aptamer regeneration during application processes.[58] In the case of the aptamer 6H7, we have eluted the target protein competitively by exposing the biosensor to a high concentration of imidazole (a strong chelating agent), see Figure 2. This results in an immediate increase in EOT signal

DOI: 10.1021/ac504487g
Anal. Chem. 2015, 87, 1999−2006

(corresponding to a net shift of approximately 120 nm) due to the higher refractive index of this buffer solution (n = 1.347). This elution procedure was adapted from immobilized metal ion affinity chromatography (IMAC), which is conventionally used for the purification of His-tagged proteins.[44] Whereas, imidazole is the most common and effective agent for elution and recovery of captured His-tagged proteins from an IMAC column.[59] Indeed, following this step, the relative EOT readout returns to its original value. Figure 2 demonstrates that we were able to remove the captured proteins from the biosensor surface. Consequently, the biosensors were incubated with PBS. Following this step, the biosensor was exposed to the lipase solution for subsequent optical experiments. Figure 3 depicts

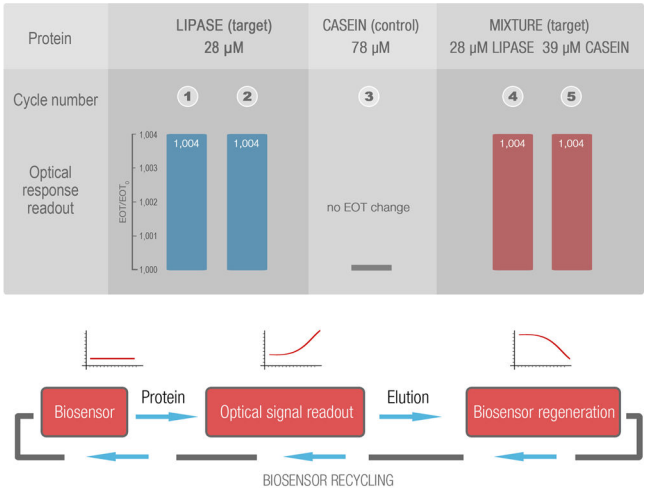

Figure 3. Biosensing results, expressed in terms of the averaged relative EOT value, for the 6H7-functionalized $PSiO_2$ exposed to 28 μM lipase for two subsequent cycles (cycles 1 and 2) and a successive third cycle of exposure to 78 μM casein (cycle 3, used as a negative control). Consequently, the biosensor was exposed to a protein mixture, containing 28 μM lipase and 39 μM casein, for two additional cycles (cycles 4 and 5). All experiments were carried out on a single biosensor sample. Schematics underneath depict the course of biosensing experiments and the mode of biosensor regeneration and cycling. Figure S-4 (see the Supporting Information) presents the relative EOT vs time data for these experiments and details how data was extracted.

the optical response of the biosensor, expressed in terms of the relative EOT shift, upon consecutive exposure to different protein solutions. The biosensor exhibited highly reproducible results, i.e., similar EOT shifts were obtained during cycling of lipase solution (28 μM). Whereas, upon subsequent exposure of the biosensor to a high concentration solution of a nontarget protein, i.e., casein (78 μM), no EOT shift was observed, demonstrating the high specificity of this biosensing platform. Furthermore, successive introduction of target/nontarget protein mixtures, containing lipase and casein (at a concentration of 28 μM and 39 μM, respectively), resulted in reproducible EOT shifts, corresponding to the concentration of the lipase target. It should be noted that all these experiments were carried out using a single biosensor, demonstrating the stability of our biosensing scheme and the ability to reuse the biosensor for numerous subsequent experiments. Figure S-4 (see the Supporting Information) presents the relative EOT vs time data for these experiments and details how data was extracted for Figure 3.

A key challenge in PSi biosensors is to effectively stabilize the nanostructure during experiments in biological solutions, as PSi oxidation and dissolution in aqueous environments lead to significant signal baseline drifts, signal loss, and ultimately to structural collapse of the PSi thin film.[25,40,60] Also in the case of the aptamer-functionalized $PSiO_2$ biosensors, baseline drifts were observed during the prolonged exposure to buffer solutions (EOT/EOT_0 = 1.0040 after 4 h of buffer flow). Nevertheless, we were able to reuse the biosensors for numerous subsequent experimental cycles. The aptamer-functionalized $PSiO_2$ biosensor was used for 12 subsequent sensing cycles, showing their excellent reusability (see Table S-2 in the Supporting Information). To the best of our knowledge, this is the first report on PSi-based optical affinity biosensors utilizing aptamers as capture probes, demonstrating their successful reuse while retaining detection accuracy, as presented in Figure 3. It should be noted that all experiments were carried out in solution and following the regeneration step (see Figure 3), and the biosensor was dried under a stream of nitrogen and stored overnight. After usage for a >7 day time period, the PSi film showed poor optical properties. Visual assessment of the biosensor suggested residues of salts and protein to have clogged the pores and therefore impaired its performance.

The dynamic range of the biosensor was studied by exposing the biosensor to a set of lipase solutions with different concentrations (0–56 μM). Figure 4 summarizes the results of

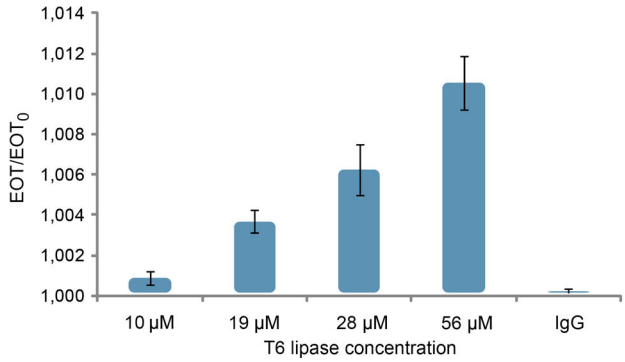

Figure 4. Optical response (relative EOT) of the biosensor vs lipase concentration. The concentration row, including the negative control with IgG (nontarget protein), was carried out on a single biosensor and repeated again on a different biosensor scaffold.

these experiments, depicting the maximal relative EOT value attained for each protein concentration. All experiments were carried out using a 6H7-functionalized $PSiO_2$ surface by performing biosensing experiments with varying lipase concentration. All experiments were performed in triplicates, and IgG is introduced as a nontarget protein control. Indeed, no optical shifts were observed upon exposure to IgG, demonstrating again the excellent selectivity of the 6H7 aptamer. A good linear correlation between the relative EOT signal and the protein concentration is obtained (R^2 = 0.985).

Biosensing in Complex Biological Fluids. One of the major obstacles in the application of label-free biosensors is the ability to detect the target molecule in complex biological fluid in which it resides.[61,62] This is ascribed to the strong interference from nonspecific binding of nontarget proteins onto the transducer/solution interface.[63] Thus, to study the ability of our biosensor to selectively detect target molecules in

DOI: 10.1021/ac504487g
Anal. Chem. 2015, 87, 1999–2006

the presence of overabundant nonspecific proteins, the aptamer-immobilized $PSiO_2$ was exposed to an overnight bacterial culture grown in LB medium as well as to bacteria lysate solution, both are rich in overabundant nonspecific proteins (but do not contain target his-tagged proteins). Figure 5 shows the optical response of the biosensor, expressed as the

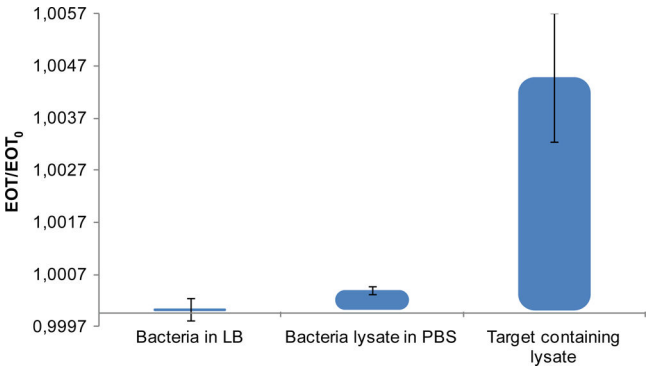

Figure 5. Optical response (relative EOT) of the biosensor to different complex fluids. A single biosensor was subsequently exposed to an overnight bacterial culture grown in LB medium, a solution of bacteria lysate in PBS, and a target-containing bacterial lysate solution.

maximal relative EOT value attained, upon exposure to these complex biological fluids. For the bacterial culture suspension, negligible EOT changes were observed; exposure to the bacteria lysate solution (total protein concentration is 1.8 mg/mL) induced a minor increase in the relative EOT value of 6 nm. These values are similar to those observed upon exposure to the biosensor to nontarget protein solutions in buffer at protein concentrations corresponding to 2 mg/mL (see Figures 3 and 4). On the other hand, introduction of the biosensor to a bacteria lysate solution, overexpressing target his-tagged proteins (total protein concentration is 19.6 mg/mL), resulted in a profound change in the relative EOT of 67 nm. Please note that experiments with pure lipase samples were conducted in concentrations of 0–56 μM, corresponding to a range of 0–2.47 mg/mL. These results demonstrate the ability of this biosensing platform to selectively detect its target protein in a complex solution of bacteria lysate. This is attributed to the excellent specificity of the 6H7 aptamer and to its viable immobilization strategy and surface modification, minimizing nonspecific adsorption of unrelated molecules. Thus, when designing a PSi-based biosensor with other aptamer–target pairs, nonspecific interactions between the capture probe, the modified surface, the appropriate target as well as possible interfering substances, must be carefully studied and optimized accordingly. This is critical when targeting proteins, as properties such as the isoelectric point, molecular weight, and folding will affect both target recognition and unintended adsorption onto the biosensor.[7]

Current work in our lab is focused on a few aspects: (i) reducing the overall analysis time by optimizing the assay; (ii) exploring the use of more sophisticated PSi structures such as rugate filters, to improve the sensor resolution and (iii) employment of aptamers with lower affinity constants to address the sensitivity aspect. We expect these advancements to result in biosensors exhibiting superior sensitivity according to the dissociation constant of the aptamers (i.e., in nanomolar range) and will make them indeed comparable to the performance of antibody-based PSi biosensors.

CONCLUSIONS

In this proof-of-concept work, a label-free optical biosensor based on aptamer-conjugated porous Si (Fabry–Pérot layers) was designed and characterized. For the first time, a model aptamer was covalently immobilized onto the oxidized PSi nanostructure and the resulting biosensor scheme demonstrated specific binding of target proteins, detected and quantified by RIFTS. Exposure to the target proteins, also in mixture solutions (containing target and nontarget proteins) and even complex fluids (bacteria in culture media and their lysates), resulted in highly robust and reproducible changes in the optical reflectivity spectrum of the biosensor corresponding to the affinity constant of the used aptamer model system. Control experiments revealed negligible binding of nontarget proteins, even in complex biological fluids, confirming the excellent selectivity of these aptamer-based biosensors toward their target analytes. Importantly, the biosensors show exceptional stability and could be easily regenerated by a short rinsing step for multiple biosensing analyses.

The presented optical label-free biosensor scheme holds a great promise for the design of versatile bioanalytical assays, allowing for rapid detection and quantification of analytes in a simple and reliable manner. The superior properties of aptamers as recognition elements, mainly their availability for various targets and their excellent selectivity and stability, combined with the advantages of PSi-optical transducers, can be exploited for construction of simple, flexible, inexpensive, robust, and portable biosensing platforms. Where many biosensing schemes fail due to their lack of stability in real world samples and settings, the presented system can fill this gap and provide a real alternative to antibody-based assays.

ASSOCIATED CONTENT

Supporting Information

Additional information as noted in text. This material is available free of charge via the Internet at http://pubs.acs.org.

AUTHOR INFORMATION

Corresponding Author

*Phone: +972-4-8295071. E-mail: esegal@tx.technion.ac.il.

Notes

The authors declare no competing financial interest.

ACKNOWLEDGMENTS

We thank Prof. Ayelet Fishman and her Ph.D. student, Adi Dror, from the Department for Biotechnology and Food Engineering, at the Technion-Israel Institute of Technology, for supplying target proteins. We are grateful to Prof. Rolf Brendel and Sascha Wolter at the Institute for Solar Energy Research Hamelin, Germany, for performing the spectroscopic ellipsometry measurements. E.S. and K.U. acknowledge the core services and support from the Lorry I. Lokey Center for Life Science and Engineering.

REFERENCES

(1) Tuerk, C.; Gold, L. *Science* **1990**, *249*, 505–510.
(2) Ellington, A. D.; Szostak, J. W. *Nature* **1990**, *346*, 818–822.
(3) Song, S.; Wang, L.; Li, J.; Fan, C.; Zhao, J. *Trends Anal. Chem.* **2008**, *27*, 108–117.
(4) O'Sullivan, C. *Anal. Bioanal. Chem.* **2002**, *372*, 44–48.
(5) Walter, J. G.; Heilkenbrinker, A.; Austerjost, J.; Timur, S.; Stahl, F.; Scheper, T. *Z. Naturforsch., B* **2012**, *67b*, 976–986.

DOI: 10.1021/ac504487g
Anal. Chem. 2015, 87, 1999–2006

(6) You, K.; Lee, S.; Im, A.; Lee, S. *Biotechnol. Bioproess Eng.* **2003**, *8*, 64−75.
(7) Lönne, M.; Zhu, G.; Stahl, F.; Walter, J.-G. In *Biosensors Based on Aptamers and Enzymes*; Gu, M. B., Kim, H.-S., Eds.; Springer: Berlin, Heidelberg, Germany, 2014; pp 121−154.
(8) Famulok, M.; Mayer, G. *Acc. Chem. Res.* **2011**, *44*, 1349−1358.
(9) Gu, M. B.; Kim, H.-S. *Biosensors Based on Aptamers and Enzymes*; Springer: Berlin, Heidelberg, Germany, 2014; Vol. *140*, p 331.
(10) Sefah, K.; Phillips, J. A.; Xiong, X.; Meng, L.; Van Simaeys, D.; Chen, H.; Martin, J.; Tan, W. *Analyst* **2009**, *134*, 1765−1775.
(11) Han, K.; Liang, Z.; Zhou, N. *Sensors* **2010**, *10*, 4541−4557.
(12) Cho, H.; Yeh, E.-C.; Sinha, R.; Laurence, T. A.; Bearinger, J. P.; Lee, L. P. *ACS Nano* **2012**, *6*, 7607−7614.
(13) Zhou, J.; Ellis, A. V.; Kobus, H.; Voelcker, N. H. *Anal. Chim. Acta* **2012**, *719*, 76−81.
(14) Giamberardino, A.; Labib, M.; Hassan, E. M.; Tetro, J. A.; Springthorpe, S.; Sattar, S. A.; Berezovski, M. V.; DeRosa, M. C. *PLoS One* **2013**, *8*, e79087.
(15) Kim, D. K.; Kerman, K.; Hiep, H. M.; Saito, M.; Yamamura, S.; Takamura, Y.; Kwon, Y. S.; Tamiya, E. *Anal. Biochem.* **2008**, *379*, 1−7.
(16) Bai, H.; Wang, R.; Hargis, B.; Lu, H.; Li, Y. *Sensors* **2012**, *12*, 12506−12518.
(17) Tombelli, S.; Minunni, M.; Luzi, E.; Mascini, M. *Bioelectrochemistry* **2005**, *67*, 135−141.
(18) Ashley, J.; Li, S. F. *Biosens. Bioelectron.* **2013**, *48*, 126−131.
(19) Tran, D. T.; Knez, K.; Janssen, K. P.; Pollet, J.; Spasic, D.; Lammertyn, J. *Biosens. Bioelectron.* **2013**, *43*, 245−251.
(20) Couture, M.; Zhao, S. S.; Masson, J.-F. *Phys. Chem. Chem. Phys.* **2013**, *15*, 11190−11216.
(21) Leonard, P.; Hearty, S.; Brennan, J.; Dunne, L.; Quinn, J.; Chakraborty, T.; O'Kennedy, R. *Enzyme Microb. Technol.* **2003**, *32*, 3−13.
(22) De Stefano, L.; Arcari, P.; Lamberti, A.; Sanges, C.; Rotiroti, L.; Rea, I.; Rendina, I. *Sensors* **2007**, *7*, 214−221.
(23) Pacholski, C. *Sensors* **2013**, *13*, 4694−4713.
(24) Jane, A.; Dronov, R.; Hodges, A.; Voelcker, N. H. *Trends Biotechnol.* **2009**, *27*, 230−239.
(25) Kilian, K. A.; Bocking, T.; Gooding, J. J. *Chem. Commun.* **2009**, *0*, 630−640.
(26) Alvarez, S. D.; Schwartz, M. P.; Migliori, B.; Rang, C. U.; Chao, L.; Sailor, M. J. *Phys. Status Solidi A* **2007**, *204*, 1439−1443.
(27) Dancil, K.-P. S.; Greiner, D. P.; Sailor, M. J. *J. Am. Chem. Soc.* **1999**, *121*, 7925−7930.
(28) Janshoff, A.; Dancil, K. P. S.; Steinem, C.; Greiner, D. P.; Lin, V. S. Y.; Gurtner, C.; Motesharei, K.; Sailor, M. J.; Ghadiri, M. R. *J. Am. Chem. Soc.* **1998**, *120*, 12108−12116.
(29) Orosco, M. M.; Pacholski, C.; Miskelly, G. M.; Sailor, M. J. *Adv. Mater.* **2006**, *18*, 1393−1396.
(30) Pacholski, C.; Yu, C.; Miskelly, G. M.; Godin, D.; Sailor, M. J. *J. Am. Chem. Soc.* **2006**, *128*, 4250−4252.
(31) Schwartz, M. P.; Derfus, A. M.; Alvarez, S. D.; Bhatia, S. N.; Sailor, M. J. *Langmuir* **2006**, *22*, 7084−7090.
(32) Schwartz, M. P.; Alvarez, S. D.; Sailor, M. J. *Anal. Chem.* **2006**, *79*, 327−334.
(33) Gaur, G.; Koktysh, D.; Weiss, S. M. *Proc. SPIE*, Vol. 8594, Nanoscale Imaging, Sensing, and Actuation for Biomedical Applications X; February 19, 2013; 859408; 10.1117/12.2002889.
(34) Zhang, J.; Wu, Y.; Zhang, B.; Li, M.; Jia, S.; Jiang, S.; Zhou, H.; Zhang, Y.; Zhang, C.; Turner, A. P. F. *Anal. Lett.* **2012**, *45*, 986−992.
(35) Gupta, B.; Zhu, Y.; Guan, B.; Reece, P. J.; Gooding, J. J. *Analyst* **2013**, *138*, 3593−3615.
(36) Tsang, C. K.; Kelly, T. L.; Sailor, M. J.; Li, Y. Y. *ACS Nano* **2012**, *6*, 10546−10554.
(37) Pacholski, C.; Sartor, M.; Sailor, M. J.; Cunin, F.; Miskelly, G. M. *J. Am. Chem. Soc.* **2005**, *127*, 11636−11645.
(38) Segal, E.; Perelman, L. A.; Cunin, F.; Di Renzo, F.; Devoisselle, J. M.; Li, Y. Y.; Sailor, M. J. *Adv. Funct. Mater.* **2007**, *17*, 1153−1162.
(39) Shtenberg, G.; Massad-Ivanir, N.; Moscovitz, O.; Engin, S.; Sharon, M.; Fruk, L.; Segal, E. *Anal. Chem.* **2012**, *85*, 1951−1956.
(40) Massad-Ivanir, N.; Shtenberg, G.; Segal, E. *Adv. Exp. Med. Biol.* **2012**, *733*, 37−45.
(41) Bonanno, L. M.; DeLouise, L. A. *Biosens. Bioelectron.* **2007**, *23*, 444−448.
(42) Krismastuti, F. S. H.; Pace, S.; Voelcker, N. H. *Adv. Funct. Mater.* **2014**, *24*, 3639−3650.
(43) Kökpinar, Ö.; Walter, J.-G.; Shoham, Y.; Stahl, F.; Scheper, T. *Biotechnol. Bioeng.* **2011**, *108*, 2371−2379.
(44) Doyle, S. A.; Murphy, M. B. *Aptamers and methods for their in vitro selection and uses thereof.* U.S. Patent Application 20050142582, June 30, 2005.
(45) Zhu, G.; Lübbecke, M.; Walter, J.; Stahl, F.; Scheper, T. *Chem. Eng. Technol.* **2011**, *34*, 2022−2028.
(46) Walter, J. G.; Kökpinar, O.; Friehs, K.; Stahl, F.; Scheper, T. *Anal. Chem.* **2008**, *80*, 7372−7378.
(47) Massad-Ivanir, N.; Shtenberg, G.; Zeidman, T.; Segal, E. *Adv. Funct. Mater.* **2010**, *20*, 2269−2277.
(48) Sailor, M. J. *Porous Silicon in Practice*; Wiley-VCH: Weinheim, Germany, 2011; p 250.
(49) Massad-Ivanir, N.; Shtenberg, G.; Tzur, A.; Krepker, M. A.; Segal, E. *Anal. Chem.* **2011**, *83*, 3282−3289.
(50) Massad-Ivanir, N.; Friedman, T.; Tzur-Balter, A.; Nahor, A.; Eichler, S.; Bonanno, L. M.; Sa'ar, A.; Segal, E. *Soft Matter* **2012**, *8*, 9166−9176.
(51) Shtenberg, G.; Massad-Ivanir, N.; Fruk, L.; Segal, E. *ACS Appl. Mater. Interfaces* **2014**, *6*, 16049−16055.
(52) Barth, A. *Prog. Biophys. Mol. Biol.* **2000**, *74*, 141−173.
(53) Parikh, S. J.; Mukome, F. N.; Zhang, X. *Colloids Surf., B: Biointerfaces* **2014**, *119*, 38−46.
(54) Zhou, J.; Rossi, J. J. *Mol. Ther. Nucleic Acids* **2014**, *3*, e169.
(55) Wang, H.-Q.; Wu, Z.; Tang, L.-J.; Yu, R.-Q.; Jiang, J.-H. *Nucleic Acids Res.* **2011**, *39*, e122.
(56) Deng, Q.; German, I.; Buchanan, D.; Kennedy, R. T. *Anal. Chem.* **2001**, *73*, 5415−5421.
(57) Lee, J.-O.; So, H.-M.; Jeon, E.-K.; Chang, H.; Won, K.; Kim, Y. *Anal. Bioanal. Chem.* **2008**, *390*, 1023−1032.
(58) Walter, J.-G.; Stahl, F.; Scheper, T. *Eng. Life Sci.* **2012**, *12*, 496−506.
(59) Cheung, R. C.; Wong, J. H.; Ng, T. B. *Appl. Microbiol. Biotechnol.* **2012**, *96*, 1411−1420.
(60) Bonanno, L. M.; Segal, E. *Nanomedicine* **2011**, *6*, 1755−1770.
(61) Li, L.-L.; Ge, P.; Selvin, P. R.; Lu, Y. *Anal. Chem.* **2012**, *84*, 7852−7856.
(62) Huang, D.; Niu, C.; Li, Z.; Ruan, M.; Wang, X.; Zeng, G. *Analyst* **2012**, *137*, 5607−5613.
(63) Swensen, J. S.; Xiao, Y.; Ferguson, B. S.; Lubin, A. A.; Lai, R. Y.; Heeger, A. J.; Plaxco, K. W.; Soh, H. T. *J. Am. Chem. Soc.* **2009**, *131*, 4262−4266.

DOI: 10.1021/ac504487g
Anal. Chem. 2015, 87, 1999−2006

Supporting Information

LABEL-FREE OPTICAL BIOSENSORS BASED ON APTAMER-FUNCTIONALIZED POROUS SILICON SCAFFOLDS

*Katharina Urmann[1,2], Johanna-Gabriela Walter[1], Thomas Scheper[1], Ester Segal[2]**

[1] Institute for Technical Chemistry, Leibniz University of Hanover, Callinstr. 5, 30167 Hanover, Germany

[2] Department of Biotechnology and Food Engineering, Technion Israel Institute of Technology, Technion City, 32000 Haifa, Israel; phone: +972-4-8295071; e-mail: esegal@tx.technion.ac.il

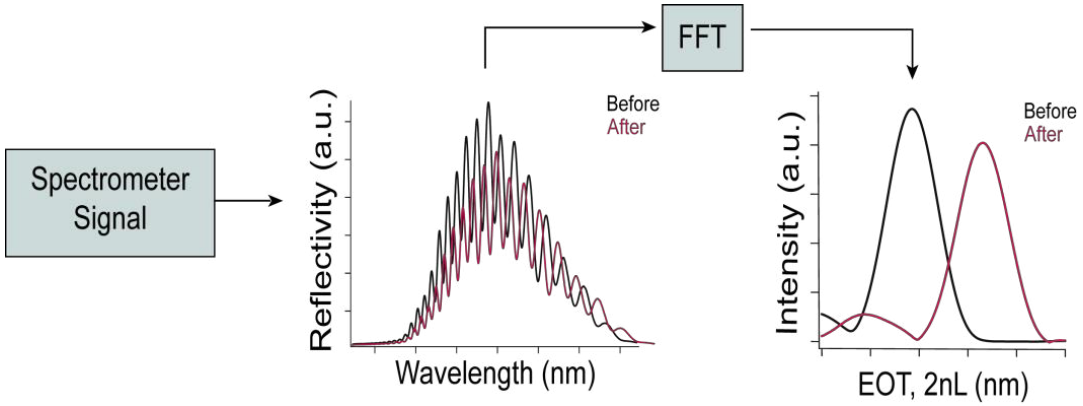

Figure S-1. RIFTS signal processing steps. Reflectivity spectra are recorded with a CCD camera spectrometer and a fast Fourier transformation is applied. The signal is then expressed as the relative change in EOT before and after exposure of the aptamer-functionalized $PSiO_2$ scaffold to the target protein solution.

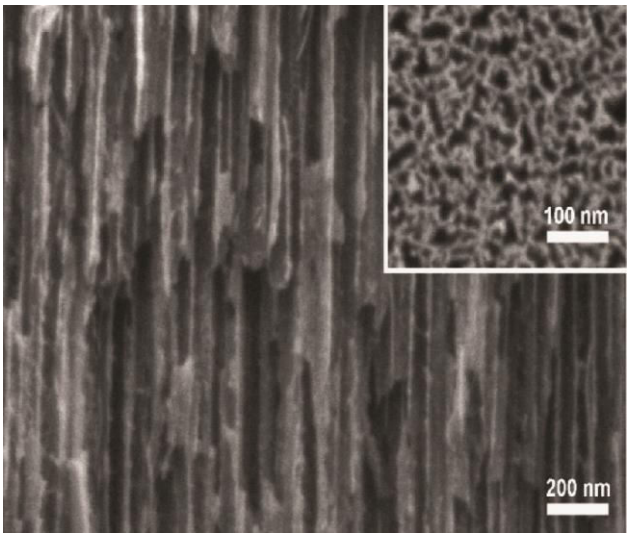

Figure S-2. Cross-section and top-view high-resolution scanning electron microscopy images section, depicting the interconnected porous structure with pore sizes between 50 and 80 nm.

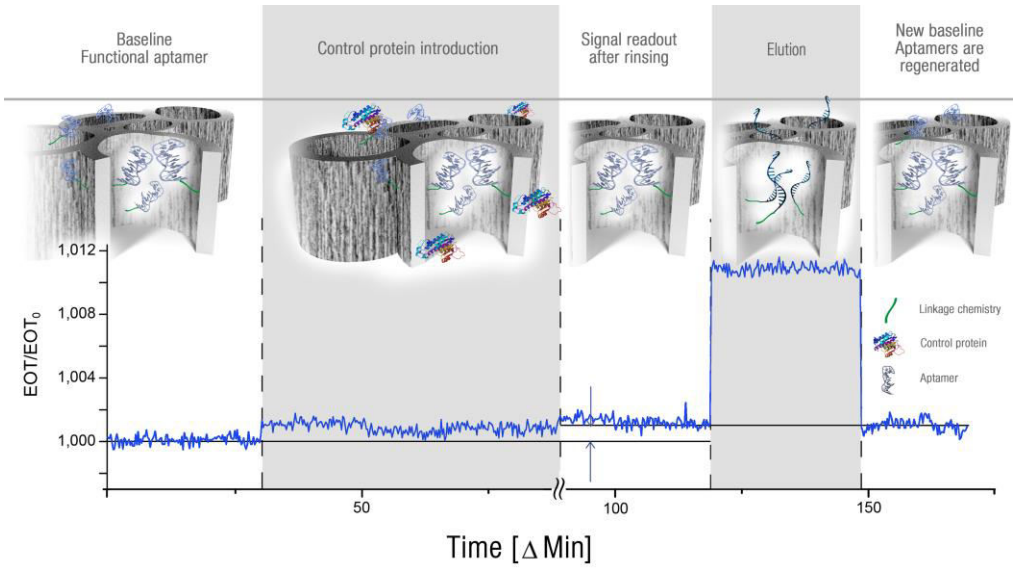

Figure S-3. Relative EOT value vs. time of 6H7-functionalized $PSiO_2$ during a control experiment. A baseline is obtained in buffer solution followed by the introduction of casein solution (78 µM). The signal barely increases due to unspecific interactions (corresponding to a net shift of 5 nm). After a rinse step to remove the unbound molecules, a stable readout signal is attained. Elution with imidazole and a short incubation in the aptamer's selection buffer restores the biosensor for subsequent use. Note that during buffer exchange and rinsing, EOT measurements are briefly paused.

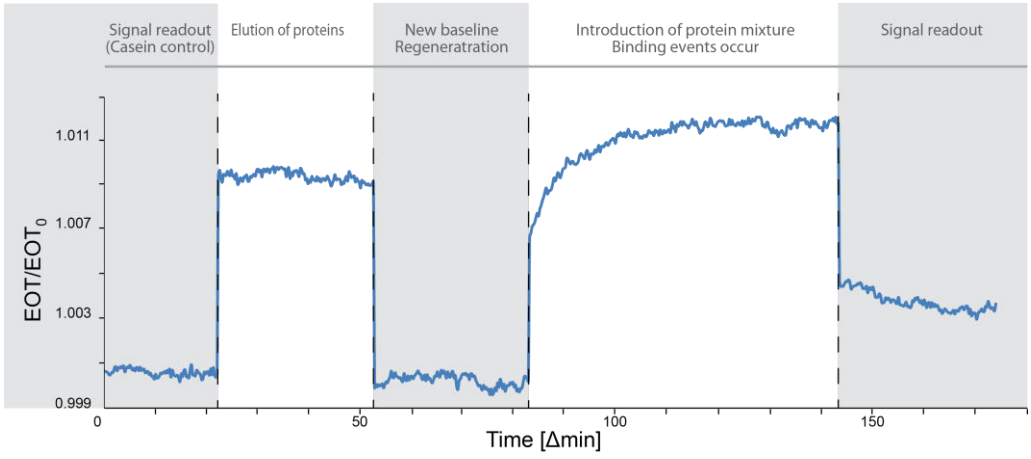

Figure S-4. Excerpt of relative EOT value vs. time data of 6H7-functionalized $PSiO_2$ during a series of repeated sensing cycles. Relative EOT values from baseline and readout sections are averaged in order to express the biosensor signal as bar. This trace shows the readout signal after incubation with casein as control protein, as well as the following

elution step and a complete cycle of biosensing with a mixture of lipase and casein. Values from these traces were extracted and summarized in Figure 3. Note that during buffer exchange and rinsing, EOT measurements are briefly paused.

Table S-1. Results of $PSiO_2$ scaffold characterization.

Etching conditions		**HRSEM**		**Gravimetry**	**SLIM**		**Ellipsometry**	
Etch time (s)	Current density (mA/cm^2)	Pore Diameter (nm)	Thickness (nm)	Total Porosity (%)	Open Porosity (%)	Thickness (nm)	Porosity (%)	Thickness (nm)
30	300	65 ± 10	5440 ± 80	78 ± 1	79 ± 1	4975 ± 88	79 ± 4	5000 ± 30

Table S-2. Relative change in EOT of a single biosensor to 28 μM lipase; 12 consecutive biosensing cycles spanning over a period of 7 days.

Cycle number	**EOT/EOT_0**
3	1,0069
7	1,0091
8	1,0099
9	1,0061
11	1,0077

Cycles 1, 2, 4-6, 10 and 12 included exposure of the sensor to control proteins, mixtures and other lipase concentrations. The sensor was dried and stored overnight after cycle 1, 3, 5, 7, 9 and 11.

5.2 Whole cell detection of live *Lactobacillus Acidophilus* on aptamer-decorated porous silicon biosensors

This work depicts the consequent advancement of the idea to utilize aptamers as capture probes in optical porous silicon biosensors for the design of a highly versatile and simple biosensing platform. The paper not only presents a different mode of biosensing with $PSiO_2$ (with targets being size-excluded from the nanostructure), but also emphasizes the broad range of targets that can be specifically bound by aptamer receptors. Herein, aptamer Hemag1P, which specifically binds the important probiotic *Lactobacillus acidophilus*, was utilized for direct bacteria capture onto oxidized PSi Fabry–Pérot thin films. Monitoring changes in the reflectivity spectrum (using reflective interferometric Fourier transform spectroscopy) allows for bacteria detection in a label-free, simple and rapid manner. The performance of the biosensor was optimized by tuning the PSi nanostructure, its optical properties, as well as the immobilization density of the aptamer. We demonstrate the high selectivity and specificity of this simple “direct-capture” biosensing scheme by comparisons with non-target bacteria cultures and mixtures. Furthermore, we show its ability to distinguish between live and dead bacteria populations. The resulting biosensor presents a robust and rapid method for the specific detection of live *L. acidophilus* at concentrations relevant for probiotic products and as low as 10^6 cells per mL. Rapid monitoring of probiotic bacteria is crucial for quality, purity, and safety control as the use of probiotics in functional foods and pharmaceuticals becomes increasingly popular.

Analyst

PAPER

Cite this: *Analyst*, 2016, **141**, 5432

Whole-cell detection of live *lactobacillus acidophilus* on aptamer-decorated porous silicon biosensors†

K. Urmann,[a,b] S. Arshavsky-Graham,[b] J. G. Walter,[a] T. Scheper[a] and E. Segal*[b]

Received 6th April 2016,
Accepted 28th June 2016

DOI: 10.1039/c6an00810k

www.rsc.org/analyst

This work describes the design of optical aptamer-based porous silicon (PSi) biosensors for the direct capture of *Lactobacillus acidophilus*. Aptamers are oligonucleotides (single-stranded DNA or RNA) that can bind their targets with high affinity and specificity, making them excellent recognition elements for biosensing applications. Herein, aptamer Hemag1P, which specifically targets the important probiotic *L. acidophilus*, was utilized for direct bacteria capture onto oxidized PSi Fabry–Pérot thin films. Monitoring changes in the reflectivity spectrum (using reflective interferometric Fourier transform spectroscopy) allows for bacteria detection in a label-free, simple and rapid manner. The performance of the biosensor was optimized by tuning the PSi nanostructure, its optical properties, as well as the immobilization density of the aptamer. We demonstrate the high selectivity and specificity of this simple "direct-capture" biosensing scheme and show its ability to distinguish between live and dead bacteria. The resulting biosensor presents a robust and rapid method for the specific detection of live *L. acidophilus* at concentrations relevant for probiotic products and as low as 10^6 cells per mL. Rapid monitoring of probiotic bacteria is crucial for quality, purity and safety control as the use of probiotics in functional foods and pharmaceuticals is becoming increasingly popular.

Introduction

Aptamers are short single-stranded oligonucleotides with specific target affinity which are yielded from an iterative selection process called SELEX (Systematic Evolution of Ligands by Exponential Enrichment), first established in 1990.[1,2] Compared to antibodies, these oligonucleotides possess a number of advantages: aptamers can exhibit similarly high affinities while their production is fully performed *in vitro*, assuring fast, low-cost and reproducible synthesis.[3,4] Aptamers can be designed to bind any desired target[3] and their selection under conditions of the native target conformation and surrounding matrix fosters a highly selective and affine aptamer sequence as a result. When employed as capture probes in biosensors, the aptamers' versatile chemical modification options facilitate their surface conjugation in a desired orientation and density[5–8] and their small molecule size and high stability are highly advantageous.[9–11]

When designing biosensors targeting whole cells, aptamer technology enables the development of highly affine capture probes even without exact knowledge of the molecular composition of the targeted structure. Whole-cell SELEX approaches utilize the cells in their native conformation and targeted structures do not need to be available in a purified form, as it would be necessary for antibody generation.[3,4,12] Indeed, aptamer capture probes have been generated against a variety of bacteria (*e.g. Escherichia coli*,[13] *Campylobacter jejuni*,[14] *Mycobacterium tuberculosis*,[15] *Staphylococcus aureus*[16] and *Salmonella enterica*[17]) and many aptamer-based capture assays have been reviewed recently.[18] For *Lactobacillus acidophilus* (*L. acidophilus*), a common lactic acid bacteria, the aptamer Hemag1P was developed by Hamula *et al.*[19] *L. acidophilus* is the most commonly used probiotic bacteria with several health benefits, including stimulation of the immune system and better digestibility.[20,21] *L. acidophilus* is a Gram-positive, rod-shaped bacterium, widely found in fermented and dairy-containing food products.

The Hemag1P aptamer is a 78-nucleotide long sequence, selected against whole, live *L. acidophilus* cells by a SELEX approach. The aptamer is believed to target the abundantly present S-proteins on the outer bacteria membrane. This

[a]*Institute of Technical Chemistry, Leibniz University of Hannover, Callinstr. 5, 30167 Hannover, Germany*
[b]*Department of Biotechnology and Food Engineering, Technion Israel Institute of Technology, Technion City, 32000 Haifa, Israel. E-mail: esegal@tx.technion.ac.il; Tel: +972-4-8295071*

†Electronic supplementary information (ESI) available. See DOI: 10.1039/c6an00810k

Results

hypothesis was confirmed by flow cytometry studies of the aptamer-target interactions comparing *Lactobacillus* strains with and without S-layer proteins and its affinity was reported to be 13 ± 3 nM.[19] Since its selection, Hemag1P has been employed twice as a capture probe. A preliminary work by Zhang *et al.*[22] demonstrated the capture of fluorescently labelled *L. acidophilus* onto a Hemag1P-functionalized chip.[22] Zuo *et al.*[23] have developed a fluorescence-based biosensor in which fluorophore-labelled Hemag1P was adsorbed to a graphene oxide (GO). Bacteria detection was facilitated by monitoring changes in GO fluorescence quenching.[23] Yet, these two studies required tedious labelling and employed a fluorescence microscope for signal readout. Thus, their potential application is confined to a laboratory setting.

Label-free optical biosensors can be designed using porous silicon-based systems. In the past few years, porous silicon (PSi) has received much attention as an optical transducer due to its facile fabrication, large surface-to-volume ratio and numerous available surface chemistries.[24–37] Many PSi-based biosensors use reflective interferometric Fourier transform spectroscopy (RIFTS) to monitor target capture within the porous layer.[32,38–40] However, for cellular targets (such as microorganisms), which are too large to penetrate into the pores, monitoring changes in the intensity of the reflectivity spectrum upon "direct cell capture" onto antibody-modified PSi allows their detection and quantification.[41,42] This biosensing scheme has allowed for a sensitive detection of *E. coli* bacteria using a peptidomimetic antimicrobial compound as a recognition element.[43] However, these biosensors are non-specific in their nature and require cell lysis to induce a response. Thus, in the present work, we design a highly specific biosensor for detection of *L. acidophilus* employing the Hemag1P aptamer as the capture probe. The biosensing concept relies on monitoring changes in the amplitude (intensity) of the FFT peak, which is obtained from the raw reflectivity spectra of the PSi, during exposure to bacteria suspensions. Bacteria capture onto the biosensor surface induce intensity changes. Recent work on aptamer-functionalized PSi has demonstrated their immense potential for designing highly stable and specific PSi biosensors for protein detection.[44,45] Herein, we describe the design and characterization of a label-free optical PSi-based aptasensor, where an oxidized PSi ($PSiO_2$) Fabry–Pérot thin film, used as the optical transducer, is conjugated with the *L. acidophilus* binding aptamer Hemag1P. We demonstrate the high selectivity and specificity of this simple "direct-capture" biosensing scheme and show its ability to distinguish between live and dead bacteria. The resulting biosensor presents a robust and rapid method for the specific detection of live *L. acidophilus* in concentrations as low as 10^6 cells per mL.

Experimental

Materials

Silicon wafers (0.0009 Ω cm resistivity, p-type, <100>-oriented, heavily boron-doped) were purchased from Siltronix Corp. Aqueous HF (48%) and absolute ethanol were supplied by Merck. (3-Mercaptopropyl)trimethoxysilane (MPTMS), maleimide, ethylenediaminetetraacetic acid (EDTA), 5,5′-dithiobis-(2-nitrobenzoic acid) (DTNB, Ellman reagent), culturing media components and all buffer salts were purchased from Sigma-Aldrich Chemicals. Buffers and media were all prepared with deionized water (18.2 MΩ cm) and filtered prior to use. Media were autoclaved prior to their use. Solvents (toluene, acetone) were purchased from Gadot Israel. The sequence of aptamer Hemag1P (5′-AGC AGC ACA GAG GTC AGA TGT AGC CCT TCA ACA TAG TAA TAT CTC TGC ATT CTG TGT GCC TAT GCG TGC TAC CGT GAA-3′) was published by Hamula *et al.*[19] and purchased with a 5′-acrylamide phosphoramidite (Acrydite™ phosphoramidite; Mosaic Technologies) modification from Integrated DNA Technologies. Other aptamers included in this work as controls are listed in Table 1. Hemag1P was selected in 50 mM Tris-HCl (pH 7.4), 100 mM NaCl, 5 mM KCl, 1 mM $MgCl_2$ (this buffer composition is subsequently abbreviated as SB). TE-buffer was composed of 10 mM Tris-HCl (pH 8.0) and 1 mM EDTA. PBS-buffer was composed of 137 mM NaCl, 2.7 mM KCl, 10 mM Na_2HPO_4 and 1.8 mM KH_2PO_4 (pH 7.0). Bacteria strain *Lactobacillus acidophilus* ATCC 4356 was obtained from Gamidor Diagnostics and *Escherichia coli* strain K12, as a negative control, was generously supplied by Prof. Sima Yaron (Technion – Israel Institute of Technology).

Bacteria culturing, sample preparation and cell count

L. acidophilus was grown in MRS medium (CM0359, OXOID) under 5% CO_2 atmosphere at 37 °C. Bacterial growth was monitored by optical density (OD) measurements at 600 nm in order to determine the logarithmic phase of growth. To correlate OD_{600} values with bacteria cell concentration, a standard plate-counting technique[47] was performed. Briefly, bacteria were grown to the mid-logarithmic phase (OD_{600} of 0.44) and plated on MRS agar plates in replicates. Plates were then incu-

Table 1 Aptamer and oligonucleotide sequences and their modification

Sequence name	Sequence	Modification
Hemag1P	AGCAGCACAGAGGTCAGATGTAGCCCTTCAACATAGTAATATCTCTGCATTCTGTGTGCCTAT GCGTGCTACCGTGAA	5′-Acrydite
T10-Hemag1P	TTTTTTTTTTAGCAGCACAGAGGTCAGATGTAGCCCTTCAACATAGTAATATCTCTGCATTCTGTGTGCC TATGCGTGCTACCGTGAA	5′-Acrydite
6H7[46]	GCTATGGGTGGTCTGGTTGGGATTGGCCCCGGGAGCTGGC	5′-Acrydite

Results

bated for 48 h in 5% CO_2 atmosphere at 37 °C and the formed colonies were counted. Based on counting, an OD_{600} value of 0.44 was correlated to a cell concentration of 3.5×10^7 CFU mL^{-1}.

E. coli K12 was cultivated in Luria–Bertani (LB) medium (composed of 5 g of NaCl, 5 g of yeast extract and 10 g of tryptone in 1 L of deionized water) at 37 °C while shaking. Bacterial growth was monitored by OD measurements and bacteria concentration was calculated from OD_{600} value according to the correlation of 1 OD_{600} = 10^8 cells per mL.[41]

For biosensing experiments, *L. acidophilus* was grown overnight in MRS medium and a subculture was grown the next morning until a cell density corresponding to an OD_{600} value of 0.44. *E. coli* K12 was grown overnight in LB medium and a subculture was grown the next morning until an OD_{600} value of 0.5. Samples of the cultures (1 mL) were spun down in a standard lab centrifuge (10 min at 5000*g*), replacing the supernatant by 1 mL SB. Following the re-suspension of the cell pellet, the centrifugation and buffer replacement were repeated two more times before the final cell suspension was either further diluted or used directly for biosensing experiments.

For the biosensing experiments with mixed bacterial populations, upon the final centrifugation and supernatant replacement, a bacteria pellet was re-suspended in 1 mL SB, after which, another bacteria pellet was introduced to form a mixed culture suspension.

For biosensing experiments with non-viable bacteria, bacteria suspensions were heat-treated as suggested by Bunthof *et al.*[48] Bacterial suspensions were placed on a dry heating block for 15 min at 70 °C and then stored on ice until further use.

Preparation and characterization of aptamer-conjugated $PSiO_2$ biosensors

Si wafers were electrochemically etched in a 3 : 1 (v/v) aqueous HF (48%) : ethanol solution. Two different etching conditions were used: (i) 30 s at 300 mA cm^{-2} current density and (ii) 375 s at 24 mA cm^{-2}. CAUTION: HF is a highly corrosive liquid and must be handled with extreme care and under secured working conditions! A strip of aluminium foil was brought in contact with the backside of a Si wafer (exposed area 1.33 cm^2) and mounted in an etching cell made from Teflon material. A platinum wire was used as the counter electrode. After etching, the wafer surface was rinsed with ethanol and subsequently dried under dry nitrogen gas flow. The obtained freshly etched PSi samples were thermally oxidized in a tube furnace (Thermolyne) at 800 °C for 1 h in ambient air, resulting in oxidized PSi ($PSiO_2$) films.

For $PSiO_2$ biofunctionalization, the porous film was incubated in a solution of 20 mM MPTMS in toluene for 1 h. After removal of the solution, the surface was rinsed with toluene, ethanol and acetone (for 2 min each) and dried under a stream of nitrogen. The silanized sample was rinsed with TE buffer prior to 1 h incubation with the aptamer solutions (50 μL) and successive rinsing with TE and PBS buffers. 2 mg mL^{-1} maleimide were dissolved in PBS, then applied to the aptamer-modified sample, and allowed to react for 1 h. Subsequently, the resulting biosensor was rinsed with PBS and finally incubated (30 min) in SB to allow proper aptamer folding.

Characterization of $PSiO_2$ films. The structural properties of the fabricated $PSiO_2$ films, *i.e.*, thickness, pore size and porosity, were characterized by electron microscopy, gravimetry (for porosity), and SLIM (spectroscopic liquid infiltration method), as described in detail by Massad-Ivanir *et al.*[42]

High-resolution scanning electron microscopy (HRSEM) of $PSiO_2$ films was performed with a Carl Zeiss Ultra Plus instrument at an accelerating voltage of 1 keV.

For gravimetric characterization, the silicon samples were weighed prior (m_1) and after etching and oxidation (m_2). Subsequently, the oxide layer was dissolved in a 3 : 1 (v/v) solution of aqueous HF (48%) and ethanol and the remnant porous layer was removed by incubation in 1 M aqueous KOH solution. The remaining sample was weighed again (m_3) and the porosity (P) was determined by the following equation:[49]

$$P(\%) = \frac{m_1 - m_2}{m_1 - m_3} \times 100 \quad (1)$$

The SLIM method provides a nondestructive determination of thickness and porosity based on data from reflectance spectra obtained while different liquids infiltrate into the pores.[49] The differences between the spectra are attributed to the change in optical thickness as the medium in the pores changes, under the assumption that all void spaces are filled equally.[50] The optical thickness ($2nL$, where n is the average refractive index of the porous film and L is its thickness) of the $PSiO_2$ is determined from the interferometric reflectance spectrum of the porous film in air and while immersed in ethanol and acetone, having refractive indices of 1.359 and 1.357, respectively. The refractive index of the SiO_2 portion of the film is assumed to be 1.455. Values of $2nL$ are then fitted to a two-component Bruggeman model of refractive index for the composite-layer, which yields a unique solution for both the porosity and the thickness of the samples.[42,50]

Characterization of $PSiO_2$ biofunctionalization. Surface modifications were verified using attenuated total reflectance Fourier transform infrared (ATR-FTIR) spectroscopy. Spectra were recorded using a Thermo 6700 FTIR instrument equipped with a Smart iTR diamond ATR device.

Silanization of the samples was characterized by the Ellmann assay for free thiol groups.[51] Herein, the silanized $PSiO_2$ samples were incubated for 15 min in 2.5 mL Ellman buffer (100 mM sodium phosphate, pH 8.0, 1 mM EDTA) supplemented with 50 μl Ellman solution (4 mg mL^{-1} of DNTB in Ellman buffer). The supernatant was collected after the reaction and its absorbance was measured at 412 nm using a Varioskan flash plate reader (Thermo Scientific).

Bacteria biosensing

The biosensors were placed in fixed flow cell apparatus, as previously described[44] and their interferometric reflectance

Results

spectra were collected using an Ocean Optics charge-coupled device (CCD) USB 4000 spectrometer fitted with a microscope objective lens coupled to a bifurcated fiber-optic cable. A tungsten light source was focused onto the center of the flow cell with a spot size of approximately 1–2 mm^2. Reflectivity data were continuously recorded every minute in the wavelength range of 400–1000 nm, with a spectral acquisition time of 100 ms. As previous work on probiotic bacteria indicated their sensitivity to light,[52,53] a shutter was used to block the light from reaching the sample surface between the measurements. This is to exclude possible effect of light on bacteria growth, behavior and interaction with the aptamer-conjugated surface. Both illumination of the surface and detection of the reflected light were performed along an axis coincident with the surface normal. The collected spectra were analyzed by applying fast Fourier transformation (FFT), as previously described by Massad-Ivanir *et al.*[41] with the FFT intensity changes expressed as percentages and calculated using the following equation:

$$\text{Intensity decrease}\,(\%) = \frac{I_1 - I_2}{I_1} \times 100\% \qquad (2)$$

where I_1 is the average intensity during the baseline establishment and I_2 is the average intensity during the incubation of the sensor with SB after exposure to the bacteria and the respective subsequent washing step.

In a typical optical biosensing experiment, a freshly-prepared aptamer-functionalized $PSiO_2$ sample was incubated with SB for 30 min to allow proper folding of the aptamer and to acquire a baseline signal. Thereafter, the respective bacteria suspensions (in SB) were introduced and allowed to incubate with the biosensor for 20 min. After removal of the bacteria suspension and thorough flushing of the cell with SB, the sample was incubated for 10 min in SB. Optical measurements were recorded every 1 min throughout the experiment. Note that during buffer exchange and rinsing steps, optical measurements were shortly paused to allow a thorough washing of the biosensor and the flow cell.

To confirm the bacteria capture on the biosensor surface, the biosensor was removed from the flow cell and immediately examined under a light microscope (ZEISS upright). Images were taken using the microscope camera (Axio Cam MRc, ZEISS).

Results and discussion

Biosensors fabrication and characterization

The first step in the biosensor preparation involves an anodization process of a Si wafer at a current density of 300 mA cm^{-2} for a duration of 30 s. These etching condition were adapted from our previous work on the design of aptamer-functionalized PSi for protein biosensing.[44] Following anodization, the resulting porous films were thermally oxidized in order to passivate the silicon hydride surface and render it into a hydrophilic $PSiO_2$ scaffold.[50] The detailed nanostructure and physical properties of the resulting $PSiO_2$ were characterized by HRSEM, gravimetry and SLIM and the results are summarized in Table S1 (ESI†). Detailed description of these techniques for the characterization of PSi films was previously reported.[42,44,49] The $PSiO_2$ films display a macroporous structure[54] of cylindrical pores with a diameter ranging between 55–75 nm, the thickness of the porous layer was ~5 μm, and a porosity of 79%.

A simple three-step biofunctionalization route was used to immobilize the aptamers to the $PSiO_2$ surface, as illustrated in Fig. 1a. The $PSiO_2$ was first silanized with (3-mercaptopropyl) trimethoxysilane (MPTMS) to result in a thiolated surface (Fig. 1a-I), which was then reacted with the acrydite-modified aptamers to form thioether bonds[55,56] (Fig. 1a-II). The latter are temperature and pH insensitive and provide stable conjugation of the aptamers to the porous nanostructure.[56,57] The third and final step (Fig. 1a-III) involved blocking of the residual thiol groups with maleimide in order to minimize subsequent non-specific reaction with buffers or sample components.

Successful aptamer immobilization was confirmed by ATR-FTIR spectroscopy and the results are presented in Fig. 1b. For neat $PSiO_2$, the typical $-(O_ySiH_x)$ vibration mode at 801 cm^{-1} and a peak at 1039 cm^{-1}, ascribed to the Si–O–Si stretching mode, were observed clearly. The aptamer-functionalized surface depicted an additional characteristic DNA band at 1635 cm^{-1} (carbonyl) as well as a new peak at 1717 cm^{-1}, which is attributed to the two C═O stretching frequencies of the maleimide blocking group.[58,59] It should be noted that other typical DNA peaks below 1500 cm^{-1} (*e.g.*, the

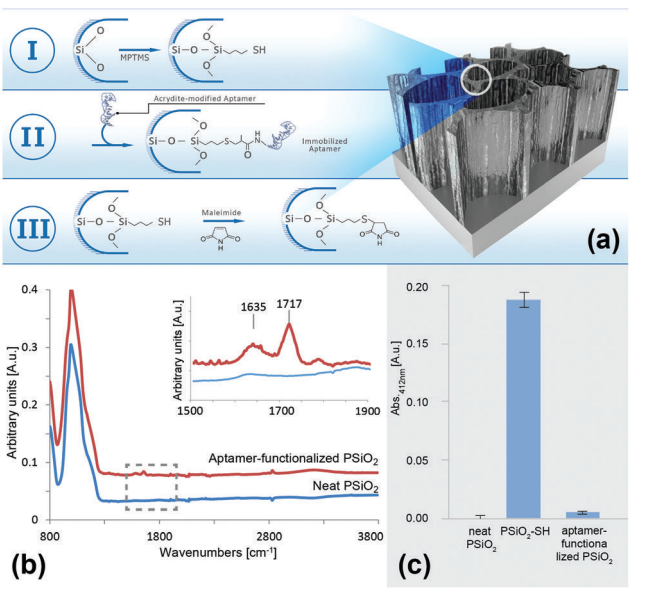

Fig. 1 (a) Three-step biofunctionalization route for aptamers immobilization onto $PSiO_2$. (I) Silanization of the $PSiO_2$ with 3-aptamer *via* formation of thioether bonds and (III) blocking of residual thiol groups with maleimide. (b) ATR-FTIR spectra of aptamer-functionalized $PSiO_2$ and neat $PSiO_2$. Inset depicts the marked area for clarity. (c) Ellman's assay results for neat $PSiO_2$, silanized $PSiO_2$ and aptamer-functionalized $PSiO_2$, presented as absorbance intensity (at 412 nm). All measurements were taken in triplicates.

Results

phosphate diester bands) could not be observed due to the strong absorption of the silicon species, as well as the maleimide C–N–C stretching which overlaps with the Si–O–Si stretching modes (around 1180 cm^{-1}).[60–62]

Another validation of the immobilization scheme was performed by using the Ellman assay for thiol-groups. This assay is based on the reduction of 5,5′-dithio-bis-(2-nitrobenzoic acid) (Ellman's reagent, DTNB) in the presence of free sulfhydryls, resulting in the formation of 2-nitro-5-thiobenzoic acid (TNB),[51] which can be easily quantified by absorbance measurements at 412 nm. Thus, following silanization (Fig. 1a-I), the resulting modified $PSiO_2$ was incubated with DTNB and the collected supernatant absorbance was measured. The absorbance values are presented in Fig. 1c and compared to those obtained for neat $PSiO_2$ and an aptamer-functionalized $PSiO_2$. Negligible absorbance was observed for both the neat and the aptamer-functionalized $PSiO_2$ samples, confirming that no free sulfhydryls were present on the surface, before silanization and following aptamer conjugation and blocking with maleimide, respectively. On the contrary, the measured absorbance for the silanized $PSiO_2$ was drastically higher, indicative of successful thiolation of the scaffold. Note that aptamer conjugation to mesoporous $PSiO_2$ was studied using the same methods and similar results as those presented above were observed (data not shown).

Optical biosensing experiments

The Hemag1P-modified $PSiO_2$ biosensors were exposed to *L. acidophilus* suspensions while the reflectivity spectra of the porous film was monitored in real time and the corresponding EOT intensity values were computed. In a typical biosensing experiment, see Fig. 2a, aptamer selection buffer (SB) was first introduced to assure correct folding of the aptamer and to establish the initial intensity baseline on the freshly prepared aptamer-functionalized biosensor. Introduction of *L. acidophilus* suspension (10^7 cells per mL in SB) induced a sharp decrease of approximately 10% in relative intensity due to light scattering by the bacteria cells on the biosensor surface; followed by incubation for 20 min with the suspension to allow proper interaction of the bacteria with the aptamer-decorated surface. The *L. acidophilus* cells targeted by the aptamer Hemag1P possess a typical size of 0.6–0.9 μm in width and 1.5–6 μm in length,[20] thus, they are too large to penetrate into the porous nanostructure and they only reside on the biosensor surface influencing the intensity of reflected light. Subsequent washing of the biosensor with SB was performed to remove unbound species; after which the intensity increased and stabilized at a net intensity decrease value of 5.5%. These results are in agreement with our previous work on direct-capture of *E. coli* with conjugated antibodies[41,43,63] and suggest successful capture of the bacteria onto the biosensor surface. However, the profound increase in the intensity during the washing step suggests that a fairly high amount of cells contained in the sample were not captured by the aptamers. A second washing step however, showed no further change in the optical signal, indicating that the remaining bacteria were tightly bound by the aptamers. Microscope images taken immediately after experiments (see Fig. 2b), reveal a large number of bacteria cells, with a typical morphology of *L. acidophilus* cells, captured onto the biosensor surface.

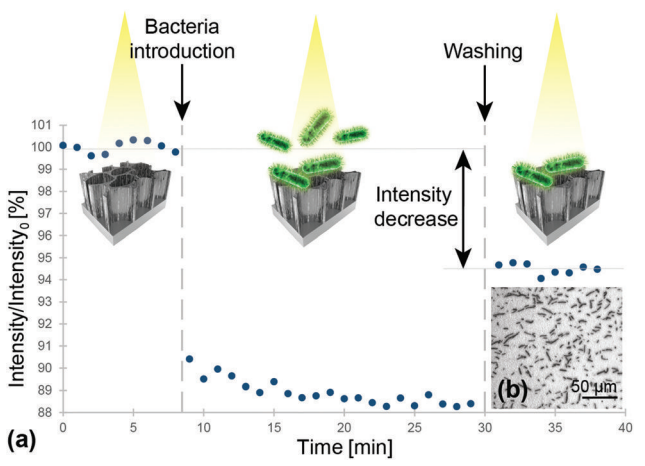

Fig. 2 (a) Relative intensity change of the Hemag1P-modified $PSiO_2$ upon exposure to *L. acidophilus* bacterial suspensions (10^7 cells per mL). First, a baseline was established in SB. After incubation with bacteria suspension, the biosensor was extensively washed before continued signal readout in SB. Note: the intensity values are normalized to the initial average intensity, marked as intensity$_o$. (b) Microscope image taken immediately after the biosensing experiment depicts *L. acidophilus* cells captured onto the aptamer-modified $PSiO_2$.

Numerous replications of these biosensing experiments have demonstrated a similar behavior to that presented in Fig. 2 and a highly reproducible net intensity decrease value of 5.5% (± 0.07%) was achieved. However, attempts to detect 10^6 cells per mL of *L. acidophilus* demonstrated negligible optical response throughout the biosensing experiments.

The aforementioned results demonstrate the successful construction of an aptamer-functionalized PSi biosensor and its successful operation in detecting high bacteria concentrations. While these concentrations are relevant for potential application of this biosensor in the food industry, we aimed to increase the dynamic range of the biosensor. Thus, we tuned the nanostructure of the PSi transducer by reducing the pore diameter to exhibit a mesoporous morphology[54] with improved optical properties[30] (see Table S1, ESI†). Moreover, the increased top surface area (see Fig. S1, ESI†) available for aptamer immobilization may facilitate the interaction between the target bacteria with the capture probe. For the mesoporous PSi transducer, noise-level was considerably reduced although the attained signal was lower (2.4% intensity decrease in comparison to 5.5%), the signal-to-noise ratio has improved significantly (see Fig. S2 and Table S2, ESI†). Based on these results, we have attempted to optimize the performance of the mesoporous PSi in terms of the aptamer surface coverage and spacing. Previous studies have revealed the vital role of the immobilized aptamer surface density, affecting the biosensor response,[64,65] especially in systems where the amount of surface-immobilized capture probes directly correlates with

Results

the biosensor binding capacity (*i.e.* one capture probe can bind one target analyte). However, in this study, as the target is several orders of magnitude larger than the capture probe, it is likely that several aptamers bind one bacteria cell. As we used a relatively high aptamer concentration (*i.e.* 50 μM) to ensure a uniform coverage of the surface, the closely packed aptamers may hamper target cells from capture. The latter is ascribed to the target's limited access to the aptamer as well as to the aptamer's improper folding into secondary structures,[66,67] leading to decreased binding capacity.[7,68] Thus, two strategies for biosensor optimization were employed: lowering of the immobilization density (utilizing 10 μM instead of 50 μM aptamer solution) and optimization of the aptamer sequence, *i.e.* extension of the sequence by ten thymine bases positioned between the aptamer sequence and the 5′ acrydite modification (T_{10}-Hemag1P).

Fig. 3 summarizes the biosensing results for the different aptamer-functionalized mesoporous $PSiO_2$. For the standard Hemag1P sequence as well as the elongated sequence, the optical signals increased at lower aptamer-density (4.9% and 4.5%, respectively) giving rise to the notion that a steric hindrance effect had occurred. At unchanged high aptamer immobilization density (50 μM employed concentration), utilization of T_{10}-Hemag1P has a profound effect and the intensity signal increases from 2.4% (for the standard sequence) to 4.3%. The improved response of the biosensor may be attributed to the enhanced flexibility of the grafted aptamer and its proper folding.[69] However, it should be noted that the unmodified Hemag1P sequence yields more reproducible results (see Fig. 3). The latter is observed for all studied bacteria concentrations. Accordingly, in order to allow reproducible and sensitive *L. acidophilus* detection, we have optimized the concentration of the Hemag1P. We found that lower aptamer concentrations (10 μM) facilitate the detection of 10^6 cells per mL *L. acidophilus* (a net intensity decrease of 0.68% was attained). As a negative control and to exclude possible effects of non-specific interactions between surface immobilized DNA and the bacteria, $PSiO_2$ films conjugated with a non-target 6H7 aptamer, which is directed against his-tagged proteins, and exposed to 10^7 cells per mL *L. acidophilus*. These experiments resulted in inconsistent low intensity changes, indicative of minor adhesion of bacteria cells to the aptamer-decorated surface.[43] Fig. 4 presents micrographs of the biosensors' surface, taken immediately after the biosensing experiments. Dense coverage of cells with a typical *L. acidophilus* morphology were observed (Fig. 4a). HRSEM images (see Fig. 4d) reveal the rod-shaped bacteria cells, with a characteristic length of ~5 μm,[20] nestled on the $PSiO_2$. Bacteria coverage was observed to decrease profoundly upon exposure to lower bacteria concentration (*i.e.* 10^6 cells per mL, see Fig. 4b) in agreement with the lower optical biosensor response. Exposure of $PSiO_2$, decorated with a non-target sequence (6H7 aptamer), to 10^7 cells per mL *L. acidophilus*, reveals a negligible number of cells bound to the surface (see Fig. 4c).

Although the change in pore size of the nanostructure improved the performance of the designed biosensor, the sensitivity is still lacking in comparison to similar biosensor systems. While Massad-Ivanir *et al.* achieved a limit of detection of 10^3 cells per mL of *E. coli* with their antibody-conjugated PSi biosensor;[42] herein, a limit of detection of only 10^6 cells per mL was observed. Nevertheless, it should be taken into consideration that for *L. acidophilus* and other probiotics, a minimum therapeutic daily dose of 10^8–10^9 viable cells is suggested and an intake of 100 g of fermented bioproducts

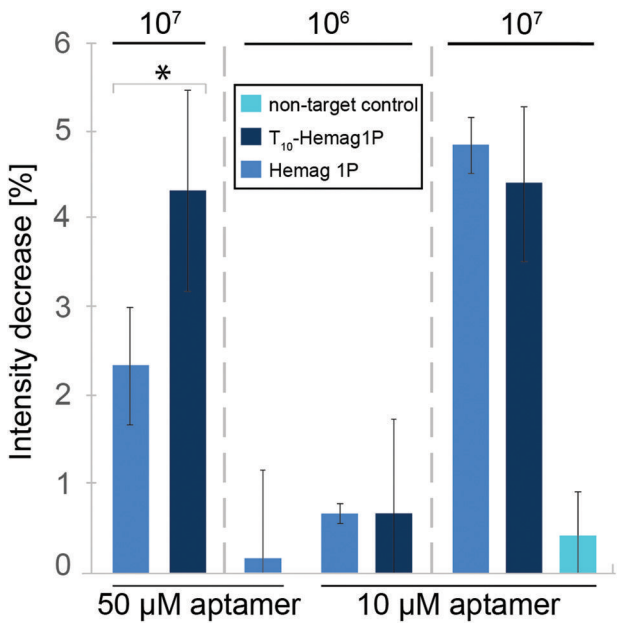

Fig. 3 Optical response upon exposure to 10^6–10^7 cells per mL of the mesoporous biosensor and its optimization. At high aptamer immobilization concentration (50 μM), the Hemag1P-based biosensor yields a reproducible signal upon introduction to 10^7 cells per mL, at lower bacteria concentration, unstable results are obtained. Using the T_{10}-elongated Hemag1P improves the biosensors signal; however, the results deviate significantly (for both 50 and 10 μM). Lower Hemag1P concentration of 10 μM, allows reproducible detection of 10^6–10^7 cells per mL. A negative control experiment with a non-target sequence (6H7 aptamer) results in minor and highly deviating intensity changes. * Statistically significant ($p < 0.05$).

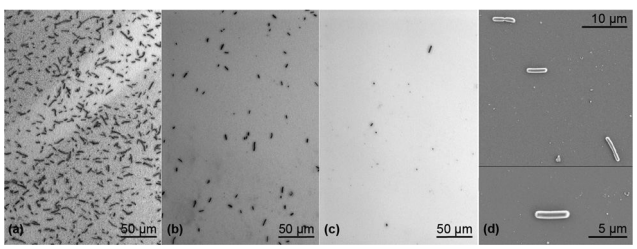

Fig. 4 Microscope images of the mesoporous biosensors, taken immediately after bacteria capture experiments: (a) 10 μM Hemag1P + 10^7 cells per mL *L. acidophilus*; (b) 10 μM Hemag1P + 10^6 cells per mL *L. acidophilus*; (c) 10 μM 6H7 control aptamer + 10^7 cells per mL *L. acidophilus*; (d) HRSEM micrographs of *L. acidophilus* captured on Hemag1P-functionalized $PSiO_2$ biosensor.

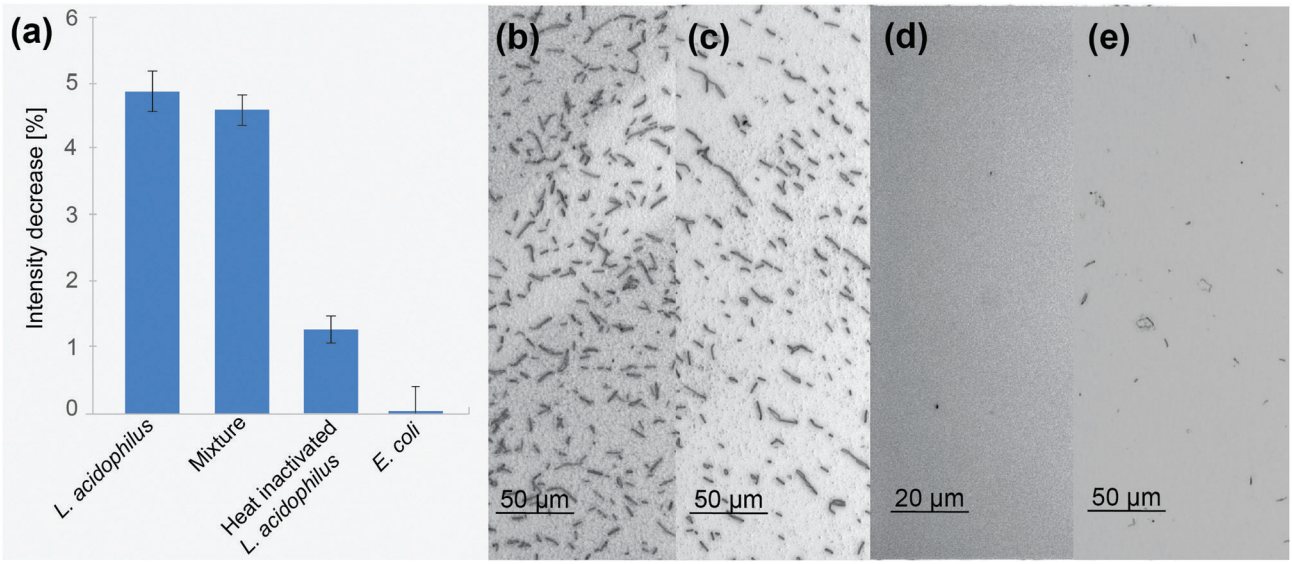

Fig. 5 (a) Optical response (intensity decrease) of the Hemag1P-functionalized biosensor to different bacteria suspensions (containing 10^7 cells per mL). Corresponding microscope images taken immediately after biosensing experiments: (b) 10^7 cells per mL *L. acidophilus*; (c) mixture of 10^7 cells per mL *E. coli* + 10^7 cells per mL *L. acidophilus*, (d) 10^7 cells per mL *E. coli* and (e) 10^7 cells per mL heat inactivated *L. acidophilus*.

with a content of 10^6–10^7 viable cells per mL is recommended.[20,70] Some probiotic products even claim much higher microorganism contents (*e.g.* 10^{11} cells per g in VSL#3 probiotic preparation[71]). Hence, with regard to its possible application, the sensitivity of the presented biosensor lies in the range of relevant concentrations and excels other systems by far in terms of its simplicity, cost, stability and speed of measurement. In the case of applications that necessitate higher sensitivity, integration of our biosensing scheme with a bacteria pre-concentration step,[72] could facilitate detection.

Biosensing in mixtures and heat inactivated samples

One of the main challenges of biosensors is the ability to perform in "real-time", detecting the target analyte in its natural environment, surrounded by interfering molecules.[44,73] To study the ability of the constructed biosensor to selectively bind its target bacteria in the presence of interfering microorganisms and molecules, the biosensor was exposed to a mixed suspension containing 10^7 cells per mL *L. acidophilus* and 10^7 cells per mL *E. coli* in SB. The latter was chosen as model Gram-negative bacteria, displaying a different membrane composition,[74] which is also of high relevancy in the food industry. Fig. 5 presents the obtained optical signals and respective microscope images taken immediately after the biosensing experiments. Herein, all biosensors used were functionalized with 10 µM Hemag1P aptamer. Exposure of a biosensor to a mixture of 10^7 cells per mL *L. acidophilus* and 10^7 cells per mL *E. coli* yielded an average intensity decrease of 4.6%, which is in agreement with the results obtained for pure suspensions of 10^7 cells per mL *L. acidophilus*, see Fig. 5a. This result was also validated by the comparable amount of bound bacteria cells on the biosensors surface as shown in Fig. 5b and c. This demonstrates the ability of the biosensor to distinguish between the different bacteria species and selectively bind the target cells with high accuracy. As a control, the biosensor was also exposed to a suspension of 10^7 cells per mL *E. coli*, resulting in a negligible intensity decrease (Fig. 5a) and no cells were observed on its surface (Fig. 5d).

Another important advantageous characteristic of a biosensor for bacteria detection would be its ability to distinguish between live and dead bacteria.[75,76] To study the response of the Hemag1P-functionalized $PSiO_2$ biosensor upon exposure to dead *L. acidophilus*, we have thermally treated the cell suspensions (15 minutes at 70 °C[48]) prior to biosensing experiments. Fig. 5a displays the biosensor's average intensity decrease upon introduction of these suspensions, revealing their significantly reduced response of 1.5% in comparison to 4.9% for a live culture. This result supports the hypothesis that the Hemag1P aptamer targets the membrane S-protein of the bacteria.[19] When *L. acidophilus* is heat treated, these membrane proteins denature and as a result the aptamer-affinity to the bacteria cells drastically decreases. We suggest that the detected signal may be attributed to a combination of non-specific adsorption of denatured cells and some viable bacteria remaining in the suspensions, see Fig. 5e. This was confirmed by bacterial growth after medium addition to the biosensor. Thus, the biosensor can distinguish between live/dead populations due to the profound difference in its response.

Conclusions

In the presented work, a label-free optical biosensor based on aptamer-functionalized porous Si (Fabry–Pérot thin film) was designed, characterized and optimized. This demonstrates the first label-free detection of *L. acidophilus* with Hemag1P

Results

aptamer as capture probe at relevant concentrations for probiotic intake.[20] Exposure to the target suspensions and mixed bacterial populations resulted in highly robust and reproducible changes in the optical reflectivity of the biosensor, given that the bacteria are viable. Control experiments revealed negligible binding of non-target species, confirming the excellent selectivity of this aptamer-based biosensor. Other important advantages of this biosensor are its ability to distinguish between live and dead target bacteria populations, as well as the short total assay time of less than one hour. Biosensing schemes for the rapid and label-free monitoring of live *L. acidophilus* are highly relevant for the functional food and pharmaceutical industry.[70,77] These products become increasingly popular as the importance of the human microbiome and its influence on a variety of diseases is revealed.[78,79] However, live bacteria cultures are essential for their probiotic activity.[70,80] Finally, the availability of other species-targeting aptamers enables to implement this biosensing concept to facilitate the fast detection and identification of bacteria species in a simple and reliable manner, overcoming the need for time-consuming and unspecific culturing techniques as well as assays requiring highly sophisticated instruments.

Acknowledgements

This work was funded by the German Research Foundation under the grant SCHE 279/32-1. ES, SA and KU acknowledge the core services and support from the Lorry I. Lokey Center for Life Science and Engineering.

Notes and references

1 C. Tuerk and L. Gold, *Science*, 1990, **249**, 505–510.
2 A. D. Ellington and J. W. Szostak, *Nature*, 1990, **346**, 818–822.
3 S. Song, L. Wang, J. Li, C. Fan and J. Zhao, *Trends Anal. Chem.*, 2008, **27**, 108–117.
4 C. L. A. Hamula, H. Zhang, F. Li, Z. Wang, X. Chris Le and X.-F. Li, *Trends Anal. Chem.*, 2011, **30**, 1587–1597.
5 M. Lönne, G. Zhu, F. Stahl and J.-G. Walter, in *Biosensors Based on Aptamers and Enzymes*, ed. M. B. Gu and H.-S. Kim, Springer, Berlin, Heidelberg, 2014, ch. 231, vol. 140, pp. 121–154.
6 G. Zhu, M. Lübbecke, J. Walter, F. Stahl and T. Scheper, *Chem. Eng. Technol.*, 2011, **34**, 2022–2028.
7 J. G. Walter, O. Kökpinar, K. Friehs, F. Stahl and T. Scheper, *Anal. Chem.*, 2008, **80**, 7372–7378.
8 R. Nezlin, *Mol. Immunol.*, 2016, **70**, 149–154.
9 M. Ilgu and M. Nilsen-Hamilton, *Analyst*, 2016, **141**, 1551–1568.
10 K. Sefah, J. A. Phillips, X. Xiong, L. Meng, D. Van Simaeys, H. Chen, J. Martin and W. Tan, *Analyst*, 2009, **134**, 1765–1775.
11 R. A. Potyrailo, A. J. Murray, N. Nagraj, A. D. Pris, J. M. Ashe and M. Todorovic, *Angew. Chem., Int. Ed.*, 2015, **54**, 2174–2178.
12 A. C. A. Roque, C. R. Lowe and M. Â. Taipa, *Biotechnol. Prog.*, 2004, **20**, 639–654.
13 H. M. So, D. W. Park, E. K. Jeon, Y. H. Kim, B. S. Kim, C. K. Lee, S. Y. Choi, S. C. Kim, H. Chang and J. O. Lee, *Small*, 2008, **4**, 197–201.
14 H. P. Dwivedi, R. D. Smiley and L. A. Jaykus, *Appl. Microbiol. Biotechnol.*, 2010, **87**, 2323–2334.
15 F. Chen, J. Zhou, F. Luo, A. B. Mohammed and X. L. Zhang, *Biochem. Biophys. Res. Commun.*, 2007, **357**, 743–748.
16 X. Cao, S. Li, L. Chen, H. Ding, H. Xu, Y. Huang, J. Li, N. Liu, W. Cao, Y. Zhu, B. Shen and N. Shao, *Nucleic Acids Res.*, 2009, **37**, 4621–4628.
17 G. Singh, P. Vajpayee, N. Rani, A. Jyoti, K. C. Gupta and R. Shanker, *Ecotoxicol. Environ. Saf.*, 2012, **78**, 320–326.
18 M. Citartan, E.-S. Ch'ng, T. S. Rozhdestvensky and T.-H. Tang, *Microchem. J.*, 2016, **128**, 187–197.
19 C. L. Hamula, H. Zhang, L. L. Guan, X. F. Li and X. C. Le, *Anal. Chem.*, 2008, **80**, 7812–7819.
20 A. M. P. Gomes and F. X. Malcata, *Trends Food Sci. Technol.*, 1999, **10**, 139–157.
21 N. P. Shah, *Int. Dairy J.*, 2007, **17**, 1262–1277.
22 C. Zhang, X. Lv, H. Qing, L. Geng and Y. Deng, 2013 ICME International Conference on Complex Medical Engineering (CME), 2013.
23 P. Zuo, X. Li, D. C. Dominguez and B.-C. Ye, *Lab Chip*, 2013, **13**, 3921–3928.
24 L. De Stefano, P. Arcari, A. Lamberti, C. Sanges, L. Rotiroti, I. Rea and I. Rendina, *Sensors*, 2007, **7**, 214–221.
25 C. Pacholski, *Sensors*, 2013, **13**, 4694–4713.
26 A. Jane, R. Dronov, A. Hodges and N. H. Voelcker, *Trends Biotechnol.*, 2009, **27**, 230–239.
27 K. A. Kilian, T. Bocking and J. J. Gooding, *Chem. Commun.*, 2009, **0**, 630–640.
28 S. D. Alvarez, M. P. Schwartz, B. Migliori, C. U. Rang, L. Chao and M. J. Sailor, *Phys. Status Solidi A*, 2007, **204**, 1439–1443.
29 K.-P. S. Dancil, D. P. Greiner and M. J. Sailor, *J. Am. Chem. Soc.*, 1999, **121**, 7925–7930.
30 A. Janshoff, K. P. S. Dancil, C. Steinem, D. P. Greiner, V. S. Y. Lin, C. Gurtner, K. Motesharei, M. J. Sailor and M. R. Ghadiri, *J. Am. Chem. Soc.*, 1998, **120**, 12108–12116.
31 M. M. Orosco, C. Pacholski, G. M. Miskelly and M. J. Sailor, *Adv. Mater.*, 2006, **18**, 1393–1396.
32 C. Pacholski, C. Yu, G. M. Miskelly, D. Godin and M. J. Sailor, *J. Am. Chem. Soc.*, 2006, **128**, 4250–4252.
33 M. P. Schwartz, A. M. Derfus, S. D. Alvarez, S. N. Bhatia and M. J. Sailor, *Langmuir*, 2006, **22**, 7084–7090.
34 M. P. Schwartz, S. D. Alvarez and M. J. Sailor, *Anal. Chem.*, 2006, **79**, 327–334.
35 J. Zhang, Y. Wu, B. Zhang, M. Li, S. Jia, S. Jiang, H. Zhou, Y. Zhang, C. Zhang and A. P. F. Turner, *Anal. Lett.*, 2012, **45**, 986–992.

Results

36 B. Gupta, Y. Zhu, B. Guan, P. J. Reece and J. J. Gooding, *Analyst*, 2013, **138**, 3593–3615.
37 E. Tenenbaum, N. Ben-Dov and E. Segal, *Langmuir*, 2015, **31**, 5244–5251.
38 C. K. Tsang, T. L. Kelly, M. J. Sailor and Y. Y. Li, *ACS Nano*, 2012, **6**, 10546–10554.
39 C. Pacholski, M. Sartor, M. J. Sailor, F. Cunin and G. M. Miskelly, *J. Am. Chem. Soc.*, 2005, **127**, 11636–11645.
40 G. Gaur, D. S. Koktysh and S. M. Weiss, *Adv. Funct. Mater.*, 2013, **23**, 3604–3614.
41 N. Massad-Ivanir, G. Shtenberg, A. Tzur, M. A. Krepker and E. Segal, *Anal. Chem.*, 2011, **83**, 3282–3289.
42 N. Massad-Ivanir, G. Shtenberg, T. Zeidman and E. Segal, *Adv. Funct. Mater.*, 2010, **20**, 2269–2277.
43 E. Tenenbaum and E. Segal, *Analyst*, 2015, **140**, 7726–7733.
44 K. Urmann, J.-G. Walter, T. Scheper and E. Segal, *Anal. Chem.*, 2015, **87**, 1999–2006.
45 K. Urmann, E. Tenenbaum, J. G. Walter and E. Segal, in *Electrochemically Engineered Nanoporous Materials Methods, Properties and Applications*, ed. D. Losic and A. Santos, Springer, 2015, pp. 93–116.
46 S. A. Doyle and M. B. Murphy, *US Patent*, 0142582A1, 2005.
47 S. P. Riley, M. E. Woodman and B. Stevenson, *in Current Protocols Essential Laboratory Techniques*, John Wiley & Sons, Inc., 2008, DOI: 10.1002/9780470089941.et0402s00.
48 C. J. Bunthof, K. Bloemen, P. Breeuwer, F. M. Rombouts and T. Abee, *Appl. Environ. Microbiol.*, 2001, **67**, 2326–2335.
49 M. J. Sailor, *Porous silicon in practice: preparation, characterization and applications*, John Wiley & Sons, 2012.
50 E. Segal, L. A. Perelman, F. Cunin, F. Di Renzo, J. M. Devoisselle, Y. Y. Li and M. J. Sailor, *Adv. Funct. Mater.*, 2007, **17**, 1153–1162.
51 G. L. Ellman, *Arch. Biochem. Biophys.*, 1959, **82**, 70–77.
52 G. Weiss, S. Rasmussen, L. H. Zeuthen, B. N. Nielsen, H. Jarmer, L. Jespersen and H. Frøkiær, *Immunology*, 2010, **131**, 268–281.
53 K. Kiviharju, M. Leisola and N. von Weymarn, *Biotechnol. Lett.*, 2004, **26**, 539–542.
54 D. R. Thevenot, K. Toth, R. A. Durst and G. S. Wilson, *Biosens. Bioelectron.*, 2001, **16**, 121–131.
55 P. J. Knerr, A. Tzekou, D. Ricklin, H. Qu, H. Chen, W. A. van der Donk and J. D. Lambris, *ACS Chem. Biol.*, 2011, **6**, 753–760.
56 I. D. Technlogies, 2014, Technical report available from www.idtdna.com.
57 Z. Li, Y. Chen, X. Li, T. I. Kamins, K. Nauka and R. S. Williams, *Nano Lett.*, 2004, **4**, 245–247.
58 J. Zhou and J. J. Rossi, *Mol. Ther. –Nucleic Acids*, 2014, **3**, e169.
59 T. S. P. Cellet, M. R. Guilherme, R. Silva, G. M. Pereira, M. R. Mauricio, E. C. Muniz and A. F. Rubira, *J. Colloid Interface Sci.*, 2012, **367**, 494–501.
60 A. M. Peterson, R. E. Jensen and G. R. Palmese, *Compos. Sci. Technol.*, 2011, **71**, 586–592.
61 H. Ishida and S. Ohba, *Polymer*, 2005, **46**, 5588–5595.
62 R. Voicu, R. Boukherroub, V. Bartzoka, T. Ward, J. T. C. Wojtyk and D. D. M. Wayner, *Langmuir*, 2004, **20**, 11713–11720.
63 N. Massad-Ivanir, G. Shtenberg and E. Segal, *J. Visualized Exp.*, 2013, e50805, DOI: 10.3791/50805.
64 R. J. White, N. Phares, A. A. Lubin, Y. Xiao and K. W. Plaxco, *Langmuir*, 2008, **24**, 10513–10518.
65 T. Doneux, A. De Rache, E. Triffaux, A. Meunier, M. Steichen and C. Buess-Herman, *ChemElectroChem*, 2014, **1**, 147–157.
66 R. Zheng, B.-W. Park, D.-S. Kim and B. D. Cameron, *Biomed. Opt. Express*, 2011, **2**, 2731–2740.
67 A. M. Giovannozzi, C. Renacco, M. Derosas, E. Enrico, A. Farano and A. M. Rossi, *Phys. Status Solidi C*, 2011, **8**, 1878–1882.
68 Z. Yang, E. Castrignanò, P. Estrela, C. G. Frost and B. Kasprzyk-Hordern, *Sci. Rep.*, 2016, **6**, 21024.
69 C. Daniel, Y. Roupioz, D. Gasparutto, T. Livache and A. Buhot, *PLoS One*, 2013, **8**, e75419.
70 K. Kailasapathy and J. Chin, *Immunol. Cell Biol.*, 2000, **78**, 80–88.
71 A. Venturi, P. Gionchetti, F. Rizzello, R. Johansson, E. Zucconi, P. Brigidi, D. Matteuzzi and M. Campieri, *Aliment. Pharmacol. Ther.*, 1999, **13**, 1103–1108.
72 X. Xie, J. Bahnemann, S. Wang, Y. Yang and M. R. Hoffmann, *Sci. Rep.*, 2016, **6**, 20516.
73 G. A. Zelada-Guillén, S. V. Bhosale, J. Riu and F. X. Rius, *Anal. Chem.*, 2010, **82**, 9254–9260.
74 W. W. Navarre and O. Schneewind, *Microbiol. Mol. Biol. Rev.*, 1999, **63**, 174–229.
75 C. Lui, N. C. Cady and C. A. Batt, *Sensors*, 2009, **9**, 3713–3744.
76 A. Singh, S. Poshtiban and S. Evoy, *Sensors*, 2013, **13**, 1763.
77 D. C. Lin, *Nutr. Clin. Pract.*, 2003, **18**, 497–506.
78 D. Knights, M. Silverberg, R. Weersma, D. Gevers, G. Dijkstra, H. Huang, A. Tyler, S. van Sommeren, F. Imhann, J. Stempak, H. Huang, P. Vangay, G. Al-Ghalith, C. Russell, J. Sauk, J. Knight, M. Daly, C. Huttenhower and R. Xavier, *Genome Med.*, 2014, **6**, 1–11.
79 M. C. Cénit, V. Matzaraki, E. F. Tigchelaar and A. Zhernakova, *Biochim. Biophys. Acta*, 2014, **1842**, 1981–1992.
80 P. S. Yeung, M. E. Sanders, C. L. Kitts, R. Cano and P. S. Tong, *J. Dairy Sci.*, 2002, **85**, 1039–1051.

Electronic Supplementary Information

WHOLE-CELL DETECTION OF LIVE LACTOBACILLUS ACIDOPHILUS ON APTAMER-DECORATED POROUS SILICON BIOSENSORS

*Katharina Urmann[1,2], Sofia Arshavsky-Graham[2], Johanna-Gabriela Walter[1], Thomas Scheper[1], Ester Segal[2]**

[1] Institute of Technical Chemistry, Leibniz University of Hannover, Callinstr. 5, 30167 Hannover, Germany

[2] Department of Biotechnology and Food Engineering, Technion Israel Institute of Technology, Technion City, 32000 Haifa, Israel; phone: +972-4-8295071; e-mail: esegal@tx.technion.ac.il

* Corresponding author

Table S1. Results of $PSiO_2$ scaffold characterization.

Etching conditions		**HRSEM**		**Gravimetry**	**SLIM**	
Etching time (s)	Current density (mA/cm^2)	Pore Diameter (nm)	Thickness (nm)	Total Porosity (%)	Open Porosity (%)	Thickness (nm)
30	300	65 ± 10	5440 ± 80	78 ± 1	79 ± 1	4975 ± 88
375	24	25 ± 5	-	54.6 ± 1	52 ± 1	5172 ± 57

Porous Si films were tuned in terms of pore size and thus porosity, in order to improve optical properties. Smaller pore sizes result in a higher number of reflection interferences as the light beam is reflected on more pore walls which is represented by a higher number of Fabry-Pérot fringes in the sample reflectivity spectrum [1, 2]. In the electrochemical etching process of porous silicon, pore diameter decreases with decreasing current density. In order to change this parameter, but not the thickness of the porous film, the product of current density and etch time has to be kept in the same range so that the total charge passing through the sample stays constant [3, 4]. Therefore, the current density was lowered to 24 mA/cm^2 and the etch duration was extended accordingly to 375 seconds. The characterization of the resulting new $PSiO_2$ scaffold is presented in Table S1. Figure S1 shows HRSEM images of both the original macroporous structure and the tuned mesoporous PSi revealing the differences in pore size. The average pore diameter in the mesoporous transducer was reduced to 25±5 nm (as determined by HRSEM) while the average thickness of the porous layer was nearly unchanged (as determined by SLIM). In addition, the porosity of the porous layer was reduced, suggesting increased free surface area as expected.

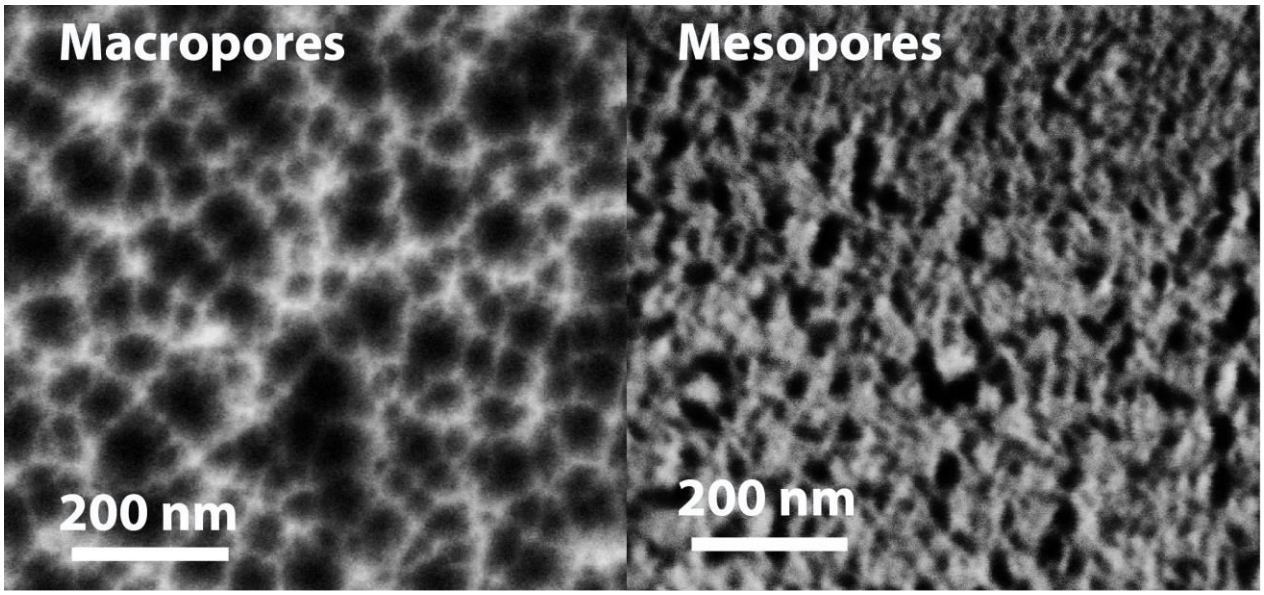

Fig S1. HRSEM top-view micrographs of porous silicon films obtained from etching conditions as listed in Table S1.

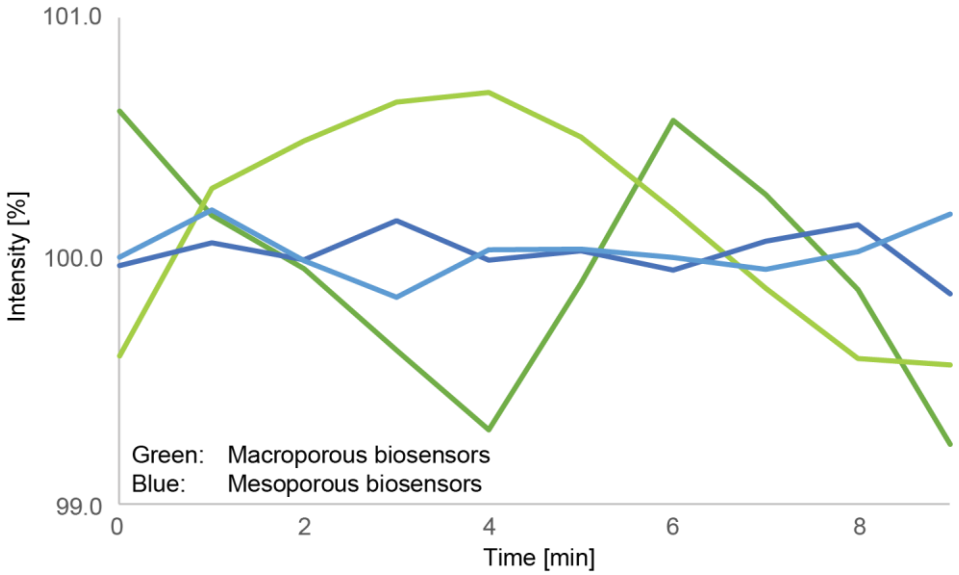

Fig S2. Typical baselines of aptamer-functionalized biosensors in SB prior to incubation with bacteria suspensions. Macroporous biosensors (green lines) show higher standard deviations between the measurements while the noise for mesoporous structures (blue lines) is significantly reduced.

Table S2. Signal-to-noise ratios calculated from baseline standard deviations and obtained biosensing signals with 10^7 cells/mL.

Biosensor structure	**Average noise** (%)	**Average signal (for 10^7 cells/mL)** (%)	**Signal-to-noise ratio**
Macroporous	0.5	5.5	11
Mesoporous	0.1	2.4	24

References:

1. S. Jang, *J. Chosun Natural Sci*, 2011, 5, 13-17.
2. M. J. Sailor, *Porous silicon in practice: preparation, characterization and applications*, John Wiley & Sons, 2012.
3. M. J. Sailor and E. C. Wu, *Advanced Functional Materials*, 2009, 19, 3195-3208.
4. E. Segal, L. A. Perelman, F. Cunin, F. DiRenzo, J. M. Devoisselle, Y. Y. Li and M. J. Sailor, *Advanced Functional Materials*, 2007, 17, 1153-1162.

5.3 Rapid and label-free detection of Protein A

In this work, we extend the examination of a RIFTS protein biosensor beyond the linear detection range. For the capture of protein A, which is a virulence factor secreted by and displayed on the cell membrane of *Staphylococcus aureus*, by a protein A-binding aptamer, we present a thorough characterization of the binding behavior and consequent modeling with the three variable Hill equation. The specific detection of protein A is a valuable tool in the fast identification and battle against infections, as it is an important biomarker for the presence of *S. aureus* which often develops methicillin-resistance. Herein, we present the simple, label-free and rapid optical detection of protein A with minimal instrumentation. We determine the system-specific apparent dissociation constant K_D at the protein concentration corresponding to the half-maximum biosensor response, extract the Hill coefficient providing information about the number of binding sites and we calculate the limit of detection as well as resolution of the biosensor system. Furthermore, to reduce the protein A concentrations necessary for a significant signal, we harness the affinity between protein A and antibodies and demonstrate a sandwich assay that enables protein A detection at concentrations as low as 1 µM.

RAPID AND LABEL-FREE DETECTION OF PROTEIN A BY APTAMER-TETHERED POROUS SILICON NANOSTRUCTURES

Katharina Urmann[a,b,‡], *Peggy Reich*[a,c,‡], *Johanna-Gabriela Walter*[a], *Dieter Beckmann*[c], *Ester Segal*[b]*, *Thomas Scheper*[a]*

‡ Equal contribution, * Corresponding authors

[a] Institute of Technical Chemistry, Leibniz Universität Hannover, Callinstr. 5, 30167 Hanover, Germany; phone: +49-511-7622269; e-mail: scheper@iftc.uni-hannover.de

[b] Department of Biotechnology and Food Engineering, Technion Israel Institute of Technology, Technion City, 32000 Haifa, Israel; phone: +972-4-8295071; e-mail: esegal@tx.technion.ac.il

[c] Institute for Bioprocessing and Analytical Measurement Techniques e.V., Rosenhof, 37308 Heilbad Heiligenstadt, Germany

KEYWORDS

Optical Biosensor, Aptamer, Porous Silicon, Label-Free, Protein A, *Staphylococcus aureus*

ABSTRACT

Protein A, which is secreted by and displayed on the cell membrane of *Staphylococcus aureus* is an important biomarker for *S. aureus*. Thus, its rapid and specific detection may facilitate the pathogen identification and initiation of proper treatment. Herein, we present a simple, label-free and rapid optical biosensor enabling specific detection of protein A. Protein A-binding aptamer serves as the capture probe and is immobilized onto a nanostructured porous silicon thin film, which serves as the optical transducer element. We demonstrate high sensitivity of the biosensor with a linear detection range between 8-23 μM. The apparent dissociation constant was determined as 13.98 μM and the LoD is 3.17 μM. Harnessing the affinity between protein A and antibodies, a sandwich assay format was developed to amplify the optical signal associated with protein A capture by the aptamer. Using this approach, we increase the sensitivity of the biosensor, resulting in a three times lower LoD.

1. INTRODUCTION

Staphylococcus aureus is a leading cause of infections and bacteremia in humans, but also causing food-borne diseases due to excretion of several enterotoxins[1]. Treatment is especially challenging as *S. aureus* has a remarkable ability to rapidly adapt its genetic characteristics and develop resistance against new antibiotics[2,3]. Hence, the most efficient way to fight *S. aureus* infections is to prevent their transmission by isolation, decontamination and strict hygienic guidelines. Moreover, studies have concluded that active screening for methicillin-resistant *Staphylococcus aureus* (MRSA) can efficiently reduce bloodstream infections, which results in high mortality[4,5].

Rapid and reliable detection and identification of MRSA is critical for effective infection control as well as for therapeutic decisions. Traditional culturing techniques using selective media are sensitive and cost-effective, but are time-consuming (several days) and therefore problematic[6,7]. Molecular methods based on polymerase chain reaction (PCR) exhibit faster turnaround times (~2-6 h) and are considered the gold standard for MRSA detection nowadays; however, they are cost-intense, require trained staff and may not keep up with new evolving genetic variants[8]. A rapid user-friendly point-of-care test for *S. aureus* is thus urgently needed to allow fast screening of patient samples and provide effective infection control.

Protein A, a virulence factor specific for *S. aureus*, is linked to peptidoglycans on the bacterial cell surface and promotes general surface adhesion[9]. Protein A binds to the von Willebrand factor (vWF), an essential protein for hemostasis, and therefore promotes wound infection. It also binds the Fc-region of human antibodies, thereby inhibiting phagocytosis, which in consequence prevents bacterial elimination[10,11]. Real-time PCR for

typing and detection of different *S. aureus* variants utilizes the specific spa gene, encoding protein A. As the gene is highly conserved, showing one mutation in 70 months[12], protein A provides an optimal molecular marker for the detection of *S. aureus*. Several assays, mostly ELISA (Enzyme Linked Immunosorbent Assay) based, for the detection of protein A using antibodies have been developed[13] and are commercially available. While these labeled techniques are highly sensitive, they suffer from several limitations, which are ascribed to the complicated required equipment and the delicate nature of the antibody receptor and its costs[14,15].

Aptamers are single-stranded DNA or RNA oligonucleotides with the ability to specifically bind their target due to their unique 3-dimensional structure. Aptamers are selected *in vitro* for a specific target using the Systematic Evolution of Ligands by Exponential Enrichment (SELEX) process[16]. Aptamers can be engineered towards specific targets, ranging from small molecules or proteins to whole cells, and synthesized with high reproducibility and at a fraction of the cost of antibodies[14,17,18]. Thus, due to these advantageous properties, a variety of aptamer-based analytical methods and biosensors have been developed in recent years, also for the detection of *S. aureus*[19-22]. Lian et al. developed a piezoelectric sensor employing *S. aureus* aptamer and demonstrated detection at bacterial concentrations as low as 59 CFU/mL in milk samples[23]. The aptamer they used was selected against *S. aureus* whole cells and as such, the molecular binding site of the aptamer on the cell surface is unknown[24]. Since *S. aureus* has many variants and is evolving quickly, the aptamer may lose its affinity, thereby limiting the applicability of this method[12].

Recently, the Strehlitz group has developed a modified SELEX process, termed FluMag-SELEX, wherein the target is immobilized on magnetic beads and fluorescent labels are

used for aptamer quantification[25]. Using this process, they selected an aptamer binding protein A with high affinity and demonstrated that it binds specifically to both, native and recombinant protein A, but not to other immunoglobulin-binding proteins like protein G.

Herein, we use the this aptamer as a receptor for the design of a label-free optical biosensor. The biosensor is based on a porous silicon (PSi) nanostructure which is used as the optical transducer. PSi-based optical biosensors have demonstrated outstanding performance in terms of rapid and reliable detection of numerous targets[26-29]. Specifically, biosensors employing interferometric Fourier transform spectroscopy (RIFTS)[30-32], which harness the series of Fabry-Pérot interference fringes from light reflections from the top and bottom interfaces of a porous thin film, allow for the design of simple and sensitive detection of a specific analyte upon its binding to surface-tethered capture probes[33-35]. Recently, the excellent integration of aptamers as capture probes with PSi-based transducers has been demonstrated, enabling exceptionally stable and reliable biosensing, applicable for both, proteins and bacteria[36-38].

In the present study, protein A-targeting aptamers are conjugated to PSi thin films and the resulting biosensors demonstrate a specific detection and quantification of protein A in a range of 2 to 50 μM with a total assay time of < 2 h. The biosensing scheme is further optimized and we show a measured limit of detection (LoD) of 1 μM.

2. MATERIAL AND METHODS

2.1 Materials

Heavily boron doped p-type Si wafers (0.0008 Ω·cm resistivity, <100>-oriented) were purchased from Sil'tronix Silicon Technologies (France). Aqueous HF (48%) and ethanol

absolute were obtained from Merck and toluene and acetone were supplied by Gadot Biochemical Industries LTD (Israel). (3-aminopropyl)-triethoxysilane (APTES), succinic acid, *N*-(3-Dimethylaminopropyl)-*N*-ethylcarbodiimide hydrochloride (EDC) and all buffer salts were purchased from Sigma-Aldrich Chemicals. Buffers were prepared with deionized water (18.2 MΩ cm), filtered and autoclaved prior to use. The protein A-binding aptamer, selected by Stoltenburg et al.[39] was used in its truncated form PA#2/8[S1-58]: 5'-ATA CCA GCT TAT TCA ATT AGC AAC ATG AGG GGG ATA GAG GGG GTG GGT TCT CTC GGC T - 3'(abbreviated as PAA). Its selection buffer (SB) was composed of 20 mM Tris, 100 mM NaCl, 5 mM KCl, 10 mM $MgCl_2$, and 1 mM $CaCl_2$. MES buffer was composed of 100 mM 2-Morpholinoethanesulfonic acid at pH 6. PAA and a completely randomized 40 nucleotides long DNA-Pool (N_{40}) were purchased with a 3'-amino-C6- modification from Integrated DNA Technologies (Coralville, USA). Proteins for biosensing experiments included recombinant protein A (PA) and IgG from human serum (both from Sigma-Aldrich Chemicals). As Tween 20 enhances protein solubility, all proteins solutions were prepared in SB supplemented with 0.005% Tween 20 (SBT).

2.2 Preparation of Oxidized PSi

Si wafers were anodized in a two-step process. First, a sacrificial layer was etched at a constant current density of 375 mA/cm^2 for 30 s in a solution of 3:1 (v/v) aqueous HF (48%) and ethanol. Etching setup details are reported elsewhere[30,40]. The resulting PSi layer was dissolved in an aqueous NaOH solution (0.1 M). Next, a second etching step was performed using the above-mentioned conditions. After each step, the silicon surface was thoroughly rinsed with ethanol and dried under a stream of nitrogen. Finally, the PSi

samples were thermally oxidized in a tube furnace (Thermolyne) at 800 °C for 1 h in ambient air, yielding oxidized PSi ($PSiO_2$) scaffolds.

2.3 Characterization of $PSiO_2$ Films

The nanostructure and the thickness of the neat $PSiO_2$ samples were studied by a Carl Zeiss Ultra Plus high-resolution scanning electron microscopy (HRSEM) at an accelerating voltage of 1 keV. The porosity of the films was characterized by gravimetry (for porosity), and the spectroscopic liquid infiltration method (SLIM)[30], as described by Massad-Ivanir *et al.*[41].

2.4 Aptamer Immobilization onto $PSiO_2$ Films

The aptamer was conjugated to the $PSiO_2$ films by a previously described coupling chemistry[36]. Briefly, the $PSiO_2$ was amino-modified by incubation (1 h) in a solution of APTES in toluene (42 mM); after which, the samples were rinsed with toluene, ethanol and acetone and dried under a nitrogen stream. Next, the $PSiO_2$ was incubated for 30 min in a freshly prepared solution of 100 mg succinic acid in 4.7 mL DMSO and 300 µL of 0.1 M $NaHCO_3$, pH 9.4 and subsequently washed with DMSO and deionized water. Successive chemical modifications were carried out in a custom made Plexiglas flow cell[36]. A 52 mM solution of EDC in MES was introduced into the flow cell and allowed to react for 1 h. Next, 50 µL of the aptamer solution (75 µM in MES) was introduced and incubated with the surface for 1 h, followed by washing with 10 mL MES. Finally, the surface was incubated for 30 min with 300 µL of 0.1 M ethanolamine solution to block remaining active sites.

2.5 Infrared Spectroscopy

Surface modification steps were followed with attenuated total reflectance Fourier transform infrared (ATR-FTIR) spectroscopy. Spectra were recorded using a Thermo 6700 FTIR instrument equipped with a Smart iTR diamond ATR device.

2.6 Measurement of Interferometric Reflectance Spectra and Protein Biosensing

The experimental setup for optical measurements and biosensing experiments is schematically illustrated in Figure 1A. The sample was mounted in a fixed flow cell to ensure that data is collected from the same spot during the entire course of measurements. Reflectivity spectra were collected by an Ocean Optics charge-coupled device (CCD) USB 4000 spectrometer coupled to a microscope objective lens with a bifurcated fiber-optic cable. A tungsten light source was connected to the second port of the fiber-optic cable and the light spot was focused onto the center of the $PSiO_2$ sample (spot size 1-2 mm^2). Surface illumination and detection of the reflected light were both performed along an axis coincident with the surface normal. Spectra were continuously recorded every 30 s at a spectral acquisition time of 100 ms and in the wavelength range of 400-1000 nm. The raw spectra (see Fig. 1B-1) were processed in real time by applying Fast Fourier Transformation (FFT). The FFT spectra, shown in Fig. 1B-2, depict a single peak, whose location along the x-axis corresponds to the effective optical thickness (EOT) of the film. The latter equals 2nL, where n is the effective refractive index and L is the physical thickness of the porous film.

Prior to biosensing experiments, the PAA-modified $PSiO_2$ were rinsed with boiling deionized water to unfold any secondary structures in the oligonucleotide and followed by incubation in SB to allow functional folding of the aptamer. In a typical biosensing experiment, a baseline was recorded in SB followed by introduction of the protein

dissolved in SBT (100 µL) and incubation for 1 h. Next, the protein solution was removed and the biosensor was rinsed extensively with SB (10 mL). Reflectivity spectra were recorded every 30 s throughout the entire experiment and data are presented as the relative change of EOT in respect to a baseline value (as depicted in Fig. 1B-3). Please note that during buffer exchange and rinsing steps, EOT measurements were shortly paused to allow a thorough washing of the biosensor and the flow cell.

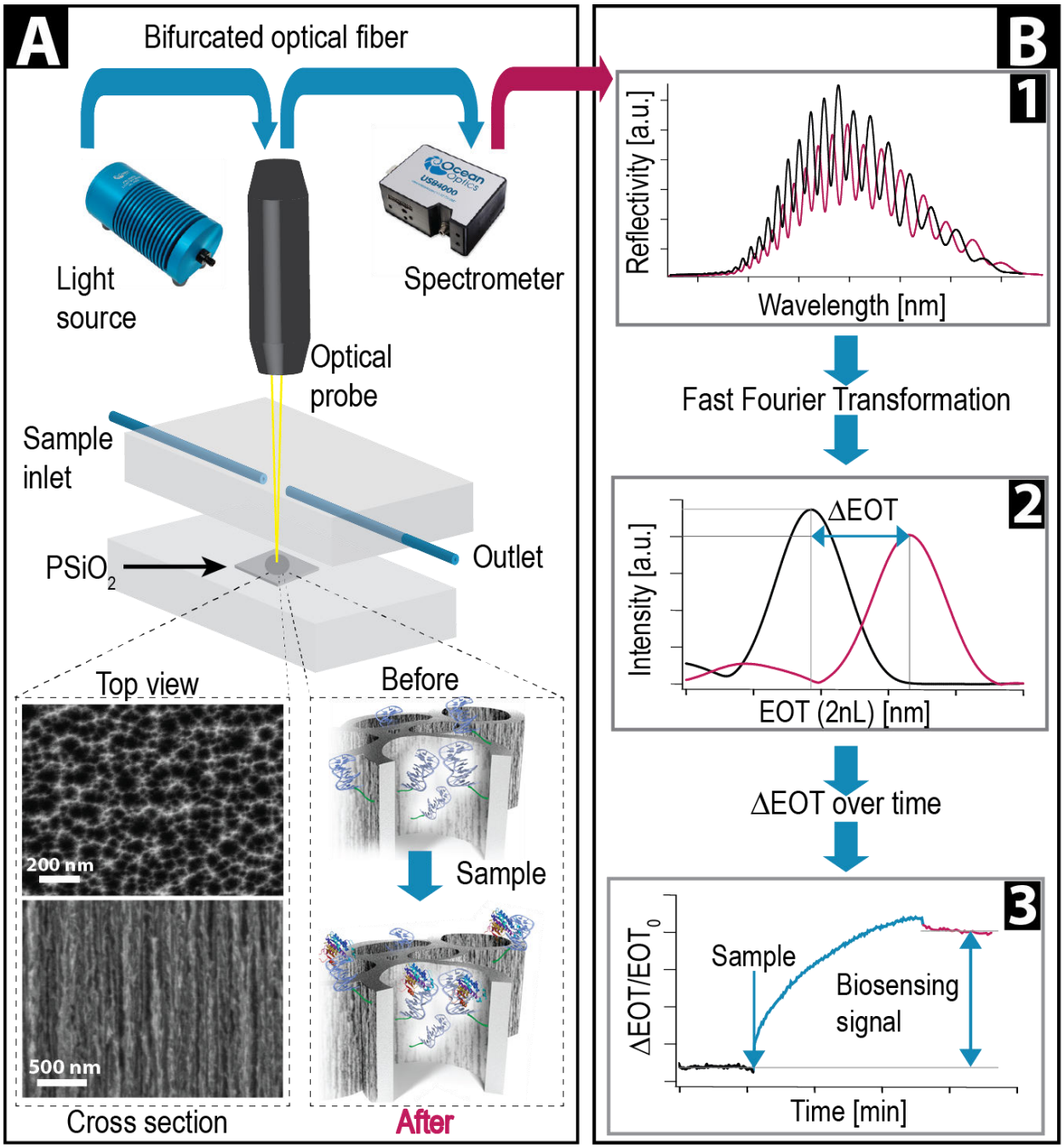

Figure 1. A: Schematic illustration of the experimental setup, depicting instrumentation and flow-cell configuration. The lower panels show HRSEM micrographs of porous silicon nanostructures (left) and schematics of aptamer-functionalized $PSiO_2$ before and after target capture (right). **B:** Reflectivity collection and processing steps. Reflectivity spectra

were recorded (1) and a Fast Fourier transformation was applied (2). The signal was then expressed as the relative change in EOT over the course of the experiment (3). The final biosensing result was extracted as the relative change in EOT before and after exposure of the aptamer-functionalized $PSiO_2$ scaffold to the sample solution (3).

2.7 Statistical and regression analysis

For statistical analysis, unpaired t-tests were performed. Resulting two-tailed P values below 0.05 were required to consider the compared groups as significantly different from each other. Non-linear regressions were performed using SigmaPlot software (Systat Software, Inc).

3. RESULTS AND DISCUSSION

3.1 Functionalization of $PSiO_2$ Films with Amino-Modified Aptamers

Porous silicon thin films were prepared from heavily boron-doped p-type crystalline Si wafers by anodization at a constant current of 375 mA/cm^2 for 30 s. In order to stabilize the PSi nanostructure and to render it more hydrophilic, the films were thermally oxidized for 1 h at 800 °C[42]. The thickness of the resulting films, as determined from HRSEM studies, is ~5500 nm and their morphology (see Fig. 1A, bottom panel) is characterized by interconnected cylindrical pores with pore size ranging between 35 and 65 nm. The porosity of the films is 70%, calculated based on SLIM and gravimetry experiments (data not shown). Thus, the film's nanostructure provides a high surface area and large porous volume for proper infiltration of biomolecules (e.g., the diameter of PA is approximately 5.3 nm, based on the number of amino acid residues[43]) and their interaction.

Previous studies by Stoltenburg et al.[39] have shown that the protein A-binding aptamers (PAA) possess higher functionality when immobilized from the 3' terminus, hence, we have used 3'-amino modified aptamers. The latter were conjugated to the $PSiO_2$ by standard carbodiimide-mediated coupling chemistry[36]. Preferably, the aptamer immobilization should be carried out in its selection buffer (SB)[44]. However, as in this case the aptamer's SB contains Tris, which could impede its conjugation to the $PSiO_2$ surface, immobilization was carried out in MES buffer instead. $PSiO_2$ surface modifications and aptamer-conjugation were verified by ATR-FTIR (see Fig. S1, SI) and were found to coincide with our previous work[36,37]. As the aptamers' ability to bind their targets depends crucially on proper folding and 3-D structure[45,46], the aptamer-modified $PSiO_2$ films were thermally treated at 100°C (well above the predicted melting temperature of the aptamer[47]) in order to allow the PAA to unfold. To support the tethered aptamers to correctly fold into their functional structure, the porous films were incubated in SB prior to subsequent biosensing experiments.

3.2 Optical Biosensing Experiments with Protein A

PAA-modified $PSiO_2$ films were exposed to different concentrations of PA solutions to investigate the target-aptamer binding behavior within the nanoporous scaffold. In a typical biosensing experiment, the reflectivity spectra of the biosensors were monitored in real time and corresponding EOT values were computed. Figure 2 presents the change in the relative EOT ($\Delta EOT/EOT_0$) upon exposure of the biosensor to recombinant PA from *S. aureus* (molecular weight 45 kDa) at a concentration of 5 µM. First, SB buffer was introduced into the flow cell to acquire a stable EOT baseline. Subsequently, the target

solution was injected and incubated with the aptamer-conjugated $PSiO_2$. Immediately after the introduction of PA, a rapid increase in the relative EOT value is observed, after which the signal steadily increases until a constant EOT value was attained (after ~ 1 h). This represents a typical binding curve: PA infiltrates into the pores and is bound by PAA inducing an increase in the EOT. Thereafter, the protein solution was removed and the biosensor surface was extensively rinsed with SB to eliminate unbound protein molecules and attaining a new stable EOT value. In a control experiment (see Fig. 2, trace b), the biosensor was exposed to a non-target protein, human IgG (molecular weight 150 kDa) at the same concentration (5 µM). The EOT is observed to rapidly increase upon the IgG introduction due to the higher refractive index of this solution. During incubation, minor changes in the EOT occur, possibly owing to unspecific adsorption of IgG to the porous scaffold.

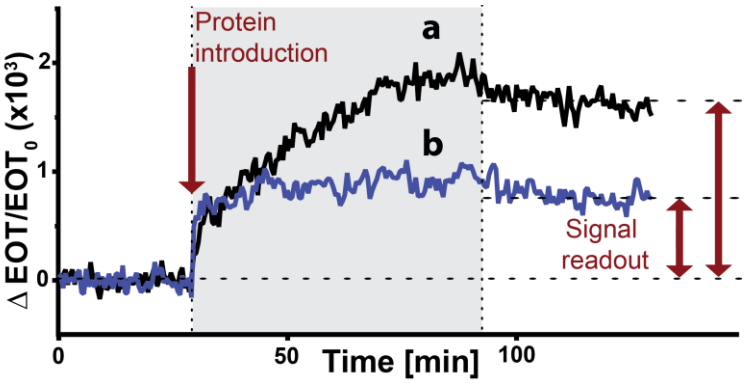

Figure 2: Relative change in EOT vs. time of PAA-functionalized $PSiO_2$ during a typical biosensing experiment. A baseline was acquired in SB followed by introduction of PA (trace a) or IgG (trace b), respectively. After rinsing to remove unbound molecules, a stable readout signal was attained. Note that during buffer exchange and rinsing, EOT measurements were briefly paused.

3.3 Non-specific Adsorption and Aptamer Selectivity

Next, control experiments were performed utilizing an amino-modified DNA-Pool, investigating non-specific adsorption and verifying aptamer selectivity. In these experiments, random sequence oligonucleotides (40-bases long, N_{40}) were immobilized onto $PSiO_2$ in the same manner and concentration as previously described for PAA and biosensing experiments were performed by exposing the N_{40}-functionalized $PSiO_2$ to IgG (5 µM). Figure 3 summarizes results of these experiments and presents the average relative change in EOT in comparison to values obtained for the PAA-functionalized biosensors upon exposure to IgG and the target PA (at a concentration of 5 µM). Both, the N_{40}-and the PAA-functionalized $PSiO_2$, exhibit comparable relative EOT changes (of 0.92 ± 0.09 and 0.85 ± 0.16 respectively) upon incubation with the IgG solution. These results suggest that the increase in EOT can be attributed to non-specific adsorption of IgG onto the porous surface and not to binding by the aptamers. Whereas, the PAA-functionalized biosensors are exposed to the PA, the attained EOT change is considerably higher (by 62 %) and these are statistically significant. Moreover, it is important to note that IgG molecules are more than 3 times larger (molecular weight 150 kDa) than PA (45 kDa) and thus, a smaller number of IgG molecules can evoke a higher optical signal. Hence, the biosensor response upon exposure to IgG is not only significantly lower in signal, but is also expected to represent the adsorption of much fewer IgG molecules in comparison to the specific binding of PA.

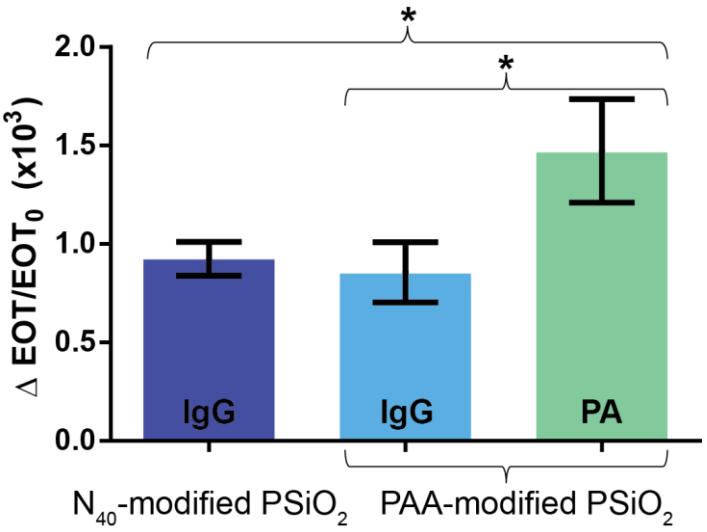

Figure 3: Averaged optical response (relative EOT) of N_{40}-functionalized $PSiO_2$ and PAA-functionalized $PSiO_2$ upon exposure to IgG or PA at a concentration of 5 µM (n > 3 for each experiment). * indicates statistically significant difference between the values (t-test, $p < 0.05$).

3.4 Binding Affinity Characterization

To determine the binding affinity, the PAA-functionalized $PSiO_2$ biosensor responses from different concentrations of PA and IgG were analyzed. Figure 4 shows the biosensor response, expressed as the relative EOT change, for different PA concentrations. The sensor response shows a consistent behavior and the relative EOT change increases with increasing concentration of PA. The data were fit to the 3-parameter hill function (see Equation 1)[48] and is presented as the solid black line in Figure 4.

$$R = R_{max}\frac{[T]^h}{K_{0.5}+[T]^h} \qquad \text{Equation 1}$$

where R is the relative change in EOT of the biosensor to the target concentration [T], R_{max} is the maximal response signal at $[T] \rightarrow \infty$, h the hill coefficient and $K_{0.5}$ the equilibrium constant, also known as the apparent dissociation constant K_D.

The three parameter hill function is a suitable model to describe biosensor characteristics from its binding curve as shown by Kurganov et al.[49]. The equilibrium constant $K_{0.5}$ (K_D) is calculated to be 13.98 ± 1.54 µM, describing the concentration at which half of the maximum signal is attained. For [T] → ∞, saturation of the biosensor occurs at a relative EOT change of 10.12 ± 0.94, corresponding to R_{max}. The sensitivity, S, of a biosensor is defined as $S = \frac{\Delta R}{\Delta [T]}$, expressing the ratio of signal change ΔR per concentration change Δ[T]. Accordingly, the sensitivity of PAA-functionalized $PSiO_2$ biosensors is determined as the slope at $K_{0.5}$ and is 0.6 (in ($\Delta EOT/EOT_0$ x 10^3)/µM), implying that the optical signal increases by ~0.6 per µM of the target PA. The hill coefficient, h, of 2.61 ± 0.69 indicates that on average the PA is bound by 2 or 3 aptamers within the $PSiO_2$ nanostructure (PA exhibits 5 identical binding sites). The correlation coefficient R^2 is 0.977, proving excellent prediction of the experimental data using this model.

It should be noted that that the K_D value obtained in this work varies from that calculated by Stoltenburg et al.[39]. The apparent K_D is known to be highly depending on the method of the affinity characterization[50]. Hence, different values for PAA affinity have been reported for measurements with either microscale thermophoresis or surface Plasmon resonance[39]. The main reason for the differences may lie in the accessibility of the aptamer binding sites due to its immobilization on a surface[51]. Recent studies by Chang et al.[52,53], comparing between literature-reported K_D values and their obtained results, highlighted that

differences in K_Ds are largely attributed to the effect of environmental and experimental conditions on aptamer binding kinetics and affinities.

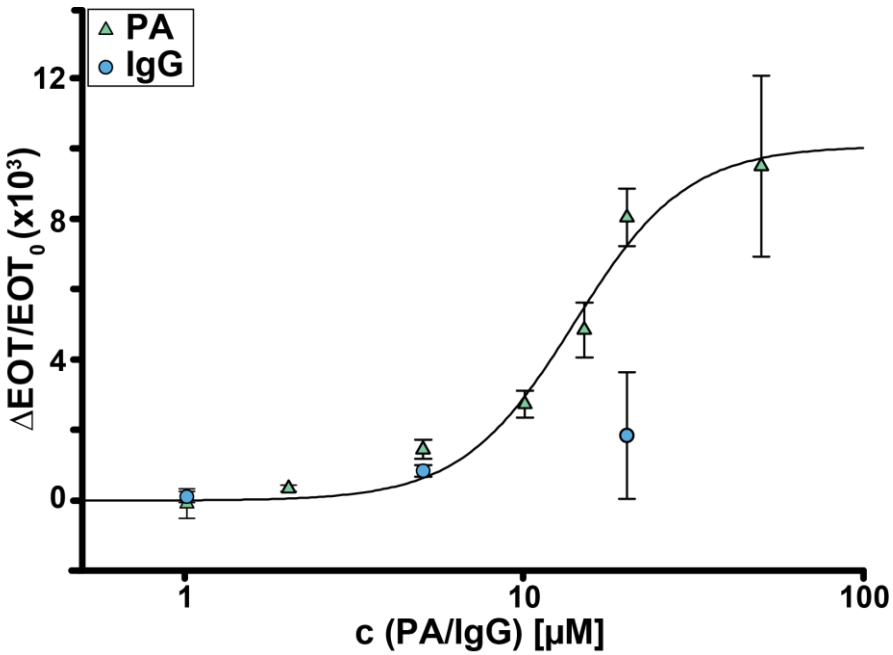

Figure 4: Aptamer-functionalized $PSiO_2$ biosensor responses, expressed as the relative EOT change, from different concentrations of PA (triangles) and IgG (circles). The solid line is a fit using equation (1), and K_D is determined, yielding 13.98 ± 1.54 µM.

3.4 Limit of Detection

The limit of detection (LoD) for the presented aptamer-based optical $PSiO_2$ biosensor was determined from the standard deviation of the relative EOT. Standard deviation between relative EOT values (measured during baseline establishment and incubation of the biosensors in SB) was calculated to be σ= 0.068 (as $\Delta EOT/EOT_0 \times 10^3$). By definition, the LoD corresponds to a protein concentration which can be reliably distinguished from the background noise. With a confidence level of 98.3% this is true for an optical signal as

high as 3*σ = 0.205 (as $\Delta EOT/EOT_0$ x10^3). Thus, by interpolation of the hill fit (see Fig. 4), the LoD was determined as 3.166 µM.

The resolution of a sensor is defined as the smallest change in analyte concentration that can be detected, $Res = \frac{noise}{S}$. Given that, a resolution of 0.113 µM was calculated for the PAA modified scaffold. It should be emphasized that the LoD and the resolution are instrument-specific and in this case, it is assumed that the instrument is the limiting factor. While aptamer-based protein A detection has been previously reported with lower LoD values (K_D = 287 ± 16.2 nM)[39], the inherently high standard deviation of RIFTS signals is accredited to the simplicity of the experimental setup. However, there are possibilities to lower the noise, e.g. by minimizing environmental influences (i.e. temperature) or by means of signal processing[54].

3.5 Enhancing the Biosensor Sensitivity: Sandwich Assay with IgG

Finally, we present a sandwich assay designed for the enhancement of optical signals induced by PA binding to the surface-tethered PAA within the nanostructured PSi films. For this assay, it is assumed that PA binds to the PAA-functionalized $PSiO_2$ biosensor even at low concentrations, however, the number of molecules being too low to cause a change in EOT above the noise level. Protein A is known for its affinity to the Fc-region of antibodies and often used for their oriented immobilization in order to retain their ability to bind their specific antigen[10,55-57]. Furthermore, it is known, that protein A has five IgG binding domains[58]. Thus, introduction of IgG should result in its binding by the aptamer-captured PA. As the molecular weight of IgG is three times larger than that of PA, a distinct change in EOT is expected even when the number of molecule is low. Figure 5 presents

the change of relative EOT over time for a characteristic experiment in which we study the response of the biosensors to a PA concentration of 1 µM, which is well below the LoD. Upon introduction of PA, no significant change in the EOT can be observed. Subsequent injection of IgG at the same low concentration (1 µM) induces a rapid response, depicting a typical binding behavior (see Fig. 5a). For comparison, Figure 5b shows the EOT signal of the biosensor to IgG exposure, while eliminating prior introduction to PA. In this case, a negligible change in the EOT is detected following the rinsing step, indicating that no specific binding has occurred.

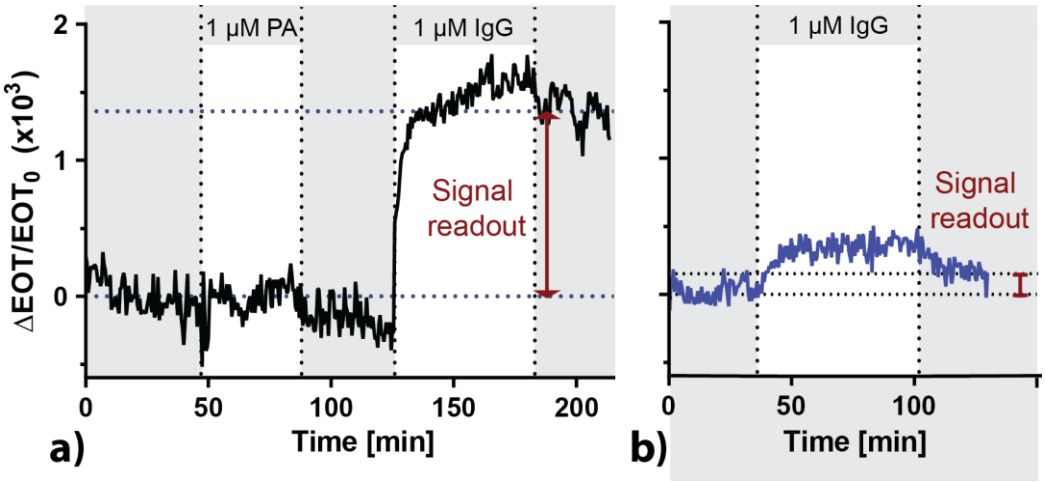

Figure 5: a) Relative change in EOT vs. time of PAA-functionalized $PSiO_2$ upon exposure to a concentration of 1 µM of PA (below the LoD) followed by incubation with IgG at the same concentration and a final rinsing step with SB. b) Optical response of the PAA-biosensor upon introduction of 1 µM IgG without prior incubation with PA.

Figure 6 summarizes the results of the developed sandwich assay. While the biosensing signals from single exposure to either PA or IgG were insignificant and below the limit of detection, the sandwich assay resulted in meaningful optical signals. While signal amplification in the presented sandwich assay relies on the specific binding between PA

and antibody, this approach can certainly be applied to other biosensors. Most protein ligands have more than one binding site for aptamers or antibodies and can thus be exposed to a secondary ligand for signal amplification.

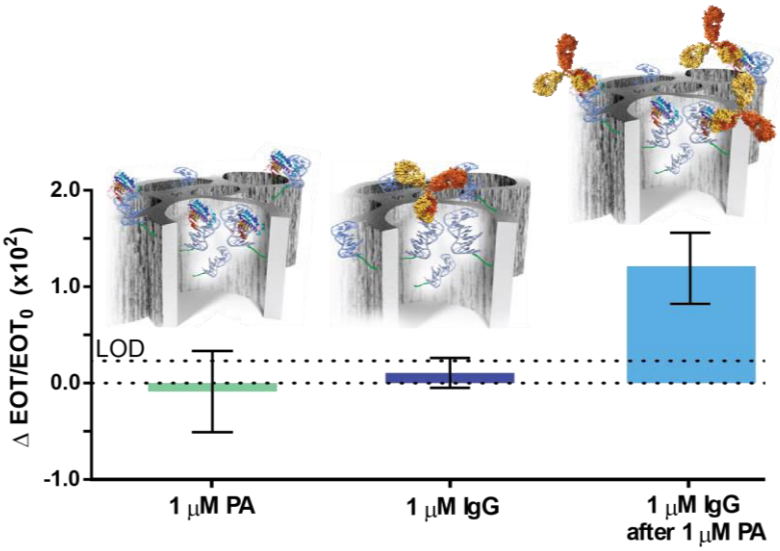

Figure 6: Sensitivity enhancement of the PAA-functionalized $PSiO_2$ biosensor. Averaged optical response (relative EOT) of the biosensor upon exposure to 1 μM of: PA, IgG or both in a successive manner. Schematic illustration of biomolecules captured by the aptamers within the porous scaffold. Upper dashed line indicates the LoD value. Differences between both single exposures (of PA or IgG) and the sandwich assay are statistically significant ($p<0.05$, $n\geq3$).

4. CONCLUSIONS

Reliable and fast detection of protein A is an important step towards improved diagnosis of *S. aureus* infections. Since direct recognition of *S. aureus* bacteria cells is hampered by the fast evolution of the bacterial genome, capture of the highly conserved protein A may provide indirect detection of *S. aureus*. Protein A-targeting aptamers have proven to be

suitable capture probes, convincing with their high selectivity, sensitivity and superior stability. Herein, PAA was successfully integrated into a simple optical biosensor scheme based on a nanostructured PSi. The biosensor displays a high sensitivity with a ten-fold higher change in the EOT signal (6%; 0.6 as $\Delta EOT/EOT_0 \times 10^3$) per µM protein A than the noise (0.7%; 0.068 as $\Delta EOT/EOT_0 \times 10^3$) in a linear range of the target concentration (8-23 µM). Its binding affinity towards protein A is determined to be 13.98 µM with an LoD value of 3.17 µM. Taking advantage of the affinity between protein A and antibodies, we demonstrate a proof-of-concept scheme for enhancing the sensitivity of the PAA-functionalized $PSiO_2$ biosensors by three fold. Subsequent introduction of IgG in a sandwich-assay format allows for the detection of protein A at a concentration of 1 µM. Thus, the short assay time combined with the simplicity of the biosensing system can potentially provide for a suitable point-of-care method for the fast identification of S. aureus infections.

ACKNOWLEDGMENT

This work was funded by the German Research Foundation under the grant SCHE 279/32-1. ES acknowledges the support by the Israel Science Foundation (Grant 1146/12). ES and KU acknowledge the core services and support from the Lorry I. Lokey Center for Life Science and Engineering. PR acknowledges the financial support of the Life Science Network stipend, administered by the German Technion Society.

REFERENCES

(1) Foster, T. J.; Geoghegan, J. A.; Schwartzman, Y.-W. T. S. L. P. In *Molecular Medical Microbiology (Second Edition)*; Academic Press: Boston, 2015, pp 655-674.

(2) Maple, P. A. C.; Hamilton-Miller, J. M. T.; Brumfitt, W. *The Lancet* **1989**, *333*, 537-540.
(3) Chambers, H. F.; DeLeo, F. R. *Nature reviews. Microbiology* **2009**, *7*, 629-641.
(4) Tacconelli, E.; De Angelis, G.; de Waure, C.; Cataldo, M. A.; Torre, G. L.; Cauda, R. *The Lancet Infectious Diseases* **2009**, *9*, 546-554.
(5) Pronovost , P.; Needham , D.; Berenholtz , S.; Sinopoli , D.; Chu , H.; Cosgrove , S.; Sexton , B.; Hyzy , R.; Welsh , R.; Roth , G.; Bander , J.; Kepros , J.; Goeschel , C. *New England Journal of Medicine* **2006**, *355*, 2725-2732.
(6) Lee, B. Y.; Singh, A.; David, M. Z.; Bartsch, S. M.; Slayton, R. B.; Huang, S. S.; Zimmer, S. M.; Potter, M. A.; Macal, C. M.; Lauderdale, D. S.; Miller, L. G.; Daum, R. S. *Clinical Microbiology and Infection* **2013**, *19*, 528-536.
(7) Francois, P.; Pittet, D.; Bento, M.; Pepey, B.; Vaudaux, P.; Lew, D.; Schrenzel, J. *Journal of Clinical Microbiology* **2003**, *41*, 254-260.
(8) Kluytmans, J. *Journal of Hospital Infection*, *65*, 100-104.
(9) DeDent, A. C.; McAdow, M.; Schneewind, O. *Journal of Bacteriology* **2007**, *189*, 4473-4484.
(10) Hartleib, J.; Köhler, N.; Dickinson, R. B.; Chhatwal, G. S.; Sixma, J. J.; Hartford, O. M.; Foster, T. J.; Peters, G.; Kehrel, B. E.; Herrmann, M. *Blood* **2000**, *96*, 2149-2156.
(11) Kim, H. K.; Emolo, C.; DeDent, A. C.; Falugi, F.; Missiakas, D. M.; Schneewind, O. *Infection and immunity* **2012**, *80*, 3460-3470.
(12) Kahl, B. C.; Mellmann, A.; Deiwick, S.; Peters, G.; Harmsen, D. *Journal of Clinical Microbiology* **2005**, *43*, 502-505.
(13) Hsin Chang, Y.; Chang, T. C.; Kao, E. F.; Chou, C. *Bioscience, Biotechnology, and Biochemistry* **1996**, *60*, 1571-1574.
(14) Song, K.-M.; Lee, S.; Ban, C. *Sensors (Basel, Switzerland)* **2012**, *12*, 612-631.
(15) Lakhin, A. V.; Tarantul, V. Z.; Gening, L. V. *Acta Naturae* **2013**, *5*, 34-43.
(16) Tuerk, C.; Gold, L. *Science* **1990**, *249*, 505-510.
(17) Bunka, D. H. J.; Stockley, P. G. *Nat. Rev. Microbiol.* **2006**, *4*, 588-596.
(18) Strehlitz, B.; Nikolaus, N.; Stoltenburg, R. *Sensors* **2008**, *8*, 4296-4307.
(19) Yuan, J.; Wu, S.; Duan, N.; Ma, X.; Xia, Y.; Chen, J.; Ding, Z.; Wang, Z. *Talanta* **2014**, *127*, 163-168.
(20) Duan, N.; Wu, S.; Zhu, C.; Ma, X.; Wang, Z.; Yu, Y.; Jiang, Y. *Analytica Chimica Acta* **2012**, *723*, 1-6.
(21) Jia, F.; Duan, N.; Wu, S.; Ma, X.; Xia, Y.; Wang, Z.; Wei, X. *Microchimica Acta* **2014**, *181*, 967-974.
(22) Baumstummler, A.; Lehmann, D.; Janjic, N.; Ochsner, U. A. *Letters in applied microbiology* **2014**, *59*, 422-431.
(23) Lian, Y.; He, F.; Wang, H.; Tong, F. *Biosensors and Bioelectronics* **2015**, *65*, 314-319.
(24) Shangguan, D.; Bing, T.; Zhang, N. In *Aptamers Selected by Cell-SELEX for Theranostics*, Tan, W.; Fang, X., Eds.; Springer Berlin Heidelberg: Berlin, Heidelberg, 2015, pp 13-33.
(25) Stoltenburg, R.; Reinemann, C.; Strehlitz, B. *Analytical and Bioanalytical Chemistry* **2005**, *383*, 83-91.
(26) Massad-Ivanir, N.; Shtenberg, G.; Tzur, A.; Krepker, M. A.; Segal, E. *Analytical Chemistry* **2011**, *83*, 3282-3289.

(27) Dancil, K. P. S.; Greiner, D. P.; Sailor, M. J. *Journal of the American Chemical Society* **1999**, *121*, 7925-7930.
(28) Bonanno, L. M.; DeLouise, L. A. *Biosensors and Bioelectronics* **2007**, *23*, 444-448.
(29) Beavers, K. R.; Mares, J. W.; Swartz, C. M.; Zhao, Y.; Weiss, S. M.; Duvall, C. L. *Bioconjugate Chemistry* **2014**, *25*, 1192-1197.
(30) Sailor, M. J. *Porous silicon in practice: preparation, characterization and applications*; John Wiley & Sons, 2012.
(31) Pacholski, C.; Yu, C.; Miskelly, G. M.; Godin, D.; Sailor, M. J. *Journal of the American Chemical Society* **2006**, *128*, 4250-4252.
(32) Pacholski, C.; Sartor, M.; Sailor, M. J.; Cunin, F.; Miskelly, G. M. *Journal of the American Chemical Society* **2005**, *127*, 11636-11645.
(33) Jane, A.; Dronov, R.; Hodges, A.; Voelcker, N. H. *Trends in Biotechnology* **2009**, *27*, 230-239.
(34) De Stefano, L.; Arcari, P.; Lamberti, A.; Sanges, C.; Rotiroti, L.; Rea, I.; Rendina, I. *Sensors* **2007**, *7*, 214-221.
(35) Jane, A. O.; Szili, E. J.; Reed, J. H.; Gordon, T. P.; Voelcker, N. H., 2007, pp 679908-679908-679911.
(36) Urmann, K.; Walter, J.-G.; Scheper, T.; Segal, E. *Analytical Chemistry* **2015**, *87*, 1999-2006.
(37) Urmann, K.; Arshavsky-Graham, S.; Walter, J. G.; Scheper, T.; Segal, E. *The Analyst* **2016**.
(38) Yoo, L.; Ahn, K.-Y.; Ahn, J.-Y.; Laurell, T.; Lee, Y. M.; Yoo, P. J.; Lee, J. *Biosensors and Bioelectronics* **2013**, *41*, 477-483.
(39) Stoltenburg, R.; Schubert, T.; Strehlitz, B. *PLoS ONE* **2015**, *10*, e0134403.
(40) Shtenberg, G.; Massad-Ivanir, N.; Engin, S.; Sharon, M.; Fruk, L.; Segal, E. *Nanoscale Res Lett* **2012**, *7*, 443.
(41) Massad-Ivanir, N.; Shtenberg, G.; Zeidman, T.; Segal, E. *Advanced Functional Materials* **2010**, *20*, 2269-2277.
(42) Segal, E.; Perelman, L. A.; Cunin, F.; Di Renzo, F.; Devoisselle, J. M.; Li, Y. Y.; Sailor, M. J. *Advanced Functional Materials* **2007**, *17*, 1153-1162.
(43) 2012.
(44) Walter, J. G.; Kökpinar, Ã.; Friehs, K.; Stahl, F.; Scheper, T. *Analytical Chemistry* **2008**, *80*, 7372-7378.
(45) Walter, J.-G.; Heilkenbrinker, A.; Austerjost, J.; Stahl, F.; Scheper, T. *Z. Naturforsch.* **2012**, *67b*, 976-986.
(46) Song, S. P.; Wang, L. H.; Li, J.; Zhao, J. L.; Fan, C. H. *Trac-Trends in Analytical Chemistry* **2008**, *27*, 108-117.
(47) Markham, N. R.; Zuker, M., 2008, pp 3-31.
(48) Hill, A. V. *The Journal of Physiology* **1910**, *40*, i-vii.
(49) Kurganov, B. I.; Lobanov, A. V.; Borisov, I. A.; Reshetilov, A. N. *Analytica Chimica Acta* **2001**, *427*, 11-19.
(50) Jing, M.; Bowser, M. T. *Analytica chimica acta* **2011**, *686*, 9-18.
(51) Urmann, K.; Modrejewski, J.; Scheper, T.; Walter Johanna, G. In *BioNanoMaterials*, 2016.
(52) Chang, A. L.; McKeague, M.; Smolke, C. D. *Methods in enzymology* **2014**, *549*, 451-466.

(53) Chang, A. L.; McKeague, M.; Liang, J. C.; Smolke, C. D. *Anal Chem* **2014**, *86*, 3273-3278.
(54) Mariani, S.; Strambini, L. M.; Barillaro, G. *Anal Chem* **2016**.
(55) Pacholski, C.; Yu, C.; Miskelly, G. M.; Godin, D.; Sailor, M. J. *Journal of the American Chemical Society* **2006**, *128*, 4250-4252.
(56) Demirel, G.; Çağlayan, M. O.; Garipcan, B.; Duman, M.; Pişkin, E. *Journal of Materials Science* **2007**, *42*, 9402-9408.
(57) Li, J.; Sailor, M. J. *Biosensors and Bioelectronics* **2014**, *55*, 372-378.
(58) Moks, T.; Abrahmsén, L.; Nilsson, B.; Hellman, U.; Sjöquist, J.; Uhlén, M. *European Journal of Biochemistry* **1986**, *156*, 637-643.

Supporting Information

RAPID AND LABEL-FREE DETECTION OF PROTEIN A BY APTAMER-TETHERED POROUS SILICON NANOSTRUCTURES

Katharina Urmann[a,b,‡], *Peggy Reich*[a,c,‡], *Johanna-Gabriela Walter*[a], *Dieter Beckmann*[c], *Ester Segal*[b]*, *Thomas Scheper*[a]*

‡ Equal contribution, * Corresponding authors

[a] Institute of Technical Chemistry, Leibniz Universität Hannover, Callinstr. 5, 30167 Hanover, Germany; phone: +49-511-7622269; e-mail: scheper@iftc.uni-hannover.de

[b] Department of Biotechnology and Food Engineering, Technion Israel Institute of Technology, Technion City, 32000 Haifa, Israel; phone: +972-4-8295071; e-mail: esegal@tx.technion.ac.il

[c] Institute for Bioprocessing and Analytical Measurement Techniques e.V., Rosenhof, 37308 Heilbad Heiligenstadt, Germany

KEYWORDS: Optical Biosensor, Aptamer, Porous Silicon, Label-Free, Protein A, *Staphylococcus aureus*

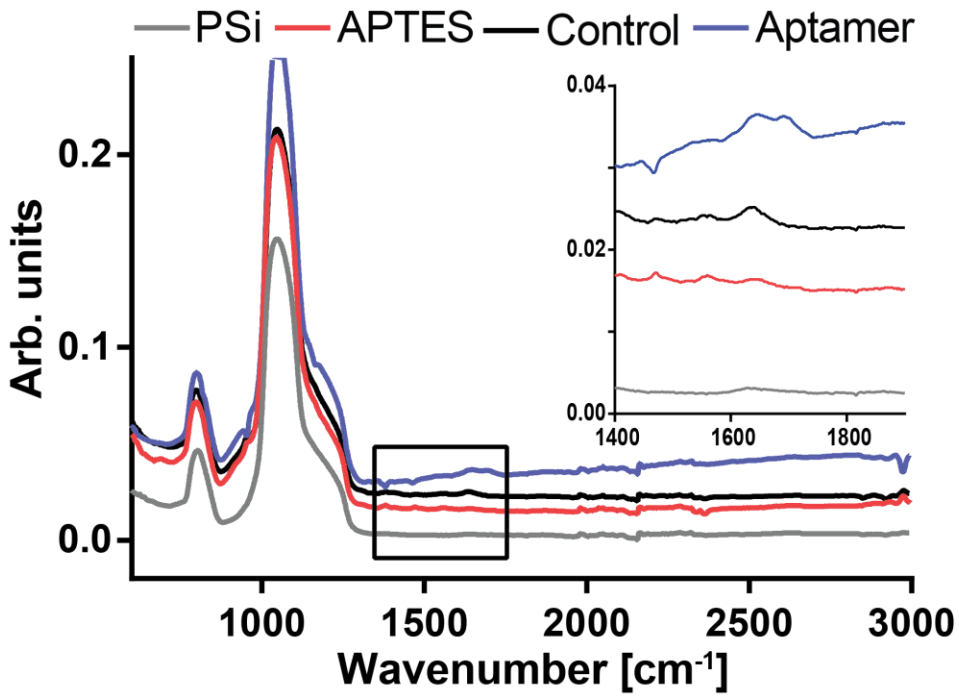

Figure S1: $PSiO_2$ ATR-FTIR spectra of a neat sample (grey), after silanization with APTES (red) and aptamer-conjugation (blue). For a control (black), $PSiO_2$ was treated similarly during all steps without exposure to aptamer. Inset for clarification.

The spectrum of neat $PSiO_2$ shows the typical SiH vibration mode at 801 cm^{-1} and a strong peak from the Si-O-Si stretching mode at 1040 cm^{-1} [1]. The silanized sample reveals peaks ascribed to bending of primary amines (1645 cm^{-1}) and protonated amines (1565 cm^{-1}), as expected after treatment with APTES [2]. The blue line shows the spectrum after conjugation of protein A binding aptamer and the blocking of residual groups: a peak around 1690 cm^{-1} is characteristic for the carbonyl groups stemming from the conjugated oligonucleotides [3]. Similarly to the control (black line), the peak for primary amines is elevated after the complete conjugation chemistry, which includes blocking with ethanolamine.

(1) Sailor, M. J. *Porous silicon in practice: preparation, characterization and applications*; John Wiley & Sons, 2012.
(2) Shtenberg, G.; Massad-Ivanir, N.; Fruk, L.; Segal, E. *ACS Applied Materials & Interfaces* **2014**, *6*, 16049-16055.
(3) Zhou, J.; Rossi, J. J. *Molecular Therapy. Nucleic Acids* **2014**, *3*, e169.

6. Unpublished work

One of the main advantages of aptamers as receptors is their availability against a wide range of target analytes, beyond those accessible to antibody development. However, due to the progress in the field of monoclonal antibody production, these traditional capture probes often challenge aptamers when they are targeting the same analyte. Thus, to allow for appropriate choice of suitable bioreceptors, a direct comparison between the performance of biosensors utilizing antibodies and aptamers for the capture of the same protein target was performed.

The following chapter presents preliminary results from studying $PSiO_2$ biosensors conjugated with either the well-known 6H7 aptamers or antibodies targeting his-tag sequences immobilized either randomly or in an oriented manner. Herein, biosensor responses for all three types of biosensors were investigated utilizing different concentrations of the same target protein tyrosinase (6x histidine). Furthermore, we focused on the evaluation of signals from exposure to non-target proteins and complex samples, emphasizing the stability and advantage of regenerability for the aptamer-conjugated biosensors.

HEAD TO HEAD: ANTIBODY VS. APTAMER – A BIOSENSOR PERFORMANCE COMPARISON

*Katharina Urmann[1,2], Sharon Nissinmann[2], Naama Massad-Ivanir[2], Johanna-Gabriela Walter[1], Thomas Scheper[1], Ester Segal[2]**

[1] Institute of Technical Chemistry, Leibniz University of Hanover, Callinstr. 5, 30167 Hanover, Germany

[2] Department of Biotechnology and Food Engineering, Technion Israel Institute of Technology, Technion City, 32000 Haifa, Israel; phone: +972-4-8295071; e-mail: esegal@tx.technion.ac.il

INTRODUCTION

Countless publications and review articles elaborate the properties, advantages and disadvantages of both aptamers and antibodies. Having been established in 1990 with the development of the SELEX (Systematic Evolution of Ligands by Exponential Enrichment) process, aptamers have since been termed "chemical antibodies" and predicted to replace antibodies in the near future [1-3]. With the possibility of selecting high affinity aptamers for a wide range of ligands (including small molecules, proteins and whole cells), their small size, high stability and outstanding performance even in complex sample matrices, many biosensing schemes have been recently designed utilizing aptamers as receptors [2,4,5]. However, aptamers have not yet replaced antibodies in many applications and there is still a steady number of reports on antibody-based biosensing. While some studies present results of different assays using antibodies or aptamers as capture probes to the same target analyte [6,7], direct performance comparisons of antibodies and aptamers binding the same target in one biosensing scheme are rare [8].

Our previous work has focused on the demonstration of various label-free optical biosensors based on porous silicon (PSi). Therein, we emphasized the advantages of PSi as a promising platform in combination with minimal instrumentation reflective interferometric Fourier transform spectroscopy (RIFTS), monitoring changes in refractive index or reflection intensity depending on the analyte of interest [9,10]. Detailed description of the optical properties of PSi, the different biosensing principles as well as various applications can be found elsewhere in literature and reviews. Moreover, our group has shown these biosensing concepts realized with both antibodies and aptamer receptors for the detection of protein and bacteria targets [9,11,12]. With the present study we are aiming to provide a direct comparison of aptamer and antibody capture probes within the same biosensing platform and for the detection of the same target to evaluate the performance and benefits of each receptor.

Herein, an oxidized porous silicon nanostructure (Fabry-Pérot thin film), used as the optical transducer, is functionalized with either the well-characterized his-tag binding aptamer (6H7) [13-15] or an anti his-tag antibody for the detection of a his-tagged protein. As a representative target, 6x-his tyrosinase from *Bacillus megatherium* was used. It is to note,

that in our previous work, the target was a his-tagged lipase. As the aptamer (and antibody respectively) target the histamine-sequence in the protein, binding affinity strongly depends on the secondary protein structure and accessibility of the target structure for the receptor. Hence, previously reported limit of detection values or absolute signals cannot be compared with the results of the present study [11]. We confirm successful conjugation of the capture probes to the oxidized PSi ($PSiO_2$) nanostructure by RIFTS and attenuated total reflectance Fourier transform infrared (ATR-FTIR) spectroscopy. The binding of protein target molecules to the receptors within the porous scaffold is monitored in real time and the limit of detection for both the aptamer- and the antibody-conjugated biosensors are extracted from a series of optical biosensing experiments. Focus is laid especially on comparing the performance of both receptors in the detection of the target protein within complex samples, namely bacteria lysates.

EXPERIMENTAL SECTION

Materials. Si wafers (p-type, boron doped, 0.0008 Ω·cm resistivity, <100>-oriented) were purchased from Siltronix Corp. Aqueous HF (48%) and ethanol absolute were purchased from Merck. All chemicals, such as (3-aminopropyl)triethoxysilane (APTES), ethyldiisopropylamine (EDIPA), glutaraldehyde 25% solution (GA), ethanolamine, *N*-(3-Dimethylaminopropyl)-*N*-ethylcarbodiimide hydrochloride (EDC), succinic acid, sodium cyanoborohydride and buffer salts were obtained from Sigma-Aldrich Chemicals. Buffers were prepared with deionized water (18.2 MΩ cm) and filtered before use. Anti-his-tag aptamer 6H7 (5'- GCT ATG GGT GGT CTG GTT GGG ATT GGC CCC GGG AGC TGG C - 3') sequence was taken from the US patent specification U.S.7329742 (Doyle and Murphy, 2008). 6H7 was selected in 50 mM K_2HPO_4, 150 mM NaCl, 0.05% Tween 20 (this buffer is subsequently abbreviated as SB-T). To prevent possible blocking of amino-modified surfaces, Tween 20 was omitted during immobilization and washing steps, as well as renaturation of the aptamer (buffer SB). Other utilized buffers were PBS and HEPES, prepared according to standard recipes. Aptamers were purchased with a 5'-amino modification from Integrated DNA Technologies. Mouse anti-his antibody was obtained from Enco. Streptavidin and biotinylated protein A were purchased from Sigma-Aldrich

Chemicals. Proteins for biosensing experiments included trypsin from porcine (Sigma-Aldrich Chemicals) and 6xhis tyrosinase from *Bacillus megatherium* (recombinant, expressed in *E. coli*), generously supplied by Prof. Ayelet Fishman. As a negative control, *Escherichia coli* strain JL-102 was cultured in Luria broth (LB) medium (10 g/L casein peptone, 10 g/L NaCl, 5 g/L yeast extract, all purchased from Sigma-Aldrich Chemicals).

Preparation of Bacteria and Bacteria Lysates. A shaking flask with 20 ml sterile LB medium was inoculated with 100 µl of a freeze culture of *E. coli* JL-102 (free of plasmids) and cultured over night, shaking at 37°C. The resulting culture was used for biosensing experiments to mimic a biologically relevant complex fluid.

2 ml of bacteria culture were spun down in a standard lab centrifuge, replacing the supernatant by 1 ml PBS selection buffer. Following the re-suspension, the culture was ultrasonicated at 4°C (Labsonic M, Sartorius Stedim Biotech). Following removal of cell debris, the suspension was centrifuged again and the supernatant taken to a fresh tube and further used as the bacteria lysate.

Preparation of Oxidized PSi. Electrochemical preparation of oxidized porous silicon layers from boron-doped p-type Si wafers was performed as previously described. Freshly etched samples were thermally oxidized described likewise (800°C for 1 h in ambient air).

Characterization of $PSiO_2$ Films. Specific properties (i.e. thickness and porosity) of the fabricated $PSiO_2$ layers were characterized by several techniques: HRSEM, gravimetry (for porosity), and SLIM (spectroscopic liquid infiltration method) methods, as previously described [16,17].

Functionalization of $PSiO_2$ Films.

Aptamers. The $PSiO_2$ samples were conjugated with 75 µM aptamer as previously described [11].

Antibodies. For unoriented conjugation with antibodies, $PSiO_2$ samples were first incubated with a solution of 1% APTES and 1% EDIPA in water for 30 min. After removing the solution, the sample was rinsed with toluene, ethanol and acetone, then dried under a nitrogen stream. Afterwards, the surface was incubated in a 2% aqueous glutaraldehyde solution for 30 min. Subsequently, the sample was washed with water and

again dried under a stream of nitrogen. In the next step, the sample was mounted in the same type of custom made Plexiglas flow cell and 50 µl of 100 µg/ml anti-his antibody solution were injected. The sample was first incubated for 1 h at room temperature and then stored over night at 8°C. Prior to the biosensing experiments, unbound antibodies were removed by thorough washing with PBS and residual reactive groups were capped by incubation of the sensor with 0.1 M aqueous solution of ethanolamine for 30 min.

For oriented immobilization of antibodies, silanization and modification with GA were performed as described above, followed by an incubation with 50 mM sodium cyanoborohydride in HEPES for 30 min. After washing with HEPES, $PSiO_2$ samples were placed in a humidity chamber and 100 µL of a freshly prepared streptavidin solution (100 µg/mL in PBS) are pipetted on the sample and incubated for 1 h. Thorough rinsing with PBS was performed before a repetition of the incubation in sodium cyanoborohydride as described before. Next, the streptavidin-surface was blocked with ethanolamine (as described previously) and then incubated with biotinylated protein A (100 µL; 100 µg/mL in PBS) for 1 h in a humidity chamber. Finally, the samples were rinsed with PBS and incubated with the antibody (50 µL; 100 µg/mL in PBS; humidity chamber) for 1 h at room temperature and then overnight in the fridge. On the next day, repeated blocking of residual groups with ethanolamine after rinsing with PBS was performed, concluding the oriented immobilization of the anti-his-tag antibodies.

Measurement of Interferometric Reflectance Spectra. Interferometric reflectance spectra of the samples were collected as described previously [11]. RIFTS was used to verify biomolecule-attachment as previously reported by Massad-Ivanir et al. [9]. Therefore, sample reflectivity spectra were taken before and after the respective modification steps in the same sample spots and the change in effective optical thickness (EOT) was determined.

Infrared Spectroscopy. Modification steps were verified using attenuated total reflectance Fourier transform infrared (ATR-FTIR) spectroscopy. Spectra were recorded using a Thermo 6700 FTIR instrument equipped with a Smart iTR diamond ATR device.

Protein Biosensing. Biosensing experiments were carried out in a flow cell configuration, described for the functionalization of $PSiO_2$ scaffolds, following the conjugation of the respective receptor. At first, spectra were recorded for a baseline of the biosensor immersed

in PBS or SB respectively. The binder-functionalized $PSiO_2$ samples were then incubated with 100 µL of the protein solution (in PBS or SB-T respectively) for 1 h. After removal of the protein solution and flushing the cell with PBS/SB, the sample was incubated for 30 min in PBS/SB. For the regeneration of the aptamer-based biosensor, the protein was eluted with 1 M imidazole, followed by the renaturation of aptamers in SB. Optical measurements were recorded every 30 s throughout the entire experiment. Please note that during buffer exchange and rinsing steps, EOT measurements were shortly paused for to allow a thorough washing of the biosensor and the flow cell.

Statistical analysis and data regression

For statistical analysis, unpaired t-tests were performed. Resulting two-tailed P values below 0.05 were required to consider the compared groups as significantly different from each other.

Non-linear regression of obtained data was performed with GraphPad Prism software utilizing the model for specific binding with hill slope. The following equation is used for modelling:

$$Y = \frac{B_{max} \cdot X^h}{(K_d^h \cdot X^h)} \qquad \text{Equation 1}$$

Herein, B_{max} is the interpolated concentration at which the maximum biosensor response is reached. K_d (also known as the apparent dissociation constant) is the target concentration needed to reach the half-maximum biosensing signal. The parameter h is the Hill coefficient.

RESULTS AND DISCUSSION

Functionalization of $PSiO_2$ films with receptor biomolecules.

Electrochemical etching with a constant current density of 375 mA/cm^2 for 30 s was performed to create porous silicon thin films from highly boron-doped p-type crystalline Si wafers. For stabilization of the PSi structure and increased hydophilicity, freshly-etched films were thermally oxidized for 1 h at 800 °C [18]. Resulting $PSiO_2$ samples were characterized by their morphological properties by HRSEM, SLIM and gravimetry (data

not shown). In brief, $PSiO_2$ layers were around 5500 nm thick at an approximate porosity of 70 %. HRSEM studies depicted characteristic interconnected cylindrical pores within the $PSiO_2$ films and revealed pore sizes between 35 and 65 nm. The large porous volume and surface area provide an ideal structure for the anchoring and capture of biomolecules and the pore sizes allow for their infiltration (e.g. tyrosinase has an approximate diameter of 4.6 nm [19]).

Amino-modified aptamer 6H7 was immobilized onto the $PSiO_2$ samples as previously reported at a concentration of 75 µM [11]. Surface modification steps were followed with and confirmed by ATR-FTIR (data not shown).

For the immobilization of antibodies, two different strategies were chosen: (1) straightforward conjugation of a random amine-group within the antibody to an aldehyde-modified surface and (2) oriented conjugation of the antibody Fc-region to a protein A-modified surface. Unoriented conjuation encompassed silanization of $PSiO_2$ samples with APTES resulting in a terminal amine-group, followed by a reaction with glutaraldehyde. Thereafter, an aldehyde-group on the $PSiO_2$ was available for the attachment of a primary amine within the antibody. Therefore, antibody at a final concentration of 100 µg/mL was incubated with the surface over night. Finally, biosensors were rinsed and residual aldehydes blocked by incubation with ethanolamine. Attachment of functional groups and conjugation of biomolecules within the porous scaffold leads to a red-shift of the PSi reflectivity spectrum [20]. This is due to the change of the average refractive index of the matrix which is governed by the Fabry-Pérot equation describing the reflection interferences:

$$m \cdot \lambda = 2 \cdot n \cdot L \qquad \text{Equation 2}$$

Therein, m is an integer, λ the light wavelength, n the average refractive index of the material and L the constant thickness of the porous layer. The term 2nL represents the effective optical thickness. Thus, a change in EOT indicates a change in the refractive index. Sample EOT was measured before and after the respective surface modification (resulting in the delta) and the averaged values are presented in Figure 1.

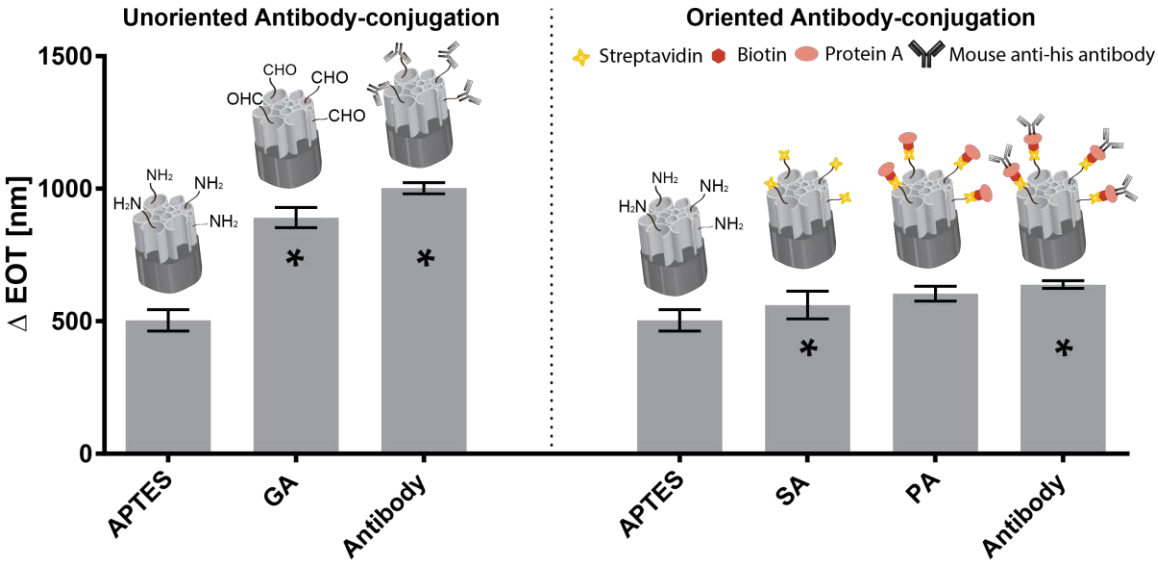

Figure 1. Changes in the EOT upon respective surface modifications of PSiO2 biosensors. Measurements were taken in quadruplicates and stars indicate statistically significant differences ($p<0.05$).

While the changes in EOT upon each step of the unoriented antibody-conjugation were significant and easy to observe, the strategy for oriented antibody-immobilization includes several steps where the differences in EOT are minor (due to the attachment of small moieties). However, the accumulated changes in EOT confirm the attachment of the antibody on a statistically significant basis.

Biosensing experiments

Biosensing experiments were carried out as previously described with different concentration of the his-tagged tyrosinase protein, bacteria lysates, non-target proteins for negative control and mixtures [11]. While aptamer-functionalized $PSiO_2$ has been regenerated by protein elution to perform subsequent series of increasing concentrations on the same biosensor, antibody-modified biosensors were each used only once and then discarded. For each biosensing experiment, biosensors were first incubated in selection buffer or PBS, respectively, to establish a stable baseline. Reflectivity spectra were therefore recorded every 30 s. Next, the investigated sample was injected to the chamber and allowed to react with the respective bioreceptor. This resulted in immediate and profound increases in the

optical signal, reaching saturation after about 1 h. Following brief pausing of the reflectivity measurements, the biosensors were rinsed with buffer (SB or PBS) extensively in order to remove unbound molecules. Subsequently, signal acquisition was continued to obtain the final biosensing signal. In case of aptamer-conjugated biosensors, the previously described steps were followed by an incubation with elution buffer for 15 min and subsequent washing and incubation with SB to establish a new baseline. Typical signal traces for each of the three tested biosensors, expressed as the relative change in EOT to the average signal during baseline establishment ($\Delta EOT/EOT_0$) are presented in Fig. 2.

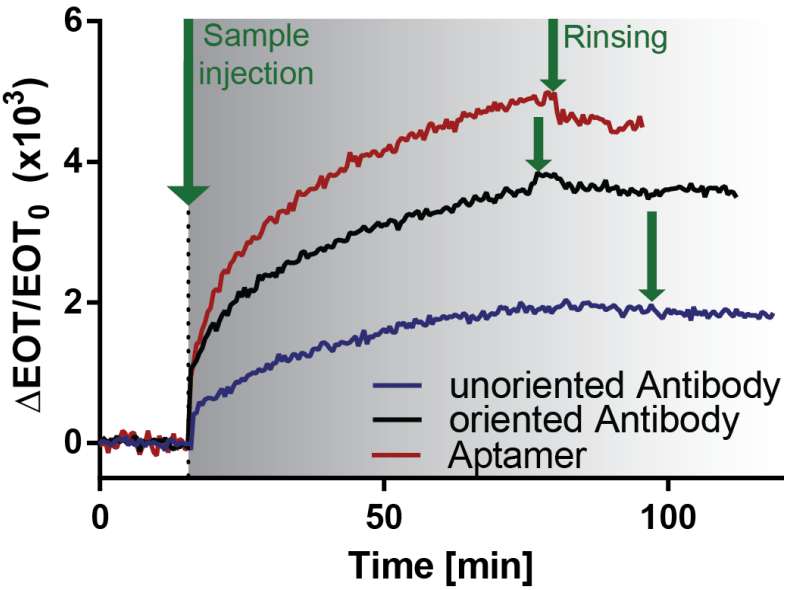

Figure 2. Relative change in EOT vs. time of respective biofunctionalized $PSiO_2$ during typical biosensing experiments. A baseline was obtained in SB or PBS respectively followed by the injection of tyrosinase (16.5 µM). After rinsing to remove unbound molecules (indicated by green arrows), a stable readout signal was attained. Note that during buffer exchange and rinsing, EOT measurements were briefly paused.

Selectivity and performance in complex samples.

$PSiO_2$ biosensors modified with 6H7-aptamer have previously demonstrated high selectivity towards their his-tagged target protein and robustness against unspecific adsorption even in complex media with an abundancy of non-target proteins (*i.e.* bacteria lysates)[11]. In the present study, we have consequently compared the biosensor responses

obtained upon unspecific adsorption of non-target proteins as well as bacteria lysates and lysates spiked with target protein tyrosinase for the three types of biosensors. The results are summarized in Figure 3.

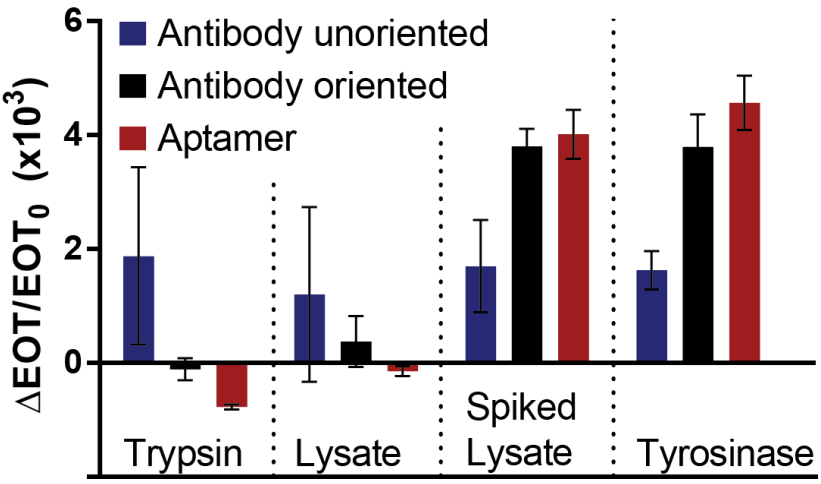

Figure 3. Biosensor responses upon introduction of different samples: trypsin as a non-target protein (concentration 16.5 µM), bacterial lysates and lysates spiked with 16.5 µM tyrosinase and pure tyrosinase (concentration 16.5 µM) for comparison. (n ≥ 3)

Exposure of biosensors - conjugated with antibodies in random orientation - to pure his-tag protein solutions and other types of non-target proteins or mixtures, results in signals indiscernible from each other. This is not only due to the high deviations between responses obtained in several repeats of the experiments, but also the relatively low signals in general. The inconsistent display of antibody-regions other than the antigen binding sites due to undirected immobilization may promote unspecific adsorption to the biosensor. Surface coverage with antibodies and stability of the utilized surface chemistry should be investigated further to investigate their influence on biosensing signals.

The results for both, biosensors functionalized with aptamers and oriented antibodies, show good selectivity, low unspecific adsorption and robust biosensing signals for target protein in complex media, which are in good agreement with biosensor responses from pure analyte solutions. While the antibody-conjugated $PSiO_2$ shows minor adsorption from the

complex protein mixture of the bacterial lysates, aptamer-modified scaffolds were not prone to any adsorption, confirming previous reports[11].

Target binding behavior.

For direct comparison of biosensor responses for the different biosensor types (modified with (i) antibodies, (ii) oriented antibodies and (iii) aptamers), respective functionalized $PSiO_2$ scaffolds were exposed to different concentrations of the his-tagged target protein tyrosinase. Figure 4 presents the average biosensor responses to the different samples and the corresponding curve fit (lines) utilizing a model for specific binding with Hill slope (see equation 1).

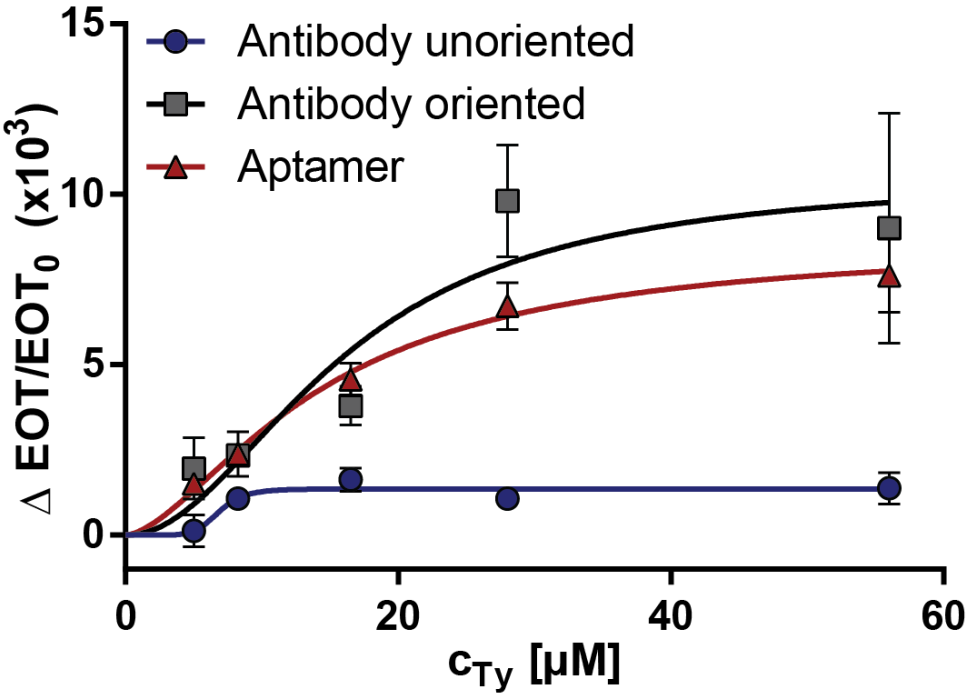

Figure 4. Measured responses and deviations of different $PSiO_2$ biosensors to a series of tyrosinase concentrations. Triangles correspond to aptamer-conjugated biosensors, squares correspond to biosensors with oriented antibodies and circles represent signals from antibody-conjugated biosensors. The lines show the curves fitted for specific binding with Hill slope. ($n \geq 3$)

Conjugation of antibodies to porous silicon functionalized with glutaraldehyde via a primary amine in the antibody-structure, results in random orientation of the antibodies owed to the large number of amines in an antibody-structure. Thus, the functionality of the capture probes and the protein layer that is presented to the target-structure varies enormously between the biosensors and repetitions of the same experiments. Moreover, target binding to these biosensors was generally low so that no statistically significant difference between the signals measured for different protein concentrations could be observed (see Fig. 4 blue line and circles). We conclude that the simple immobilization of antibodies via a random amine-functionality is not suitable for the fabrication of robust and specific $PSiO_2$ biosensors.

Contrary, careful directed immobilization of the same anti-his-tag antibodies results in a target binding behavior that can be modeled according to equation 1. Signals at protein concentrations in the linear range of the biosensor (8.25 μM to 28 μM) are statistically significant in their differences. The R^2 value for the fitted curve is 0.73, representing the relatively high deviations between experiment repeats (see Fig. 4, black line and squares). This can be due to the necessity of repeated fabrication of antibody-conjugated biosensors due to their short storability and the inability to regenerate the biosensors for repeated use. The best fit is achieved with the aptamer-functionalized biosensors ($R^2 = 0.94$). Robust biosensing signals were obtained and biosensor responses were statistically significant different in the linear detection range (see Fig. 4, red line and triangles).

Limit of detection.

For the determination of the limit of detection (LoD) for each of the biosensor types, the respective noise was calculated (as the standard deviation between relative EOT values measured during baseline establishment and incubation of the biosensors in SB). The results are shown in Table 1. The LoD is defined as the minimum protein concentration which evokes a signal that can be reliably distinguished from the background noise. Thus, the fitted binding curves were interpolated for each biosensor type for a y-value corresponding to $3x\sigma$. The calculated values are shown in Table 1.

Table 1. Limit of detection.

	Antibody unoriented	**Antibody oriented**	**Aptamer**
Noise [$\Delta EOT/EOT_0$ x10^3]	0.042314	0.044022	0.045849
3xσ [$\Delta EOT/EOT_0$ x10^3]	0.126942	0.132065	0.137548
LoD [μM]	**5.026617**	**1.859828**	**1.13771**

These values represent a theoretical limit of detection and it is not confirmed that the respective protein concentrations would indeed result in a signal as calculated. Especially for the curves with less accurate fit (*i.e.* lower R^2), the actual protein concentration necessary to achieve a signal distinguishable from the noise may deviate.

Nevertheless, robust signals at a concentration of 5 μM tyrosinase (see Fig. 4) already demonstrate improved target binding of this analyte in comparison to the previously tested protein lipase [11]. Therein, the lowest protein concentration resulting in a significant signal was 11 μM [11]. This may be attributed to the tyrosinase secondary structure and the better accessibility of the histidine sequence for the binding aptamer.

CONCLUSIONS

This preliminary study presents a direct comparison for the specific detection of his-tagged tyrosinase with antibody and aptamer capture probes, utilizing porous silicon optical biosensors. One of the main results is that a simple random immobilization of antibodies does not result in $PSiO_2$ biosensors capable of specific target detection. Although, the conjugation of anti-his-tag-antibodies was confirmed by RIFTS, their random orientation within the porous nanostructure makes them prone to unspecific adsorption of non-related molecules and severly hampers the capacity for specific target capture. This is represented by low signals indistinguishable from each other at different target protein concentrations and controls.

Laborious directed conjugation of the antibodies via an anchored protein A layer, however, results in $PSiO_2$ biosensors suitable for the detection of his-tagged tyrosinase at low

unspecific adsorption of non-target molecules. While the agreement of experimental data and modeled biosensor response is not as good (R^2 = 0.73), further investigation with optimized immobilization densities and additional tested concentrations may result in a better curve fit and thus more robust biosensor responses. Nevertheless, this conjugation chemistry is significantly more complicated, cost-intense and time consuming while resulting in antibody-biosensors for one-time use and with limited storability.

Aptamer-functionalized optical biosensors, showed the best performance in this study. Biosensor responses corresponded well with the specific binding model and no unspecific adsorption of interfering molecules, even in complex matrices, was observed. The affinity of the target tyrosinase and the associated biosensing signals and detection limits present an improvement from the previously reported biosensing scheme [11].

We hypothesized that antibodies may provide higher sensitivity and therefore enable protein detection at lower concentration, however, under the presented conditions, aptamer-functionalized $PSiO_2$ have no disadvantages compared to the antibody biosensors. On the contrary, they can be fabricated much easier, cost-effective and fast, while allowing for robust multiple biosensing cycles on the same biosensor.

Adjustment of immobilization density or the choice of a different target/receptor pair may eventually result in an advantage of antibodies over aptamers regarding the biosensor sensitivity. However, in this comparison for the capture of his-tagged tyrosinase with 6H7 aptamer or mouse anti-his-tag antibodies, the aptamer prevails in all categories.

REFERENCES

(1) Bunka, D. H. J.; Stockley, P. G. *Nat Rev Micro* **2006**, *4*, 588-596.

(2) Song, S.; Wang, L.; Li, J.; Fan, C.; Zhao, J. *Trends in Analytical Chemistry* **2008**, *27*, 108-117.

(3) Hianik, T.; Wang, J. *Electroanalysis* **2009**, *21*, 1223-1235.

(4) Duan, N.; Wu, S. J.; Dai, S. L.; Gu, H. J.; Hao, L. L.; Ye, H.; Wang, Z. P. *The Analyst* **2016**, *141*, 3942-3961.

(5) Feng, C.; Dai, S.; Wang, L. *Biosensors and Bioelectronics* **2014**, *59*, 64-74.

(6) Zhang, X.; Sun, M.; Kang, Y.; Xie, H.; Wang, X.; Song, H.; Li, X.; Fang, W. *Toxicon* **2015**, *106*, 89-96.

(7) Liu, R.; Huang, Y.; Ma, Y.; Jia, S.; Gao, M.; Li, J.; Zhang, H.; Xu, D.; Wu, M.; Chen, Y.; Zhu, Z.; Yang, C. *ACS Applied Materials & Interfaces* **2015**, *7*, 6982-6990.

(8) Liss, M.; Petersen, B.; Wolf, H.; Prohaska, E. *Analytical Chemistry* **2002**, *74*, 4488-4495.

(9) Massad-Ivanir, N.; Shtenberg, G.; Tzur, A.; Krepker, M. A.; Segal, E. *Analytical Chemistry* **2011**, *83*, 3282-3289.

(10) Tenenbaum, E.; Segal, E. *The Analyst* **2015**, *140*, 7726-7733.

(11) Urmann, K.; Walter, J.-G.; Scheper, T.; Segal, E. *Analytical Chemistry* **2015**, *87*, 1999-2006.

(12) Urmann, K.; Arshavsky-Graham, S.; Walter, J. G.; Scheper, T.; Segal, E. *The Analyst* **2016**.

(13) Kökpinar, Ö.; Walter, J.-G.; Shoham, Y.; Stahl, F.; Scheper, T. *Biotechnology and Bioengineering* **2011**, *108*, 2371-2379.

(14) Doyle, S. A.; Murphy, M. B. *US Patent 0142582 A1* **2005**.

(15) Zhu, G.; Lübbecke, M.; Walter, J.; Stahl, F.; Scheper, T. *Chemical engineering & technology* **2011**, *34*, 2022-2028.

(16) Massad-Ivanir, N.; Shtenberg, G.; Zeidman, T.; Segal, E. *Advanced Functional Materials* **2010**, *20*, 2269-2277.

(17) Sailor, M. J. *Porous Silicon in Practice*; Wiley-VCH: Weinheim, 2011, p 250.

(18) Segal, E.; Perelman, L. A.; Cunin, F.; Di Renzo, F.; Devoisselle, J. M.; Li, Y. Y.; Sailor, M. J. *Advanced Functional Materials* **2007**, *17*, 1153-1162.

(19) Protein Size Calculator, available at www.calctool.org, accessed 02/09/2016.

(20) Pacholski, C.; Yu, C.; Miskelly, G. M.; Godin, D.; Sailor, M. J. *Journal of the American Chemical Society* **2006**, *128*, 4250-4252.

7. Discussion

This chapter summarizes the main results and achievements of this research, as presented in the previous sections.

PSi fabrication and characterization

Throughout this work, optical transducers based on $PSiO_2$ were prepared by electrochemical etching of crystalline p-type silicon wafers. According to the applied current density and etching duration, their morphological properties differ (see table 3). Freshly etched PSi samples were all thermally oxidized to create more stable and hydrophilic scaffolds. Structural properties, such as pore sizes, layer thickness and porosity were characterized by HRSEM, SLIM, gravimetry and ellipsometry. The results are summarized in table 3.

Table 3. Etching conditions and structural properties of $PSiO_2$.

Etching conditions		**HRSEM**		**Gravimetry**	**SLIM**		**Ellipsometry**		**Wafer resistivity**
Etch time	Current density	Pore Diameter	Thickness	Total Porosity	Open Porosity	Thickness	Porosity	Thickness	
(s)	(mA/cm^2)	(nm)	(nm)	(%)	(%)	(nm)	(%)	(nm)	(Ω·cm)
30	300	65 ± 10	5440 ± 80	78 ± 1	79 ± 1	4975 ± 88	79 ± 4	5000 ± 30	0.0008
375	24	25 ± 5	-	54.6 ± 1	52 ± 1	5172 ± 57	-	-	0.0008
30	375	50 ± 15	-	62 ± 1	68 ± 5	4948 ± 302	-	-	0.00095

The porous silicon scaffolds were characterized by cylindrically shaped pores that were interconnected. HRSEM images of a typical $PSiO_2$ film are included in Fig. 4.1 (page 46, lower panel, left). While the current density strongly influences the resulting pore size, etching duration directly reflects on the thickness of the resulting layers. Furthermore, the resistivity of the wafer has a profound effect on the efficacy of the etching process and thus influences both pore size and layer thickness. Pore sizes were chosen and adjusted depending on the application of the scaffold: $PSiO_2$ for protein biosensors (see 5.1, 5.3 and 6) required pore sizes large enough to accommodate both aptamer receptors as well as captured target protein molecules. For analytes not infiltrating the nanostructure (see 5.2), smaller pores had beneficial optical properties

Once the $PSiO_2$ films were fabricated and thoroughly characterized, we have continued to study different strategies for the conjugation of aptamers onto the outer surface and within the porous layers of the films.

Aptamer conjugation

Following the fabrication and characterization of the porous silicon thin films, covalent conjugation of the aptamer capture probes was required to functionalize the $PSiO_2$ layers.

As discussed in section 2.2 in detail, aptamer immobilization and subsequent functionality of the receptors necessitates consideration of various factors, such as immobilization density, aptamer orientation and the possible use of spacer molecules.

The infiltration of the aptamers into the porous silicon scaffold and their conjugation within presents a challenge: spatial confinement within the nano-scale pores and the high negative charge of oligonucleotides can hamper efficient immobilization. On the other hand, numerous functionalities on the aptamer-termini are available during their chemical synthesis and also porous silicon is highly compatible with a wide range of chemical modifications through silanes.

Thus, during this work two different strategies for $PSiO_2$-functionalization with aptamers were employed, verifying the success of each modification step by various methods, such as ATR-FTIR, confocal microscopy, and Ellmann assay (see Fig. 5.1.1 and 5.2.1).

The respective detailed strategies for chemical modifications are presented in scheme 5.1.1 and Fig. 5.2.1. Herein, the first scheme utilized standard carbodiimide-mediated coupling of amino-modified aptamers to a previously treated surface exhibiting a carboxy-functionality. This strategy relies on standard procedures and can be rapidly performed using inexpensive reagents. The second strategy, wherein acrydite-modified aptamers were directly conjugated to a mercapto-silanized surface has fewer synthetic steps and is shorter. However, modification of aptamers with acrydite during their chemical synthesis is limited to the 5' end of oligonucleotides and hence, this approach is not suitable for aptamers which require immobilization at their 3' terminus.

Additionally, biosensors were functionalized with antibodies. Herein, results showed that simple conjugation of antibodies via an amine-functionality to $PSiO_2$ displaying an aldehyde group, resulted in biosensors with low functionality and tendency for unspecific adsorption of proteins. Directed conjugation of antibodies, retaining their functionality and achieving a good surface coverage is considerably more laborious: after silanization and reaction with glutaraldehyde, streptavidin was conjugated to the $PSiO_2$ scaffolds. In the next step, biotinylated protein A was bound to the surface. Finally, the affinity of protein A to the F_c region of antibodies allowed for the oriented capture of such within the $PSiO_2$ nanostructure. The detailed schematics for the different conjugation approaches are shown in Fig. 6.1 (upper panel). It should be emphasized again that directed immobilization of aptamers is possible in only two steps (see Fig. 5.2.1). Due to the presence of only one functional group, which can be chosen and positioned as needed, oriented conjugation can be achieved easily.

Biosensing

Porous silicon nanostructured films exhibiting Fabry-Pérot interference can be exploited as optical transducers in two different modes: when the pore sizes allow for infiltration of the analyte molecule, the average refractive index of the matrix changes upon its capture. This results in a shift towards higher EOT and can be easily monitored as a shift in position of the FFT peak (see Fig. 7.1, upper panel). For cellular targets, such as bacteria, which cannot infiltrate mesoporous silicon structures, cells captured on the surface cause increased light scattering which can be monitored as a decrease in the FFT peak's intensity (see Fig. 7.1, lower panel).

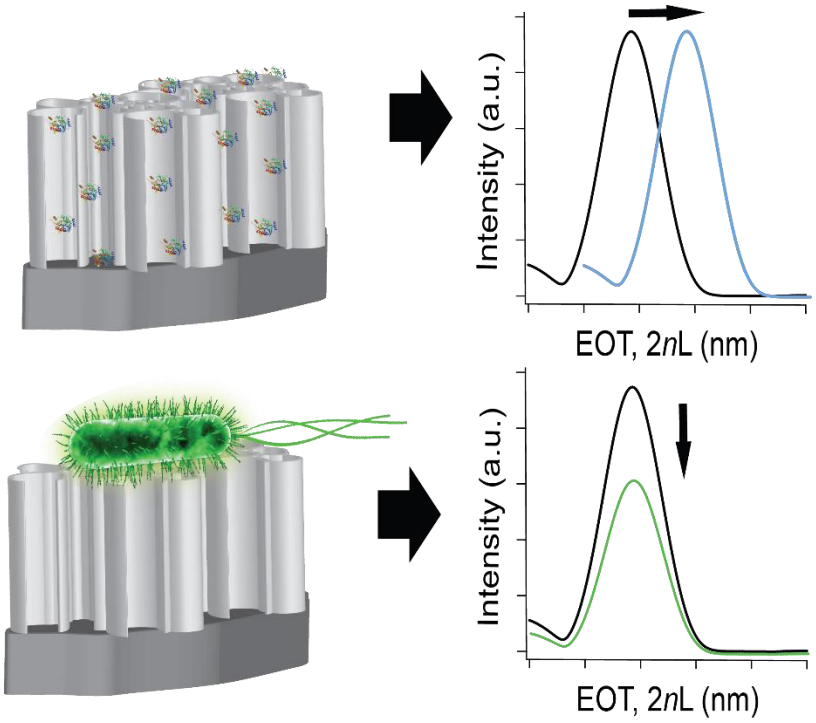

Figure 7.1. Different biosensing modes for aptamer-functionalized $PSiO_2$ layers. Upper panel shows the principle for analytes small enough to infiltrate the porous layer, causing a shift in FFT peak. Lower panel shows bacteria capture on top of the porous layer, causing an intensity-decrease in the FFT peak.

Functionalization of such optical transducers with aptamers as specific receptors enables the design of a vast number of different biosensors. As aptamers can be

selected against virtually any target, this is especially relevant for analytes, against which antibodies are not readily available.

Protein biosensing

In our first demonstrated proof-of-concept for the detection of his-tagged proteins, we focused on the linear detection range (11-56 µM) of the biosensor and emphasized the unique regenerability of the utilized aptamer and the highly selective performance of the biosensor in complex samples, such as bacteria lysates. Figures 5.1.4 and 5.1.1 illustrate the biosensor response versus the target-protein concentrations as well as controls, while Fig. 5.1.3 highlights the robust changes in EOT up to 15 biosensing cycles with target proteins and protein mixtures on the same $PSiO_2$-biosensor.

For the evaluation of PSi biosensors with a second aptamer/protein analyte pair, we chose to further investigate the detection range of the biosensor and to analyze common biosensor characteristics such as limit of detection, apparent dissociation constant, and resolution. Figure 5.3.3 presents the total binding of protein A to an aptamer-modified $PSiO_2$ layer and the unspecific adsorption of a non-target molecule to the scaffold, as well as the corresponding curves fitted with the three parameter Hill equation. Biosensor parameters determined for the binding of recombinant protein A to the truncated aptamer selected by Stoltenburg ***et al.*** [(138)] are shown in table 4.

Table 4. Biosensor parameters for the detection of protein A.

Linear detection range	Apparent dissociation constant	Limit of detection	Sensitivity
8-23 µM	13.98 ±1.54 µM	3.166 µM	6 % change in EOT per µM protein A

Bacteria biosensing

Utilizing the second mode of detection in RIFTS biosensors and simultaneously highlighting the broad range of aptamer targets, we presented a porous silicon-based aptasensor for the direct capture of *Lactobacillus acidophilus* bacteria cells.

While this system has indeed high relevance in the food industry, it mostly serves as a model for the concept of whole-cell detection with aptamer-tethered PSi nanostructures.

We demonstrated the efficient and rapid capture of *L. acidophilus* cells from pure and mixed populations of bacteria with high selectivity (see Fig. 5.2.3, 5.2.4 and 5.2.5). Additionally, the molecular recognition of membrane-protein structures enabled the aptamer to distinguish between live cultures and those that were heat-inactivated. Thus, the presented biosensing system allows for rapid and direct capture of live *L. acidophilus* cells at concentrations relevant for their application in probiotic products.

Optimization strategies

Over the course of this work, several aspects of the aptamer-functionalized porous silicon nanostructures were optimized and adjusted to ensure good aptamer-functionality, robust optical signals, and their amplification to reach lower limits of detection.

As outlined in section 2.2, aptamer immobilization density and the use of spacer molecules can have a severe impact on their functionality and induce steric hindrance. For the application of surface-tethered aptamers to directly capture bacteria cells, we found that lowering the aptamer concentration (10 µM instead of 50 µM) per fixed surface area has a similar effect as increasing the spacing by extension of the aptamer sequence. In both cases, greater flexibility of the aptamers without interference with neighboring capture probes enhanced the functional folding and access to the target structures, which resulted in increased biosensing signals (see Fig. 5.2.3)

Moreover, two specific optimizations have been established for the respective systems:

For bacteria capture, where no infiltration of targets into the porous structure is necessary and thus also immobilization of the aptamers within the pores is not relevant, the $PSiO_2$ nanostructure has been tuned in terms of its morphological

properties. In order to enhance the robustness and stability of the optical signal, pore sizes have been decreased, resulting in a higher number of Fabry-Pérot fringes in the reflectivity spectrum and thus in turn a higher signal-to-noise ratio (see Fig. 5.2.S1, 5.2.S2 and table 5.2.S2).

Protein A is known to have a specific affinity to human IgG. Thus, for the detection of protein A with protein A-binding aptamers, we were able to harness this affinity to demonstrate a sandwich assay for the amplification of biosensing signals in a simple RIFTS biosensor. While exposure of aptamer-functionalized biosensors to sample concentrations below the biosensor detection limit for each, protein A and IgG separately, does not result in any significant signal, subsequent exposure of a biosensor to first protein A and then human IgG resulted in a pronounced EOT signal (see Fig. 5.3.5 and 5.3.6). While the change in refractive index due to binding of few protein A molecules could not be observed by RIFTS, subsequent attachment of IgG which has a significantly higher molecular mass, induced a measurable EOT signal. This mechanism for signal amplification can be applied to other aptamer/target pairs and utilization of a second aptamer for the same target coupled to a higher mass particle or molecule is imaginable to enhance the signal further.

Comparison between aptamers and antibodies

The differences between antibodies and aptamers in terms of their production and properties are obvious. However, studies reporting on direct comparison of their performance as receptors in biosensors are rare and often leave the question, which recognition element results in better biosensors, open. In a preliminary study, we compared the behavior of biofunctionalized $PSiO_2$ to different non-target proteins, mixtures and different target protein concentrations (see Fig. 6.2 and 6.3). We studied three types of biosensors, (i) aptamer-conjugated, (ii) with randomly conjugated antibodies and (iii) with antibodies immobilized oriented. We found that aptamer-functionalized biosensors performed best in terms of robust signal following the model of specific target binding (see Fig. 6.4). Moreover, the calculated limit of detection (see Table 6.1) was the lowest for aptamer-tethered

biosensors and they could be regenerated for multiple uses, while their fabrication is easier and they have longer shelf life.

8. Conclusion

The major achievements of this work are:

- Introduction of aptamers as a new class of receptor probes in optical porous silicon biosensors
- Straightforward fabrication of tunable porous silicon nanostructures and simple strategies for the controlled conjugation of oligonucleotide sequences.
- Fabrication of highly stable biosensors that exhibit – due to the superior stability of aptamers and porous silicon – long shelf lives, especially compared to antibody-based assays.
- Reliable optical biosensing for two exemplary aptamer/target protein pairs, wherein one model-system (for capture of his-tagged proteins) additionally demonstrated easy regenerability for multiple usage. Therein, instrumentation was minimalistic and sample and reagent consumption low. The system has immense potential for multiplexing (i.e. immobilization of different aptamers on the same biosensor to detect several analytes simultaneously) and miniaturization of the experimental setup.
- Second detection mode for the RIFTS platform, highlighting the versatility of possible aptamer targets: with minimal changes in the $PSiO_2$ nanostructure and slightly different analysis of the data, we showed specific capture of whole bacteria cells onto the surface of the biosensor by aptamer receptors.
- Complete characterization of aptamer-functionalized $PSiO_2$ biosensors and additional comparison to antibody-functionalized biosensors targeting the same target.
- Sandwich assay format as proof-of-concept for the amplification of obtained biosensing signals by attachment of a secondary binding molecule that enhances the biosensor response at low analyte concentrations.

The demonstrated biosensor system based on aptamer capture probes and porous silicon transducers represents a universal detection scheme with enormous potential for further development: the simplicity of the system allows for miniaturization of the required instruments and combination with microfluidics, as it has been already demonstrated for porous silicon biosensors [146], could enable convenient point-of-care application. Integration of automated liquid handling would advance the system to high-throughput multiplexing and seamless integration into production processes for online monitoring of multiple analytes.

References

1. Tuerk, C., and Gold, L. (1990) Systemic evolution of ligands by exponential enrichment: RNA ligands to bacteriophage T4 DNA polymerase, *Science 249*, 505-510.
2. Ellington, A. D., and Szostak, J. W. (1990) In vitro selection of RNA molecules that bind specific ligands, *Nature 346*, 818-822.
3. Bunka, D. H. J., and Stockley, P. G. (2006) Aptamers come of age – at last, *Nat Rev Micro 4*, 588-596.
4. Berglund, L., Björling, E., Oksvold, P., Fagerberg, L., Asplund, A., Al-Khalili Szigyarto, C., Persson, A., Ottosson, J., Wernérus, H., Nilsson, P., Lundberg, E., Sivertsson, Å., Navani, S., Wester, K., Kampf, C., Hober, S., Pontén, F., and Uhlén, M. (2008) A Genecentric Human Protein Atlas for Expression Profiles Based on Antibodies, *Molecular & Cellular Proteomics 7*, 2019-2027.
5. Bradbury, A., and Plueckthun, A. (2015) Standardize antibodies used in research, *Nature 518*, 27-29.
6. Song, S., Wang, L., Li, J., Fan, C., and Zhao, J. (2008) Aptamer-based biosensors, *Trends in Analytical Chemistry 27*, 108-117.
7. Hamula, C. L. A., Zhang, H., Li, F., Wang, Z., Chris Le, X., and Li, X.-F. (2011) Selection and analytical applications of aptamers binding microbial pathogens, *Trends in Analytical Chemistry 30*, 1587-1597.
8. Lönne, M., Zhu, G., Stahl, F., and Walter, J.-G. (2014) Aptamer-Modified Nanoparticles as Biosensors, In *Biosensors Based on Aptamers and Enzymes* (Gu, M. B., and Kim, H.-S., Eds.), pp 121-154, Springer Berlin Heidelberg.
9. Zhu, G., Lübbecke, M., Walter, J., Stahl, F., and Scheper, T. (2011) Characterization of Optimal Aptamer-Microarray Binding Chemistry and Spacer Design, *Chemical engineering & technology 34*, 2022-2028.
10. Walter, J. G., Kökpinar, O., Friehs, K., Stahl, F., and Scheper, T. (2008) Systematic Investigation of Optimal Aptamer Immobilization for Protein-Microarray Applications, *Analytical Chemistry 80*, 7372 - 7378.
11. Sailor, M. J. (2011) *Porous Silicon in Practice*, Wiley-VCH, Weinheim.
12. Jane, A., Dronov, R., Hodges, A., and Voelcker, N. H. (2009) Porous silicon biosensors on the advance, *Trends in Biotechnology 27*, 230-239.
13. Kilian, K. A., Boecking, T., and Gooding, J. J. (2009) The importance of surface chemistry in mesoporous materials: lessons from porous silicon biosensors, *Chemical Communications*, 630-640.
14. Bonanno, L. M., and Segal, E. (2011) Nanostructured porous silicon/polymer-based hybrids: from biosensing to drug delivery, *Nanomedicine 6*, 1755-1770.
15. Salonen, J., and Lehto, V.-P. (2008) Fabrication and chemical surface modification of mesoporous silicon for biomedical applications, *Chemical Engineering Journal 137*, 162-172.
16. Archer, M., Christophersen, M., and Fauchet, P. M. (2004) Macroporous Silicon Electrical Sensor for DNA Hybridization Detection, *Biomedical microdevices 6*, 203-211.
17. Bonanno, L. M., and DeLouise, L. A. (2007) Steric crowding effects on target detection in an affinity biosensor, *Langmuir 23*, 5817-5823.
18. Bonanno, L. M., and DeLouise, L. A. (2010) Tunable Detection Sensitivity of Opiates in Urine via a Label-Free Porous Silicon Competitive Inhibition Immunosensor, *Analytical Chemistry 82*, 714-722.

19. Massad-Ivanir, N., Shtenberg, G., Tzur, A., Krepker, M. A., and Segal, E. (2011) Engineering Nanostructured Porous SiO(2) Surfaces for Bacteria Detection via "Direct Cell Capture", *Analytical Chemistry 83*, 3282-3289.
20. Chan, S., Horner, S. R., Fauchet, P. M., and Miller, B. L. (2001) Identification of gram negative bacteria using nanoscale silicon microcavities, *Journal of the American Chemical Society 123*, 11797-11798.
21. Massad-Ivanir, N., and Segal, E. (2014) 12 - Porous silicon for bacteria detection, In *Porous Silicon for Biomedical Applications* (Santos, H. A., Ed.), pp 286-303, Woodhead Publishing.
22. Shtenberg, G., and Segal, E. (2014) Porous Silicon Optical Biosensors, In *Handbook of Porous Silicon* (Canham, L., Ed.), pp 1-11, Springer International Publishing.
23. Pacholski, C. (2013) Photonic Crystal Sensors Based on Porous Silicon, *Sensors 13*, 4694-4713.
24. Dancil, K. P. S., Greiner, D. P., and Sailor, M. J. (1999) A porous silicon optical biosensor: Detection of reversible binding of IgG to a protein A-modified surface, *Journal of the American Chemical Society 121*, 7925-7930.
25. Janshoff, A., Dancil, K. P. S., Steinem, C., Greiner, D. P., Lin, V. S. Y., Gurtner, C., Motesharei, K., Sailor, M. J., and Ghadiri, M. R. (1998) Macroporous p-type silicon Fabry-Perot layers. Fabrication, characterization, and applications in biosensing, *Journal of the American Chemical Society 120*, 12108-12116.
26. Lin, V. S.-Y., Motesharei, K., Dancil, K.-P. S., Sailor, M. J., and Ghadiri, M. R. (1997) A Porous Silicon-Based Optical Interferometric Biosensor, *Science 278*, 840-843.
27. Salis, A., Setzu, S., Monduzzi, M., and Mula, G. (2011) Porous Silicon-based Electrochemical Biosensors, In *Biosensors - Emerging Materials and Applications* (Serra, P. A., Ed.), InTech.
28. Thévenot, D. R., Toth, K., Durst, R. A., and Wilson, G. S. (2001) Electrochemical biosensors: recommended definitions and classification, *Biosensors and Bioelectronics 16*, 121-131.
29. Turner, A. P. F. (1989) Current Trends in Biosensor Research and Development, *Sensor Actuator 17*, 433-450.
30. Kahn, K., and Plaxco, K. W. (2010) Principles of Molecular Recognition, In *Recognition Receptors in Biosensors* (Zourob, M., Ed.), pp 3-46, Springer, New York Dordrecht Heidelberg London.
31. Zourob, M. (2010) *Recognition Receptors in Biosensors*, Springer, New York Dordrecht Heidelberg London.
32. Piletsky, S. A., and Whitcombe, M. J., (Eds.) (2013) *Designing Receptors for the Next Generation of Biosensors*, Vol. 12, Springer, Heidelberg New York Dordrecht London.
33. Tonegawa, S. (1983) Somatic Generation of Antibody Diversity, *Nature 302*, 575-581.
34. Kim, J. P., Lee, B. Y., Hong, S., and Sim, S. J. (2008) Ultrasensitive carbon nanotube-based biosensors using antibody-binding fragments, *Analytical Biochemistry 381*, 193-198.
35. Holliger, P., and Hudson, P. J. (2005) Engineered antibody fragments and the rise of single domains, *Nat Biotechnol 23*, 1126-1136.
36. Roque, A. C. A., Lowe, C. R., and Taipa, M. A. (2004) Antibodies and genetically engineered related molecules: Production and purification, *Biotechnology Progress 20*, 639-654.

37. Shreder, K. (2000) Synthetic haptens as probes of antibody response and immunorecognition, *Methods 20*, 372-379.
38. Hopkins, N. A. E. (2010) Antibody engineering for Biosensor Applications, In *Recognition Receptors in Biosensors* (Zourob, M., Ed.), pp 451-529, Springer, New York Dordrecht Heidelberg London.
39. Clark, L. C., and Lyons, C. (1962) Electrode Systems for Continuous Monitoring in Cardiovascular Surgery, *Annals of the New York Academy of Sciences 102*, 29-&.
40. Hundeck, H. G., Weiss, M., Scheper, T., and Schubert, F. (1993) Calorimetric Biosensor for the Detection and Determination of Enantiomeric Excesses in Aqueous and Organic Phases, *Biosens. Bioelectron. 8*, 205-208.
41. Leca-Bouvier, B. D., and Blum, L. C. (2010) Enzyme for Biosensing Applications, In *Recognition Receptors in Biosensors* (Zourob, M., Ed.), pp 177-220, Springer, New York Dordrecht Heidelberg London.
42. Axarli, I., Prigipaki, A., and Labrou, N. E. (2005) Engineering the substrate specificity of cytochrome P450CYP102A2 by directed evolution: production of an efficient enzyme for bioconversion of fine chemicals, *Biomolecular Engineering 22*, 81-88.
43. Chambers, J. P., Arulanandam, B. P., Matta, L. L., Weis, A., and Valdes, J. J. (2008) Biosensor recognition elements, *Curr Issues Mol Biol 10*, 1-12.
44. Ostermeier, M. (2005) Engineering allosteric protein switches by domain insertion, *Protein Engineering Design & Selection 18*, 359-364.
45. Turner, A. P. F. (2000) Biochemistry - Biosensors sense and sensitivity, *Science 290*, 1315-1317.
46. Liao, J. C., Mastali, M., Li, Y., Gau, V., Suchard, M. A., Babbitt, J., Gornbein, J., Landaw, E. M., McCabe, E. R., Churchill, B. M., and Haake, D. A. (2007) Development of an advanced electrochemical DNA biosensor for bacterial pathogen detection, *Journal of Molecular Diagnostics 9*, 158-168.
47. Farabullini, F., Lucarelli, F., Palchetti, I., Marrazza, G., and Mascini, M. (2007) Disposable electrochemical genosensor for the simultaneous analysis of different bacterial food contaminants, *Biosens Bioelectron 22*, 1544-1549.
48. Shin, Y., Perera, A. P., and Park, M. K. (2013) Label-free DNA sensor for detection of bladder cancer biomarkers in urine, *Sensors and Actuators B-Chemical 178*, 200-2006.
49. Stahl, F. (2005) Analysis of genregulation - DNA chip technology, *Chem Unserer Zeit 39*, 188-194.
50. Gerasimova, Y. V., Ballantyne, J., and Kolpashchikov, D. M. (2013) Detection of SNP-containing human DNA sequences using a split sensor with a universal molecular beacon reporter, *Methods Mol Biol 1039*, 69-80.
51. Wang, J. (2000) From DNA biosensors to gene chips, *Nucleic Acids Res 28*, 3011-3016.
52. Eckstein, F., and Gish, G. (1989) Phosphorothioates in Molecular-Biology, *Trends in Biochemical Sciences 14*, 97-100.
53. Vester, B., and Wengel, J. (2004) LNA (Locked nucleic acid): High-affinity targeting of complementary RNA and DNA, *Biochemistry 43*, 13233-13241.
54. Vainrub, A., and Pettitt, B. M. (2002) Coulomb blockage of hybridization in two-dimensional DNA arrays, *Physical Review E 66*.
55. Rao, A. N., and Grainger, D. W. (2014) Biophysical properties of nucleic acids at surfaces relevant to microarray performance, *Biomaterials Science 2*, 436-471.

56. Nielsen, P. E., Egholm, M., Berg, R. H., and Buchardt, O. (1991) Sequenceselective recognition of DNA by strand displacement with a thymine-substituted polyamide, *Science 254*, 1498-1500.
57. Mateo-Martí, E., and Pradier, C.-M. (2010) A Novel Type of Nucleic Acid-based Biosensors: the Use of PNA Probes, Associated with Surface Science and Electrochemical Detection Techniques In *Intelligent and biosensor* (Somerset, V. S., Ed.), InTech.
58. Ellington, A. D., and Szostak, J. W. (1990) In vitro selection of RNA molecules that bind specific ligands, *Nature 346*, 818-822.
59. Robertson, D. L., and Joyce, G. F. (1990) Selection in vitro of an RNA enzyme that specifically cleaves single-stranded DNA, *Nature 344*, 467-468.
60. Tuerk, C., and Gold, L. (1990) Systematic evolution of ligands by exponential enrichment: RNA ligands to bacteriophage T4 DNA polymerase, *Science 249*, 505-510.
61. Stoltenburg, R., Nikolaus, N., and Strehlitz, B. (2012) Capture-SELEX: Selection of DNA Aptamers for Aminoglycoside Antibiotics, *Journal of Analytical Methods in Chemistry*.
62. Stoltenburg, R., Reinemann, C., and Strehlitz, B. (2005) FluMag-SELEX as an advantageous method for DNA aptamer selection, *Analytical and Bioanalytical Chemistry 383*, 83-91.
63. Nitsche, A., Kurth, A., Dunkhorst, A., Panke, O., Sielaff, H., Junge, W., Muth, D., Scheller, F., Stocklein, W., Dahmen, C., Pauli, G., and Kage, A. (2007) One-step selection of Vaccinia virus-binding DNA aptamers by MonoLEX, *BMC Biotechnol 7*, 48.
64. Patel, D. J. (1997) Structural analysis of nucleic acid aptamers, *Current Opinion in Chemical Biology 1*, 32-46.
65. Hermann, T., and Patel, D. J. (2000) Biochemistry - Adaptive recognition by nucleic acid aptamers, *Science 287*, 820-825.
66. Strehlitz, B., Nikolaus, N., and Stoltenburg, R. (2008) Protein detection with aptamer biosensors, *Sensors 8*, 4296-4307.
67. Walter, J.-G., Stahl, F., and Scheper, T. (2012) Aptamers as affinity ligands for downstream processing, *Engineering in Life Sciences 12*, 496-506.
68. Walter, J.-G., Heilkenbrinker, A., Austerjost, J., Stahl, F., and Scheper, T. (2012) Aptasensors for Small Molecule Detection, *Z. Naturforsch. 67b*, 976-986.
69. Loenne, M., Zhu, G., Stahl, F., and Walter, J.-G. (2014) Aptamer-modified Nanoparticles as Biosensors, In *Biosensors Based on Aptamers and Enzymes - Advances in biochemical engineering/biotechnology* (Gu, M. B., and Kim, H.-S., Eds.), pp 121-154, Springer.
70. Heilkenbrinker, A., Reinemann, C., Stoltenburg, R., Walter, J.-G., Jochums, A., Stahl, F., Zimmermann, S., Strehlitz, B., and Scheper, T. (submitted) Identification of the target binding site of ethanolamine binding aptamers and its exploitation for ethanolamine detection, *Analytical Chemistry*.
71. Hamaguchi, N., Ellington, A., and Stanton, M. (2001) Aptamer beacons for the direct detection of proteins, *Analytical Biochemistry 294*, 126-131.
72. Stoltenburg, R., Reinemann, C., and Strehlitz, B. (2007) SELEX--a (r)evolutionary method to generate high-affinity nucleic acid ligands, *Biomolecular Engineering 24*, 381-403.
73. Kökpinar, Ö., Walter, J.-G., Shoham, Y., Stahl, F., and Scheper, T. (2011) Aptamer-based Downstream Processing of His-tagged Proteins Utilizing Magnetic Beads, *Biotechnology and Bioengineering 108*, 2371-2379.

74. Zhu, G., and Walter, J.-G. (accepted) Aptamer-Modified Magnetic Beads in Affinity Separation of Proteins, In *Affinity Chromatography: Methods and Protocols, Second Edition* (Reichelt, S., Ed.), Springer.

75. Lee, E. J., Lim, H. K., Cho, Y. S., and Hah, S. S. (2013) Peptide nucleic acids are an additional class of aptamers, *Rsc Advances 3*, 5828-5831.
76. Bredehorst, R., Glökler, J., Grunwald, T., Matzas, M., and Spillner, E. (2005) Method for determining an unknown PNA sequence and uses thereof, (SPECIFICATION, E. P., Ed.).
77. Harraz, F. A. (2014) Porous silicon chemical sensors and biosensors: A review, *Sensors and Actuators B: Chemical 202*, 897-912.
78. DeLouise, L. A., Kou, P. M., and Miller, B. L. (2005) Cross-correlation of optical microcavity biosensor response with immobilized enzyme activity. Insights into biosensor sensitivity, *Analytical Chemistry 77*, 3222-3230.
79. Deng, Z., and Alocilja, E. C. (2008) Characterization of Nanoporous Silicon-Based DNA Biosensor for the Detection of <emphasis>Salmonella</emphasis> Enteritidis, *Sensors Journal, IEEE 8*, 775-780.
80. de Leon, S. B., Sa'ar, A., Oren, R., Spira, M. E., and Yitzchaik, S. (2004) Neurons culturing and biophotonic sensing using porous silicon, *Applied Physics Letters 84*, 4361-4363.
81. Stewart, M. P., and Buriak, J. M. (2000) Chemical and Biological Applications of Porous Silicon Technology, *Adv. Mater. 12*, 859-869.
82. Birner, A., Wehrspohn, R. B., Gosele, U. M., and Busch, K. (2001) Silicon-based photonic crystals, *Adv. Mater. 13*, 377-388.
83. Lugo, J. E., Ocampo, M., Kirk, A. G., Plant, D. V., and Fauchet, P. M. (2007) Electrochemical Sensing of DNA with Porous Silicon Layers, *Journal of New Materials for Electrochemical Systems 10*, 113-116.
84. Song, M. J., Yun, D. H., Min, N. K., and Hong, S. I. (2007) Electrochemical biosensor array for liver diagnosis using silanization technique on nanoporous silicon electrode, *Journal of bioscience and bioengineering 103*, 32-37.
85. Setzu, S., Salis, S., Demontis, V., Salis, A., Monduzzi, M., and Mula, G. (2007) Porous silicon-based potentiometric biosensor for triglycerides, *physica status solidi (a) 204*, 1434-1438.
86. Zhang, J., Wu, Y., Zhang, B., Li, M., Jia, S., Jiang, S., Zhou, H., Zhang, Y., Zhang, C., and Turner, A. P. F. (2012) Label-Free Electrochemical Detection of Tetracycline by an Aptamer Nano-Biosensor, *Analytical Letters 45*, 986-992.
87. Starodub, V. M., Fedorenko, L. L., Sisetskiy, A. P., and Starodub, N. F. (1999) Control of myoglobin level in a solution by an immune sensor based on the photoluminescence of porous silicon, *Sensors and Actuators B: Chemical 58*, 409-414.
88. Cullis, A. G., and Canham, L. T. (1991) Visible light emission due to quantum size effects in highly porous crystalline silicon, *Nature 353*, 335-338.
89. Canham, L. T., and (Firm), K. (1997) *Properties of porous silicon / edited by Leigh Canham*, Institution of Electrical Engineers, London.
90. Bisi, O., Ossicini, S., and Pavesi, L. (2000) Porous silicon: a quantum sponge structure for silicon based optoelectronics, *Surface Science Reports 38*, 1-126.
91. Yoo, L., Ahn, K.-Y., Ahn, J.-Y., Laurell, T., Lee, Y. M., Yoo, P. J., and Lee, J. (2013) A simple one-step assay platform based on fluorescence quenching of macroporous silicon, *Biosensors and Bioelectronics 41*, 477-483.

92. Gaur, G., Koktysh, D., and Weiss, S. M. (2013) Porous silicon biosensors using quantum dot signal amplifiers, In *Nanoscale Imaging, Sensing, and Actuation for Biomedical Applications X*, pp 859408-859408-859411, Proc. SPIE.
93. Simion, M., Kusko, M., Mihalache, I., and Bragaru, A. (2013) Dual detection biosensor based on porous silicon substrate, *Mater. Sci. Eng. B-Adv. Funct. Solid-State Mater. 178*, 1268-1274.
94. Fan, X., White, I. M., Shopoua, S. I., Zhu, H., Suter, J. D., and Sun, Y. (2008) Sensitive optical biosensors for unlabeled targets: A review, *Analytica Chimica Acta 620*, 8-26.
95. Massad-Ivanir, N., Shtenberg, G., Tzur, A., Krepker, M. A., and Segal, E. (2011) Engineering nanostructured porous SiO2 surfaces for bacteria detection via "direct cell capture", *Anal Chem 83*, 3282-3289.
96. Bonanno, L. M., and DeLouise, L. A. (2009) Tunable Detection Sensitivity of Opiates in Urine via a Label-Free Porous Silicon Competitive Inhibition Immunosensor, *Analytical Chemistry 82*, 714-722.
97. Pacholski, C., Yu, C., Miskelly, G. M., Godin, D., and Sailor, M. J. (2006) Reflective Interferometric Fourier Transform Spectroscopy: A Self-Compensating Label-Free Immunosensor Using Double-layers of Porous SiO2, *Journal of the American Chemical Society 128*, 4250-4252.
98. Bonanno, L. M., and DeLouise, L. A. (2007) Whole blood optical biosensor, *Biosensors and Bioelectronics 23*, 444-448.
99. Kilian, K. A., Boecking, T., Gaus, K., Gal, M., and Gooding, J. J. (2007) Peptide-modified optical filters for detecting protease activity, *Acs Nano 1*, 355-361.
100. Orosco, M. M., Pacholski, C., Miskelly, G. M., and Sailor, M. J. (2006) Protein-coated porous-silicon photonic crystals for amplified optical detection of protease activity, *Adv. Mater. 18*, 1393-1396.
101. Pacholski, C., Sartor, M., Sailor, M. J., Cunin, F., and Miskelly, G. M. (2005) Biosensing using porous silicon double-layer interferometers: reflective interferometric Fourier transform spectroscopy, *Journal of the American Chemical Society 127*, 11636-11645.
102. Grieshaber, D., MacKenzie, R., Vörös, J., and Reimhult, E. (2008) Electrochemical Biosensors - Sensor Principles and Architectures, *Sensors 8*, 1400-1458.
103. Thevenot, D. R., Toth, K., Durst, R. A., and Wilson, G. S. Electrochemical biosensors: recommended definitions and classification, *Biosensors and Bioelectronics 16*, 121-131.
104. De Filippo, F., De Lisio, C., Maddalena, P., Lérondel, G., and Altucci, C. (2000) Measurement of Porous Silicon Dielectric Constant by VUV Laser Harmonic Radiation, *physica status solidi (a) 182*, 261-266.
105. Tuerk, C., and Gold, L. (1990) Systematic Evolution of Ligands by Exponential Enrichment - Rna Ligands to Bacteriophage-T4 DNA-Polymerase, *Science 249*, 505-510.
106. Jayasena, S. D. (1999) Aptamers: An emerging class of molecules that rival antibodies in diagnostics, *Clinical Chemistry 45*, 1628-1650.
107. Heilkenbrinker, A., Reinemann, C., Stoltenburg, R., Walter, J. G., Jochums, A., Stahl, F., Zimmermann, S., Strehlitz, B., and Scheper, T. (2015) Identification of the target binding site of ethanolamine-binding aptamers and its exploitation for ethanolamine detection, *Analytical Chemistry 87*, 677-685.
108. Urmann, K., Walter, J.-G., Scheper, T., and Segal, E. (2015) Label-Free Optical Biosensors Based on Aptamer-Functionalized Porous Silicon Scaffolds, *Analytical Chemistry 87*, 1999-2006.

109. Kökpinar, Ö., Walter, J. G., Shoham, Y., Stahl, F., and Scheper, T. (2011) Aptamer-Based Downstream Processing of His-Tagged Proteins Utilizing Magnetic Beads, *Biotechnology and Bioengineering 108*, 2371-2379.
110. Lönne, M., Bolten, S., Lavrentieva, A., Stahl, F., Scheper, T., and Walter, J. G. (2015) Development of an aptamer-based affinity purification method for vascular endothelial growth factor, *Biotechnology Reports 8*, 16-23.
111. Walter, J. G., Stahl, F., and Scheper, T. (2012) Aptamers as affinity ligands for downstream processing, *Engineering in Life Sciences 12*, 496-506.
112. Schax, E., Lönne, M., Scheper, T., Belkin, S., and Walter, J. G. (2015) Aptamer-based depletion of small molecular contaminants: A case study using ochratoxin A, *BIOTECHNOL BIOPROC E 20*, 1016-1025.
113. Meyer, M., Scheper, T., and Walter, J. G. (2013) Aptamers: Versatile probes for flow cytometry, *Appl Microbiol Biotechnol 97*, 7097-7109.
114. Modrejewski, J., Walter, J.-G., Kretschmer, I., Kemal, E., Green, M., Belhadj, H., Blume, C., and Scheper, T. (2015) Aptamer-modified polymer nanoparticles for targeted drug delivery, *BioNanoMaterials 17*, 43-51.
115. Walter, J. G., Petersen, S., Stahl, F., Scheper, T., and Barcikowski, S. (2010) Laser ablation-based one-step generation and bio-functionalization of gold nanoparticles conjugated with aptamers, *Journal of Nanobiotechnology 8*.
116. Patel, D. J., Suri, A. K., Jiang, F., Jiang, L. C., Fan, P., Kumar, R. A., and Nonin, S. (1997) Structure, recognition and adaptive binding in RNA aptamer complexes, *Journal of Molecular Biology 272*, 645-664.
117. Walter, J. G., KÃ¶kpinar, Ã., Friehs, K., Stahl, F., and Scheper, T. (2008) Systematic investigation of optimal aptamer immobilization for protein-microarray applications, *Analytical Chemistry 80*, 7372-7378.
118. Balamurugan, S., Obubuafo, A., Soper, S. A., and Spivak, D. A. (2008) Surface immobilization methods for aptamer diagnostic applications, *Anal Bioanal Chem 390*, 1009-1021.
119. Ocana, C., and del Valle, M. (2014) A comparison of four protocols for the immobilization of an aptamer on graphite composite electrodes, *Microchimica Acta 181*, 355-363.
120. Zhu, G. H., Lubbecke, M., Walter, J. G., Stahl, F., and Scheper, T. (2011) Characterization of Optimal Aptamer-Microarray Binding Chemistry and Spacer Design, *Chemical Engineering & Technology 34*, 2022-2028.
121. Lin, P. H., Chen, R. H., Lee, C. H., Chang, Y., Chen, C. S., and Chen, W. Y. (2011) Studies of the binding mechanism between aptamers and thrombin by circular dichroism, surface plasmon resonance and isothermal titration calorimetry, *Colloids and Surfaces B-Biointerfaces 88*, 552-558.
122. Witt, M., Walter, J.-G., and Stahl, F. (2015) Aptamer Microarrays-Current Status and Future Prospects, *Microarrays 4*, 115-132.
123. Justino, C. I. L., Freitas, A. C., Pereira, R., Duarte, A. C., and Rocha Santos, T. A. P. (2015) Recent developments in recognition elements for chemical sensors and biosensors, *TrAC Trends in Analytical Chemistry 68*, 2-17.
124. Liang, H., Zhang, X. B., Lv, Y. F., Gong, L., Wang, R. W., Zhu, X. Y., Yang, R. H., and Tan, W. H. (2014) Functional DNA-Containing Nanomaterials: Cellular Applications in Biosensing, Imaging, and Targeted Therapy, *Accounts Chem. Res. 47*, 1891-1901.
125. Wang, Z. H., Yu, J. B., Gui, R. J., Jin, H., and Xia, Y. Z. (2016) Carbon nanomaterials-based electrochemical aptasensors, *Biosens. Bioelectron. 79*, 136-149.

126. Wang, G., Wang, Y., Chen, L., and Choo, J. (2010) Nanomaterial-assisted aptamers for optical sensing, *Biosensors and Bioelectronics 25*, 1859-1868.
127. Bunka, D. H. J., and Stockley, P. G. (2006) Aptamers come of age - at last, *Nat. Rev. Microbiol. 4*, 588-596.
128. Walter, J.-G., Kökpinar, Ö., Friehs, K., Stahl, F., and Scheper, T. (2008) Systematic Investigation of Optimal Aptamer Immobilization for Protein−Microarray Applications, *Analytical Chemistry 80*, 7372-7378.
129. Balamurugan, S., Obubuafo, A., McCarley, R. L., Soper, S. A., and Spivak, D. A. (2008) Effect of Linker Structure on Surface Density of Aptamer Monolayers and Their Corresponding Protein Binding Efficiency, *Analytical Chemistry 80*, 9630-9634.
130. White, R. J., Phares, N., Lubin, A. A., Xiao, Y., and Plaxco, K. W. (2008) Optimization of Electrochemical Aptamer-Based Sensors via Optimization of Probe Packing Density and Surface Chemistry, *Langmuir 24*, 10513-10518.
131. Daniel, C., Roupioz, Y., Gasparutto, D., Livache, T., and Buhot, A. (2013) Solution-Phase vs Surface-Phase Aptamer-Protein Affinity from a Label-Free Kinetic Biosensor, *PLoS ONE 8*, e75419.
132. Hasegawa, H., Savory, N., Abe, K., and Ikebukuro, K. (2016) Methods for Improving Aptamer Binding Affinity, *Molecules (Basel, Switzerland) 21*, 421.
133. Urmann, K., Arshavsky-Graham, S., Walter, J. G., Scheper, T., and Segal, E. (2016) Whole-cell detection of live lactobacillus acidophilus on aptamer-decorated porous silicon biosensors, *The Analyst*.
134. Lim, J. Y., and Donahue, H. J. (2007) Cell sensing and response to micro- and nanostructured surfaces produced by chemical and topographic patterning, *Tissue Eng. 13*, 1879-1891.
135. Teixeira, A. I., Abrams, G. A., Bertics, P. J., Murphy, C. J., and Nealey, P. F. (2003) Epithelial contact guidance on well-defined micro- and nanostructured substrates, *Journal of Cell Science 116*, 1881-1892.
136. Doyle, S. A., and Murphy, M. B. (2005) Aptamers and methods for their in vitro selection and uses thereof, US.
137. Hamula, C. L., Zhang, H., Guan, L. L., Li, X. F., and Le, X. C. (2008) Selection of aptamers against live bacterial cells, *Analytical Chemistry 80*, 7812-7819.
138. Stoltenburg, R., Schubert, T., and Strehlitz, B. (2015) In vitro Selection and Interaction Studies of a DNA Aptamer Targeting Protein A, *PLoS ONE 10*, e0134403.
139. Segal, E., Perelman, L. A., Cunin, F., Di Renzo, F., Devoisselle, J. M., Li, Y. Y., and Sailor, M. J. (2007) Confinement of Thermoresponsive Hydrogels in Nanostructured Porous Silicon Dioxide Templates, *Advanced Functional Materials 17*, 1153-1162.
140. Massad-Ivanir, N., Shtenberg, G., Zeidman, T., and Segal, E. (2010) Construction and Characterization of Porous SiO(2)/Hydrogel Hybrids as Optical Biosensors for Rapid Detection of Bacteria, *Advanced Functional Materials 20*, 2269-2277.
141. Ellman, G. L. (1959) Tissue sulfhydryl groups, *Archives of biochemistry and biophysics 82*, 70-77.
142. Riley, S. P., Woodman, M. E., and Stevenson, B. (2008) Culture of Escherichia coli and Related Bacteria, In *Current Protocols Essential Laboratory Techniques*, John Wiley & Sons, Inc.
143. Bunthof, C. J., Bloemen, K., Breeuwer, P., Rombouts, F. M., and Abee, T. (2001) Flow Cytometric Assessment of Viability of Lactic Acid Bacteria, *Appl. Environ. Microbiol. 67*, 2326-2335.

144. Weiss, G., Rasmussen, S., Zeuthen, L. H., Nielsen, B. N., Jarmer, H., Jespersen, L., and Frøkiær, H. (2010) Lactobacillus acidophilus induces virus immune defence genes in murine dendritic cells by a Toll-like receptor-2-dependent mechanism, *Immunology 131*, 268-281.
145. Kiviharju, K., Leisola, M., and von Weymarn, N. (2004) Light sensitivity of Bifidobacterium longum in bioreactor cultivations, *Biotechnology Letters 26*, 539-542.
146. Vilensky, R., Bercovici, M., and Segal, E. (2015) Oxidized Porous Silicon Nanostructures Enabling Electrokinetic Transport for Enhanced DNA Detection, *Advanced Functional Materials 25*, 6725-6732.

Chapter 4
Porous Silicon Biosensors Employing Emerging Capture Probes

Katharina Urmann, Elena Tenenbaum, Johanna-Gabriela Walter and Ester Segal

Abstract The application of porous silicon (PSi) for biosensing was first described by Thust et al. in 1996, demonstrating a potentiometric biosensor for the detection of penicillin. However, only in the past decade PSi has established as a promising nanomaterial for label-free biosensing applications. This chapter focuses on the integration of new emerging capture probes with PSi-based biosensing schemes. An overview of natural and synthetic receptors and their advantageous characteristics for the potential application in PSi biosensors technology is presented. We also review and discuss several examples, which successfully combine these new bioreceptors with PSi optical and electrochemical transducers, for label-free biosensing.

4.1 Introduction

Although porous silicon (PSi) was already discovered in the 1950s, it only gained scientific attention in the 1990s when Leigh Canham reported bright photoluminescence of the material [1]. While the interest in PSi for optoelectronic switches, displays and lasers quickly faded due to its poor chemical and mechanical stability, it became a material of choice for sensors design. PSi unique combination of properties i.e., high surface area and volume, tunable nanostructure, versatile surface chemistry and compatibility with other silicon microfabrication technologies,

K. Urmann · J.-G. Walter
Institute of Technical Chemistry, Gottfried-Wilhelm Leibniz Universität Hannover, Hannover, Germany

K. Urmann · E. Tenenbaum · E. Segal (✉)
Department of Biotechnology and Food Engineering, Technion-Israel Institute of Technology, Haifa, Israel
e-mail: esegal@tx.technion.ac.il

E. Segal
Russell Berrie Nanotechnology Institute, Technion-Israel Institute of Technology, Haifa, Israel

D. Losic and A. Santos (eds.), *Electrochemically Engineered Nanoporous Materials*, Springer Series in Materials Science 220,
DOI 10.1007/978-3-319-20346-1_4

allow for the design of sophisticated biosensing platforms [1, 2]. Indeed, a growing number of biosensing schemes employing PSi as a transducer are reported in recent years. By 2013, the yearly number of new publications already reached 40. Included here are not only electrochemical biosensors taking advantage of the semiconductor electrical properties, but also many optical biosensing schemes, which utilize the unique optical properties of this nanostructured material. The most common fabrication method of PSi is electrochemical etching in the presence of hydrofluoric acid (HF). This method allows to easily define the properties of the formed porous layer in terms of pore dimensions, morphology and porosity, by adjustment of the etching parameters (e.g., current density, anodization time, HF concentration) [3, 4]. By controlling the current density during the etching process, different porous structures can be fabricated such as single porous layers, double layers, photonic crystals and microcavities [2].

The freshly-etched PSi is unstable in ambient environment and in aqueous medium as the Si hydride-terminated surface is prone to nucleophilic attack by water molecules. A simple method to stabilize PSi is to grow an oxide layer on the surface to slow spontaneous oxidation ($PSiO_2$ formation). The resulting $PSiO_2$ layer provides a convenient means for subsequent surface modification, as it enables the simple reaction with different alkyl silanes [2, 5, 6]. Reactive groups at the distal end of the silane molecules, such as amines and thiols, provide attachment points for biorecognition elements. Silanization of oxidized PSi has been used to create biorecognition interfaces composed of DNA [5], antibodies [7–9] and small molecules [10].

Porous silicon has proven to be a suitable transducer, showing excellent sensitivity, and allowing for label-free detection of many analytes of interest [11, 12]. PSi optical biosensors are based on changes in the photoluminescence or the reflectivity spectra upon exposure to the target analyte, which replace the media in the pores. A change in the refractive index (RI) of the liquid in the pores affects the average RI of the porous film, and is commonly observed as quenching of the PSi photoluminescence or as a wavelength shift in the reflectivity spectrum. For analytes that are size excluded from penetrating into the porous nanostructure, changes in the reflected light intensity are observed as a result from a change in the RI contrast at the PSi-medium (air or other) interface [13].

Optical transducers received significant attention in the field of PSi-based biosensors since the pioneering work of Sailor and co-workers [14–16], and there are already few commercially-available optical sensing systems (Silicon Kinetics, Inc.). Nevertheless, PSi is also studied as an electrochemical transducer for biosensing applications [17]. The two main electrochemical transduction types are potentiometry and amperometry. Potentiometric biosensors measure the potential difference occurring as a result of an acidic/alkaline substance formation. These substances are usually a product of an enzymatic reaction, where the catalyzing enzyme is immobilized onto the PSi surface. Amperometric biosensors measure current density resulting from redox reactions, catalyzed by immobilized enzymes. Amperometric PSi-based biosensors are less applicable due to the relatively poor conductivity of PSi and therefore, coupling of metal electrodes to the PSi may increase their sensitivity [17, 18].

Apart from the transducer quality, the properties of the biorecognition elements to be used for analyte binding have a critical effect on the performance of any biosensor system. The use of novel capture probes is emerging for new assay designs and for targeting a wide variety of analytes. These capture probes: aptamers, peptide nucleic acid (PNA), synthetic antibodies, antimicrobial peptides (AMPs) or enzymes, hold in store many advantages over the common bioreceptors. These include improved conformational stability, higher affinity towards the target analyte, and reduced production costs. We believe that the integration of these novel biorecognition elements with the advantageous properties of PSi will improve the performance of PSi-based biosensors dramatically, especially in terms of sensitivity. Low limits of detection will allow these biosensors to meet the requirements in the fields of food safety, medical diagnostics or homeland security.

4.2 Emerging Bioreceptors

All biosensors rely on an element facilitating molecular recognition—the so-called bioreceptor, which specifically binds the target analyte. Binding between the bioreceptor and the analyte occurs due to biomolecular recognition which is based on the complementarities of the surfaces of the two binding partners [19]. Different molecular interactions can contribute to binding: Hydrogen bonding, van der Waals forces, electrostatic interactions, π-π interactions, and combination of thereof are working in concert to enable high specific and high affinity binding. Moreover, during the binding event, successive replacement of water from the binding sites of the bioreceptor and the analyte takes place, resulting in an increase of enthalpy, making binding favorable. In aqueous solutions—which are most often the media to be analyzed by biosensors—this so-called hydrophobic effect has a profound role and may even dominate the bioreceptor-analyte complex formation [20].

In this section a brief overview on bioreceptors will be given with an emphasis on emerging new types of recognition elements. This section makes no claim to be complete, more comprehensive reviews can be found elsewhere (e.g. [21, 22]). The main features of the bioreceptors described in this chapter are summarized in Table 4.1.

4.2.1 Natural Bioreceptors

The first biosensor systems utilized bioreceptors provided by living organisms. Examples for such biological recognition elements are antibodies and enzymes. These naturally occurring receptors have been developed by nature via evolutional processes. Today, biotechnology allows not only the construction of completely new bioreceptors, which will be discussed in Sect. 4.2.2, but also facilitates rational modification of naturally occurring bioreceptors e.g. manipulation of their binding

Table 4.1 Main features of the bioreceptors

Bioreceptor	Classification	Targets/Analytes	Advantages	Disadvantages
Antibody	Natural/engineered	Proteins, small molecules	High affinity, well established production and application	Low stability, not readily available for all analytes
Enzyme	Natural/engineered	Small molecules	High affinity	Not available for all analytes of interest
AMP (antimicrobial peptides)	Natural/engineered	Bacteria	High affinity, chemical stability when compared to antibodies, broad antimicrobial spectrum	Not specific towards certain strain
DNA	Synthetic	DNA/RNA	Ease of production, well established technologies	Prone to nucleases, negative charge
PNA (peptide nucleic acid)	Artificial	DNA/RNA	Higher affinity when compared to DNA, resistant to nucleases	Poor solubility (depending on the length and sequence)
Aptamer	Artificial	Proteins, small molecules, cells (including pathogens)	High affinity and specificity, in vitro selection and production	Less established selection and application techniques, negative charge
MIP	Artificial	Proteins, DNA	High stability	High amount of target required

site to permit new specificities. Therefore, a precise discrimination between natural and synthetic bioreceptors is difficult and the line between them is blurred. In this subsection we are summarizing some naturally occurring bioreceptors as well as engineered variants derived from these molecules.

4.2.1.1 Antibodies

The most prominent example for bioreceptors may be antibodies. In nature, antibodies are produced by the immune system in an evolutional process resulting in high affinity and specificity. The human immune system is estimated to possess a repertoire of 10^{15} distinct antibody structures from which appropriate antibodies are chosen by recombinant selection [23]. This allows the production of antibodies directed against numberless potential antigens. This diversity in combination with the well-established techniques of antibody development and production are responsible for the broad use of antibodies in biosensing systems. The dominance of antibodies was especially boosted by the development of monoclonal antibody technology, facilitating the production of large amounts of antibodies directed against one single epitope of the antigen in cell culture. Instead of using the complete, intact antibody, Fab fragments or even smaller fragments can be used as bioreceptors [24–26].

Based on their generation in living organisms—cells or animals—antibodies possess some limitations. For instance, antibodies directed against small molecules in general, and especially against toxic or non-immunogenic molecules, are difficult to generate. Here the analyte has to be coupled to a protein before immunization [27] and the obtained antibodies have to be purified in order to isolate the fraction binding to the target of interest. The development of antibodies against small molecules is thus laborious, time-consuming and expensive.

Detailed understanding of the genetic background of antibodies has resulted in the possibility to manipulate antibodies structure [25]. Recombinant expression of antibodies allows the design of chimeric antibodies; the binding sites of antibodies can be selected by phage display techniques using genetic engineered phage libraries. In antibody phage display, the minimized antibodies are fused to a coat protein of the virus, resulting in phages presenting the antibody on the phage surface. The phages are then used for the selection of antibody fragments with the desired binding properties, they not only display the antibody fragment on their surface, but also carry the corresponding genetic information and can thus be used for the amplification of these features [28].

Although these modern selection techniques have overcome the limitations associated with the development of antibodies in living organisms, other problems remain unsolved. These include poor antibody stability and their limitation to near-physiological conditions.

4.2.1.2 Enzymes

Enzymes do not only bind a substance—the so-called substrate—they also convert it to a product. The binding of the substrate to the active binding pocket of the enzyme is driven by the forces described above and results in high specificity. Moreover, the catalytic process results in detectable reaction products like protons and electrons, which can be exploited for signal amplification. Enzymes were the first recognition elements used in biosensors. The pioneering work of Clark and Lyons [29], immobilizing glucose oxidase on an electrode to allow for the determination of glucose concentration, has boosted the development of numerous enzymatic biosensor platforms, exploiting the outstanding specificity of enzymes [30].

Drawbacks of naturally occurring enzymes are their rather low stability with regard to environmental conditions (temperature and pH) [31], and the lack of specific enzymes for all analytes of interest. Here, genetic engineering can broaden up the diversity of possible substrates and fine-tune the characteristics of the bioreceptor [32]. An interesting approach to develop enzymes, which can be tailored to allow the detection of specific analytes of interest, was described by Ostermeier (2005) [33]. Target binding sites were engineered and inserted into the regulatory subunit of an allosteric enzyme. Binding of the target to the regulatory subunit resulted in a structural switch affecting the activity of the catalytic site [33, 34].

4.2.1.3 Antimicrobial Peptides

Antimicrobial peptides (AMPs) are positively charged short (10–50 amino acids) oligopeptides occurring as natural antibiotics and immunomodulating substances which have been evolved as a part of the innate immune system [35]. Various types of AMPs have already been identified including defensins, cecropins, magainins and cathelicidins [36]. AMPs are stable molecules, which can survive under flow or heat conditions, as well as different salt concentrations and pH variations. They can also bind to a broad spectrum of microorganisms. As such, they have already been successfully used for the detection of pathogens in various formats of diagnostic assays [37]. Although their affinity towards many bacteria strains might also be a drawback for biosensing applications, it is interesting to mention that it has been shown that the natural AMP Magainin I exhibits preferential binding towards some pathogenic species [38].

Besides naturally occurring peptides, synthetic peptides which mimic the biophysical characteristics of naturally occurring AMPs can be generated by combinational synthesis. For a synthetic peptide, consisting of 10 of the 20 essential amino acids, 20^{10} (2×10^{11}) distinct peptides are possible, but the diversity can be further expanded by the use of non-essential and unnatural amino acids [39]. These huge libraries have to be screened for peptides with the desired binding properties by high throughput screening. Molecular modeling is expected to improve and simplify the identification of peptides derived by combinational synthesis. Peptides with desired affinity against a given target can also be selected by phage display technology. These synthetic peptides have the advantages of simple cost-effective synthesis procedure, stability in the presence of proteases and the ability to design their binding properties [40].

4.2.2 Synthetic Receptors

As already mentioned, natural bioreceptors are limited by their low stability, poor performance in organic solvents, and/or their availability against a specific analyte. Therefore, technologies have been developed to advance naturally occurring bioreceptors or to even completely substitute them by novel types of bioreceptors. Using modern DNA technology, naturally occurring bioreceptors can be further evolved to result in engineered receptors with improved properties. In addition, completely synthetic bioreceptors are developed by rational design, computational chemistry, combinatorial chemistry, molecular imprinting, self assembly or combinations of these techniques [41].

4.2.2.1 DNA and PNA

DNA oligonucleotides can be used as bioreceptors for the detection of complementary DNA sequences. Here, the hybridization between the DNA and the oligonucleotide is exploited for the detection of the DNA—or more specifically—the source of the DNA. Thus, oligonucleotides are most valuable for a variety of targets ranging from pathogens in infectious diseases [42] and food-borne contaminations [43], cancer biomarkers [44], to the diagnosis of genetic diseases by microarray-based multiplexed detection of genes and gene alterations [45–47].

One drawback associated with DNA oligonucleotides as bioreceptors is their susceptibility to degradation by nucleases. In this context, the use of phosphorothioates can improve DNA stability [48] and locked nucleic acids (LNAs) have been developed, which contain at least one bicyclic furanose unit that nucleases do not accept as a substrate [49]. Other disadvantages associated with DNA are the limited sensitivity and rapidity of the sensing. Conventionally, the DNA originating from the sample to be analyzed needs to be amplified via PCR prior to sensing, resulting in a lengthy procedure. Moreover, the negatively charged phosphate backbone of the oligonucleotides is also the source of some concerns. The negative charge results in electrostatic repulsion, which further increases upon duplex-formation and causes Coulomb blockage of the hybridization [50, 51]. To circumvent these problems, a new type of nucleic acid oligomers has been developed. In peptide nucleic acids (PNAs) [52], the negatively charged phosphate backbone of natural oligonucleotides is replaced by a neutral peptide-like backbone composed of repeated N-(2-aminoethyl)glycine units linked by amide bonds. The number of bonds between the bases in the obtained PNA is similar to that in DNA, resulting in a proper inter-base spacing, which allows for hybridization of DNA and PNA. The use of PNA in DNA biosensors offers some major advantages. PNA is not recognized by nucleases and proteases and is thus stable in biological fluids. Due to the lack of electrostatic repulsion, existing between two DNA oligonucleotides, the binding between PNA and DNA is even stronger and more specific than the formation of DNA duplexes. Thus, PNA is considered to offer extraordinary specific detection of DNA to facilitate the identification of single-nucleotide mismatches [53].

Despite their improved properties, PNAs are limited to the detection of DNA sequences. Another type of oligonucleotide—termed aptamer—broadens up the specificity of oligonucleotide-based detection to virtually all types of analytes.

4.2.2.2 Aptamers

Aptamers are single-stranded oligonucleotides composed of RNA or DNA generated by in vitro selection techniques like SELEX (systematic evolution of ligands by exponential enrichment) [54–56], modified SELEX procedures [57, 58] or MonoLEX [59]. During the selection, aptamers are isolated from combinational oligonucleotide libraries containing up to 10^{15} individual sequences based on their

affinity and specificity towards the desired target molecules. Once an aptamer sequence has been identified, the aptamer can be produced by chemical synthesis.

In contrast to conventional DNA, which binds complementary DNA based on Watson-Crick base-pairing and is usually thought of as a rather linear molecule, aptamers fold into unique three-dimensional (3D) structures that enable the molecular recognition of their corresponding targets [60, 61]. Thus, they are often described as nucleic acid-based alternatives to antibodies. While the development of antibodies depends on the immunization of animals and their production via cell culture techniques, aptamers are selected by in vitro techniques and can be produced via chemical synthesis. Consequently, aptamers can be selected against virtually all types of targets, including those with low immunogenicity or high toxicity. Moreover, aptamers can be selected under non-physiological conditions in order to generate aptamers that are functional under desired conditions. Thus, in case of aptamers, a tailor-made bioreceptor can be designed and optimized to meet the requirements of specific applications [62, 63].

In the special context of biosensing, the major advantages of aptamers over their amino acid-based counterparts include their superior stability, ease of regeneration (to allow subsequent usage in multiple sensing cycles), and highly reproducible production by chemical synthesis. During this synthesis, the aptamer can be modified at defined positions; for instance linker molecules can be incorporated to facilitate highly controlled immobilization of the aptamer on the transducers surface. Moreover, due to their oligonucleotide nature, aptamers offer completely new biosensing schemes, as we reviewed recently [64, 65]. For instance, oligonucleotides complementary to the target-binding site of the aptamer can be designed and hybridized to the aptamer. Thus, in the presence of the target, the target will replace the complementary oligonucleotide, while the release of the oligonucleotide can be detected and quantified via different labeling techniques. This strategy has been already successfully applied for the detection of ethanolamine, which is the smallest analyte against which an aptamer has been selected [66]. In more sophisticated sensing schemes, the aptamer can simultaneously act as both the bioreceptor and the transducer. In these so called aptamer beacons, the aptamer can be modified with a quencher and a fluorophore positioned in close proximity, resulting in low fluorescence in the absence of the target. Binding to the target results in conformational changes; fluorophore and quencher depart from each other to yield an increase in the fluorescence intensity [67].

One concern associated with aptamers is their sensitivity to degradation by nucleases. Today, this problem can be easily overcome by different modifications [68] and even non-modified aptamers are already successfully applied in complex biological samples [69, 70]. In addition, the high negative charge presented by the aptamer molecule may result in failure to select aptamers, which are directed against negatively charged species, and may also induce non-specific binding to aptamer-modified surfaces. To overcome these issues, PNA aptamers have been developed in recent years. Lee et al. have synthesized a PNA aptamer using the same base sequence known from a DNA aptamer directed against thrombin [71]. However, it remains uncertain whether this simple transition from DNA to PNA

may be applicable for other aptamers, in which the folding of the aptamer may be influenced strongly by the negatively charged phosphate backbone. In this context, the direct selection of aptamers from a PNA library, which has already been used to develop PNA aptamers directed against dihydrofolate reductase [72], may prove to be a more versatile tool.

4.2.2.3 Molecularly Imprinted Polymers

Molecularly imprinted polymers (MIPs) are synthesized by contacting the target of interest with a complementary mixture of functional monomers to allow complex formation. Subsequently, the monomers are polymerized to form a matrix, which entraps the target. Removal of the target leaves behind a cavity with a surface complementary to the target.

Depending on the used monomers, the MIP offers some advantages over natural and other artificial bioreceptors, including their inherent stability with regard to temperature, pH, and organic solvents, low cost, and ease of preparation [41, 73]. The affinity and specificity of MIPs are generally inferior in comparison to that of antibodies and aptamers; e.g. apparent dissociation constants within the micro molar range have been determined for MIPs [74]. Moreover, MIPs produced by available techniques are polyclonal binders [75, 76], also restricting their specificity. The major disadvantage of MIPs is the large amount of target that is required for MIP production. In the case of antibodies, small amounts of the antigen (corresponding to the target) are needed for the immunization of the animal, after which large quantities of the antibody can be expressed with no need for additional target. The same applies for the production of aptamers; the target is only required during the SELEX process. Accordingly, the obtained DNA sequence can be used for the reproduction of the bioreceptor. In contrast, each cavity within the MIP requires one target molecule.

4.2.3 Today's Use of Bioreceptors and Future Perspectives

Today biosensors employ a broad diversity of different bioreceptors, as discussed in previous sections. Nevertheless, most biosensors still rely on conventional bioreceptors based on nature's well-known binding mechanisms. These include DNA detection, which is based on Watson-Crick base pairing, proteins are most frequently detected using antibodies, and small molecules are mostly detected by enzymes. Figure 4.1 summarizes the number of academic publications (between 1980–2013) dealing with biosensors, categorized in accordance to the type of employed bioreceptor. Clearly, enzymes, DNA and antibodies are dominating the field, but new capture probes are emerging and gaining significant momentum. Among these novel types of bioreceptors, AMPs and especially aptamers have

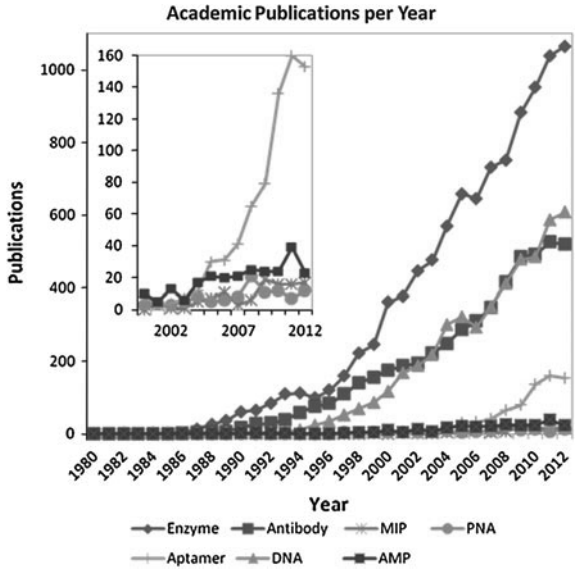

Fig. 4.1 Publications dealing with biosensors utilizing different natural and artificial bioreceptors. Search for publications was performed using the term "biosensor" in combination with the terms "enzyme", "antibody", "MIP", "PNA", "aptamer", "DNA", or "AMP". Data was created using MEDSUM: an online MEDLINE summary tool by Galsworthy, MJ. Hosted by the Institute of Biomedical Informatics (IBMI), Faculty of Medicine, University of Ljubljana, Slovenia. URL: www.medsum.info

attracted much attention (insert in Fig. 4.1). Our perspective is that aptamers have the potential to dominate the field in the future due to the fact that they can be developed to target almost all classes of analytes and produced at relatively low cost.

4.3 Porous Silicon-Based Biosensors

Over the past decade, a great number of PSi-based biosensors were reported in the literature [2, 12, 77]. With its most attractive property, the large surface area of up to 500 m^2/cm^3, PSi allows dense immobilization of different capture probes: enzymes [78], DNA fragments [79], antibodies [7], or any of the aforementioned emerging bioreceptors. Optical biosensors make up for the largest share in PSi-based assays and can be further categorized to two subgroups, based on the optical transduction mechanism, to include biosensors based on changes in photoluminescence [10, 80] and those based on changes in reflectivity [5, 81]. Upon infiltration of the target analyte molecules into the porous layer and their subsequent binding to the respective bioreceptors, which are immobilized onto the pore walls, a

Appendix

Table 4.2 Examples of PSi-based biosensor schemes categorized in terms of the type of bioreceptor employed

Capture probe	Analyte	Detection method	Porous architecture	Working range	Reference
Antibody	*E. coli* Streptavidin Opiates	Optical-reflectivity	Single mesoporous layer	10^4–10^5 cells/ml	[9]
		Optical-fluorescence	Single nanoporous layer	n/a	[87]
		Optical-reflectivity	Single mesoporous layer	0.018–10.8 μM	[88]
Enzyme	Specifically cleaved peptide fragments Proteins (e.g. cholesterol)	Optical-reflectivity	Single mesoporous layer	n/a	[89]
		Electrical-amperometry	Single mesoporous layer	1–50 mM	[84]
Peptide	Enzyme	Optical-reflectivity	1D Photonic crystal	0.037–37 μM	[90]
DNA	DNA	Electrical-impedance	Single macroporous layer	0.1–5 μM	[5]
PNA	DNA	Optical-reflectivity	Single mesoporous layer	n/a	[91]
Aptamers	ATP	Optical-fluorescence	Single macroporous layer	0.1–100 μM	[92]
	Tetracycline	Electrical-impedance	Single mesoporous layer	2–100 nM	[86]
	His-tag proteins	Optical-reflectivity	Single mesoporous layer	11–56 μM	[93]

change in the RI of the thin film can be observed, as a modulation in the photoluminescence or as a wavelength shift in the reflectivity spectra, respectively. Other biosensors based on PSi are mainly electrochemical, relying on PSi semiconductor characteristics [82]. Examples include voltammetric approaches [83] as well as amperometric [84], potentiometric characterization [85] and impedance-based sensors [86].

Another appealing characteristic of PSi transducers is the ability to easily tailor their nanostructure [1]: pore sizes to accommodate the interacting species, pore architecture, as well as surface chemistry, can be varied and tuned to meet the needs of any specific application.

Table 4.2 provides an overview of existing PSi-based biosensor schemes and the type of bioreceptor employed. Without the claim of being complete, it shows that a wide diversity of bioreceptors in concert with different transduction approaches is used for the development of PSi-based biosensors.

4.3.1 Optical Biosensors

While the discovery of photoluminescence in PSi kick-started scientists' attention on the material, this emission of secondary photons upon light induced excitation has not established itself as a prevalent transduction methodology for biosensors development. This is in spite of the promising early studies by Starodub et al. [94], in which specific protein binding to the corresponding antibody was demonstrated by a decrease in the PSi photoluminescence. The complex photoluminescence mechanisms, associated with electron transfer and interfacial charging [1, 95, 96], pose a major challenge in the development of reliable biosensors [97]. Yet, a recent study demonstrated the quenching of a reporter-label inside the porous structure in a very interesting manner [92], this work will be discussed in more detail in the next section.

Fluorescent labels have also been used in assays to combine both, a fluorescent signal and reflectivity spectra [98] or electrical impedance [87], respectively. Nonetheless, label-free methods are often preferred. The necessity of additional steps for labeling the capture probes or target, add cost and complexity to the assay and may interfere with target recognition. Other disadvantages of labeled approaches include the rapid photobleaching of fluorescent organic dyes conjugated to the biomolecules of interest, as well as challenges associated with quantitative analysis due to the fluorescence signal bias, as the number of fluorophores on each molecule cannot be precisely controlled [99].

For label-free PSi biosensors based on reflectance, two different signals can be monitored: the shift in the wavelength due to RI variation [16] and a change in the intensity of the reflected light due to scattering effects [9]. Different PSi architectures e.g., single and double layers [88, 100], microcavities [78, 101], and photonic crystals [90, 102], have been used for the construction of reflectivity-based optical biosensors. The tunable architecture of PSi allows incorporating additional functionalities within the optical transducer, such as internal reference channels, and size exclusion features. Pacholski et al. [103] demonstrated a double layer biosensor, where a layer with smaller pore size serves for separation of biomolecules by size exclusion and also as an internal signal reference channel. This nanostructure allowed for simultaneous detection of a macromolecule (*bovine* serum albumin) and a small molecule (sucrose). This concept was later exploited by Bonanno and DeLouise [101] using a microcavity structure for filtering, enabling a label-free detection of rabbit IgG in complex media (such as whole blood samples).

We believe that a combination of the advantageous properties of the novel capture probes, described in the previous section, with PSi can bring forth a new generation of high performance biosensing concepts. While there are certainly many more publications to be expected within the next years, in this review, we focus on few recent studies, which have demonstrated promising results. The first example of a fluorescence-based optical biosensor employing PSi in combination with novel capture probes, is a one-step assay presented by Yoo et al. [92]. In this assay, a macroporous PSi is modified with streptavidin through physical adsorption followed

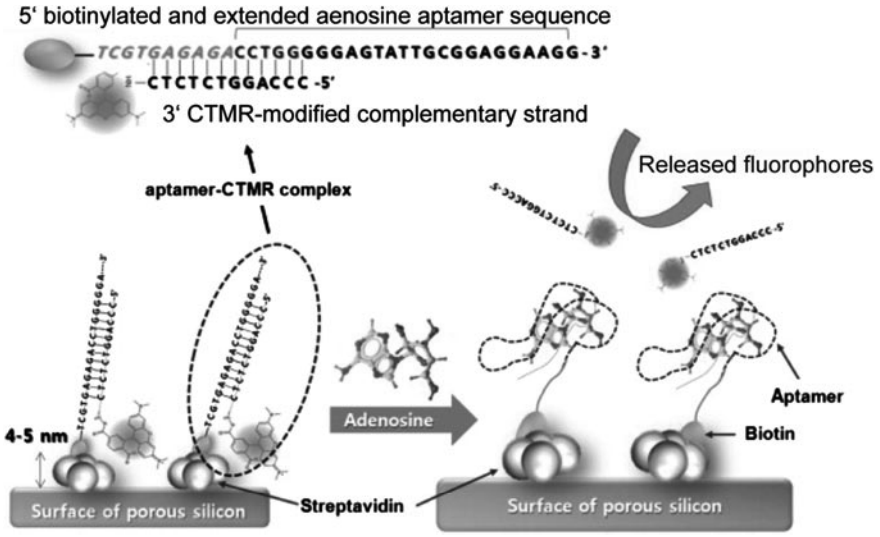

Fig. 4.2 Schematic illustration of the assay for adenosine detection based on fluorescence-quenching in an aptamer-based macroporous silicon structure. Adapted with permission [92]

by the introduction of biotin-conjugated DNA aptamer, directed against the target adenosine. The biosensor is geared up by hybridization of a complementary strand modified with the fluorescent reporter probe, carboxytetramethylrhodamine (CTMR), to the aptamer. A detailed scheme of the assay is presented in Fig. 4.2. Close proximity of the CTMR to the PSi surface effectively quenches the fluorescence, while a target-induced dissociation of the complementary strand in the presence of adenosine target, restores the fluorescence by releasing the fluorophore. The macroporous silicon structure is produced by electrochemical etch with a characteristic pore size distribution between 0.8 and 1.6 μm, and its protein adsorption capacity is determined to be 93.75 μg/cm^2. The high hydrophilicity and high surface area of the scaffold allows for simple and dense immobilization of the protein probes [104] building further up to the attachment of the aptamer receptor. The quenching of organic dyes on the scaffold was found to be most efficient when close proximity of the molecules to the silicon matrix is kept, as this ensures efficient energy transfer [105, 106], whereas oxide layers or other spacers can hinder this phenomenon in distances >30 nm from the scaffold [105–107]. Additional quenching effects are not only achieved by the suitable transducer here, but also by the guanines abundantly contained in the aptamer sequence due to electron transfer from aromatic compounds [108]. This combination of fluorescence quenching renders the biosensor highly effective to sensitive target detection and indeed, the proposed platform showed reliable detection in sub-micromolar concentrations. While basal adenosine blood-levels range from 20 to 200 nM [109], hypoxic tissue

or inflammatory response easily boost the concentrations to the 10–100 fold [110, 111]. Therefore, the presented assay has the potential to differentiate between normal blood-level and increased adenosine concentrations. In comparison to conventional analytical methods for the detection of adenosine, e.g. HPLC or enzyme-based electrochemical sensors, which are not suitable for fast and high throughput analysis [112, 113], usage of aptamers as receptor molecules profits from easy labeling procedures, high affinity and specificity of this novel capture probe [114]. However, previously developed aptasensors either lack in sufficient sensitivity [115] or require implementation of other nanomaterials such as graphene [116] or single-walled carbon nanotubes [117], involving laborious and time intensive production processes, whereas the use of PSi as transducer provides a simple platform and invites this proof-of-concept study to be extended with other aptamer-target pairs. Nevertheless, the assay should be studied with real samples, as components in complex biological fluids may impede with the quenching and de-quenching effects and nonspecific adsorption onto the biosensor surface should be assessed. Moreover, assay time dependency should to be carefully studied, especially when application in the field might necessitate washing steps prior to analysis.

Our own research efforts are aimed at the development of a generic biosensor scheme that utilizes aptamers as capture probes. Herein, we exploit the aptamers' superior properties in terms of stability and reversible folding. Our work [93, 118] describes, for the first time, the design and characterization of a label-free optical PSi-based aptasensor. An oxidized porous silicon nanostructure (Fabry-Pérot thin film), serving as the optical transducer, is conjugated with a well-characterized his-tag binding aptamer (6H7) [119, 120]. This aptamer system has been previously used in protein downstream processing and was thoroughly studied in microarray applications as described by Walter et al. [121]. In a first step, we confirmed successful immobilization of the aptamer throughout the oxidized PSi ($PSiO_2$) scaffold. Aptamer-protein binding events, occurring within the nano-scale pores, are monitored in real time, confirming affinity of the aptamer-immobilized $PSiO_2$ towards the target proteins in μM range (as anticipated by this specific aptamer binding characteristics) [69]. The assay scheme is outlined in Fig. 4.3, showing a typical biosensing experiment in which the reflectivity spectra of the porous film are monitored in real time and corresponding effective optical thickness (EOT) values are computed. The figure presents the change in the relative EOT values ($EOT/EOT_{t=0}$) upon exposure of the 6H7-functionalized $PSiO_2$ to lipase (T6 from *Geobacillus stearothermophilus*, molecular weight 44 kDa), which is used as a model his-tagged protein. After baseline establishment with an appropriate buffer, the analyte solution is introduced and the biosensor is incubated with the solution. A rapid increase in the relative EOT value is observed, which is attributed to the infiltration of the protein solution into the pores and to binding events of the his-tagged protein to the 6H7 aptamer. Subsequently, the target solution is removed and the biosensor is thoroughly rinsed with a buffer to remove unbound species, inducing a sharp decrease in the relative EOT after which a stable signal is attained. Thus, the significant change in EOT, corresponding to a net shift of 40 nm, is attributed to binding of the target protein to the aptamer-functionalized surface.

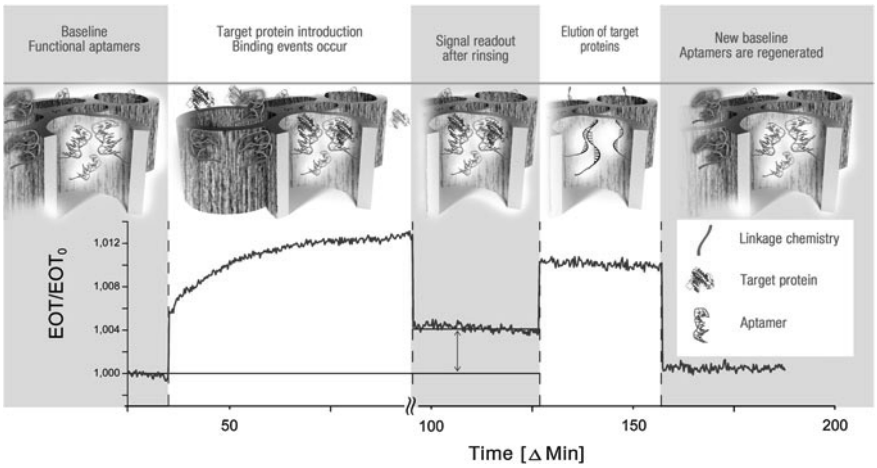

Fig. 4.3 Relative EOT value versus time of 6H7-functionalized $PSiO_2$ during a typical biosensing experiment. A baseline is obtained in buffer solution followed by the introduction of lipase solution, binding events occur and the signal increases rapidly. After a rinse step to remove unbound molecules, a stable readout signal is attained. Competitive elution with 1 M imidazole leads to the release of the captured target protein and the rapid removal of such in the following rinse step. Following a short incubation in the aptamer's selection buffer, the biosensor can be restored for subsequent use. Note that during buffer exchange and rinsing, EOT measurements are briefly paused. Adapted with permission [93]

The stability of the EOT signal during the rinsing step implies that the captured protein molecules are tightly bound to the aptamer under these conditions.

During the 6H7 aptamer selection, gentle elution conditions for the resulting sequence to release the captured target were pre-defined, resulting in an aptamer engineered to undergo reversible changes of confirmation when exposed to high concentrations of imidazole. Therefore, the resulting biosensor can withstand repeated cycles of denaturation and renaturation, exhibiting outstanding stability and reusability for numerous subsequent experiments. Indeed, exposing the biosensor to the elution buffer, see Fig. 4.3, results in an immediate increase in EOT signal (due to the higher refractive index of this buffer solution) and induces the release of the target molecules. Following this step and another thorough rinse of the biosensor, the relative EOT readout returns to its original value and a new cycle can be initiated (see Fig. 4.4).

The notably high selectivity and specificity of the proposed biosensing scheme is demonstrated in several controls: aptamer-conjugated $PSiO_2$ are exposed to non-target protein solutions, mixtures of proteins as well as to complex biological fluids such as bacteria in their culturing medium and bacterial lysates. All these experiments confirmed the very low non-specific adsorption of unrelated molecules on the aptamer-functionalized surface, indicating that the biosensor is suitable for application in real samples.

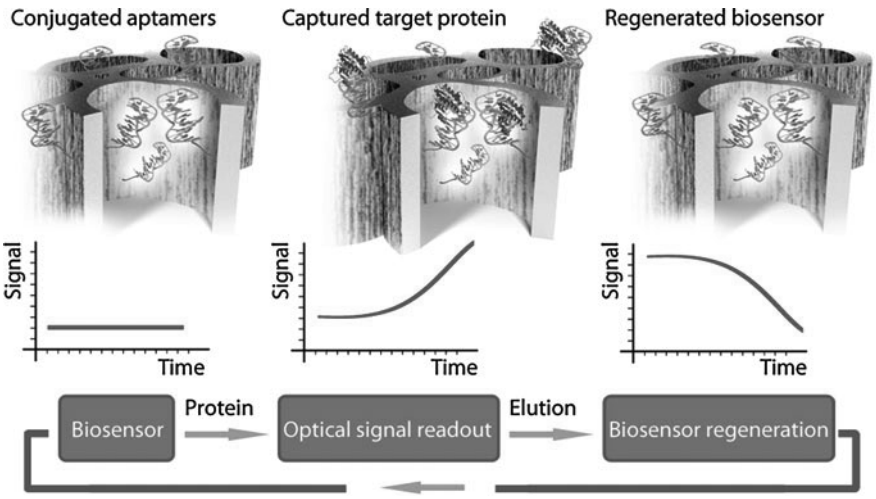

Fig. 4.4 The concept of the aptamer-porous silicon biosensor. Adapted with permission from [93]

A limitation of the presented biosensing scheme lies in the sensitivity of the sensor. Due to the poor dissociation constant of the 6H7 aptamer [69], a linear response could only be shown in the micromolar range. However, as the study has a proof-of-concept character, we expect to adapt this principle for other aptamers displaying nanomolar dissociation constants against highly relevant target molecules. This will allow the design of simple, flexible, inexpensive, robust and portable biosensing platforms combining the superior properties of aptamer capture probes and PSi-optical transducers.

4.3.2 Electrochemical Biosensors

In electrochemical biosensors, the investigated reaction usually produces or consumes an electro-active moiety due to the activity of the recognition element in the device. An important characteristic of these biosensors is a direct spacial contact between the electrochemical transducer and the bioreceptor, enabling a measurement of either current (amperometric), potential or charge accumulation (potentiometric) between the electrodes [122, 123]. These changes in electrical properties of the biosensor system are induced by the occurrence of analyte attachment to the recognition element. A similar technique that does not require labeling, relies on the measurement of impedance spectra. Here, the observed change in the characteristic impedance spectrum of the sensor is solely based on the binding of the target molecule.

The dielectric constant, space-charge distribution and therefore conductance and capacitance of the PSi transducer are the signal-producing properties in different

electrochemical sensing techniques. These depend on the Si-dopant, the interacting surface area (hence layer thickness and porosity), as well as the number of available binding sites [2, 5, 77, 124]. In order to sensitively follow changes of these properties during target capture, a thorough characterization of the biosensor surface in respect to all relevant parameters is essential.

Zhang et al. successfully demonstrated the application of the well-known tetracycline-aptamer in an electrochemical impedance spectroscopy setup. The aptamer is immobilized within $PSiO_2$ structures via standard silanization and coupling chemistry [125, 126]. The sensor's faradic impedance is measured and compared to a neat PSi sample, showing a decrease in impedance due to aptamer attachment. Upon exposure of the aptamer-functionalized $PSiO_2$ to different concentrations of tetracycline, further decrease in impedance is observed, while the neat PSi (no aptamer) retains constant impedance when subject to different target solutions. The recorded results in form of Nyquist plots are fitted as a function of the semicircle-diameter corresponding to the electron-transfer resistance, as presented in Fig. 4.5. The biosensor shows a linear response in the range between 2.079 and 62.37 nM with the lowest concentration detectable of about 2 nM and the maximum of 100 nM, above which the signal plot remains constant. Utilization of PSi as the transducer allows for bioreceptor immobilization in higher densities in comparison to planar surfaces [127] and accordingly improves the biosensor sensitivity. Although, enzyme-linked immunosorbent assay (ELISA) approaches have shown superior sensitivity levels ($\sim$2 ng/ml [128]), aptasensors still offer a number of advantages especially concerning simplicity of the assay and stability of the fabricated sensors. The work by Zhang et al. [125, 126] does not state or investigate the dissociation constant (K_D) of the aptamer sequence obtained in their SELEX process. Therefore, it is not possible to assess whether the detection method or the K_D value might be the limiting factor for the obtained sensitivity. Thus, further

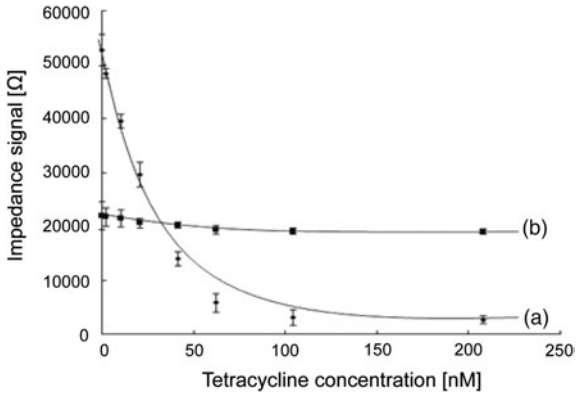

Fig. 4.5 Fitted biosensor signal upon exposure to different target concentrations. Trace **a** shows the response for an aptamer-functionalized PSi biosensor, while trace **b** serves as negative control showing the response of neat PSi (no aptamer). Adapted with permission from [86]

studies using aptamer/target pairs with known dissociation constants in combination with PSi-based impedance assays may result in promising detection schemes, which are highly sensitive yet simple.

A potentiometric PSi-based biosensor for triglyceride (TG) detection was developed by Setzu et al. [85]. As high levels of TG in the bloodstream are linked with cardiovascular problems, there is an increasing demand for simple and rapid TG monitoring systems [129]. The operation principle of the biosensor is the lipase-catalyzed hydrolysis of the TG tributyrin to glycerol and free butyric acid. Fatty acid production induces changes in the solution pH, which are measured using an open circuit potential (OCP) configuration. The enzyme is physisorbed onto an n-type PSi scaffold, which is 50 μm thick. Despite the thickness of the layer, the enzymatic reaction is not limited by the diffusion of tributyrin within the porous film. In fact, the adsorbed lipase follows the Michaelis Menten law, which is widely used to describe enzymatic reactions. It is interesting to mention that the biosensor is reusable and has a relatively long shelf life. Thus, the performance of this biosensing scheme is impressive; however, more work is needed in order to establish a reliable calibration curve, which correlates the change in the OCP to the TG concentration. Nevertheless, this work significantly advances previous potentiometric PSi-based schemes for monitoring of triglycerides [130], in which the enzyme was not loaded into the PSi matrix but rather added to the electrolyte solution together with the tributyrin.

The study by Setzu et al. suggests a promising approach for the detection of analytes, which are the substrates of enzyme-mediated biological reactions. Further studies should optimize the immobilization method (adsorption/covalent immobilization), as well as the enzyme concentration so that the enzymatic reaction will be confined to the linear range of the Michaelis-Menten curve. Also, time of reaction should be optimized and fixed for all measurements.

4.4 Conclusions

In this book chapter, we briefly reviewed novel capture probes and described their properties, emphasizing their advantages and disadvantages when applied in biosensors. We focused on PSi-based biosensors, which combine these new bioreceptors with different transduction schemes. These studies, although few in number, demonstrate the compatibility of PSi with a wide range of novel receptor molecules. As for now, many of the reported biosensors are still in a proof-of-concept stage applying model-systems; nonetheless, we believe that further improvements of the sensors systems will soon enable real applications. PSi, facilitating different transduction strategies, and the broad range of available bioreceptors, both provide a versatile toolbox for developing biosensors that can be tailored to fit the needs of uncountable analytical applications. It is important to keep in mind that for the development of a biosensor, the chosen bioreceptor and PSi-based detection method need to be thoroughly validated for this specific application. It could be

concluded from the given examples, that sensitivity and limit of detection are crucial parameters to determine the applicability of a biosensor. Not only the resolution and sensitivity of the detection have to be considered, but also binding properties of the bioreceptor/target pair as well as possible cross-reactions with other substances involved. Critical studies on these performance-determining issues need to be conducted.

As one of the most promising methods, label-free optical biosensing provides the easiest and most generally applicable method. Excellent examples of effective and reliable biosensors utilizing label-free optical schemes with traditional bioreceptors have already been reported; these biosensing approaches can be further improved by the implementation of novel receptor molecules that will not only enhance the resulting system performance but may also generate new designs (e.g. target-induced dissociation of complementary oligonucleotides from aptamers).

References

1. M.J. Sailor, *Porous Silicon in Practice* (Wiley-VCH, Weinheim, 2011), p. 250
2. A. Jane et al., Porous silicon biosensors on the advance. Trends Biotechnol. **27**(4), 230–239 (2009)
3. L.M. Bonanno, E. Segal, Nanostructured porous silicon-polymer-based hybrids: from biosensing to drug delivery. Nanomedicine **6**(10), 1755–1770 (2011)
4. J. Salonen, V.-P. Lehto, Fabrication and chemical surface modification of mesoporous silicon for biomedical applications. Chem. Eng. J. **137**(1), 162–172 (2008)
5. M. Archer, M. Christophersen, P.M. Fauchet, Macroporous silicon electrical sensor for DNA hybridization detection. Biomed. Microdevices **6**(3), 203–211 (2004)
6. K.A. Kilian, T. Boecking, J.J. Gooding, The importance of surface chemistry in mesoporous materials: lessons from porous silicon biosensors. Chem. Commun. **6**, 630–640 (2009)
7. L.M. Bonanno, L.A. DeLouise, Steric crowding effects on target detection in an affinity biosensor. Langmuir **23**(10), 5817–5823 (2007)
8. L.M. Bonanno, L.A. DeLouise, Tunable detection sensitivity of opiates in urine via a label-free porous silicon competitive inhibition immunosensor. Anal. Chem. **82**(2), 714–722 (2010)
9. N. Massad-Ivanir et al., Engineering nanostructured porous SiO(2) surfaces for bacteria detection via "direct cell capture". Anal. Chem. **83**(9), 3282–3289 (2011)
10. S. Chan et al., Identification of gram negative bacteria using nanoscale silicon microcavities. J. Am. Chem. Soc. **123**(47), 11797–11798 (2001)
11. N. Massad-Ivanir, E. Segal, *12—Porous Silicon for Bacteria Detection*, in *Porous Silicon for Biomedical Applications*, ed. by H.A. Santos (Woodhead Publishing, Finland, 2014), pp. 286–303
12. G. Shtenberg, E. Segal, *Porous Silicon Optical Biosensors*, in *Handbook of Porous Silicon*, ed. by L. Canham, (Springer International Publishing, Switzerland, 2014), pp. 1–11
13. C. Pacholski, Photonic crystal sensors based on porous silicon. Sensors **13**(4), 4694–4713 (2013)
14. K.P.S. Dancil, D.P. Greiner, M.J. Sailor, A porous silicon optical biosensor: detection of reversible binding of IgG to a protein A-modified surface. J. Am. Chem. Soc. **121**(34), 7925–7930 (1999)

Appendix

15. A. Janshoff et al., Macroporous p-type silicon Fabry-Perot layers. Fabrication, characterization, and applications in biosensing. J. Am. Chem. Soc. **120**(46), 12108–12116 (1998)
16. V.S.-Y. Lin et al., A porous silicon-based optical interferometric biosensor. Science **278** (5339), 840–843 (1997)
17. A. Salis et al., *Porous Silicon-based Electrochemical Biosensors*, in *Biosensors—Emerging Materials and Applications*, ed. by P.A. Serra.(InTech, Croatia, 2011)
18. D.R. Thévenot et al., Electrochemical biosensors: recommended definitions and classification. Biosens. Bioelectron. **16**(1–2), 121–131 (2001)
19. A.P.F. Turner, Current trends in biosensor research and development. Sens. Actuators **17**(3–4), 433–450 (1989)
20. K. Kahn, K.W. Plaxco, *Principles of Molecular Recognition*, in *Recognition Receptors in Biosensors*, ed by M. Zourob (Springer, New York, 2011), pp. 3–46
21. M. Zourob, *Recognition Receptors in Biosensors* (Springer, New York Dordrecht Heidelberg London, 2010)
22. S.A. Piletsky, M.J. Whitcombe (eds.), *Designing Receptors for the Next Generation of Biosensors*. in Springer Series on Chemical Sensors and Biosensors, ed. by G. Urban. Vol. 12 (Springer, Heidelberg, 2013)
23. S. Tonegawa, Somatic generation of antibody diversity. Nature **302**(5909), 575–581 (1983)
24. J.P. Kim et al., Ultrasensitive carbon nanotube-based biosensors using antibody-binding fragments. Anal. Biochem. **381**(2), 193–198 (2008)
25. P. Holliger, P.J. Hudson, Engineered antibody fragments and the rise of single domains. Nat. Biotechnol. **23**(9), 1126–1136 (2005)
26. A.C.A. Roque, C.R. Lowe, M.A. Taipa, Antibodies and genetically engineered related molecules: production and purification. Biotechnol. Prog. **20**(3), 639–654 (2004)
27. K. Shreder, Synthetic haptens as probes of antibody response and immunorecognition. METHODS: A Companion to Methods in Enzymology **20**(3), 372–379 (2000)
28. N.A.E. Hopkins, *Antibody engineering for Biosensor Applications*, in *Recognition Receptors in Biosensors*, ed. by M. Zourob (Springer, New York, 2010), pp. 451–529
29. L.C. Clark, C. Lyons, Electrode systems for continuous monitoring in cardiovascular surgery. Ann. N. Y. Acad. Sci. **102**(1), 29–000 (1962)
30. H.G. Hundeck et al., Calorimetric biosensor for the detection and determination of enantiomeric excesses in aqueous and organic phases. Biosens. Bioelectron. **8**(3–4), 205–208 (1993)
31. B.D. Leca-Bouvier, L.C. Blum, *Enzyme for Biosensing Applications*, in *Recognition Receptors in Biosensors*, ed. by M. Zourob (Springer, New York ,2010), pp. 177–220
32. I. Axarli, A. Prigipaki, N.E. Labrou, Engineering the substrate specificity of cytochrome P450CYP102A2 by directed evolution: production of an efficient enzyme for bioconversion of fine chemicals. Biomol. Eng. **22**(1–3), 81–88 (2005)
33. M. Ostermeier, Engineering allosteric protein switches by domain insertion. Protein Eng. Des. Sel. **18**(8), 359–364 (2005)
34. J.P. Chambers et al., Biosensor recognition elements. Curr. Issues Mol. Biol. **10**, 1–12 (2008)
35. R.E.W. Hancock, H.-G. Sahl, Antimicrobial and host-defense peptides as new anti-infective therapeutic strategies. Nat. Biotech. **24**(12), 1551–1557 (2006)
36. C.D. Fjell et al., Designing antimicrobial peptides: form follows function. Nat. Rev. Drug. Discov. **11**(1), 37–51 (2012)
37. L. Shriver-Lake et al., *Antimicrobial Peptides for Detection and Diagnostic Assays*, in *Designing Receptors for the Next Generation of Biosensors*, ed. by S.A. Piletsky, M. J. Whitcombe (Springer, Heidelberg, 2013), pp. 85–104
38. M.S. Mannoor et al., Electrical detection of pathogenic bacteria via immobilized antimicrobial peptides. Proc Natl Acad Sci U S A **107**(45), 19207–19212 (2010)
39. I.E. Tothill, *Peptides as Molecular Receptors*, in *Recognition Receptors in Biosensors*, ed. by M. Zourob (Springer, New York, 2010), pp. 249–274

Appendix

40. S. Rotem et al., Analogous oligo-acyl-lysines with distinct antibacterial mechanisms. FASEB J. **22**(8), 2652–2661 (2008)
41. A.P.F. Turner, Biochemistry—biosensors sense and sensitivity. Science **290**(5495), 1315–1317 (2000)
42. J.C. Liao et al., Development of an advanced electrochemical DNA biosensor for bacterial pathogen detection. J. Mol. Diagn. **9**(2), 158–168 (2007)
43. F. Farabullini et al., Disposable electrochemical genosensor for the simultaneous analysis of different bacterial food contaminants. Biosens. Bioelectron. **22**(7), 1544–1549 (2007)
44. Y. Shin, A.P. Perera, M.K. Park, Label-free DNA sensor for detection of bladder cancer biomarkers in urine. Sens. Actuators B-Chem. **178**, 200–2006 (2013)
45. F. Stahl, Analysis of genregulation—DNA chip technology. Chem. unserer Zeit **39**(3), 188–194 (2005)
46. Y.V. Gerasimova, J. Ballantyne, D.M. Kolpashchikov, Detection of SNP-containing human DNA sequences using a split sensor with a universal molecular beacon reporter. Methods Mol. Biol. **1039**, 69–80 (2013)
47. J. Wang, From DNA biosensors to gene chips. Nucleic Acids Res. **28**(16), 3011–3016 (2000)
48. F. Eckstein, G. Gish, Phosphorothioates in molecular-biology. Trends Biochem. Sci. **14**(3), 97–100 (1989)
49. B. Vester, J. Wengel, LNA (Locked nucleic acid): high-affinity targeting of complementary RNA and DNA. Biochemistry **43**(42), 13233–13241 (2004)
50. A. Vainrub, B.M. Pettitt, Coulomb blockage of hybridization in two-dimensional dna arrays. Phys. Rev. E. **66**(4) (2002)
51. A.N. Rao, D.W. Grainger, Biophysical properties of nucleic acids at surfaces relevant to microarray performance. Biomater. Sci. **2**(4), 436–471 (2014)
52. P.E. Nielsen et al., Sequence selective recognition of DNA by strand displacement with a thymine-substituted polyamide. Science **254**, 1498–1500 (1991)
53. E. Mateo-Martí, C.-M. Pradier, *A Novel Type of Nucleic Acid-based Biosensors: the Use of PNA Probes, Associated with Surface Science and Electrochemical Detection Techniques* in *Intelligent and biosensor*, ed. by V.S. Somerset (InTech, Croatia, 2010)
54. A.D. Ellington, J.W. Szostak, In vitro selection of RNA molecules that bind specific ligands. Nature **346**(6287), 818–822 (1990)
55. D.L. Robertson, G.F. Joyce, Selection in vitro of an RNA enzyme that specifically cleaves single-stranded DNA. Nature **344**(6265), 467–468 (1990)
56. C. Tuerk, L. Gold, Systematic evolution of ligands by exponential enrichment: RNA ligands to bacteriophage T4 DNA polymerase. Science **249**(4968), 505–510 (1990)
57. R. Stoltenburg, N. Nikolaus, B. Strehlitz, Capture-selex: selection of dna aptamers for aminoglycoside antibiotics. J. Anal. Methods Chem 415697, 14 (2012)
58. R. Stoltenburg, C. Reinemann, B. Strehlitz, FluMag-SELEX as an advantageous method for DNA aptamer selection. Anal. Bioanal. Chem. **383**(1), 83–91 (2005)
59. A. Nitsche et al., One-step selection of Vaccinia virus-binding DNA aptamers by MonoLEX. BMC Biotechnol. **7**, 48 (2007)
60. D.J. Patel, Structural analysis of nucleic acid aptamers. Curr. Opin. Chem. Biol. **1**(1), 32–46 (1997)
61. T. Hermann, D.J. Patel, Biochemistry—adaptive recognition by nucleic acid aptamers. Science **287**(5454), 820–825 (2000)
62. B. Strehlitz, N. Nikolaus, R. Stoltenburg, Protein detection with aptamer biosensors. Sensors **8**(7), 4296–4307 (2008)
63. J.-G. Walter, F. Stahl, T. Scheper, Aptamers as affinity ligands for downstream processing. Eng. Life Sci. **12**(5), 496–506 (2012)
64. J.-G Walter et al., Aptasensors for small molecule detection. Z. Naturforsch. **67b** 976–986 (2012)
65. M. Loenne et al., *Aptamer-modified Nanoparticles as Biosensors*, in *Biosensors Based on Aptamers and Enzymes—Advances in biochemical engineering/biotechnology*, ed. by M.B. Gu, H.-S. Kim (Springer, Heidelberg, 2014), pp. 121–154

66. A. Heilkenbrinker et al., Identification of the target binding site of ethanolamine binding aptamers and its exploitation for ethanolamine detection. Anal. Chem. **87**(1), 677–685 (2015)
67. N. Hamaguchi, A. Ellington, M. Stanton, Aptamer beacons for the direct detection of proteins. Anal. Biochem. **294**(2), 126–131 (2001)
68. R. Stoltenburg, C. Reinemann, B. Strehlitz, SELEX–a (r)evolutionary method to generate high-affinity nucleic acid ligands. Biomol. Eng. **24**(4), 381–403 (2007)
69. Ö. Kökpinar et al., Aptamer-based downstream processing of his-tagged proteins utilizing magnetic beads. Biotechnol. Bioeng. **108**(10), 2371–2379 (2011)
70. G. Zhu, J.-G. Walter, *Aptamer-Modified Magnetic Beads in Affinity Separation of Proteins*, in *Affinity Chromatography: Methods and Protocols,* 2nd edn. ed. by S. Reichelt (Springer Protocols, Humana Press, 2015), pp. 67–82
71. E.J. Lee et al., Peptide nucleic acids are an additional class of aptamers. Rsc Advances **3**(17), 5828–5831 (2013)
72. R. Bredehorst et al., *Method for determining an unknown PNA sequence and uses thereof*, ed. by E.P. Specification 2005
73. G. Vasapollo et al., Molecularly imprinted polymers: present and future prospective. Int. J. Mol. Sci. **12**(9), 5908–5945 (2011)
74. S.A. Piletsky et al., Substitution of antibodies and receptors with molecularly imprinted polymers in enzyme-linked and fluorescent assays. Biosens. Bioelectron. **16**(9–12), 701–707 (2001)
75. T.A. Sergeyeva et al., Selective recognition of atrazine by molecularly imprinted polymer membranes. Development of conductometric sensor for herbicides detection. Anal. Chim. Acta **392**(2–3), 105–111 (1999)
76. R.J. Umpleby et al., Characterization of the heterogeneous binding site affinity distributions in molecularly imprinted polymers. J. Chromatogr. B-Anal. Technol. Biomed. Life Sci. **804** (1), 141–149 (2004)
77. F.A. Harraz, Porous silicon chemical sensors and biosensors: a review. Sens. Actuators B: Chem. **202**, 897–912 (2014)
78. L.A. DeLouise, P.M. Kou, B.L. Miller, Cross-correlation of optical microcavity biosensor response with immobilized enzyme activity. Insights biosens. sensitivity Anal. Chem. **77**(10), 3222–3230 (2005)
79. Z. Deng, E.C. Alocilja, Characterization of nanoporous silicon-based dna biosensor for the detection of salmonella enteritidis. Sens. J. IEEE **8**(6), 775–780 (2008)
80. S.B. de Leon et al., Neurons culturing and biophotonic sensing using porous silicon. Appl. Phys. Lett. **84**(22), 4361–4363 (2004)
81. M.P. Stewart, J.M. Buriak, Chemical and biological applications of porous silicon technology. Adv. Mater. **12**(12), 859–869 (2000)
82. A. Birner et al., Silicon-based photonic crystals. Adv. Mater. **13**(6), 377–388 (2001)
83. J.E. Lugo et al., Electrochemical sensing of dna with porous silicon layers. J. New Mater. Electrochem. Syst. **10**(2), 113–116 (2007)
84. M.J. Song et al., Electrochemical biosensor array for liver diagnosis using silanization technique on nanoporous silicon electrode. J. Biosci. Bioeng. **103**(1), 32–37 (2007)
85. S. Setzu et al., Porous silicon-based potentiometric biosensor for triglycerides. physica status solidi(a). **204**(5), 1434–1438 (2007)
86. J. Zhang et al., Label-free electrochemical detection of tetracycline by an aptamer nano-biosensor. Anal. Lett. **45**(9), 986–992 (2012)
87. M. Simion et al., Dual detection biosensor based on porous silicon substrate. Mater. Sci. Engi. B-Adv. Funct. Solid-State Mater. **178**(19), 1268–1274 (2013)
88. L.M. Bonanno, L.A. DeLouise, Tunable detection sensitivity of opiates in urine via a label-free porous silicon competitive inhibition immunosensor. Anal. Chem. **82**(2), 714–722 (2009)
89. G. Shtenberg et al., Picking up the pieces: a generic porous si biosensor for probing the proteolytic products of enzymes. Anal. Chem. **85**(3), 1951–1956 (2012)

Appendix

90. K.A. Kilian et al., Peptide-modified optical filters for detecting protease activity. ACS Nano **1** (4), 355–361 (2007)
91. K.R. Beavers et al. *Porous Silicon Functionalization for Drug Delivery and Biosensing by In Situ Peptide Nucleic Acid Synthesis*. in *Porous Semiconductors—Science and Technology* (Alicante-Benidorm, Spain, 2014)
92. L. Yoo et al., A simple one-step assay platform based on fluorescence quenching of macroporous silicon. Biosens. Bioelectron. **41**, 477–483 (2013)
93. K. Urmann et al., Label-free optical biosensors based on aptamer-functionalized porous silicon scaffolds. Anal. Chem. **87**(3), 1999–2006 (2015)
94. V.M. Starodub et al., Control of myoglobin level in a solution by an immune sensor based on the photoluminescence of porous silicon. Sens. d Actuators B: Chem. **58**(1–3), 409–414 (1999)
95. A.G. Cullis, L.T. Canham, Visible light emission due to quantum size effects in highly porous crystalline silicon. Nature **353**(6342), 335–338 (1991)
96. L.T. Canham, K. (Firm), *Properties of porous silicon EMIS datareviews series no. 18.* ed. by Leigh Canham (Institution of Electrical Engineers, London, 1997)
97. O. Bisi, S. Ossicini, L. Pavesi, Porous silicon: a quantum sponge structure for silicon based optoelectronics. Surf. Sci. Rep. **38**(1–3), 1–126 (2000)
98. G. Gaur, D. Koktysh, S.M. Weiss. Porous silicon biosensors using quantum dot signal amplifiers. Proc. of SPIE 8594, 859408 (2013)
99. X. Fan et al., Sensitive optical biosensors for unlabeled targets: a review. Anal. Chim. Acta **620**(1–2), 8–26 (2008)
100. C. Pacholski et al., Reflective interferometric fourier transform spectroscopy: a self-compensating label-free immunosensor using double-layers of porous SiO2. J. Am. Chem. Soc. **128**, 4250–4252 (2006)
101. L.M. Bonanno, L.A. DeLouise, Whole blood optical biosensor. Biosens. Bioelectron. **23**(3), 444–448 (2007)
102. M.M. Orosco et al., Protein-coated porous-silicon photonic crystals for amplified optical detection of protease activity. Adv. Mater. **18**(11), 1393–1396 (2006)
103. C. Pacholski et al., Biosensing using porous silicon double-layer interferometers: reflective interferometric Fourier transform spectroscopy. J. Am. Chem. Soc. **127**(33), 11636–11645 (2005)
104. A. Ressine, G. Marko-Varga, T. Laurell, *Porous silicon protein microarray technology and ultra-/superhydrophobic states for improved bioanalytical readout*, in *Biotechnology Annual Review*, ed. by M.R. El-Gewely (Elsevier 2007), pp. 149–200
105. L. Danos, R. Greef, T. Markvart, Efficient fluorescence quenching near crystalline silicon from Langmuir-Blodgett dye films. Thin Solid Films **516**(20), 7251–7255 (2008)
106. H.M. Nguyen et al., Efficient radiative and nonradiative energy transfer from proximal cdse/zns nanocrystals into silicon nanomembranes. ACS Nano **6**(6), 5574–5582 (2012)
107. L. Gu, M. Orosco, M.J. Sailor, *Detection of protease activity by FRET using porous silicon as an energy acceptor.* physica status solidi (a), **206**(6) pp. 1374–1376 (2009)
108. J.R. Unruh et al., Orientational dynamics and dye-dna interactions in a dye-labeled dna aptamer. Biophys. J. **88**(5), 3455–3465 (2005)
109. B.P. Ramakers et al., Measurement of the endogenous adenosine concentration in humans in vivo: methodological considerations. Curr. Drug Metab. **9**(8), 679–685 (2008)
110. J. Stagg, M.J. Smyth, Extracellular adenosine triphosphate and adenosine in cancer. Oncogene **29**(39), 5346–5358 (2010)
111. G. Schulte, B.B. Fredholm, Signalling from adenosine receptors to mitogen-activated protein kinases. Cell. Signal. **15**(9), 813–827 (2003)
112. L. Bekar et al., Adenosine is crucial for deep brain stimulation-mediated attenuation of tremor. Nat. Med. **14**(1), 75–80 (2008)
113. L.A. Conlay et al., Caffeine alters plasma adenosine levels. Nature **389**(6647), 136–136 (1997)

Appendix

114. D.E. Huizenga, J.W. Szostak, A DNA aptamer that binds adenosine and ATP. Biochemistry **34**(2), 656–665 (1995)
115. J. Zhang et al., Aptamer-based multicolor fluorescent gold nanoprobes for multiplex detection in homogeneous solution. Small **6**(2), 201–204 (2010)
116. S. Guo et al., Solid-state label-free integrated aptasensor based on graphene-mesoporous silica-gold nanoparticle hybrids and silver microspheres. Anal. Chem. **83**(20), 8035–8040 (2011)
117. L. Zhang et al., A carbon nanotubes based ATP apta-sensing platform and its application in cellular assay. Biosens. Bioelectron. **25**(8), 1897–1901 (2010)
118. K. Urmann et al. *Highly Generic Aptamer-Based Porous Si Optical Biosensors*. in *Porous Semiconductors—Science and Technology*.(Alicante-Benidorm, Spain, 2014)
119. S.A. Doyle, M.B. Murphy, U.S. Patent *Aptamers and methods for their in vitro selection and uses thereof* 2005
120. G. Zhu et al., Characterization of optimal aptamer-microarray binding chemistry and spacer design. Chem. Eng. Technol. **34**(12), 2022–2028 (2011)
121. J.G. Walter et al., Systematic investigation of optimal aptamer immobilization for protein-microarray applications. Anal. Chem. **80**(19), 7372–7378 (2008)
122. D. Grieshaber et al., Electrochemical biosensors—sensor principles and architectures. Sensors **8**(3), 1400–1458 (2008)
123. D.R. Thevenot et al., Electrochemical biosensors: recommended definitions and classification: biosens Bioelectron. **16**(1–2), 121–131 (2001)
124. F. De Filippo et al., *Measurement of Porous Silicon Dielectric Constant by VUV Laser Harmonic Radiation.* physica status solidi (a), 2000. **182**(1) pp. 261–266
125. J. Zhang et al., Nano-porous light-emitting silicon chip as a potential biosensor platform. Anal. Lett. **40**(8), 1549–1555 (2007)
126. J. Zhang et al., A label free electrochemical nanobiosensor study. Anal. Lett. **42**(17), 2905–2913 (2009)
127. Y.-J. Kim et al., Electrochemical aptasensor for tetracycline detection. Bioprocess Biosyst. Eng. **33**(1), 31–37 (2010)
128. C.C. Weber et al., Broad-spectrum protein biosensors for class-specific detection of antibiotics. Biotechnol. Bioeng. **89**(1), 9–17 (2005)
129. C.S. Pundir, J. Narang, Determination of triglycerides with special emphasis on biosensors: a review. Int. J. Biol. Macromol. **61**, 379–389 (2013)
130. R.R.K. Reddy et al., Estimation of triglycerides by a porous silicon based potentiometric biosensor. Curr. Appl. Phys. **3**(2–3), 155–161 (2003)

Review

Katharina Urmann[a], Julia Modrejewski[a], Thomas Scheper and Johanna-G. Walter*

Aptamer-modified nanomaterials: principles and applications

DOI 10.1515/bnm-2016-0012
Received May 31, 2016; accepted July 27, 2016

Abstract: Aptamers are promising alternative binders that can substitute antibodies in various applications. Due to the advantages of aptamers, namely their high affinity, specificity and stability, along with the benefits originating from the chemical synthesis of aptamers, they have attracted attention in various applications including their use on nanostructured material. This necessitates the immobilization of aptamers on a solid support. Since aptamer immobilization may interfere with its binding properties, the immobilization of aptamers has to be investigated and optimized. Within this review, we give general insights into the principles and factors controlling the binding affinity of immobilized aptamers. Specific features of aptamer immobilization on nanostructured surfaces and nanoparticles are highlighted and a brief overview of applications of aptamer-modified nanostructured materials is given.

Keywords: applications; aptamer; immobilization; nanomaterial; nanoparticle.

Introduction

Aptamers are synthetic short single stranded oligonucleotides composed of DNA or RNA. Based on their unique three-dimensional structure, aptamers exhibit specific binding to their corresponding target molecule, which can be a small molecule, a macromolecule, or a complete cell. Due to this specificity and their high affinity, aptamers can be used to substitute antibodies in different applications. In comparison to antibodies, aptamers offer several advantages which are mainly based on their in-vitro generation and their oligonucleotide nature: aptamers are selected in an in-vitro process termed systematic evolution of ligands by exponential enrichment (SELEX) [1]. Due to this animal-free process, aptamers can be selected to exhibit binding of the target under non-physiological conditions and the selection of aptamers is also possible for highly toxic or non-immunogenic molecules [2]. Once aptamers are selected and their sequence is revealed, they can be produced by chemical synthesis, a process not only resulting in high and consistent product quality, but also facilitating the precise introduction of labels or other modifications at defined positions within the aptamer sequence.

Aptamers have already been applied successfully e.g. for the detection of proteins and small molecules [3, 4], the purification of proteins [5–7] and depletion of small molecules [8], as well as in cell targeting and drug delivery [9–11]. In most of the developed aptamer-based methods, the aptamer has to be immobilized on a solid support, which might be a nano-structured surface. Aptamer binding to the corresponding target molecule depends on the correct three-dimensional folding of the aptamer [12]. Therefore, it is crucial to immobilize aptamers without affecting their ability to fold into this binding-competent structure. Within the first section of this review article we will highlight factors that may interfere with correct folding of aptamers on solid supports and give general suggestions for the immobilization of functional aptamers.

Immobilization of aptamers

As mentioned before, functional groups can be incorporated into the aptamer sequence and can subsequently be used for the immobilization of the aptamer on a solid support.

[a]**Katharina Urmann and Julia Modrejewski:** These authors contributed equally to this work.
***Corresponding author: Johanna-G. Walter,** Institut für Technische Chemie, Leibniz Universität Hannover, Callinstrasse 5, 30167 Hannover, Germany, e-mail: walter@iftc.uni-hannover.de
Katharina Urmann: Institut für Technische Chemie, Leibniz Universität Hannover, Callinstrasse 5, 30167 Hannover, Germany; and Department of Biotechnology and Food Engineering, Technion – Israel Institute of Technology, 32000 Haifa, Israel
Julia Modrejewski and Thomas Scheper: Institut für Technische Chemie, Leibniz Universität Hannover, Callinstrasse 5, 30167 Hannover, Germany

For different types of materials, different modifications can be utilized, for example the introduction of terminal thiol groups is allowing for the straight-forward immobilization of aptamers on gold surfaces. Since the chemical synthesis enables precise control of the position of functional groups, the aptamer can be immobilized in a highly controlled orientation, i.e. via one of the termini of the aptamer. This controlled orientation facilitates high binding activity by avoiding a loss of functionality resulting from immobilization in random orientation. Nonetheless, several factors influencing aptamer folding have to be carefully considered during the immobilization of aptamers and in many cases, optimization of aptamer conjugation has to be performed to obtain functional aptamer-modified surfaces [13].

Effects of immobilization to aptamer performance

In order to immobilize aptamers in a functional manner, the conjugation process must not interfere with aptamer folding [14, 15]. Here, the user has to consider that during most of the selection processes, aptamers are present free in solution. Thus, aptamers can adopt their binding-competent folding while they are in solution but might lose their binding competence after immobilization mainly due to three different factors [13]:

First, the surface may directly interfere with aptamer folding. This is especially problematic when truncated versions of the aptamer sequence are used. To overcome steric hindrance caused by too close proximity of aptamer and surface, the use of spacer molecules can be recommended. Here, rather simple spacers like polyethylenglycol moieties can be used and either be provided on the surface or fused between the aptamer sequence and the aptamer modification used for immobilization chemistry [16]. Also the elongation of the aptamer sequence, e.g. by introduction of several thymin bases, can provide additional space to allow for proper aptamer folding. One other factor that might interfere with correct folding of the aptamer is its orientation. Therefore, a screening of different aptamer orientations (3′ terminal versus 5′ terminal immobilization) may be useful to optimize aptamer performance.

The second feature of aptamers that has to be considered is their highly negative charge. Immobilizing aptamers on positively charged surfaces may result in complete unfolding of aptamers – which interact with the surface electrostatically. This can be prevented by capping of the surface [13].

Finally, the third factor influencing the folding of conjugated aptamers is the immobilization density. While generally, high immobilization densities are desired to guarantee high binding capacity for the aptamer target, too high aptamer density may prevent formation of the correct three-dimensional structure. Here, one has to consider that the immobilized aptamer must be provided with sufficient space to fold encountering no steric interference caused by neighboring aptamers. Moreover, the negative charge of aptamers can provoke electrostatic repulsion of neighboring aptamers, thereby forcing the aptamers to erect into a rather linear conformation not able to bind the target molecule. Therefore, the aptamer density, which can be easily influenced by the aptamer concentration applied during the immobilization process, has to be optimized experimentally.

Methods to investigate immobilized aptamers

As elaborated briefly in the previous subsection, several parameters including the aptamer density, aptamer orientation, surface charge, and the presence of spacers influence the performance of immobilized aptamers. Thus, methods for the investigation and optimization of aptamer conjugation are needed. Surface plasmon resonance (SPR) measurements allow for the quantitative investigation of the binding affinities of immobilized aptamers. SPR measurements are especially useful to reveal immobilization-induced reduction of aptamer affinity when they are compared with immobilization-free methods for the determination of dissociation constants such as isothermal titration calorimetry (ITC) or microscale thermophoresis (MST) [17]. The comparison of dissociation constants obtained by different methods may uncover negative effects evoked by immobilization. Nonetheless, SPR measurements suffer from a limited degree of parallelization, thus require a large set of experiments to screen different immobilization conditions and additionally require rather large amounts of aptamer and target. In our group, aptamer microarrays have shown to be a suitable alternative for the systematic investigation and optimization of aptamer immobilization [13, 16, 18]. Here, many different immobilization conditions (e.g. different aptamer orientations and immobilization densities, as well as different spacer moieties) can be screened in parallel on one single microarray. When aptamers are utilized as a receptor probe in a biosensing scheme, depending on the type and complexity, optimization of aptamer-conjugation directly within the biosensing platform may be the most suitable approach. Aptamer performance can be set in relation with the output signal and optimized accordingly.

Aptamer-modified nanostructured surfaces

Many different materials are accessible to a wide variety of surface chemistries for the attachment of biomolecules, such as aptamers. One reason for immobilization of aptamers to nanostructured surfaces specifically can be to increase the aptamer-density on the material due to higher surface area of such materials and thus increased area of interaction between aptamer and target analyte [19, 20]. Another main reason are the desirable intrinsic properties of nanostructured materials in combination with the binding characteristics of the immobilized aptamers which are opening possibilities for a variety of applications. In the following chapter, we will discuss some of the main considerations when conjugating aptamers to nanomaterials and present a number of applications with their corresponding materials, where such concepts were realized in an outstanding manner.

Special considerations for aptamer immobilization on nanostructured surfaces

Nanomaterials and nanostructured materials of different kinds have recently gained increased attention for their application in concert with aptamer-receptors tethered to their surface [21–23]. Applications thereof, see Tables 1 and 2, can mainly be found in the field of biosensors and for the capture and purification of cellular targets (e.g. cancer cells, bacteria cells). However, in contrast to immobilization of oligonucleotides on planar surfaces, aptamer-conjugation to nanomaterials requires a number of additional considerations which are discussed in the following.

Increased immobilization-density of aptamers conjugated to a surface (i.e. by means of larger surface area in nanomaterials), also brings the risk of higher steric hindrance effects, commonly occurring [4, 13, 38, 39]. This phenomenon was recently studied by Daniel et al. on a planar gold-coated prism for SPR measurements with the thrombin-binding aptamer as model [39]. The researchers conducting the study consequently compared binding affinities of the thrombin to surface-immobilized aptamers and in a competitive mode when additional aptamers are present in solution. They varied grafting-density as well as concentrations of free aptamer and found that increasing grafting-density has a negative effect on the binding affinity (K_D) of the surface-conjugated aptamer, while it has no effect on the K_D of aptamer in solution. In order to ensure sufficient spacing and thus maintain aptamer-functionality, even on this planar surface, additional spacing between aptamer and surface had to be applied.

Nanoscale surface features (e.g. roughness, groves, pores) and spatial confinement of aptamers when immobilized on nanomaterials adds another dimension to the challenge of controlling steric hindrance effects. Even though close proximity of capture probe and target supported by nanostructure architecture (e.g. in a porous matrix) can enhance their interaction [40], high grafting-density and crowding within the nanostructures can hamper aptamer-functionality and accessibility of the target-binding sites [38, 41]. Herein, also electrostatic interactions can have a particular effect: high amounts of negative charges accumulated by conjugated aptamers on a surface can prevent access of target analytes to the binding sites, which is enhanced by spatial confinement and limited free surface. Hence, besides reduced crowding, reduced negative charges can be a reason for better capture efficiency at

Table 1: Aptamer-modified nanostructured surfaces for cell capture.

Aptamer-target	NS material	Immobilization	Application	Comments	References
Antiepithelial cell adhesion molecule	Nano-structured glass slides	Phenyldiisothio-cyanate – NH2 aptamer	Circulating tumor cell capture		[24]
EGFR (RNA aptamer)	Nanotextured PDMS	Silanization, isothiocyanate groups, NH2-DNA, prehybridization with salmon sperm, hybridization of RNA aptamer	Circulating tumor cell capture		[25]
T lymphocyte	Silicon nanowires	MPTMS, heterobifunctional linker (GMBS), DNA aptamer	Cell capture	Release mechanism	[26]
TD05	Polymer-modified silicon nanowires	Click chemistry [copper-catalysed azide–alkyne cycloaddition (CuAAC)]	Circulating tumor cell capture		[27]
Lactobacillus acidophilus	Porous SiO_2	Acrydite-coupling on SH-surface	Optical biosensor		[28]

Table 2: Aptamer-modified nanostructured surfaces for sensing applications.

Aptamer-target	NS material	Immobilization	Application	Comments	References
Dopamine	Au-hexagons on fused silica	SH-oligos on Au layer	SERS sensor		[29]
Vasopressin	Au-layer deposited on silicon pillars	SH-oligos on Au layer	SERS sensor	Target analyte was labeled with TAMRA (5-carboxytetramethylrhodamine)	[30]
Thrombin	Single wall carbon nanotubes on FET	Carbodiimidazole-activated Tween 20 onto SWCNTs, NH_2 aptamer	Field effect transistor (FET)		[31]
Thrombin	Carboxylic-acid-functionalized polypyrrole (CPPy) nanotubes on glass substrate	Condensation reaction between carboxylic acid and amine groups (substrate or aptamers) mediated by 4-(4,6-dimethoxy-1,3,5-triazin-2-yl)-4-methylmorpholinium chloride	Field effect transistor (FET)		[32]
His-tagged protein	Porous SiO_2	EDC mediated coupling of NH_2 aptamer	Optical biosensor		[4]
Adenosin	Porous SiO_2	Avidin/biotin	Fluorescence-quenching	TID of cDNA with carboxy-tetramethyl-rhodamine/CTMR-label	[33]
Thrombin	Multiwalled carbon nanotubes on glassy carbon electrodes/gold-coated quartz crystal	Avidin/biotin, electrostatic adsorption	EQCM, amperometric, impedimetric	Methylene blue composites	[34, 35]
Human cellular prions	Multiwalled carbon nanotubes on gold electrodes	Avidin/biotin sandwich with conjugated ferrocenes	Amperometric		[36]
OTA	AuNPs/$MoSe_2$ modified glassy carbon electrode	Electrodeposition of AuNPs on $MoSe_2$, SH-oligos on AuNPs	Electrochemical sensing	TID of cDNA from aptamer upon target binding, dyeing of ssDNA with methylene blue	[37]

lower aptamer immobilization densities [28, 38]. Furthermore, while enhanced surface roughness due to nanoscale features on the surface can improve interaction of the target (i.e. cells) with the substrate, it may also render it prone to unspecific adsorption (e.g. matrix components) [42, 43]. Thus, when nanomaterials are functionalized with aptamers, special attention has to be paid to careful optimization of spacer-arms and immobilization density as well as to orientation of the aptamer (see Section "Effects of immobilization to aptamer performance").

Exemplary applications of aptamer-tethering to nanostructured surfaces are presented in the following.

Application of aptamer-modified nanostructured surfaces

Cell capture

Circulating tumor cells (CTCs) are an interesting target for the early detection, understanding and therapy of different cancer types [44, 45]. Since they occur in low numbers in the blood stream of patients with solid tumors, there is a strong need for effective methods to enrich and isolate these cells [46–48]. Over the past few years, efficient approaches have been developed, many of which take advantage of highly specific aptamers that have been selected for targeted capture of such cells with high affinity. Combination of aptamer capture probes and nanostructured materials has brought forth a number of excellent studies taking advantage of increased surface roughness and receptor-density by means of the used nanomaterials or by appropriate treatment of substrates in order to create nanoscale features [49].

One example was presented by Wang et al. [24], demonstrating an increase of target cell capture by almost 50% with only one additional step of nanostructuring their glass slides prior to functionalization with anti-EpCAM (epithelial cell adhesion molecule) aptamers for the specific capture of EpCAM-expressing PC3 cells. Aiming to mimic the surface roughness of extracellular matrix (with feature sizes between 260 and 410 nm [50]), Wang and colleagues exposed borosilicate glass to a reactive ion etching (REI) process yielding average features of 374.3 nm under optimized conditions. Such homogeneously nanostructured glass slides were then subject to further functionalization and finally conjugation with aptamers before being studied for the effectiveness of cell capture onto them. As a result, the group showed a 76% cell-capture efficiency for the nanostructured slides in comparison to only 30% of PC3 cells captured on the planar slides.

In a similar study, Wan et al. [25] compared the specific capture of human glioblastoma and meninges-derived primary fibroblast cells (hGBM) by a RNA-aptamer, targeting cell membrane overexpressed epidermal growth factor receptors (EGFRs) on planar and nanotextured polydimethylsiloxane (PDMS) substrate. While a treatment with NaOH on the PDMS template resulted in an increased PDMS surface roughness (with feature sizes of about 289 nm after complete functionalization with RNA capture probes), untreated templates resulted in a PDMS substrate with minor features of 22 nm. Herein, the authors draw a direct connection of the surface roughness and the amount of subsequently immobilized aptamers. Thus, enhanced cell capture on the nanotextured PDMS was concluded to be a synergistic effect of increased aptamer density and simulation of basement membrane structure through appropriate roughness on the substrate, both promoting cell attachment.

Besides their excellent biocompatibility [51], silicon nanowires (SiNWs) have also shown high efficiency in cell capturing, especially when functionalized with specific aptamer-capture probes [26, 27]. Significantly increasing the aptamer density on the exposed substrate surface and through their topography preferred by cells, the nanowire structures facilitate the contact between capture probe and cell receptors and provide a suitable 3D structure for cell contacts [52–55], see Figure 1C. Nanowires have demonstrated capture efficiencies two orders of magnitude higher, in comparison to planar silicon substrates, and enable controlled release of captured cells through reversible aptamer-folding [26]. While such a SiNW-system has been demonstrated for the capture of T-lymphocyte cells [26], an example of SiNWs grafted with Ramos-cell specific aptamers and glycopolymers, showed high capturing-efficiency at notably low cell-concentrations and directly in serum-containing medium [27]. Herein, the utilized glycopolymer has a cell-affinity itself, binding glucose transporter proteins on the cell membrane, but only the combination with cell-specific aptamers created a highly efficient multifunctional surface for the capture of CTCs.

In the aforementioned examples, the aptamer-functionalized nanostructures and their high surface to volume ratio, had the main purpose to promote cell attachment through cell-compatible roughness and nanoscale features. Not in all applications, where cells are captured, their detection based on labeling or cell staining is suitable. Instead, depending on the nature of the utilized nanomaterial, it can be additionally exploited as the signal transducer: visible white light reflection from Faby-Pérot thin films can easily be recorded with a spectrometer. Porous silicon thin films display such

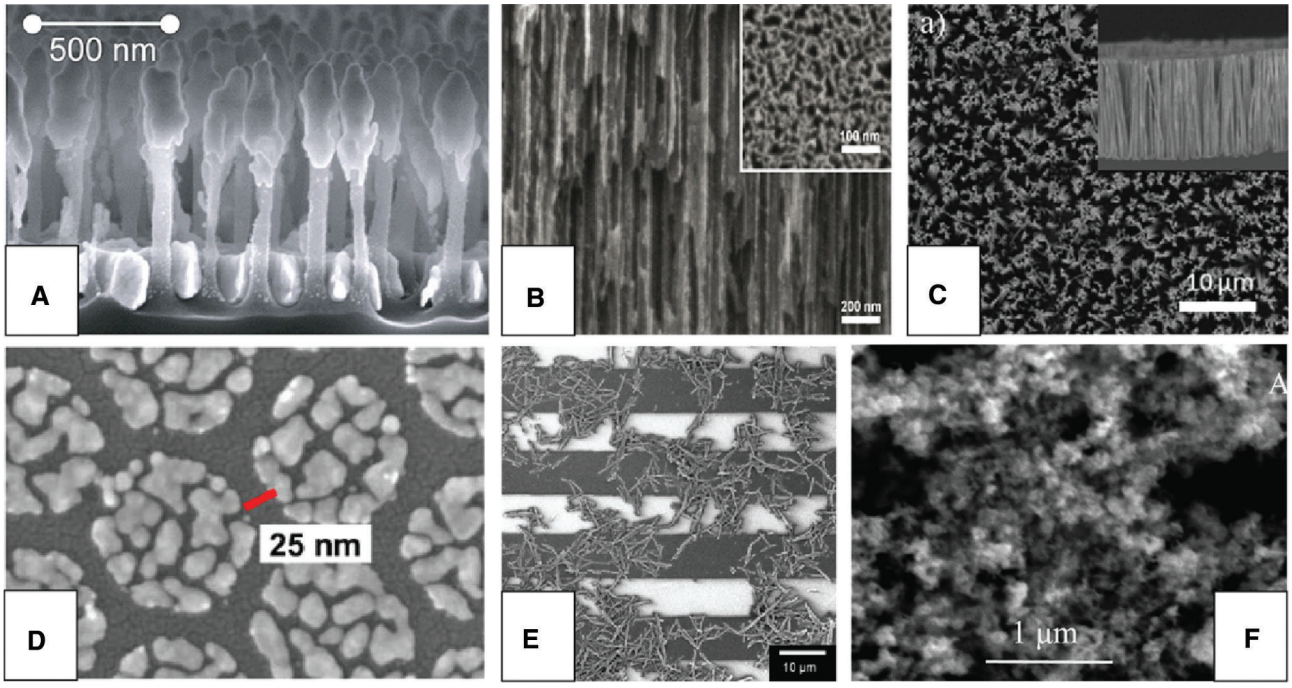

Figure 1: SEM micrographs of different nanomaterials.
(A) Au-capped nanopillars [30]. (B) Porous silicon oxide structure cross section and top-view (inset) [4]. (C) Silicon nanowires top view and cross section (inset) [27]. (D) Au-hexagon structures [29]. (E) CPPy nanotube-networks on electrodes [32]. (F) Molybdenum selenide flower-like nanostructures [56]. Adapted with permission from the respective references.

light interferences and are commonly used for biosensing applications in a reflective interferometer Fourier transform spectroscopy (RIFTS) mode [57–59], see Figure 1B. Additionally, cell capture on porous nanostructures has been reported [28, 60, 61]. The technique enables rapid capture and detection of cells with minimal instrumentation and without the need of labeling. One example where the advantages of aptamers have been combined with optical porous silicon structures was recently demonstrated for distinct capture of live probiotic bacteria [28]. Herein, the importance of spacing between aptamer and biosensor surface as well as immobilization density was highlighted as it directly affected optical signals and the ability of the structure to capture bacteria cells. The porous silicon matrix in concert with the tethered highly specific aptamers, showed fast and robust optical signals upon bacteria capture on the nanostructured surface and importantly, could distinguish between live and dead bacteria populations based on the specificity of the utilized aptamer [28].

Due to the availability of aptamers against many other bacteria species, several systems for their capture have recently been reported (e.g. against *Escherichia coli* O157:H7 [62], *Salmonella typhimurium* [63] or *Staphylococcus* aureus [64]), however, to the best of our knowledge, none of the so far published examples, harnesses the advantages of nanostructured surfaces, but are rather designed utilizing different types of nanoparticles.

Biosensing

A classification of biosensors is usually firstly made by separating label-free and label-based approaches. Secondly, biosensors of different signal transductions (optical, electrical etc.) can be divided. In the following, we are presenting several examples of biosensors, covering all types, and outlining their beneficial combination of nanomaterials and aptamer capture probes.

Contrary to the previously described cell capture methods, in biosensors, most schemes involving the use of nanomaterials, take advantage of them for the purpose of signal transduction and/or amplification. The most popular material, chosen not only for its intrinsic properties but also due to facile and well-characterized immobilization of oligonucleotides, is probably gold. While it is being widely utilized as planar material for functional-coating or as electrode material [65], researchers have also increased efforts in studying gold nanostructures due to their plasmonic properties as well as absorbance, coupling and scattering properties which are depending on their geometry [29, 30, 37].

Chemisorption of thiols to elemental gold is a well-known mechanism resulting in stable self-assembled monolayers (SAM) [66, 67]. With the facile possibility of post-synthesis functionalization of oligonucleotides with thiols, the immobilization of thiolated DNA to gold in any form, has proven to be a viable strategy and remains widely utilized [68] as can be seen from the examples presented in the following.

Surface-enhanced Raman spectroscopy (SERS) is a promising technique for the sensitive detection of chemical or biological species. Herein, characteristic molecular vibrations are observed as the inelastic scattering of monochromatic light by surface-tethered species. The use of noble metal nanostructures (i.e. gold) enhances the signals obtained significantly due to (i) the localized surface plasmons on the gold surface that get excited and (ii) the formation of a target-analyte complex enabling charge transfers [22, 29, 69]. It is crucial, that distinct Raman signals are observed only upon binding of the target molecule. One example by Peters et al. [29], presents the detection of dopamine, also investigating the influence of different gold nano-geometries on the signal output. Herein, hexagonal Au is used as substrate for the immobilization of the capturing aptamer, see Figure 1D. Raman signals are observed only when the target is present and bound.

Unlike the previously mentioned assay, in an example by Yang et al. [30], an additional TAMRA-tag (5-carboxytetramethylrhodamine) on the targeted vasopressin protein hormone is necessary to achieve distinct and enhanced Raman signals upon target capture. The authors of this study on a SERS biosensor pay specific attention to optimization of the aptamer immobilization density, aptamer orientation and surface effects on the Au coated silicon nanopillars. One interesting aspect they emphasize, is the treatment of the gold layer with mercaptohexanol (MCH), which on the one hand blocks access of analyte and buffer components to the gold surface (causing unspecific adsorption), and on the other hand, supports the vertical orientation of the aptamers when conjugated to the surface (by preventing interaction of aptamer and gold surface, thereby enhancing functional structures). However, the authors do not report if they observed a ligand exchange induced by prolonged exposure to MCH. This is highly relevant when choosing utilized MCH concentrations and incubation times [30, 70]. Their hypothesis is confirmed by significantly higher Raman peak intensities for samples treated with MCH. With their optimized setup, highly reliable and quantitative detection of picomolar concentrations was achieved. In achieving sensitive signals, the utilized nanostructure, namely silicon nanopillars, was of the essence: trapping target molecules between the nanopillars resulted in intense Raman scattering enhanced by the localized plasmon resonance induced by the gold-capped pillars leaning towards each other, see Figure 1A.

Among the label-free methods, field effect transistors (FET) have recently gained a lot of attention due to the advantages of nanostructured materials that can be integrated to the gate of the transistor [71]. In one example by So et al., the well-studied and in this case amine-modified thrombin-aptamer was conjugated to single walled carbon nanotubes (CNTs) within a FET via carbodiimidazole chemistry. Thanked to the small size of the aptamers and the conducting properties of the nanotubes, the FET enabled robust thrombin detection at low nanomolar concentrations with the additional possibility of biosensor regeneration for consecutive sensing cycles. It should be noted that in label-free FETs where the use of CNTs provides significant advantages, their nanostructure is not means of signal attainment, but a suitable and highly beneficial material enabling the observation of changes in its conductance upon target binding. Other nanomaterials such as graphene or SiNWs are also widely used as FET-gate materials due to their tunable material properties [71]. Another novel nanomaterial that has been demonstrated for the use as FET-gate material are carboxylic-acid-functionalized polypyrrole (CPPy) nanotubes. In a study by Yoon et al. [32], similarly as previously described for CNTs, the conducting polymer nanotubes, possessing a carboxy-functionality, were conjugated to the electrodes and gate surface and subsequently modified with amine-terminated aptamers targeting thrombin. Besides the facile synthesis of the material, its stable attachment to the FET basis and a reliable biosensing performance at thrombin concentrations between 50 and 500 nM, the authors show the beneficial effects of the formation of interconnected CPPy networks on the gate surface between source and drain electrode, evoking higher signal amplification as well as the improved sensor sensitivity at high aptamer-densities [32], see Figure 1E.

Oxidized porous silicon ($PSiO_2$) nanostructures serving as optical transducers are an example where the nanomaterial not only provides increased surface area but also facilitates signal transduction: when an aptamer is immobilized onto a $PSiO_2$ structure, it can serve for the capture of target proteins while the induced changes in optical properties of the functionalized scaffold can be recorded with a spectrometer. This simple experimental setup was proven successfully with an aptamer directed against his-tagged proteins, demonstrating rapid protein detection in a reversible manner and with outstanding

simplicity [4]. Herein, the signal upon target capture, arises through the changes in refractive index of the nanostructured matrix induced by the formation of the aptamer-target complex. Noteworthy is the reversibility of the target binding and complete regeneration of the sensor for multiple consecutive biosensing cycles resulting in highly reproducible signals.

Likewise utilizing multifunctional porous silicon substrates, Yoo et al. demonstrated a biosensor for the detection of adenosine [33]. Herein, the authors take advantage of the target induced dissociation of a TAMRA-labeled complementary strand from the aptamer-functionalized porous silicon surface. Thereby the fluorescence of the label, which was previously effectively quenched by the silicon surface properties, is restored and a fluorescence signal can be observed. The authors demonstrate this simple one-step assay with submicromolar concentrations of adenosine and propose the application of this scheme for the detection of other biomolecules. Despite the simple design, the assay relies on a labeled component impeding the reuse of the biosensor and additionally requires fluorescence detection which implies the necessity of sophisticated laboratory instruments.

Electrochemical aptasensors for thrombin utilizing amperometry or impedance spectroscopy (EIS) as well as electrochemical quartz crystal microbalance (EQCM) have been studied extensively by the group of Hianik [34, 35, 72–75]. Pre-treatment of their multiwalled CNTs (MWCNTs) with methylene blue (MG) has shown significant improvements in sensitivity for most of their biosensing schemes [34, 35]. This is not attributed to a direct effect on the target affinity of the biosensor, but rather improved immobilization of aptamers due to the MB's positive charge counterbalancing the negative charges of the carboxy-terminated MWCNTs and aptamers respectively. Thus, MWCNT-MB composites possess a higher aptamer-density after functionalization and subsequently display lower detection limits. Furthermore, MB in its role as a phenothiazine dye provides means of signal detection by its change in redox-status upon interaction of immobilized aptamers and its target analyte. The group has demonstrated a wide range of detection schemes and consequently improved the performance of their biosensors. Noteworthy is also their investigation of so called aptabodies [73]. Heterodimers of two anti-thrombin aptamers modified each with a poly-A or poly-T tag respectively form Y-shaped aptabodies due to the complementarity of the tags, subsequently each possessing two binding sites for the target protein. Contrary to improved sensitivity in EQCM, investigations for EIS emphasize the fragile balance of aptamer density and steric hindrance phenomena as well as charge-related affinity losses: the authors were not able to further improve biosensor sensivity from their reported 0.3 nM for the EQCM biosensing scheme and assume a negative effect of the high density negative charges on the coordination of the binding motifs [34, 35].

Going beyond the commonly demonstrated thrombin model-systems, a highly relevant application of an electrochemical aptasensor has been demonstrated by Miodek et al. [36]. For the sensitive detection of human cellular prions, the authors combined several elements: a MWCNT-coated gold surface served as electrode, while a layer of fourth generation polyamidoamine dendrimers coupled to the MWCNTs further increased available surface functionalities for the following conjugation of modified ferrocene markers [76]. Finally, traditional biotin-streptavidin was used to immobilize prion specific aptamers. Binding of human cellular prions significantly impacted the electron transfer in the system, enabling specific detection of prions at concentrations as low as 0.5 pM and notably, applicability directly in blood plasma [36].

The range of the presented examples in this review makes no pretence to be complete, however, in the authors' opinion it reflects the variety of nanomaterials, aptamer-immobilization strategies and different target analytes well and shall give the reader a good idea of the capabilities and limitations of currently studied aptasensors employing nanostructured materials.

Combination of nanostructured surfaces and nanoparticles

In search of mechanisms to amplify attained signals and enhance specificity, some assays rely on sandwich formats where aptamer-conjugated nanoparticles can serve as secondary capture probes and labels [77, 78]. While the advantages and different applications for aptamer-functionalized nanoparticles will be discussed in the next chapter, herein, we would like to give one example where both, a nanostructured material and nanoparticles are implemented with aptamer-assisted target capture.

In the study by Huang et al. [37], molybdenum selenide nanoflowers were prepared by a simple hydrothermal method on the surface of an electrode. This material was chosen due to its high surface area, the exceptional intrinsic electrical conductivity and finally its electrocatalytical activity induced by the selenite component, see Figure 1F. They constructed a highly sensitive electrochemical sensor for the detection of ochratoxin A (OTA) by integration of oligonucleotide-functionalized gold nanoparticles (AuNPs). Therein, the aptamers were

also hybridized with a second complementary sequence. Methylene blue (MB) was utilized as the electrochemical probe due to its specific interaction with single stranded DNA (ssDNA). Upon target binding, complementary DNA was released and thus became available (as ssDNA) for interaction with MB. This can be observed by the change in redox currents. With this construction of a combination between nanostructured surfaces and additional nanoparticles, the authors achieved a highly sensitive assay with detection limits as low as 0.08 pM OTA.

Aptamer-modified nanoparticles

Special considerations for aptamer immobilization on nanoparticles

For aptamer conjugation to nanoparticles, the surface charge of the nanoparticles has to be considered. Direct immobilization of aptamers on cationic surfaces, such as polyethylenimine (PEI), may lead to an aptamer-PEI-complex which interferes with correct aptamer folding and thereby renders the aptamer useless as targeting molecule. Thus, nanoparticles composed of neutral material [e.g. polymers such as polylactic acid (PLA) or polylactic-co-glycolic acid (PGLA)] may be most convenient for conjugation with aptamers [79].

An important goal during aptamer-immobilization is maintaining the binding affinity and selectivity the aptamer displays in solution [14]. This is usually accomplished by covalent binding of the aptamer to a surface bound linker and, in some cases, non-covalent attachment by physisorption [14]. In the last few years, many advantages in synthesis and characterization of different nanoparticles such as metallic, silica, magnetic, hydrogel or polymeric nanoparticles and CNTs have been revealed [80]. These nanomaterials generally possess a large surface area in combination with a unique size and shape. Due to their small sizes, nanoparticles can potentially move through cell and tissue barriers and their cellular uptake can be compared much easier as for larger drug delivery systems [81, 82]. The large surface-area-to-volume ratio leads to a greater drug delivery efficiency [81]. Additionally, the high surface area allows for high loading of targeting or drug molecules [83]. Furthermore, nanoparticles display composition and size dependent physical properties such as SPR, fluorescence and/or magnetism [80].

One advantage of aptamer immobilization on nanoparticle surfaces, for example, is the influence of aptamer on the nanoparticle stability. Wang et al. showed that gold nanoparticles were more stable in high salt concentrations when modified with aptamers [84]. High salt concentrations shield the electric field and un-modified nanoparticles form aggregates more frequently due to dipole interactions [85]. To stabilize gold nanoparticles against aggregation, negatively charged aptamers can be coupled to nanoparticle surfaces and prevent the aggregation due to the electrostatic repulsion forces between similarly charged surfaces [85].

Application of aptamer-modified nanoparticles

The modification of nanoparticles with specific aptamers has proven advantageous in different areas of applications. The properties of aptamer-modified nanoparticles can among others be used for biosensing. If cell-specific aptamers are used, resulting conjugates can be used for cell targeting and targeted drug delivery [80].

There are four different types of nanoparticles conjugated with aptamers which are commonly used for biological imaging applications: Gold nanoparticles (AuNP), quantum dots (QD), silica nanoparticles (SiNP) and magnetic nanoparticles (MNP).

In the following, we present examples for applications of aptamer-modified nanoparticles in cell and intracellular targeting, drug delivery and biosensing.

Cell targeting

One prominent application of aptamer-modified nanoparticles is cell targeting. To date, countless aptamers for various cellular targets are available. Targets can be cell-surface bound proteins, viruses, and so on [86]. Table 3 summarizes several applications of aptamer-modified nanoparticles along with the used aptamer, its target, the mode of detection and the type of NP.

Most applications aim to target cancer cells. Gao et al. developed biodegradable nanoparticles consisting of polyethylene glycol (PEG) and polycaprolactone (PCL), which are also functionalized with AS1411 aptamer and loaded with doxorubicin (DOX). They were able to target and enhance cellular uptake by glioma cells in vitro [89].

Another example for cell targeting is found in literature: Farokhzad et al. developed a nanoparticle-aptamer bioconjugate for targeting prostate cancer cells. They synthesized nanoparticles consisting of poly(lactic acid)-block-polyethylene glycol (PLA-PEG) and coupled an aptamer to their surface which selectively binds to

Table 3: Overview about aptamers, their targets and types of nanoparticles on which they could be conjugated (continued).

Aptamer	Target	Detection	Type of NP	References
A9	Prostate-specific membrane antigen (PSMA)		QD	[87]
A10	PSMA	Colorimetric	SPION[a]	[88]
AS1411	Nucleolin	Fluorescent	Polymer-NP, MSN	[89–91]
MUC1	Mucin-1	Fluorescent	QD, SiNP	[90]
TTA1	Tenascin-C	Fluorescent	MNP	[92]
A30	HER-2	Fluorescent	AuNP[b]	[93]
Sgc8c	CCRP-CEM cells	Fluorescent	AgNP[c]	[1]
TD05	Ramos (B-cell lymphoma)	Fluorescent	QD	[90]
S6	A549	Fluorescent	Polymer-NP, QD	[90]
SA17, SA61	*S. aureus*	Light scattering	AuNPs	[94]

[a]SPION, Superparamagnetic iron oxide nanoparticle; [b]AuNP, gold nanoparticle; [c]AgNP, silver nanoparticle.

prostate-specific membrane antigen (PSMA) [80, 93, 95]. Farokhzad and coworkers successfully demonstrated that their nanoparticle-aptamer conjugates targeted prostate cancer epithelial cells and were internalized by them [93].

The imaging and targeting of PSMA has also been realized by using superparamagnetic iron oxide nanoparticles (SPION) functionalized with the A10 aptamer [88]. The A10 aptamer is an RNA aptamer specifically binding an extracellular domain of the PSMA. SPIONs are characterized by low toxicity and detection limits, for example. An important application of SPIONs is to serve as a magnetic resonance imaging (MRI) contrast agent for cancer diagnosis [96]. As mentioned, Wang and coworkers developed A10 aptamer-modified thermally cross-linked SPIONs enabling the detection (by MRI) and treatment of PSMA [88].

Jalalian and coworkers developed epirubicin loaded SPIONs functionalized with 5TR1 aptamer, which binds specifically to mucin-1, a glycoprotein which is overexpressed on many epithelial tumors and adenocarcinomas [97]. They investigated the internalization of the aptamer-modified particles and cell viability after incubation with drug loaded and modified particles. Detection of the internalization was performed by using flow cytometry analysis. Cell viability was assessed by MTT assay [97].

Aptamer-modified QDs are used particularly for cancer cell imaging [98]. MUC-1 aptamer-conjugated QDs for the detection of mucin-1 positive cells serve as an example for fluorescent cell imaging [90]. QDs are also widely used for targeting breast cancer cells (MCF-7). Gedi and Kim successfully targeted such cells with aptamer-modified QDs, resulting in a strong red fluorescence signal [99].

Ulusoy and coworkers developed aptamer-modified QDs for the detection and imaging of lung cancer cells [100]. They used the S15 aptamer directed against the lung cancer cell line A549 [101]. Fluorescence microscopy showed that aptamer-modified QDs were successfully internalized by lung cancer cells while unmodified QDs were not taken up [100].

Silica is a biocompatible but inorganic material often used for biological applications such as artificial implants [83]. It was found that silica is an appropriate compound for the development of drug releasing systems. Mesoporous silica nanoparticles (MSN) are responsive to external (e.g. light or magnetic field) and internal stimuli (e.g. enzymes or pH). They are also used for imaging, controlled release of therapeutics and cell targeting. When MSNs are conjugated with aptamers, they can be used for targeting cancer cells [102]. Li and coworkers developed MSNs and conjugated them to AS1411 aptamer which is specific to nucleolin, a protein overexpressed on several types of cancer cells [89, 102]. The conjugated MSNs have successfully targeted MCF-7 cells [102, 103]. Investigating the success of cell targeting, Li and coworkers prepared fluorescein-modified MSNs, conjugated to AS1411 aptamer and then incubated them with MCF-7 cells. Utilizing confocal microscopy, the targeting and internalization of the particles were observed [102].

Su and coworkers coated MSNs with carbon quantum dots and conjugated them with aptamers for the electroluminescent detection of MCF-7 cells. The aptamer used was directed against mucin1. Specifically, Su et al. used a surface which was cast with a three dimensional graphene (3D-GR). Additionally, AuNPs were attached to the 3D-GR to improve the electronic transmission. Subsequently, MCF-7 cells were seeded on the modified electrode and were incubated with aptamer-modified MSNs. Detection was carried out with electrochemical impedance spectroscopy [103].

MNP are widely used for cell targeting as biological samples mostly exhibit no magnetic properties. Thus, MNPs may yield ultrasensitive detection with no interfering background signals [92]. MNPs conjugated with aptamers have been applied for cell targeting especially in cancer cell targeting. An example is the detection of Tenascin-C in glioma cells. Iliuk and coworkers used the GB-10 aptamer specifically binding to the Tenascin-C receptor on glioma cells and conjugated it to MNPs. The interaction between aptamer-modified MNPs and cancer cells was determined by scanning electron microscopy. Only aptamer-modified particles interacted with the glioma cells [104].

Not only cancer cells or their receptors can be targeted, but also bacteria like *Staphylococcus aureus* [94]. Chang and coworkers selected two aptamers against *S. aureus* and conjugated them to AuNPs. They modified AuNPs with one of the selected aptamers (SA17 and SA61) and detected the interaction between aptamer-modified particles and *S. aureus* cells by direct detection (resonance light-scattering signals).

Aptamer-modified AuNPs are also used for the detection of *Escherichia coli* (*E. coli*) O157:H7 and *Salmonella typhimurium* (*S. typhimurium*). Aptamers can stabilize AuNPs against aggregation in presence of high salt concentrations. Furthermore, AuNPs change color when they aggregate. Wu and coworkers took advantage of these properties and modified AuNPs with aptamers. Subsequently, they incubated *E. coli* and *S. typhimurium* with the conjugates. The conformation of the aptamers changed upon binding to the bacteria. Thus, the particles could not be stabilized by aptamers anymore and after applying high salt-concentrations, AuNPs aggregated and the dispersion changed its color. Color change was detected by UV/Vis spectroscopy [105].

As illustrated by the presented applications, aptamer-modified nanoparticles are very promising candidates for cell targeting and diagnostic detection. Especially in the context of in vivo imaging, there are still some problems to be solved. The main issue is the investigation of long term in vivo cytotoxicity.

Drug delivery

Drug delivery systems aim for specific transportation of pharmaceuticals to the desired site of action. By targeted delivery of drugs, solely to diseased cells, systemic side effects should be avoided. To enable specific delivery, a targeting ligand and its specific binding of the target cells as well as efficient intracellularization is necessary. The key advantage of such drug delivery systems is the ability to change pharmacokinetics. Additionally, the targeted distribution of drugs results in reduced effects on non-targeted tissues [106]. Aptamer-conjugated nanoparticles serving as targeting delivery systems commonly consist of iron oxid nanoparticles, gold nanoparticles, CNTs, dendrimers, quantum dots, liposomes or polymeric nanoparticles [106]. The drug can either be encapsulated within the nanoparticle or attached to the nanoparticle surface [81, 107]. Zhang and coworkers developed an aptamer-nanoparticle conjugate for co-delivery of both, an entrapped and a surface-attached drug. The surface-attached drug release was approximately 80%, while the entrapped drug release was 45% in the same time interval. These properties may find application for time-controlled drug delivery [108]. Different research groups showed the effect of aptamer-functionalized and drug-loaded nanoparticles on cancer cells [89, 91]. For example, Aravind et al. used polymeric nanoparticles consisting of poly(lactic-co-glycolic acid) (PGLA), loaded with paclitaxel (PTX) and immobilized with AS1411. They successfully targeted cancer cells in vitro. Additionally, they showed that cell viability of cancer cells decreased after incubation with aptamer-modified and drug-loaded particles. Thus, after targeting the cancer cells, drug release was induced [91].

Today there are many targeted drug delivery systems which are able to specifically enhance cellular uptake and increase cytotoxicity in vitro. Some groups have already investigated the applicability of aptamer-modified nanoparticles for targeted drug delivery in vivo. For example, Liu et al. showed that aptamer-modified nanoparticles could accumulate at tumor sites in mice. They used ApS6 and ApS10 directed against breast cancer cells and demonstrated that the systemic toxicity to other organs was decreased, compared to systematic strategies of administration [109]. A problem which has to be solved, is the multicancer drug resistance. Multidrug resistance (MDR) hampers the efficacy of chemotherapy [110]. Utilization of aptamer-modified nanoparticles is one approach to solve this problem by enhancement of intracellular drug concentration in cancer cells can be achieved with nanoparticles. Simultaneously, the toxicity to healthy cells is minimal. Due to their small size, nanoparticles are able to cross the leaky and hyperpermeable tumor vascular [111]. It is also possible to incorporate anticancer drugs and an additional chemosensitizer. Such delivery systems, consisting of two different drugs to overcome multi drug resistance have been reported. Sengupta and coworkers, for example, developed a nanoparticle delivery system loaded with combretastatin and doxorubicin

[112]. The drug attached to the nanoparticle surface was released first (combretastatin) and caused the destruction of tumors vasculature. Doxorubicin, which was entrapped within the nanoparticles, was released secondly and subsequently caused cytotoxicity [112]. This may be a suitable approach to overcome MDR.

Intracellular sensing

While the aforementioned examples deal with the specific targeting of cell surface bound receptors, aptamer-modified nanoparticles can also be exploited for the detection of targets within cells. Different types of nanoparticles were already applied for intracellular imaging, such as quantum dots, silica nanoparticles or graphene oxide nanoparticles [113]. Furthermore, AgNPs, AuNPs and QDs functionalized with aptamers were used for intracellular protein imaging [114–116]. It is possible to target specific proteins and trace their endocytic pathway [114]. AuNPs are the most commonly used nanoparticles in intracellular sensing. Zheng et al. developed an assay with aptamer-modified AuNPs which could detect intracellular adenosine triphosphate (ATP) concentrations [117]. Wang and coworkers used aptamer-modified silica nanoparticles to detect ATP [118]. They immobilized a Cy-5 labeled aptamer on nanoparticle surfaces and upon exposure to ATP, the aptamer changed its structure. Formation of an aptamer-target-complex induced the release of the immobilized aptamer and finally a strong fluorescence signal is observed in the presence of ATP. If ATP is absent, no fluorescence is detectable. The detection limit was reported to be ~34 μM [118].

Biosensing

Recently, aptamer-based biosensors (aptasensors) have attracted particular attention. The best known aptamer-modified nanoparticles for biosensing are metallic nanoparticles like gold and silver nanoparticles [119]. Besides, aptamer-functionalized MNP are used for small-molecule and protein detection (e.g. for detection of human R-thrombin protein, SPIONs were functionalized with aptamers) [80]. Aptamer-modified magnetic particles bind the target protein and MRI is used for detection. In presence of the target protein, a MRI contrast change is detectable [120].

There are three main categories of aptasensors: electrochemical, optical and mass sensitive sensor systems [121]. Table 4 quotes different aptasensors, their detection limit, corresponding analyte targeted by the aptamer and application.

Mass sensitive aptasensors are a category of label-free bioassays which include wave-based sensors like surface-plasmon resonance (SPR), acoustic wave-based sensors [quartz crystal microbalance (QCM)] and surface acoustic wave (SAW) sensors [121]. Mass sensitive aptasensors are capable of displaying changes on the sensor surface without any additional labeling. Furthermore, they can operate in real-time. Applications of mass sensitive aptasensors have been reported for the detection of large molecules like proteins or cells. Small molecules are hard to detect due to the minor change in mass induced by binding of small molecules to the sensor [104].

Optical sensors can be divided into fluorescent and colorimetric sensors [121]. Many colorimetric sensors are based on size dependent optical properties. An example

Table 4: Different aptasensors for targeting biomolecules (continued).

Sensor	Detection limit	Target	Application	References
Colorimetric	–	Cocaine	AuNP	[122]
Colorimetric	20 nM	Thrombin	AuNP	[86]
Colorimetric	5 μM	Ibuprofen	AuNP	[123]
Colorimetric	17 nM	Glutathione	AuNP	[86, 124]
Fluorescence	5 nM	OTA	AuNP	[86]
Fluorescence	0.5 μM (signal-off mode)	Cocaine	QD	[125]
Fluorescence	10 μM	ATP	Graphene	[86]
Electrochemical	0.1 nM	ATP	AuNP	[86]
Electrochemical	0.5 μM	Cocaine	AuNP	[86]
Electrochemical	9.4 nM	Kanamycin	AuNP; self-assembled nano-composite	[126]
Electrochemical	0.5 nM	Heavy metals	AuNP	[126]
Electrochemical	5 nM	BPA	AuNP	[126]
Fluorescent flow	5 mM	ATP	QD	[127]
FRET		OTA	AuNP	[128]

for colorimetric sensing are aptamer-conjugated AuNPs [126]. Colloidal gold nanoparticles exhibit a red color and when they aggregate, their color changes to blue due to SPR effects [116, 129]. SPR is dependent on shape and particle size, as well as the distance between AuNPs; consequently their absorption wavelength changes upon formation of agglomerates [126].

Another example for a colorimetric aptasensor was demonstrated for the detection of digoxin. Herein, Emrani and coworkers used AuNPs and coupled aptamers on the surface of the particles. When digoxin was absent, the aptamers were attached to the surface of the AuNPs by electrostatic interaction between aptamer and particles. Thus, the particles were stabilized against high salt-concentrations and consequently aggregation. In presence of digoxin, the aptamer changed its structure and an aptamer-digoxin-complex was formed. AuNPs aggregated after adding NaCl and the red colored colloidal AuNPs change their color into blue upon aggregation [130].

Fluorescence-based biosensors could be designed with fluorescent labeled aptamers or with label-free aptamers [131]. Many fluorescence biosensors apply the competitive binding principle. This is based on the competition of binding of the analyte or hybridization of a complementary strand to the aptamer. One example for competitive binding is a QD-based aptasensor for the detection of cocaine or the detection of human neutrophil elstase (HNE) [126, 132].

The fluorescence of the sensors could either be achieved by (i) direct modification of the aptamer with fluorophores, (ii) structural changes could cause fluorescence of a dye or (iii) the fluorescence resonance energy transfer (FRET) between two dyes could be affected [131]. As mentioned above, an example for a fluorescence-based aptasensor was reported by Sharma et al. for the detection of cocaine with aptamer-conjugated QDs [126]. Herein, distinction is made between two different types of sensors: signal-on and signal-off sensors. In case of the signal-on sensor, an oligonucleotide is labeled with the fluorescent dye Cy-5. FRET (between Cy-5 and QDs) quenches the signal and no fluorescence is detectable. If cocaine is present, an aptamer-cocaine-complex is formed resulting in the restoration of fluorescence exhibited by the labeled oligonucleotide [125, 126, 131]. In case of the signal-off sensor, the aptamer is hybridized to a complementary (Cy-5 labeled) strand and coupled to the QD surface. If cocaine is absent, the fluorescence of Cy-5 is detectable due to FRET between QD and Cy-5. In case of cocaine presence, the aptamer-target-complex is formed and the Cy-5 labeled oligonucleotide is released from the QD surface. Thus, decreased Cy-5 fluorescence signal indicates the presence of cocaine [125, 126, 131].

Aptasensors can also be of electrochemical nature and implement aptamer-functionalized gold nanoparticles. Li and coworkers self-assembled AuNPs on a gold electrode. Subsequently, the aptamer was immobilized on the nanoparticle surface and the electrical potential was measured. Upon detection of cocaine, a higher electrical potential was measured [133].

Conclusions

Potential applications of aptamer-modified nanoparticles or nanostructured materials are almost as multifarious as aptamer-sequences and their corresponding targets themselves. We believe that they will contribute to the solution of many analytical or other problems based on target recognition in the future. Even though the need of optimization for every aptamer-target pair and every utilized nanostructure persists, we are convinced that the set of considerations presented in this review can be a helpful resource when conjugating aptamers to nanoparticles or nanostructured surfaces. The applications presented here are demonstrating the success of such optimization processes for a wide range of cell-capture and biosensor applications based on aptamer-modified nanomaterials.

Author's statement

Conflict of interest: Authors state no conflict of interest.

Materials and methods

Informed consent: Informed consent has been obtained from all individuals included in this study.

Ethical approval: The research related to human use has been complied with all the relevant national regulations, institutional policies and in accordance the tenets of the Helsinki Declaration, and has been approved by the authors' institutional review board or equivalent committee.

References

1. Tuerk C, Gold L. Systematic evolution of ligands by exponential enrichment: RNA ligands to bacteriophage T4 DNA polymerase. Science. 1990;249:505–10.
2. Jayasena SD. Aptamers: an emerging class of molecules that rival antibodies in diagnostics. Clin Chem. 1999;45:1628–50.
3. Heilkenbrinker A, Reinemann C, Stoltenburg R, Walter JG, Jochums A, Stahl F, et al. Identification of the target binding site of ethanolamine-binding aptamers and its exploitation for ethanolamine detection. Anal Chem. 2015;87:677–85.

4. Urmann K, Walter J-G, Scheper T, Segal E. Label-free optical biosensors based on aptamer-functionalized porous silicon scaffolds. Anal Chem. 2015;87:1999–2006.
5. Kokpinar O, Walter JG, Shoham Y, Stahl F, Scheper T. Aptamer-based downstream processing of his-tagged proteins utilizing magnetic beads. Biotechnol Bioeng. 2011;108:2371–9.
6. Lönne M, Bolten S, Lavrentieva A, Stahl F, Scheper T, Walter JG. Development of an aptamer-based affinity purification method for vascular endothelial growth factor. Biotechnol Rep. 2015;8:16–23.
7. Walter JG, Stahl F, Scheper T. Aptamers as affinity ligands for downstream processing. Eng Life Sci. 2012;12:496–506.
8. Schax E, Lönne M, Scheper T, Belkin S, Walter JG. Aptamer-based depletion of small molecular contaminants: A case study using ochratoxin A. Biotechnol Bioproc E. 2015;20:1016–25.
9. Meyer M, Scheper T, Walter JG. Aptamers: versatile probes for flow cytometry. Appl Microbiol Biotechnol. 2013;97:7097–109.
10. Modrejewski J, Walter J-G, Kretschmer I, Kemal E, Green M, Belhadj H, et al. Aptamer-modified polymer nanoparticles for targeted drug delivery. BioNanoMaterials. 2015;17:43–51.
11. Walter JG, Petersen S, Stahl F, Scheper T, Barcikowski S. Laser ablation-based one-step generation and bio-functionalization of gold nanoparticles conjugated with aptamers. J Nanobiotechnol. 2010;8:21.
12. Patel DJ, Suri AK, Jiang F, Jiang LC, Fan P, Kumar RA, et al. Structure, recognition and adaptive binding in RNA aptamer complexes. J Mol Biol. 1997;272:645–64.
13. Walter JG, Kökpinar O, Friehs K, Stahl F, Scheper T. Systematic investigation of optimal aptamer immobilization for protein-microarray applications. Anal Chem. 2008;80:7372–8.
14. Balamurugan S, Obubuafo A, Soper SA, Spivak DA. Surface immobilization methods for aptamer diagnostic applications. Anal Bioanal Chem. 2008;390:1009–21.
15. Ocana C, del Valle M. A comparison of four protocols for the immobilization of an aptamer on graphite composite electrodes. Microchim Acta 2014;181:355–63.
16. Zhu GH, Lubbecke M, Walter JG, Stahl F, Scheper T. Characterization of optimal aptamer-microarray binding chemistry and spacer design. Chem Eng Technol. 2011;34:2022–8.
17. Lin PH, Chen RH, Lee CH, Chang Y, Chen CS, Chen WY. Studies of the binding mechanism between aptamers and thrombin by circular dichroism, surface plasmon resonance and isothermal titration calorimetry. Colloids Surf B Biointerfaces. 2011;88:552–8.
18. Witt M, Walter J-G, Stahl F. Aptamer microarrays – current status and future prospect. Microarrays. 2015;4:115–32.
19. Justino CIL, Freitas AC, Pereira R, Duarte AC, Santos TAPR. Recent developments in recognition elements for chemical sensors and biosensors. TrAC Trends Anal Chem. 2015;68:2–17.
20. Liang H, Zhang XB, Lv YF, Gong L, Wang RW, Zhu XY, et al. Functional DNA-containing nanomaterials: cellular applications in biosensing, imaging, and targeted therapy. Acc Chem Res. 2014;47:1891–901.
21. Wang ZH, Yu JB, Gui RJ, Jin H, Xia YZ. Carbon nanomaterials-based electrochemical aptasensors. Biosens Bioelectron. 2016;79:136–49.
22. Wang G, Wang Y, Chen L, Choo J. Nanomaterial-assisted aptamers for optical sensing. Biosens Bioelectron. 2010;25:1859–68.
23. Bunka DHJ, Stockley PG. Aptamers come of age – at last. Nat Rev Microbiol. 2006;4:588–96.
24. Wang L, Zhu C, Zheng Q, He X. Preparation of homogeneous nanostructures in 5 minutes for cancer cells capture. J Nanomater. 2015;2015:6.
25. Wan Y, Mahmood MAI, Li N, Allen PB, Kim Y-t, Bachoo R, et al. Nanotextured substrates with immobilized aptamers for cancer cell isolation and cytology. Cancer. 2012;118:1145–54.
26. Chen L, Liu X, Su B, Li J, Jiang L, Han D, et al. Aptamer-mediated efficient capture and release of T lymphocytes on nanostructured surfaces. Adv Mater. 2011;23:4376–80.
27. Xue L, Lyu Z, Luan Y, Xiong X, Pan J, Chen G, et al. Efficient cancer cell capturing SiNWAs prepared via surface-initiated SET-LRP and click chemistry. Polym Chem. 2015;6:3708–15.
28. Urmann K, Arshavsky-Graham S, Walter JG, Scheper T, Segal E. Whole-cell detection of live lactobacillus acidophilus on aptamer-decorated porous silicon biosensors. Analyst. 2016, doi: 10.1039/C6AN00810K.
29. Peters RF, Gutierrez-Rivera L, Dew SK, Stepanova M. Surface enhanced Raman spectroscopy detection of biomolecules using EBL fabricated nanostructured substrates. J Vis Exp. 2015, doi:10.3791/52712:e52712.
30. Yang J, Palla M, Bosco FG, Rindzevicius T, Alstrøm TS, Schmidt MS, et al. Surface-enhanced Raman spectroscopy based quantitative bioassay on aptamer-functionalized nanopillars using large-area Raman mapping. ACS Nano. 2013;7:5350–9.
31. So H-M, Won K, Kim YH, Kim B-K, Ryu BH, Na PS, et al. Single-walled carbon nanotube biosensors using aptamers as molecular recognition elements. J Am Chem Soc. 2005;127:11906–7.
32. Yoon H, Kim J-H, Lee N, Kim B-G, Jang J. A novel sensor platform based on aptamer-conjugated polypyrrole nanotubes for label-free electrochemical protein detection. ChemBioChem. 2008;9:634–41.
33. Yoo L, Ahn K-Y, Ahn J-Y, Laurell T, Lee YM, Yoo PJ, et al. A simple one-step assay platform based on fluorescence quenching of macroporous silicon. Biosens Bioelectron. 2013;41:477–83.
34. Evtugyn G, Porfireva A, Ryabova M, Hianik T. Aptasensor for Thrombin based on carbon nanotubes-methylene blue composites. Electroanalysis. 2008;20:2310–6.
35. Porfireva AV, Evtugyn GA, Ivanov AN, Hianik T. Impedimetric aptasensors based on carbon nanotubes – poly(methylene blue) composite. Electroanalysis. 2010;22:2187–95.
36. Miodek A, Castillo G, Hianik T, Korri-Youssoufi H. Electrochemical aptasensor of human cellular prion based on multiwalled carbon nanotubes modified with dendrimers: a platform for connecting redox markers and aptamers. Anal Chem. 2013;85:7704–12.
37. Huang K-J, Shuai H-L, Chen Y-X. Layered molybdenum selenide stacking flower-like nanostructure coupled with guanine-rich DNA sequence for ultrasensitive ochratoxin A aptasensor application. Sens Actuators B Chem. 2016;225:391–7.
38. White RJ, Phares N, Lubin AA, Xiao Y, Plaxco KW. Optimization of electrochemical aptamer-based sensors via optimization of probe packing density and surface chemistry. Langmuir. 2008;24:10513–8.
39. Daniel C, Roupioz Y, Gasparutto D, Livache T, Buhot A. Solution-phase vs surface-phase aptamer-protein affinity from a label-free kinetic biosensor. PLoS One. 2013;8:e75419.
40. Hasegawa H, Savory N, Abe K, Ikebukuro K. Methods for improving aptamer binding affinity. Molecules (Basel, Switzerland). 2016;21:421.
41. Balamurugan S, Obubuafo A, McCarley RL, Soper SA, Spivak DA. Effect of linker structure on surface density of aptamer

Appendix

monolayers and their corresponding protein binding efficiency. Anal Chem. 2008;80:9630–4.
42. Lim JY, Donahue HJ. Cell sensing and response to micro- and nanostructured surfaces produced by chemical and topographic patterning. Tissue Eng. 2007;13:1879–1891.
43. Teixeira AI, Abrams GA, Bertics PJ, Murphy CJ, Nealey PF. Epithelial contact guidance on well-defined micro- and nanostructured substrates. J Cell Sci. 2003;116:1881–92.
44. Plaks V, Koopman CD, Werb Z. Circulating tumor cells. Science (New York, N.Y.). 2013;341:1186–8.
45. Glaves D, Mayhew E. Selective therapy of metastasis. I. Quantitation of tumorigenic circulating and covert cancer cells disseminated from metastatic and nonmetastatic tumors. Canc Drug Del. 1984;1:293–302.
46. Butler TP, Gullino PM. Quantitation of cell shedding into efferent blood of mammary adenocarcinoma. Cancer Res. 1975;35:512–6.
47. Alix-Panabières C, Pantel K. Circulating tumor cells: liquid biopsy of cancer. Clin Chem. 2013;59:110–8.
48. Liotta LA, Kleinerman J, Saidel GM. Quantitative relationships of intravascular tumor cells, tumor vessels, and pulmonary metastases following tumor implantation. Cancer Res. 1974;34: 997–1004.
49. Bettinger CJ, Langer R, Borenstein JT. Engineering substrate topography at the micro- and nanoscale to control cell function. Angew Chem Int Ed. 2009;48:5406–15.
50. Wang L, Asghar W, Demirci U, Wan Y. Nanostructured substrates for isolation of circulating tumor cells. Nano Today. 2013;8:374–87.
51. Garipcan B, Odabas S, Demirel G, Burger J, Nonnenmann SS, Coster MT, et al. In vitro biocompatibility of n-type and undoped silicon nanowires. Adv Eng Mater. 2011;13:B3–9.
52. Fischer KE, Alemán BJ, Tao SL, Daniels RH, Li EM, Bünger MD, et al. Biomimetic nanowire coatings for next generation adhesive drug delivery systems. Nano Lett. 2009;9:716–20.
53. Wang S, Wang H, Jiao J, Chen K-J, Owens GE, Kamei K-i, et al. Three-dimensional nanostructured substrates toward efficient capture of circulating tumor cells. Angew Chem Int Ed. 2009;48:8970–3.
54. Wang S, Liu K, Liu J, Yu ZTF, Xu X, Zhao L, et al. Highly efficient capture of circulating tumor cells by using nanostructured silicon substrates with integrated chaotic micromixers. Angew Chem Int Ed. 2011;50:3084–8.
55. Dasgupta NP, Sun J, Liu C, Brittman S, Andrews SC, Lim J, et al. 25th anniversary article: semiconductor nanowires–synthesis, characterization, and applications. Adv Mater. 2014;26:2137–84.
56. Tang H, Dou K, Kaun C-C, Kuang Q, Yang S. $MoSe_2$ nanosheets and their graphene hybrids: synthesis, characterization and hydrogen evolution reaction studies. J Mater Chem A. 2014;2:360–4.
57. Pacholski C, Yu C, Miskelly GM, Godin D, Sailor MJ. Reflective interferometric fourier transform spectroscopy: a self-compensating label-free immunosensor using double-layers of porous SiO_2. J Am Chem Soc. 2006;128:4250–2.
58. Guinan T, Godefroy C, Lautrédou N, Pace S, Milhiet P-E, Voelcker N, et al. Interaction of antibiotics with lipid vesicles on thin film porous silicon using reflectance interferometric Fourier transform spectroscopy. Langmuir. 2013;29:10279–86.
59. Shtenberg G, Segal E. Porous silicon optical biosensors. In: Canham L, editor. Handbook of Porous Silicon. Cham, Switzerland: Springer International Publishing; 2014:857–68.
60. Tenenbaum E, Segal E. Optical biosensors for bacteria detection by a peptidomimetic antimicrobial compound. Analyst. 2015;140:7726–33.
61. Massad-Ivanir N, Shtenberg G, Tzur A, Krepker MA, Segal E. Engineering nanostructured porous SiO_2 surfaces for bacteria detection via “direct cell capture”. Anal Chem. 2011;83:3282–9.
62. Khang J, Kim D, Chung KW, Lee JH. Chemiluminescent aptasensor capable of rapidly quantifying Escherichia Coli O157:H7. Talanta. 2016;147:177–83.
63. Duan N, Chang BY, Zhang H, Wang ZP, Wu SJ. Salmonella typhimurium detection using a surface-enhanced Raman scattering-based aptasensor. Int J Food Microbiol. 2016;218: 38–43.
64. Cheng D, Yu MQ, Fu F, Han WY, Li G, Xie JP, et al. Dual recognition strategy for specific and sensitive detection of bacteria using aptamer-coated magnetic beads and antibiotic-capped gold nanoclusters. Anal Chem. 2016;88:820–5.
65. Lucarelli F, Marrazza G, Turner APF, Mascini M. Carbon and gold electrodes as electrochemical transducers for DNA hybridisation sensors. Biosens Bioelectron. 2004;19:515–30.
66. Palegrosdemange C, Simon ES, Prime KL, Whitesides GM. Formation of self-assembled monolayers by chemisorption of derivatives of oligo(ethylene glycol) of structure HS(CH2)11(OCH2CH2) mOH on gold. J Am Chem Soc. 1991;113:12–20.
67. Walczak MM, Popenoe DD, Deinhammer RS, Lamp BD, Chung CK, Porter MD. Reductive desorption of alkanethiolate monolayers at gold: a measure of surface coverage. Langmuir. 1991;7:2687–93.
68. Hegner M, Wagner P, Semenza G. Immobilizing DNA on gold via thiol modification for atomic force microscopy imaging in buffer solutions. FEBS Lett. 1993;336:452–6.
69. Hu M, Chen J, Li Z-Y, Au L, Hartland GV, Li X, et al. Gold nanostructures: engineering their plasmonic properties for biomedical applications. Chem Soc Rev. 2006;35: 1084–94.
70. Wijaya A, Hamad-Schifferli K. Ligand customization and DNA functionalization of gold nanorods via round-trip phase transfer ligand exchange. Langmuir. 2008;24:9966–9.
71. Adzhri R, Arshad KM, Gopinath SCB, Ruslinda AR, Fathil MFM, Ayub RM, et al. High-performance integrated field-effect transistor-based sensors. Anal Chim Acta. 2016;917:1–18.
72. Evtugyn G, Porfireva A, Ivanov A, Konovalova O, Hianik T. Molecularly Imprinted polymerized methylene green as a platform for electrochemical sensing of aptamer–thrombin interactions. Electroanalysis. 2009;21:1272–7.
73. Hianik T, Porfireva A, Grman I, Evtugyn G. Aptabodies – new type of artificial receptors for detection proteins. Protein Pept Lett. 2008;15:799–805.
74. Hianik T, Wang J. Electrochemical Aptasensors – Recent achievements and perspectives. Electroanalysis. 2009;21:1223–35.
75. Porfirieva A, Evtugyn G, Hianik T. Polyphenothiazine modified electrochemical aptasensor for detection of human α-thrombin. Electroanalysis. 2007;19:1915–20.
76. Miodek A, Castillo G, Hianik T, Korri-Youssoufi H. Electrochemical aptasensor of cellular prion protein based on modified polypyrrole with redox dendrimers. Biosens Bioelectron. 2014;56:104–11.
77. Ocana C, del Valle M. Three different signal amplification strategies for the impedimetric sandwich detection of thrombin. Anal Chim Acta. 2016;912:117–24.

78. Kwon MJ, Lee J, Wark AW, Lee HJ. Nanoparticle-enhanced surface plasmon resonance detection of proteins at attomolar concentrations: comparing different nanoparticle shapes and sizes. Anal Chem. 2012;84:1702–7.
79. Amiji MM. Nanotechnology for Cancer Therapy. Boca Raton, FL, USA: CRC Press; 2006.
80. Yang L, Zhang XB, Ye M, Jiang JH, Yang RH, Fu T, et al. Aptamer-conjugated nanomaterials and their applications. Adv Drug Deliver Rev. 2011;63:1361–70.
81. Singh R, Lillard JW. Nanoparticle-based targeted drug delivery. Exp Mol Pathol. 2009;86:215–23.
82. Farokhzad OC, Langer R. Impact of nanotechnology on drug delivery. ACS Nano. 2009;3:16–20.
83. Slowing II, Vivero-Escoto JL, Wu CW, Lin VSY. Mesoporous silica nanoparticles as controlled release drug delivery and gene transfection carriers. Adv Drug Deliver Rev. 2008;60:1278–88.
84. Wang LH, Liu XF, Hu XF, Song SP, Fan CH. Unmodified gold nanoparticles as a colorimetric probe for potassium DNA aptamers. Chem Commun. 2006;36:3780–2.
85. Sperling RA, Parak WJ. Surface modification, functionalization and bioconjugation of colloidal inorganic nanoparticles. Phil Trans R Soc A. 2010;368:1333–83.
86. Kim YS, Raston NHA, Gu MB. Aptamer-based nanobiosensors. Biosens Bioelectron. 2016;76:2–19.
87. Chu TC, Shieh F, Lavery LA, Levy M, Richards-Kortum R, Korgel BA, et al. Labeling tumor cells with fluorescent nanocrystal-aptamer bioconjugates. Biosens Bioelectron. 2006;21:1859–66.
88. Wang AZ, Bagalkot V, Vasilliou CC, Gu F, Alexis F, Zhang L, et al. Superparamagnetic iron oxide nanoparticle-aptamer bioconjugates for combined prostate cancer imaging and therapy. ChemMedChem. 2008;3:1311–5.
89. Gao HL, Qian J, Cao SJ, Yang Z, Pang ZQ, Pan SQ, et al. Precise glioma targeting of and penetration by aptamer and peptide dual-functioned nanoparticles. Biomaterials. 2012;33:5115–23.
90. Dougherty CA, Cai WB, Hong H. Applications of aptamers in targeted imaging: state of the art. Curr Top Med Chem. 2015;15:1138–52.
91. Aravind A, Varghese SH, Veeranarayanan S, Mathew A, Nagaoka Y, Iwai S, et al. Aptamer-labeled PLGA nanoparticles for targeting cancer cells. Cancer Nanotechnol. 2012;3:1–12.
92. Liu QL, Jin C, Wang YY, Fang XH, Zhang XB, Chen Z, et al. Aptamer-conjugated nanomaterials for specific cancer cell recognition and targeted cancer therapy. NPG Asia Mater. 2014;6:e95.
93. Farokhzad OC, Jon S, Khademhosseini A, Tran T-NT, LaVan DA, Langer R. Nanoparticle-aptamer bioconjugates: a new approach for targeting prostate cancer cells. Cancer Res. 2004;64:7668–72.
94. Chang YC, Yang CY, Sun RL, Cheng YF, Kao WC, Yang PC. Rapid single cell detection of Staphylococcus aureus by aptamer-conjugated gold nanoparticles. Sci Rep. 2013;3:1863.
95. Levy-Nissenbaum E, Radovic-Moreno AF, Wang AZ, Langer R, Farokhzad OC. Nanotechnology and aptamers: applications in drug delivery. Trends Biotechnol. 2008;26:442–9.
96. Rosen JE, Chan L, Shieh DB, Gu FX. Iron oxide nanoparticles for targeted cancer imaging and diagnostics. Nanomedicine. 2012;8:275–90.
97. Jalalian SH, Taghdisi SM, Hamedani NS, Kalat SAM, Lavaee P, ZandKarimi M, et al. Epirubicin loaded super paramagnetic iron oxide nanoparticle-aptamer bioconjugate for combined colon cancer therapy and imaging in vivo. Eur J Pharm Sci. 2013;50:191–7.
98. Li ZM, Huang P, He R, Lin J, Yang S, Zhang XJ, et al. Aptamer-conjugated dendrimer-modified quantum dots for cancer cell targeting and imaging. Mater Lett. 2010;64:375–8.
99. Gedi V, Kim YP. Detection and characterization of cancer cells and pathogenic bacteria using aptamer-based nano-conjugates. Sensors. 2014;14:18302–27.
100. Ulusoy M, Walter JG, Lavrentieva A, Kretschmer I, Sandiford L, Le Marois A, et al. One-pot aqueous synthesis of highly strained CdTe/CdS/ZnS nanocrystals and their interactions with cells. RSC Adv. 2015;5:7485–94.
101. Zhao ZL, Xu L, Shi XL, Tan WH, Fang XH, Shangguan DH. Recognition of subtype non-small cell lung cancer by DNA aptamers selected from living cells. Analyst. 2009;134:1808–14.
102. Li LL, Yin Q, Cheng JJ, Lu Y. Polyvalent mesoporous silica nanoparticle-aptamer bioconjugates target breast cancer cells. Adv Healthc Mater. 2012;1:567–72.
103. Su M, Liu H, Ge L, Wang YH, Ge SG, Yu JH, et al. Aptamer-based electrochemiluminescent detection of MCF-7 cancer cells based on carbon quantum dots coated mesoporous silica nanoparticles. Electrochim Acta. 2014;146:262–9.
104. Iliuk AB, Hu LH, Tao WA. Aptamer in bioanalytical applications. Anal Chem. 2011;83:4440–52.
105. Wu WH, Li M, Wang Y, Ouyang HX, Wang L, Li CX, et al. Aptasensors for rapid detection of Escherichia coli O157:H7 and Salmonella typhimurium. Nanoscale Res Lett. 2012;7:658.
106. de Aguiar Ferreira C, Branco de Barros AL. Aptamer functionalized nanoparticles for cancer targeting. J Mol Pharm Org Process Res. 2013;1:105.
107. Wu X, Chen J, Wu M, Zhao JXJ. Aptamers: active targeting ligands for cancer diagnosis and therapy. Theranostics. 2015;5:322–44.
108. Zhang LF, Radovic-Moreno AF, Alexis F, Gu FX, Basto PA, Bagalkot V, et al. Co-delivery of hydrophobic and hydrophilic drugs from nanoparticle–aptamer bioconjugates. ChemMedChem. 2007;2:1268–71.
109. Liu J, Wei T, Zhao J, Huang YY, Deng H, Kumar A, et al. Multifunctional aptamer-based nanoparticles for targeted drug delivery to circumvent cancer resistance. Biomaterials. 2016;91:44–56.
110. Kapse-Mistry S, Govender T, Srivastava R, Yergeri M. Nanodrug delivery in reversing multidrug resistance in cancer cells. Front Pharmacol. 2014;5:159.
111. Dong XW, Mumper RJ. Nanomedicinal strategies to treat multidrug-resistant tumors: current progress. Nanomedicine. 2010;5:597–615.
112. Sengupta S, Eavarone D, Capila I, Zhao GL, Watson N, Kiziltepe T, et al. Temporal targeting of tumour cells and neovasculature with a nanoscale delivery system. Nature. 2005;436:568–72.
113. Xing H, Wong NY, Xiang Y, Lu Y. DNA aptamer functionalized nanomaterials for intracellular analysis, cancer cell imaging and drug delivery. Curr Opin Chem Biol. 2012;16:429–35.
114. Chen LQ, Xiao SJ, Hu PP, Peng L, Ma J, Luo LF, et al. Aptamer-mediated nanoparticle-based protein labeling platform for intracellular imaging and tracking endocytosis dynamics. Anal Chem. 2012;84:3099–110.
115. Chen LQ, Xiao SJ, Peng L, Wu T, Ling J, Li YF, et al. Aptamer-based silver nanoparticles used for intracellular protein imaging and single nanoparticle spectral analysis. J Phys Chem B. 2010;114:3655–9.

Appendix

116. Lonne M, Zhu GH, Stahl F, Walter JG. Biosensors based on aptamers and enzymes. Adv Biochem Eng Biotechnol. 2014;140:121–54.
117. Zheng D, Seferos DS, Giljohann DA, Patel PC, Mirkin CA. Aptamer nano-flares for molecular detection in living cells. Nano Lett. 2009;9:3258–61.
118. Wang, YY, Wang, YS, Liu, B. Fluorescent detection of ATP based on signaling DNA aptamer attached silica nanoparticles, Nanotechnology. 2008;19:415605.
119. Chiu TC, Huang CC. Aptamer-functionalized nano-biosensors. Sensors. 2009;9:10356–88.
120. Yigit MV, Mazumdar D, Kim HK, Lee JH, Dintsov B, Lu Y. Smart "turn-on" magnetic resonance contrast agents based on aptamer-functionalized superparamagnetic iron oxide nanoparticles. ChemBioChem. 2007;8:1675–8.
121. Song SP, Wang LH, Li J, Zhao JL, Fan CH. Aptamer-based biosensors. Trends Anal Chem; TrAC. 2008;27:108–17.
122. Stojanovic MN, Landry DW. Aptamer-based colorimetric probe for cocaine. J Am Chem Soc. 2002;124:9678–9.
123. Kim YS, Kim JH, Kim IA, Lee SJ, Gu MB. A novel colorimetric aptasensor using gold nanoparticle for a highly sensitive and specific detection of oxytetracycline. Biosens Bioelectron. 2011;26:4058–63.
124. Xu H, Wang YW, Huang XM, Li Y, Zhang H, Zhong XH. Hg^{2+}-mediated aggregation of gold nanoparticles for colorimetric screening of biothiols. Analyst. 2012;137:924–31.
125. Zhang CY, Johnson LW. Single quantum-dot-based aptameric nanosensor for cocaine. Anal Chem. 2009;81:3051–5.
126. Sharma R, Ragavan KV, Thakur MS, Raghavarao KSMS. Recent advances in nanoparticle based aptasensors for food contaminants. Biosens Bioelectron. 2015;74:612–27.
127. Bogomolova A, Aldissi M. Real-time aptamer quantum dot fluorescent flow sensor. Biosens Bioelectron. 2011;26:4099–103.
128. Duan N, Wu SJ, Zhu CQ, Ma XY, Wang ZP, Yu Y, et al. Dual-color upconversion fluorescence and aptamer-functionalized magnetic nanoparticles-based bioassay for the simultaneous detection of Salmonella typhimurium and Staphylococcus aureus. Anal Chim Acta. 2012;723:1–6.
129. Lee JH, Yigit MV, Mazumdar D, Lu Y. Molecular diagnostic and drug delivery agents based on aptamer-nanomaterial conjugates. Adv Drug Deliv Rev. 2010;62:592–605.
130. Emrani AS, Danesh NM, Lavaee P, Jalalian SH, Ramezani M, Abnous K, et al. Sensitive and selective detection of digoxin based on fluorescence quenching and colorimetric aptasensors. Anal Methods. 2015;7:3419–24.
131. Wang RE, Zhang Y, Cai J, Cai W, Gao T. Aptamer-based fluorescent biosensors. Curr Med Chem. 2011;18:4175–84.
132. He JL, Wu ZS, Zhang SB, Shen GL, Yu RQ. Fluorescence aptasensor based on competitive-binding for human neutrophil elastase detection. Talanta. 2010;80:1264–8.
133. Li XX, Qi HL, Shen LH, Gao Q, Zhang CX. Electrochemical aptasensor for the determination of cocaine incorporating gold nanoparticles modification. Electroanalysis. 2008;20:1475–82.

Curriculum vitae

Katharina Urmann
urmann@tx.technion.ac.il | urmann@iftc.uni-hannover.de

Academic degrees

10.2013 – 09.2016 — **TECHNION - Israel Institute of Technology** and **Gottfried-Wilhelm-Leibniz University** — Haifa, Israel and Hannover, GER
Dual doctorate program: Ph.D. and Dr. rer. nat.
Advisors: Prof. Dr. Ester Segal and Prof. Dr. Thomas Scheper

- Dissertation title: **"Aptamer-based optical biosensors"**

10.2010 - 10.2012 Hannover, GER — **Gottfried-Wilhelm-Leibniz University**
Studies program: ***Life Science***
Master of Science

10.2006 - 08.2010 Frankfurt, GER — **University of Applied Sciences Frankfurt (Main)**
Studies program: ***Bio-Process Engineering***
Bachelor of Engineering

Experience

07.2015 - 08.2015 — ***Summer School for Silicon Nanotechnology,*** **Department of Chemistry and Biochemistry – UNIVERSITY OF CALIFORNIA SAN DIEGO** — San Diego, USA
Advisor: Prof. Dr. Michael J. Sailor

10.2012 - 10.2013 — ***Research assistant,*** **Institute of Technical Chemistry – GOTTFRIED-WILHELM-LEIBNIZ UNIVERSITY** — Hannover, GER

Faculty of Biotechnology and Food Engineering, TECHNION - Israel Institute of Technology — Haifa, Israel
Advisor: Prof. Dr. Ester Segal

- 04.2012 - 10.2012: Master thesis project: **"Aptamer-based optical sensors"** **Awarded with Karl-Schuegerl prize (2nd) of Leibniz University for excellent thesis in Bio-Process Engineering**
- 03.2011: Internship project title: **"Characterization of double layer porous silicon scaffolds"**

12.2010 - 03.2012 — ***Student assistant,*** **Institute of Technical Chemistry – GOTTFRIED-WILHELM-LEIBNIZ UNIVERSITY** — Hannover, GER

05.2010 - 07.2010	***Intern, Centre de Biochimie Structurale -*** ***CENTRE NATIONAL DE LA RECHERCHE SCIENTIFIQUE*** ***Advisor: Dr. Catherine Teyssier***	Montpellier, FRA
08.2009 - 02.2010	***Department for Research and Development Prototyping*** ***Health Care and Drugs – BEIERSDORF AG*** ***Advisor: Karl-Heinz Woeller***	Hamburg, GER

- Bachelor's thesis project: **"Investigation of correlations between adhesive-force and drug-release through different additives in an innovative plaster-system"**

Public professional activities

01.2014 - present	**Founding member and chairwoman of the Young German Technion Society** ***German Technion Society, Berlin, Germany***

Competencies

ADVANCED TRAININGS

- Gene technology, biosafety and biosecurity – State approved course §15 GenTSV for project leaders and responsible persons for biosafety
- Qualification course for water pollution control officers §§ 64-65 WHG
- Certification as quality management / GMP representative

LANGUAGE SKILLS

German: native proficiency
English: full professional proficiency
French: working proficiency
Hebrew: elementary proficiency